NONLINEAR THERMOELASTIC STATIC VIBRATION AND BUCKLING BEHAVIOUR OF FUNCTIONALLY GRADED SHELL PANEL

Vishesh Ranjan Kar

Nonlinear Thermoelastic Static Vibration and Buckling Behaviour of Functionally Graded Shell Panel

Thesis submitted to

National Institute of Technology, Rourkela

For the award of the degree

of

Doctor of Philosophy

by

Vishesh Ranjan Kar

Roll. No.: 512ME130

Under the guidance of

Dr. Subrata Kumar Panda

Department of Mechanical Engineering

National Institute of Technology, Rourkela

October 2015

Dedicated to……

My Family

CERTIFICATE OF APPROVAL

Certified that the thesis entitled NONLINEAR THERMOELASTIC STATIC VIBRATION AND BUCKLING BEHAVIOUR OF FUNCTIONALLY GRADED SHELL PANEL submitted by VISHESH RANJAN KAR to National Institute of Technology, Rourkela, for award of the degree of Doctor of Philosophy has been accepted by the external examiners and that the student has successfully defended the thesis in the viva-voce examination held today.

Signature:
Name: Prof. S. K. Sahu
(Member of the DSC)

Signature:
Name: Prof. T. Roy
(Member of the DSC)

Signature:
Name: Prof. H. Roy
(Member of the DSC)

Signature:
Name: Prof. S. K. Panda
(Supervisor)

Signature:
Name:
(External Examiner)

Signature:
Name: Prof. J. Srinivas
(Chairman)

Declaration

I certify that

a. The work contained in the thesis is original and has been done by myself under the general supervision of my supervisor.
b. The work has not been submitted to any other Institute for any degree or diploma.
c. I have followed the guidelines provided by the Institute in writing the thesis.
d. I have conformed to the norms and guidelines given in the Ethical Code of Conduct of the Institute.
e. Whenever I have used materials (data, theoretical analysis, and text) from other sources, I have given due credit to them by citing them in the text of the thesis and giving their details in the references.
f. Whenever I have quoted written materials from other sources, I have put them under quotation marks and given due credit to the sources by citing them and giving required details in the references.

Signature of the Student

CERTIFICATE

This is to certify that the thesis entitled **Nonlinear Thermoelastic Static Vibration and Buckling Behaviour of Functionally Graded Shell Panel**, submitted by **Mr. Vishesh Ranjan Kar** to National Institute of Technology, Rourkela, is a record of bona fide research work under my supervision and I consider it worthy of consideration for the award of the degree of Doctor of Philosophy of the Institute.

_____

Prof. S. K. Panda

Assistant Professor
Department of Mechanical Engineering
National Institute of Technology, Rourkela
Odisha: 769008

Date:

Acknowledgement

Pre-eminently, I believe myself fortunate enough to have Dr. Subrata Kumar Panda as a supervisor. I would like to thank him for his invaluable guidance, continuous encouragement and thoughtfulness towards the accomplishment of my Ph.D. work. It has been my contentment to have him as a guide, exemplar and mentor. His suggestions and advice have been a precious teaching for my work and my life. I will admire his indispensable help for the rest of my life.

It is my duty to record my sincere thanks and heartfelt gratitude to Prof. S. K. Sarangi, Director, National Institute of Technology Rourkela, for support, encouragement and blessings during the course of this work.

I express my sincere gratitude to Prof. S. S. Mohapatra, Head, Department of Mechanical Engineering, National Institute of Technology Rourkela and all faculty members for their support and encouragement during the course of this work.

I would also like to take this opportunity to thank the members of the Doctoral Scrutiny Committee Prof. J. Srinivas, Prof. S. K. Sahu, Prof. T. Roy and Prof. H. Roy of NIT, Rourkela for their valuable suggestions during the progress of this work.

I am very much thankful to my lab mates Vijay, Pankaj, Pradeep, Girish, Rohit, Abdul, Kulmani, Ravi, Diprodyuti, Sushree, Ajay, Suraj, Chetan and Rahul for their understanding, patience and extending helping hand during the work.

Lastly but certainly not the least, I extended my sincere gratitude to my parents, elder brother and sisters, nieces, in-laws, wife Padmaja, son Anvay and relatives for their help and love without which the thesis could not have reached the present form. Above all, I would like to thank almighty for his continued blessings that have helped me complete this work successfully.

National Institute of Technology, Rourkela
Rourkela - 769008, India (Vishesh Ranjan Kar)

Abstract

Functionally graded material (FGM) has created the interest of many researchers due to its tailor-made material properties. FGMs are the advanced form of composites that exhibit an inhomogeneous character especially designed for the high-temperature applications such as aircraft engines, rocket heat shields, thermal barrier coatings, heat exchanger tubes, etc. This material has been developed by taking the gradual variation of metal and ceramic constituents in a very efficient manner to suit the needs of the engineering structure. The effective material properties of the FGM follow the rule-based grading of two counterparts as discussed above, metals and ceramics. Shell structures made of FGMs are subjected to different kind of loading during their service life, and the structural responses (deformations, buckling/post-buckling, and linear/nonlinear natural frequencies) are affected considerably due to that. In this regard, a general nonlinear mathematical model has been developed for the FGM doubly curved shell panel using Green-Lagrange geometrical nonlinear kinematics in the framework of the higher-order shear deformation theory. The effective material properties of FGM shell panels are evaluated using Voigt's micromechanical model via the power-law distribution. The material properties each constituent are assumed to be temperature-dependent. In addition, to achieve the true flexure of the structure, all the nonlinear higher-order terms are included in the mathematical model. The system governing equation of the FGM structure is obtained using the variational principle, and the direct iterative method is employed to compute the desired nonlinear responses in conjunction with suitable isoparametric finite element steps. The convergence behaviour of the proposed numerical model has been checked and validated further by comparing the responses with those available published literature. The linear and the nonlinear flexural, free vibration and the buckling responses of the FGM single/doubly curved shell panels are examined under thermo-mechanical loading. Finally, the effects of different geometrical and material parameters, support conditions, loading types on the deflection, frequency and critical buckling load parameter of the FGM single/doubly curved shell panels are examined and discussed in detail. This is also believed that the present study would be beneficial to the analysis and the design of FGM structure and/or structural component for real-life problems.

Keywords: Functionally graded materials. Single/doubly curved panel, Higher-order, Green-Lagrange, Nonlinear FEM, Thermo-mechanical loading, Flexural, Free Vibration, Post-Buckling, Thermoelasticity.

CONTENTS

List of Symbols

Most of the symbols are defined as they occur in the thesis. Some of the most common symbols, which are repeatedly used, are listed below.

x, y, z	Cartesian co-ordinate axes.
u, v and w	Displacements corresponding to x, y and z direction, respectively
R_x, R_y	Principal radii of curvatures of shell panel
θ_x, θ_y	The rotations with respect to y and x direction
u_0^*, θ_x^*, v_0^*, θ_y^*	Higher order terms of Taylor series expansion
λ, λ_0	Global and mid-plane displacement vectors
a, b and h	Length, width and thickness of the shell panel
$\{\varepsilon_l\}$, $\{\varepsilon_{nl}\}$	Linear and nonlinear strain tensors
$\{\bar{\varepsilon}_l\}$, $\{\bar{\varepsilon}_{nl}\}$	Linear and nonlinear mid-plane strain vectors
$\{\sigma\}$	Stress tensor
$\{\varepsilon\}$	Strain tensor
P	Effective material properties
$P_0, P_{-1}, P_1, P_2, P_3,$	Temperature coefficients
α	Thermal expansion/contraction coefficient
ΔT	Temperature rise
T_c	Temperature at the top (ceramic) surface
T_m	Temperature at the bottom (metal) surface
n	Power-law index
V_c	Volume fraction of the ceramic material
V_m	Volume fraction of the metal material
E_c	Young's modulus of the ceramic material
E_m	Young's modulus of the metal material
υ_m	Poisson's ratio of the metal material
υ_c	Poisson's ratio of the ceramic material
ρ_c	Mass density of the ceramic material
ρ_m	Mass density of the metal material
k_c	Thermal conductivity of the ceramic material
k_m	Thermal conductivity of the metal material
U_ε	Strain energy due to linear and nonlinear strains
U_m	Strain energy due to in-plane force resultants
W	Total work done due to thermomechanical load

T	Kinetic energy
$[C]$	Reduced elastic constant
$[B_l]$ and $[B_{nl}]$	Linear and nonlinear strain-displacement matrix
$\{\varepsilon_g\}$	Geometric strain vector
$[D_G]$	Material property matrix
$[K_l]$	Linear stiffness matrix
$[K_G]$	Geometric stiffness matrix
$[K_{nl}],[K_{nl1}],[K_{nl2}],[K_{nl3}]$	Nonlinear stiffness matrices
$[M]$	Mass matrix
$[T_l]$, $[T_{nl}]$, f	Thickness co-ordinate matrices
$W_{\max}$	Maximum deflection at the centre of the shell panel
$W_{\max}/h$	Amplitude ratio
ω_l	Linear frequency
$\bar{\omega}_l$	Nondimensional linear frequency
ω_{nl}	Nonlinear frequency
$\bar{\omega}_{nl}$	Nondimensional nonlinear frequency
$\bar{\omega}_{nl} / \bar{\omega}_l$	Frequency ratios
R/a	Curvature ratios
a/h	Thickness ratios
a/b	Aspect ratios

Superscript

e	Element form
T	Transpose matrix

Subscript

l	Linear
nl	Nonlinear
c	Ceramic material
m	Metal material
i	Node number
max	Maximum

Abbreviation

CLPT	Classical laminated plate theory

FSDT	First-order shear deformation theory
HSDT	Higher order shear deformation theory
FEM	Finite element method
GDQ	Generalized differential quadrature
FGM	Functionally graded material
FG	Functionally graded
ESL	Equivalent single layer
1D	One dimensional
2D	Two-dimensional
3D	Three-dimensional
Eq.	Equation
TID	Temperature-independent
TD	Temperature-dependent
UDL	Uniformly distributed load

List of Figures

List of Tables

CHAPTER 1

INTRODUCTION

1.1 Overview

Many advanced materials are being developed every now then and used in different engineering structures/structural components to make a compromise between strength and cost. This in turn creates the necessity of analysis of such materials and structures to meet the customised design and analysis requirements. In this regard, composites are widely appreciated and dominated by many weight sensitive industries from last few decades. However, it is observed that these multi-layer composites are unable to carry an extra amount of load and excessive thermal distortion due to their inherent de-lamination behaviour. De-lamination has been a major concern for the design engineers to ensure the reliability and the performances of the structures under the combined action of loading. In addition to that, the separation of layers caused by high local inter-laminar stresses result in the destruction of load transfer mechanism, reduction of stiffness, loss of structural integrity and finally leads to functional failure of the structure. In order to overcome the above issues of the modern structure, scientists and researchers quest to develop new types of material.

The concept of functionally graded material (FGM) was first conceptualised in Japan during a space project programme in which the space scientists were exploring a thermal shielding material that can withstand a thermal environment of 2000K with a

temperature difference of 1000K across the 10mm section (Koizumi, 1997). FGMs are the advanced form of composites, which exhibit an inhomogeneous character, specially designed for the thermal protective systems such as aircraft engines, rocket heat shields, thermal barrier coatings, heat exchanger tubes, etc. Besides the manmade FGM structures, some natural FGMs are already existed, such as bone, human skin, bamboo tree, etc. In general, the FGM properties are achieved through the continuous variation of material compositions from the one surface to the other. This smooth gradation relaxes the de-lamination and the residual stress which are common in the laminated composites. Broadly, the FGMs follow different rule based grading of two counterparts, namely, metals or their alloys and the ceramics. It is worthy to mention that the metals have already established their existence and capabilities in the field of engineering for many years for their excellent strength and toughness characteristics, whereas the ceramics have the enough potential in heat resistance and anti-oxidant behaviour. The typical metal/ceramic FGM can be modelled by two ways, first by considering the stepwise variation of the volume fractions of each constituent (Figure 1.1a) and second, the continuous gradation of the volume fractions (Figure 1.1b). The latter one is the more familiar with the FGM in which the incompatible functions of ceramics (such as the heat, wear, and oxidation resistance) and metals (the high toughness, high strength, machinability, and bonding capability) can be integrated without severe internal thermal stresses. Due to the tailor-made properties of the FGM, the implementation and application of this new kind of material are now being growing in every promising industry like aerospace, automobile, defence, biomedical and energy, etc.

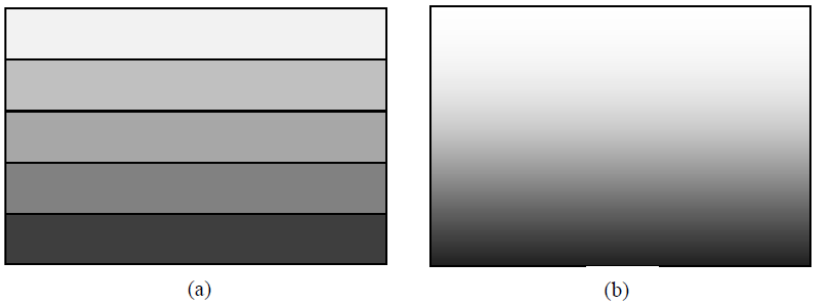

Figure 1.1 FGM model (a) stepwise and (b) continuous graded structures

It is well known that the geometry of any structure/structural component plays an important role in their strength and deformation bearing capabilities. Out of all different

geometries, shell/curved panels are widely used in many fields of engineering like modern vehicles, buildings, spacecraft etc. The shell panels may be deep/shallow, singly/doubly curved and synclastic/anticlastic curvature. The simplest form of a shell is the flat panel in which the curvatures are zero (or infinite radius of curvatures). It is true that the curved panels are much stronger and stiffer due to their continuity in geometry. In general, the shell panels are classified according to their curvatures rather than load bearing capabilities (Qatu, 2004). The shallow shell panels are the shells that have a small curvature, with a rise not greater than the one-fifth of the smallest side span of the shell panel. It is also worthy to mention that, the smallest radius of curvature must be not less than the twice of the largest side span for the extreme shallow shell panel case (Qatu, 2004). The shell panels can be categorised based on their curvatures such as spherical (both the curvatures are identical with positive Gaussian curvature), cylindrical (zero Gaussian curvature with a constant curvature in single direction), hyperbolic (negative Gaussian curvature), elliptical (positive Gaussian curvature), and conical (zero Gaussian curvature with a linearly variable curvature in single direction) panels. The shell panels with positive Gaussian curvature (spherical, elliptical) are referred as synclastic type shells whereas shell panels with negative Gaussian curvature (hyperbolic) are of the anticlastic type.

The shell panels are designed to perform under the combined loading condition including the high pressure and elevated thermal field (Shen, 2009a). This leads to the structural failure, mainly due to combined or individual effect of the excessive deformation, vibration and/or buckling of the structural component. In particular, the FGM structures need to be modelled accurately for the prediction of deformation behaviour under the hostile environment. It is also true that the FGMs are relatively expensive because of their manufacturing complexity and thus most studies have been limited to the computational analysis rather an experiment. This will help at very fast hand to determine the potential behaviour of this class of material before the final product. In this regard, various 2D and 3D models have been proposed by the researcher for the analysis of the FGM panel structures (Reddy, 2004b; Shen, 2009a; Na and Kim, 2006a, 2006b, 200c). Though the 3D elasticity theory is more precise, but it is limited due to its high computational cost and complexity in implementation including various

loading. This lacuna of 3D elasticity theory is overcome by the equivalent single-layer (ESL) theory which is derived from the 3D elasticity theory by reducing a 3D problem to 2D problem. In past, various ESL theories have been proposed for the analysis purpose of the shear deformable FG panels namely, classical laminated plate theory (CLPT), first-order shear deformation theory (FSDT) and higher-order shear deformation theory (HSDT) as well. The CLPT is based on the Kirchhoff's hypothesis, i.e., the straightness, the normality and the inextensibility of the transverse normal. This theory doesn't account the transverse shear terms and applicable to only thin plates. In continuation to that the FSDT has been developed to overcome the lacuna of the earlier, i.e., it holds all the assumptions of the CLPT except the normality condition and requires shear correction factor. It is evident from the previously reported studies that the HSDT mid-plane kinematic model gives a more accurate approximation of the transverse shear stresses and strains without any shear correction factor with fewer assumptions.

It is well known that the deflection of any structure varies linearly within a certain load limit and beyond that the behaviour becomes nonlinear. Therefore, it is essential to have a complete understanding of the nonlinear behaviour of the FG structure. In general, the nonlinearity is classified broadly in two ways, i.e., material and geometrical nonlinearity. The material nonlinearity occurs when the stress-strain relationship is no longer linear. On the other hand, the geometrical nonlinear problem relates to the strain-displacement relationship and it is no longer hold the linear behaviour. In order to address the geometrical nonlinearity of any structural engineering problem, two different strain-displacement kinematics are commonly used namely, Green-Lagrange strain (small strain and large rotation) and von-Karman strain (small strain and moderate rotation). The first kinematics (Green-Lagrange type) defines the most general type of geometrical nonlinearity whereas the latter one (von-Karman) is the reduced form of Green-Lagrange type. In general, the higher order terms of displacement gradients are neglected (Reddy, 2004a) to avoid the mathematical complexities. Therefore, the structural responses evaluated under the combined loading condition including the severe environmental effect needs more care during mathematical formulation for the realistic analysis and it may be achieved through Green-Lagrange strain terms.

Initially, the FGM structures are developed mainly for the space related structural application to overcome the shortcomings of the laminated structure under elevated thermal environment. Hence, the FGM structure needs very critical attention for the issues related to undesirable vibration under such complex environment without hampering the structural integrity. It is also true that these structures are very often exposed to the large amplitude vibration under the elevated thermal environment which in turn distorted the geometry of the structure. Due to this, the linear strain-displacement model is not enough to predict the responses and successively demand nonlinear strain-displacement field that can capture the true structural responses for the better design and safety.

In continuation of the above, it is also worthy to mention that the shell panels have significantly higher membrane stiffness than that of the bending stiffness, and, therefore, a shell panel is capable of absorbing a larger amount of membrane strain energy without excessive deformation. If the shell is loaded in such a way that most of its strain energy is in the form of membrane compression, and if there is a way that this stored-up membrane energy can be converted into the bending energy, the shell may fail dramatically in a process called “buckling”. It is also known that the buckling doesn’t mean the ultimate failure of the structural components and they are still capable of carrying extra amount of load beyond the buckling point without failure, i.e., known as post-buckling strength. It is also important to mention that the geometric strain associated with the buckling phenomenon is nonlinear in nature. Hence, to predict the buckling and the post-buckling strengths of FG shell panels, the mathematical model has to be sufficient to incorporate the geometric alteration due to the in-plane edge compression and elevated thermal load. The buckling can occur in two ways in the structural member, the first is the bifurcation buckling and the second is limit-point buckling. The bifurcation buckling is a form instability in which there is a sudden change of shape, of the structure due to the axial compressive/ tensile load. However, in the limit point buckling there is no sudden change of shape but it deviates from the primary equilibrium path after reaching the critical load i.e., known as “snap through”. The temperature increase in the structural components due to the elevated thermal environment and the constrained

thermal expansions induce buckling in the structural member and this in turn degrades the final performance.

Based on the above-discussed points, it is realised that there is a strong need of a generalised mathematical model which can predict the structural responses (vibration, bending and buckling) of the FG shell panel, precisely under the combined thermo-mechanical loading. In addition to the above, it is also necessary that the model should be capable of considering the geometric nonlinearity and the corrugated material properties under elevated thermal environment. To address the same, majority of research of FG shell panels have been focused on the theoretical analysis by involving analytical and/or numerical methods. It is true that the closed-form solution provides the exact responses of the structure, but these are limited to the simple problems only. Therefore, to solve the complex problems, various approximate techniques such as finite difference method, finite element method (FEM), mesh-free method, etc. have been utilised in past to evaluate the desired responses by incorporating the real-life situations. Out of all approximated analysis, the FEM has been dominated the engineering computations since its invention and also expanded to a variety of engineering fields. In this regard, a general nonlinear mathematical model is proposed to be developed based on the HSDT mid-plane kinematics and Green-Lagrange geometrical nonlinearity considering the temperature dependent material properties of the FGM constituent through the micromechanics approach. The present mathematical model has also included all the nonlinear higher order terms to capture the exact flexure of the FGM structure. The design and analysis of FG flat/curved panel structures based upon all such important considerations would certainly be more reliable in any real life applications.

1.2 Motivation of the Present Work

The FGM structures were conceptualised for thermal shielding applications without compromising the mechanical strength and fracture toughness of the structure. The continuous gradation of this kind of material relaxes the de-lamination and inter-laminar stresses which are common in the layered structures. This makes FGM structures be the pioneering area of research interest, especially in aerospace sectors, from past few years. It is due to the excellent amalgamation of the thermal and the mechanical

properties and the tailor-made properties in accordance with the structural requirements. During the service life, these structures are usually subjected to in-plane load and exposed to the acute thermal environment. This causes the catastrophic failure of the structure or structural component due to the individually or combined effect of excessive deflection, vibration and buckling. Based on the design requirements, curved shell panels are largely being used as structural components in various engineering sectors. The use of curved panel instead of flat one offers an extra amount of strength and the stability to the structure, along with the better aesthetics and/or ergonomics which fascinate a large group of researchers to investigate the structural responses of shell panels. Therefore, a thorough behavioural study of the structure made up of FGM has to be examined under the combined loading conditions. In addition to that, the study should also examine the effect of the temperature-dependent (TD) and the temperature independent (TID) material properties on the final responses.

As discussed earlier, the typical FGM structures are inhomogenous in nature which is achieved by grading continuously the two distinguished material phases in the thickness direction. The fabrication of this particular material with appropriate grading is very hard to achieve and still challenging to the manufacturers which increase the material processing and fabrication cost. Due to this, the experimental analysis of the FGM shell panel is not only expensive but also difficult to execute in complex environmental conditions. Hence, to investigate the structural responses, the numerical approaches can be implemented especially when the material, the geometry and the loading types are complex in nature. Therefore, a general mathematical model has to be developed which can capture the true flexural response of the FGM shell panel under unlike loading conditions.

It is evident from the exhaustive literature review that most of the previous studies focused on the linear/nonlinear bending, linear/nonlinear vibration and buckling/post-buckling behaviour of the FG flat panel under mechanical and/or thermal loading conditions. However, no work have been reported yet on the nonlinear flexural, the nonlinear vibration and the post-buckling behaviour of the temperature-dependent (TD) FG single/doubly curved shell panel in the framework of the HSDT mid-plane kinematics and Green-Lagrange geometrical nonlinearity under combined loading condition.

1.3 Objectives and Scope of the Present Work

The objective of the present work is to develop a general nonlinear mathematical model for the FG doubly-curved shallow shell panel by considering the temperature effect through-the-thickness to compute the linear and nonlinear structural responses. In order to achieve this, the geometrical nonlinearity is introduced through Green-Lagrange strain terms in the framework of the HSDT mid-plane kinematics. For the sake of true structural response, all the nonlinear higher-order terms are included in the proposed mathematical formulation. In this study, the effective material properties of the FGM are evaluated using Voigt's micromechanical model via power-law distribution and the volume fractions of each constituent are the function of position and the temperature as well. Further, the linear and nonlinear responses are computed numerically by discretising the domain through the isoparametric FEM approach in conjunction with the suitable iterative method. The point-wise descriptions of the scope of the present study are discussed below:

- Linear and nonlinear flexural behaviour of the FG shell panels of different geometries (spherical, cylindrical, hyperbolic and elliptical) under uniformly distributed transverse load is analysed using the proposed nonlinear model.

- Further, the linear and nonlinear flexural behaviour of the FG shell panels of all different geometries (spherical, cylindrical, hyperbolic and elliptical) are analysed by taking the TD and TID material properties under the combined thermomechanical load.

- The nonlinear model is extended to analyse the linear and nonlinear free vibration behaviour of the FG single/doubly (spherical, cylindrical, hyperbolic and elliptical) curved shell panels.

- It is then used to compute, the linear and nonlinear free vibration behaviour of the FG shell panels (spherical, cylindrical, hyperbolic and elliptical) including the TD and the TID material properties of the FGM constituent.

- ❖ Now, the present nonlinear model is utilised to compute the buckling and the post-buckling behaviour of the FG (spherical, cylindrical, hyperbolic and elliptical) shell panels by incorporating both the TD and the TID material properties under thermal environment.

- ❖ In continuation to that, the buckling and the post-buckling behaviour of the FG curved (spherical, cylindrical, hyperbolic and elliptical) panels under in-plane mechanical loading is also investigated by considering the presently developed nonlinear model.

- ❖ Finally, the buckling and the post-buckling behaviour of the TD-FG curved (spherical, cylindrical, hyperbolic and elliptical) panels are also investigated under combined thermomechanical loading.

A wide variety of numerical examples of the FG shell panels is investigated further for each individual case as discussed above using the developed nonlinear numerical model. The convergence behaviour of the present numerical results with mesh refinement is tested for each category of the problem. In order to assess the accuracy and applicability of the proposed nonlinear model, the present results are also compared with available published analytical and numerical solutions (FEM and meshless). In addition, a good volume of new results is also presented for each type of shell geometries with and without TD material properties and the combined loading conditions for the future references in this field of study.

1.4 Significance of the Present Model

The present nonlinear finite element formulation leads to solving the problems related to modern engineering sectors such as aerospace, automobile, defense, biomedical, and energy. In particular, the model is capable of solving problems of different kind of geometries (flat, spherical, cylindrical, hyperbolic and elliptical) associated with the structures like spacecraft (cylindrical body), rocket nozzle (*TiAl-SiC*), defense (bullet proof jackets which are shallow shell structures), automobile (engine cylinder liners, *Al-SiC*) and heat exchanger tubes (cylinder) and many more can be seen

in Udupa et al. (2014). In general, all different kind of thick and thin structural components are exposed to combined thermal (600-1000K) and mechanical load and the material properties are also affected due to the same. Based on the earlier discussion, the present model is so generic that it capable of including the geometrical distortion (nonlinearity/ small strain and large deformation) and degraded material properties (TD and TID) as occur in the real-life situations. Finally, it is believed that the present nonlinear finite element model has the potential to compute the structural responses with ease.

1.5 Organisation of the Thesis

In this chapter, the overview and the motivation of the present work are discussed and consequently the objectives and scope of the present thesis are outlined. The other contributions of the thesis are structured in the following manner.

The systematic investigations of the previous work related to the scope of the present area of interest are furnished in Chapter 2. This chapter is broadly divided into three major sections, the first section related to the review on the linear/nonlinear bending analysis, the second is related to the linear/nonlinear vibration analysis, and the third section discussed the buckling and the post-buckling behaviour of the FGM flat/curved shell panels with and without thermal field. Based on this organized literature review, the state of the art of the present problem and the knowledge gap are also outlined.

In Chapter 3, a general nonlinear mathematical model for the FGM doubly-curved shell panels is proposed and developed for the investigation of the linear/nonlinear flexural behaviour, vibration and the buckling and the post-buckling responses under the combined loading condition. The model has been developed by considering Green-Lagrange type of geometrical nonlinearity in the framework of the HSDT kinematics including the temperature-dependent material properties of the FGM constituents. In order to achieve the same, the kinematic field, the constitutive relations, the finite element formulations, and the solution techniques are provided in this chapter. In addition, the detailed regarding the computational implementation of the presently developed mathematical model is also discussed in details.

Chapter 4 presents the linear and the nonlinear flexural behaviour of the FG shell panels under thermal and/or mechanical loading. A comprehensive parametric study of different shell geometries (spherical, cylindrical, hyperbolic and elliptical) are executed and discussed for various geometrical and material parameters (Kar and Panda, 2015a; 2015b). Subsequently, the outcomes are summarised in the conclusion section.

Chapter 5 presents the linear and the nonlinear free vibration responses of the FG shell panels with and without the elevated thermal field. Numerous examples are computed for different shell geometries (spherical, cylindrical, hyperbolic and elliptical) in the results and discussion section and explained in detailed (Kar and Panda, 2014; 2015c). Base on the results, the concluding remarks are also outlined.

Chapter 6 presents the buckling and the post-buckling responses of FG shell panels under mechanical and/or thermal loading conditions. In addition to that, the effect of different parameter (geometrical and material) on the buckling and the post-buckling responses are computed using the developed nonlinear model for different shell geometries are discussed in detail.

In Chapter 7, the comprehensive concluding remarks are outlined followed by the future scope of the present work are discussed based on the present analysis.

In order to achieve the objective and scope of the present work discussed above in this chapter, there is a need to know the state of the art of the problem for that a detailed review of earlier research in the same field have been discussed thoroughly in the next chapter.

The following papers are prepared based on the work presented in the thesis.

1. Kar V R, Panda S K (2014). Nonlinear free vibration of functionally graded doubly curved shear deformable panels using finite element method, *Journal of Vibration and Control,* DOI: 10.1177/1077546314545102.
2. Kar V R, Panda S K (2015). Large deformation bending analysis of functionally graded spherical shell using FEM, *Structural Engineering and Mechanics* 53(4):661-679.

3. Kar V R, Panda S K (2015). Nonlinear flexural vibration of shear deformable functionally graded spherical shell panel, *Steel and Composite Structures*, 18(3):693-709.
4. Kar V R, Panda S K (2015). Thermoelastic analysis of functionally graded doubly curved shell panels using nonlinear finite element method, *Composite Structures*, 129: 202-212.
5. Kar V R, Panda S K (2015). Free vibration responses of temperature dependent functionally graded doubly curved panels under thermal environment, *Latin American Journal of Solids & Structures*, 12(11):2006-2024.
6. Kar V R, Panda S K, Nonlinear thermomechanical deformation behaviour of P-FGM spherical shallow shell panel, *Chinese Journal of Aeronautics*, DOI:10.1016/j.cja.2015.12.007.
7. Kar V R, Panda S K, Nonlinear thermo-mechanical behaviour of FGM cylindrical/hyperbolic/elliptical shell panel with TD and TID properties. *Journal of Pressure Vessel Technology - ASME* (Revised).
8. Kar V R, Panda S K, Geometrical nonlinear free vibration analysis of FGM spherical panel under nonlinear thermal loading with TD and TID properties. *Journal of Thermal Stresses* (Revised).
9. Kar V R, Panda S K, Geometrical nonlinear free vibration behaviour of functionally graded doubly curved panel under non-uniform thermal field. *Computational and Nonlinear Dynamics - ASME,* (Under review).
10. Kar V R, Panda S K, Thermal buckling of shear deformable functionally graded doubly curved shell panel with TD and TID properties. *Latin American Journal of Solids and Structures* (Under review).
11. Kar V R, Panda S K, Nonlinear free vibration behaviour of temperature-dependent functionally graded spherical shallow shell panel under uniform/linear temperature distribution. *Mechanics of Advanced Materials & Structures* (Communicated).
12. Kar V R, Panda S K, Nonlinear free vibration behaviour of shear deformable functionally graded doubly curved panel uniform and linear thermal field. *International Journal of Pressure Vessel & Piping* (Communicated).

13. Kar V R, Panda S K, Thermal post-buckling of FGM spherical shell panel under uniform, linear and nonlinear temperature fields. (Under preparation).
14. Kar V R, Panda S K, Post-buckling behaviour of shear deformable FGM spherical shallow shell panel under in-plane loading. (Under preparation).
15. Kar V R, Panda S K, Post-buckling behaviour of temperature-dependent FGM single/doubly curved panel under thermal environment. (Under preparation).
16. Kar V R, Panda S K, Post-buckling behaviour of FGM single/doubly curved panel under edge compression. (Under preparation).
17. Kar V R, Panda S K (2015), Effect of volume fraction on the nonlinear flexural behaviour of shear deformable functionally graded plate, 5th National Conference on Processing and Characterization of Materials (NCPCM 2015), NIT Rourkela, India. Dec 12-13.
18. Kar V R, Panda S K (2014), Thermal buckling of temperature dependent functionally graded cylindrical panel, 5th International & 26th All India Manufacturing Technology, Design and Research Conference (AIMTDR 2014) IIT Guwahati, India, Dec 12-14.
19. Kar V R, Panda S K (2014), Effect of temperature on stability behaviour of functionally graded spherical panel, 4th National Conference on Processing and Characterization of Materials (NCPCM 2014), NIT Rourkela, India. Dec 5-6. (*Scopus Indexed*: IOP Conference Series: Materials Science and Engineering 75 (2015) 012014 doi:10.1088/1757-899X/75/1/012014).
20. Kar V R, Panda S K (2014), Bending responses of functionally graded cylindrical panel, International Conference on Emerging Materials and Processes (ICEMP 2014), CSIR-IMMT, Bhubaneswar, India. Feb 26-28.
21. Kar V R, Panda S K (2014), Nonlinear bending responses of functionally graded cylindrical panels, International Conference on Functional Materials (ICFM 2014) IIT Kharagpur, India. Feb 5 -7.
22. Kar V R, Panda S K (2013), Bending behaviour of functionally graded spherical shell panels, 2nd KIIT International Symposium on Advances in Automotive Technology (2nd KIIT SAAT-2013), KIIT, Bhubaneswar, India. Dec 20-21.

23. Kar V R, Panda S K (2013), Thermal Stability Analysis of Functionally Graded Panels, International Conference on Structural Engineering and Mechanics (ICSEM 2013) NIT-Rourkela, India. Dec 20-22.
24. Kar V R, R K Singh, Panda S K (2013). Effect of gradation on bending behaviour of functionally graded spherical panels, 3th National Conference on Processing and Characterization of Materials (NCPCM 2013), NIT Rourkela, India. Dec 6-7.
25. Kar V R, Panda S K (2013), Free Vibration Responses of Functionally Graded Spherical Shell Panels using Finite Element Method, ASME 2013 Gas Turbine India Conference (ASME GTINDIA2013), CSIR-NAL, Bangalore, India. Dec 5-6. (*Scopus Indexed*: doi: 10.1115/GTINDIA20133693).
26. Kar V R, Panda S K (2013). Free vibration responses of functionally graded cylindrical shell panels using finite element method, All India Seminar on Recent Advances in Mechanical Engineering, Institute of Engineers (India), Bhubaneswar, India. March 16-17.
27. Kar V R, Panda S K (2013), Scope and study of functionally graded plate structures in automotives, 1st KIIT International Symposium on Advances in Automotive Technology (1st KIIT SAAT-2013), KIIT, Bhubaneswar, India. Jan 11-12.

CHAPTER 2

LITERATURE REVIEW

2.1 Introduction

The concept of FGM structure and their application in today's modern engineering have already been discussed in the previous chapter. Due to the applicability and effectiveness of the FG structures for the thermal protection system, in particular, attracted many researchers to study the same for last two decades. Every now and then the effort has been made by the researcher and scientist to come up with new/modified mathematical model and/or solution steps to overcome the drawbacks of former research. Many researchers have already studied the linear and nonlinear FG flat/curved panel structural responses considering with and without temperature dependent material properties in the framework of the different kinematic model using the shear deformation and classical theories. Subsequently, the studies are also modified time to time in past for more accurate prediction and to approach towards the real-life situations. In this regard, various researchers have published some detailed review articles on the FG structural responses (vibration/bending/stability) and different solution techniques (Birman and Byrd, 2007; Qatu et al., 2010; Liew et al., 2011; Jha et al., 2013; Alijani and Amabili, 2014; Swaminathan et al., 2015; Thai and Kim, 2015). In continuation that, detailed review of the individual cases have also been conducted and classified into three major categories on the available literature namely, the linear/nonlinear flexural behaviour, the

linear/nonlinear vibration analysis and the buckling/post-buckling strength of the FG flat/curved panel structures with and without considering the thermal effect. In order to maintain the conciseness, a selective review of the available past and/or current published literature is discussed in the following subsections.

2.2 Linear and Nonlinear Flexural Analysis of FG Shell Panel

In design and analysis of any structure, the flexural behaviour is one of the typical study is associated to measure the load bearing capability or the deformation behaviour of the structural component. The study becomes essential if the structure is working under large deformation regime. This section emphasises on the flexural analysis of FG flat/curved structures under mechanical and/or thermal loading with and without considering the effect of geometrical nonlinearity. In this regard, many researchers have already examined the deformation behaviour of the FGM type structure under various loading and/or environmental conditions using different analytical and/or numerical techniques. In the following subsections, the studies are majorly discussed on two different classes of problems, i.e., the flexural responses of the FG flat/curved panel under the mechanical load with and without considering the effect of temperature.

2.2.1 Flexural Analysis under Mechanical Load

Several studies have already completed on the deformation analysis of the FG flat/curved panel structures using various kinematic models and analytical/numerical approaches. In this section, some of the recent contributions on the flexural analysis of the FG flat/curved panel structures under the influence of the mechanical load are only discussed in the following lines.

Yang and Shen (2003a) employed a perturbation technique to compute the large deflection responses and the post-buckling responses of the FG plates under in-plane and transverse loads using the one-dimensional (1D) differential quadrature approximations in conjunction with Galerkin procedure. Kashtalyan (2004) proposed 3D elasticity benchmark solutions for the simply supported FG flat panel structure under transverse loading. GhannadPour and Alinia (2006 and 2009) reported the nonlinear bending

behaviour of the power-law and the exponential type FG plates under uniform pressure load using the CLPT mid-plane kinematics and von-Karman nonlinearity. Ovesy and Ghannadpour (2007) investigated the large deflection responses of simply-supported FG plate under normal pressure loading using the finite strip method. Navazi and Haddadpour (2008) examined the nonlinear bending behaviour of the FG plate using the FSDT kinematic and von-Karman type nonlinearity. Huang et al. (2008) developed the exact solutions for the thick FG plates resting on Winkler–Pasternak elastic foundations using the 3D elasticity method. Xu and Zhou (2009) employed 3D elasticity method to analyse the deformation behaviour of the simply-supported FG flat panel under the transverse load. Khabbaz et al. (2009) predicted the large deflection behaviour of the FG flat panel using the energy method based on the first and the third-order shear deformation theories. Santos et al. (2009) investigated the bending and vibration behaviour of FG cylindrical shell panel using semi-analytical axisymmetric finite element model based on the 3D linear elastic theory. Tornabene and Reddy (2013) employed the generalized differential quadrature (GDQ) method to examine the static behaviour of the layered and graded curved shells and panels resting on elastic foundations using the FSDT kinematics. Talha and Singh (2010) reported finite element solutions of vibration and static responses of the FG plates using the HSDT mid-plane kinematics. Kiani et al. (2012) computed the static, dynamic and the free vibration responses of the doubly-curved FG shell panel resting on elastic foundation analytically using the FSDT and modified Sander's shell kinematics. Oktem et al. (2012) reported the bending responses of the FG flat/curved panels using the modified higher-order theory. Xiang and Kang (2013) proposed the n^{th} order of shear deformation theory to compute the bending behaviour of simply-supported FG plate under sinusoidal load using the mesh-less global collocation method. Thai and Choi (2013) investigated the bending and the vibration behaviour of the FG plate using the simple FSDT mid-plane kinematics. Thai and Kim (2013) developed a new HSDT model to analyse the free vibration and the bending responses of the FG plates. Mojdehi et al. (2011) examined the static and the dynamic responses of the thick FG plates using the meshless local Petrov–Galerkin method.

The above review reveals that the numerous attempts have already been made in past to compute the linear and the nonlinear flexural behaviour of the FG flat/curved

panel structures. However, it is interesting to note that most of the studies are based on the FSDT/HSDT kinematics by considering the geometrical nonlinearity in the von-Karman sense. In addition, some of the available studies of FG shell panel including the thermal effect are also discussed in the following subsection.

2.2.2 Flexural Analysis under Thermomechanical Load

In general, the FGM structures are designed to work under high compressive loading including the critical thermal environment. Therefore, it is necessary to examine the exact deformation behaviour of the FGM structures under the elevated thermal load as well. Many researchers have also investigated the flexural responses of the FG flat/curved shell structures under the combined action of loading by considering the temperature dependent material properties of the FGM constituent.

Praveen and Reddy (1998) investigated the static and dynamic behaviour of FG plates under thermomechanical load using the FSDT mid-plane kinematics and von-Karman type nonlinearity. Reddy and Cheng (2001) provided 3D thermoelasticity solutions to the deformation behaviour of simply supported rectangular FG flat panel using an asymptotic method. Further, the large deflection behaviour of the flat and shallow FG shell panels under thermomechanical load is analysed by Woo and Meguid (2001) using the CLPT and von-Karman type nonlinear kinematics. Shen (2002a) reported analytical solutions of the nonlinear bending responses of the FG plate under thermomechanical loading by using the HSDT mid-plane kinematics and von-Karman type nonlinear strain-displacement relation. Yang and Shen (2003b) examined the nonlinear bending behaviour of the FG flat panel under thermomechanical loading using the perturbation technique in conjunction with 1-D differential quadrature approximation and Galerkin procedure. Later, the nonlinear bending behaviour of FG plate is examined by Na and Kim (2006a) using the 3D finite element method. In this study, Green-Lagrange type strain displacement relation is employed to account the geometric nonlinearity under uniform pressure and thermal load without considering all the nonlinear higher-order terms in the mathematical model. Shen (2007a) analysed nonlinear bending behaviour of the simply-supported smart FG plate bonded with piezoelectric actuators under thermoelectrical

loading. Zhao and Liew (2009) reported nonlinear flexural responses of FG cylindrical panel subjected to thermomechanical load using the element-free kp-Ritz method in conjunction with modified Sander's shell theory. Bayat et al. (2009) investigated the thermoelastic behaviour of temperature-dependent FG rotating discs for uniform and variable thickness using the semi-analytical approach. Shen and Wang (2010) examined the nonlinear bending responses of the simply-supported FG plate resting on Pasternak-type elastic foundation under thermomechanical load using the HSDT mid-plane displacement and von-Karman nonlinear strains. Desai and Kant (2012) analysed the bending responses FG cylinders of the finite length under thermal environment using a simple analytical cum numerical approach for the accurate prediction of the responses. Duc et al. (2014) investigated the nonlinear axisymmetric response of the FG spherical shell panel under uniform external pressure in conjunction with the temperature load using Bubnov–Galerkin method and the stress functions based on the classical shell theory. Phung-Van et al. (2014) proposed a cell-based smoothed three-node plate element (CS-MIN3) to examine the nonlinear behaviour of the FG plate under thermomechanical load. They have adopted a C^0 type HSDT kinematics and von-Karman nonlinear strains for the mathematical formulation. Zhang (2014) examined the nonlinear bending behaviour of the temperature dependent FG plate resting on the two-parameter elastic foundation under thermomechanical loading for different support conditions. In this analysis, the authors have utilised the physical neutral surface based on the HSDT model in conjunction with von-Karman strain terms and solved using Ritz method.

It is clearly evident from the above review that the most of the studies have been performed for the FG flat panels only and very few studies are attempted for the single or doubly curved structures. It is also observed that the nonlinear responses are computed for the large deformation cases using von-Karman geometrical nonlinearity kinematics and it accounts for the small strain and moderate rotations only. Now in the further subsections, various studies of the FG flat/curved panel structures are discussed for the vibration and stability cases with and without thermal load and temperature dependent material properties.

2.3 Linear and Nonlinear Free Vibration Behaviour of FG Shell Panel

In this section, the linear and nonlinear free vibration behaviour of the FG flat/curved shell panel structure under ambient and the elevated thermal environment with and without temperature-dependent material properties of the individual material constituent are discussed. In this regard, various 2D or 3D analytical and numerical methods are implemented based on the different kinematic and geometrical nonlinear models. In order to maintain the brevity, the review has been discussed into two broad categories, i.e., with and without temperature effect.

2.3.1 Free Vibration Analysis without Considering the Thermal Effect

Numerous previous investigations have been reported on the linear/nonlinear free vibration responses of the FG flat/curved shell structures under ambient conditions. Few of the recent contributions to the free vibration analysis are mentioned and discussed in the following lines.

Patel et al. (2005) examined the free vibration behaviour of the FG cylindrical shell panels using higher-order kinematics approximation through the thickness. Uymaz and Aydogdu (2007) studied the vibration responses of FG plate for various support conditions using small strain linear elasticity theory. Pradyumna and Bandyopadhyay (2008) studied the free vibration behaviour of the curved FG shell panels using the higher-order formulation in conjunction with Sanders' approximation. Santos et al. (2009) reported the free vibration responses of the FG cylindrical shell panel based on the 3D linear elastic theory using a semi-analytical axisymmetric finite element model. Viola and Tornabene (2009) proposed a three-parameter power-law based FG shell to study the free vibration responses of moderately thick FG parabolic panels of revolution using the FSDT kinematic and GDQ method. The same authors (Tornabene and Viola, 2009) also developed a four-parameter power-law FG shell structure in conjunction with their previous study.

Tornabene et al. (2009) examined the free vibration behaviour of moderately thick FG cylindrical, conical shell panel and the annular plate based on the two different

power-law distributions using the FSDT kinematics and GDQ method. Further, the work has been extended using the four-parameter power-law distribution grading by Tornabene (2009). Atmane et al. (2010) examined the free vibration behaviour of the simply-supported FG plate resting on Winkler–Pasternak elastic foundation using a new HSDT kinematic model. Hosseini-Hashemi et al. (2010) solved analytically the vibration responses of the moderately thick FG plate resting on elastic foundation using the FSDT kinematics with a modified shear correction factor. Pradyumna et al. (2010) developed higher-order based finite element model to solve the nonlinear transient behaviour of the FG doubly curved shell panel using New-mark technique. Talha and Singh (2011) employed the HSDT mid-plane kinematics and Green–Lagrange nonlinear strains to investigate the nonlinear vibration behaviour of the FG plate including all the nonlinear higher-order terms in the mathematical model. Rahimia et al. (2011) studied the vibration responses of the FG cylindrical shell panel with intermediate ring supports using Sanders' thin shell theory. Alijani et al. (2011a) investigated the nonlinear forced vibration behaviour of the simply-supported FG curved shallow shells using Donnell's type nonlinear shallow shell theory. Baferani et al. (2012) solved analytically the free vibration behaviour of the FG thin annular sector plates resting on the elastic foundation using Kirchhoff plate theory. Taj and Chakrabarti (2013) examined the dynamic responses of the FG skew shell using the finite element formulation based on Reddy's higher-order theory. Asemi et al. (2014) reported the static and the dynamic behaviour of the FG skew plate based on the 3D elasticity theory. Bich et al. (2014) utilised the FSDT and stress function to investigate the nonlinear dynamic and the free vibration behaviour of imperfect eccentrically stiffened FG thick shallow shells. Tornabene et al. (2014) presented the free vibration behaviour of the doubly-curved FG shell panel using the GDQ method. The responses are obtained using various higher-order ESL theories.

It is clear from the review that most of the vibration analysis are based on the either linear solution or the nonlinear analysis using von-Karman strains. It is also observed that the studies are limited to the flat panels. Further the linear and the nonlinear vibration behaviour of the FG shell panel under various temperature loads are summarised in the following subsection.

2.3.2 Free Vibration Analysis in Thermal Environment

In this section, the free vibration responses of the FGM structures under the thermal environment with and without temperature dependent material properties of each FG constituent is discussed in detailed. In this regard, the free vibration and dynamic responses of the FG cylindrical shell panel under thermal environment are investigated by Yang and Shen (2003c) using the semi-analytical approach based on Reddy's HSDT kinematics. Huang and Shen (2004) reported the nonlinear vibration and dynamic responses of the FG plate under thermal environment using the HSDT mid-plane kinematics and von-Karman type geometric nonlinear strain equations. Sundararajan et al. (2005) employed the FSDT mid-plane kinematics and von-Karman's nonlinearity to compute the nonlinear vibration responses of the FG plate under thermal environment. Park and Kim (2006) investigated the free vibration and post-buckling responses of FG plate under thermal environment using the FSDT kinematics and the von-Karman nonlinearity. Haddadpour et al. (2007) investigated the frequency responses of the simply-supported FG cylindrical shell panel under thermal environment using Love's shell theory and Galerkin's approach. Farid et al. (2010) investigated the free vibration behaviour of the simply-supported FG curved panel resting on the elastic foundation under thermal environment using 3D elasticity formulation. Pradyumna and Bandyopadhyay (2010) reported the vibration and buckling behaviour of the FG curved panels including the thermal effect. Alijani et al., (2011b) analysed the nonlinear vibration responses of the FG shell panel using the HSDT kinematics including the temperature effect. Valizadeh et al. (2013) employed non-uniform rational B-spline based Bubnov-Galerkin iso-geometric FEM to examine the static and dynamic behaviour of FG plates under thermal environment using the FSDT mid-plane kinematics. Pradyumna and Nanda (2013) examined the nonlinear transient behaviour of the FG doubly-curved shell panels with geometrical imperfection under the thermal environment using von-Karman type nonlinear strain terms in the framework of the FSDT kinematics. Shen and Wang (2014) reported large amplitude vibration behaviour of the FG cylindrical panel resting on the elastic foundation under thermal environment using Reddy's HSDT kinematics and von-Karman nonlinear strain-displacement relation. Zhu et al. (2014) performed the nonlinear thermomechanical analysis of FG plate using the local meshless method and

Kriging interpolation technique. Panigrahi and Pohit (2015) examined the nonlinear free vibration responses of cracked FG beams using Timoshenko beam theory and Ritz approximation.

It is obvious from the discussions that the most of the works have utilised the FSDT/HSDT mid-plane kinematic where the geometrical nonlinearity is introduced in von-Karman sense. Further, the buckling and the post-buckling behaviour of the FGM structures under the influence of the mechanical and/or thermal load has been discussed by considering the effect either individual or combined loading conditions in the following subsection.

2.4 Buckling and Post-Buckling Behaviour of FG Shell Panel

It is well known that buckling of any structure and/or structural component is attained due the influence of the in-plane loading (mechanical and/or thermal) conditions. Several studies have been reported in past to address the buckling and post-buckling behaviour of FG flat/curved shell panel structures under the axial compression and/or thermal load. In this regard, various shell/plate theories and solution techniques are adopted to perform the desired analysis and the details are discussed in the following subsection.

2.4.1 Mechanical Buckling and Post-Buckling Analysis

In this section, the studies on the buckling and the post-buckling responses of the FG flat/curved shell structures under the in-plane edge compression are discussed. Sofiyev (2003) developed a mathematical model for the analysis of the buckling behaviour of the FG cylindrical thin shell panel under external pressure and it varies with time as a power function. Sofiyev and Schnack (2004) investigated the stability behaviour of FG cylindrical shells under torsional loading where the load is varying as a linear function of the time. Sofiyev (2004) introduced the stability behaviour of the truncated FG conical shells under the external pressure varying as a power function of time by using Galerkin's method. Woo *et al.* (2005) reported the post-buckling behaviour of moderately thick FG flat and cylindrical panels under axial compression using the von-

Karman large deflections theory and the HSDT kinematics. Shen (2007b, 2007c) examined the post-buckling responses of FG flat and cylindrical shell panel under uniform temperature field using the HSDT mid-plane kinematics and the von-Karman-Donnell-type nonlinearity. Sofiyev (2007) studied the buckling behaviour of the truncated conical shells under the axial compressive load varying as a linear function of time. Darabi et al. (2008) investigated the nonlinear dynamic stability of the FG cylindrical shell under the periodic axial load using Galerkin procedure. Ebrahimi and Sepiani (2010) studied the effect of transverse shear and rotary inertia on the dynamic stability behaviour of the FG cylindrical shells under the combined static and periodic axial forces. Duc and Tung (2010a) utilised the Galerkin method to examine the post-buckling behaviour of the FG cylindrical shell panels with initial geometrical imperfection under the edge compression using the CLPT mid-plane kinematics and von-Karman–Donnell type geometrical nonlinearity. Thai and Choi (2012) investigated buckling behaviour of the FG plates for different support conditions using an efficient and simple refined theory.

It is evident from the available literature that most of the previous studies examined for the flat and single-curved shell panels. In the forthcoming section, the studies related to the buckling and the post-buckling responses under the combined mechanical and thermal loading are discussed.

2.4.2 Thermomechanical Buckling and Post-Buckling Analysis

A number of studies related to the linear and nonlinear stability analysis of FG flat/curved shell structures are reported in past. Javaheri and Eslami (2002b) derived the closed-form solution using the HSDT mid-plane kinematics to examine the buckling behaviour of the FG plate under four different temperature fields. Na and Kim (2004, 2006b) presented 3D exact solutions for the thermomechanical buckling behaviour of FG plate under uniform and non-uniform temperature fields. The same authors employed 3D FEM through an 18-noded solid element to examine the buckling and the post-buckling responses of the FG plate under uniform and non-uniform thermal fields (Na and Kim, 2006c). Yang et al. (2006a) reported the semi-analytical model based approach in

conjunction with differential quadrature method and Galerkin technique for the analysis of the post-buckling responses of the FG plate. The plate is under the influence of the axial compression and uniform temperature load and the model has been developed using the HSDT mid-plane kinematics and von-Karman nonlinearity. Wu et al. (2007) employed finite double Chebyshev polynomial approach to obtaining the thermomechanical post-buckling behaviour of the FG plate using the FSDT mid-plane kinematics and von-Karman nonlinear strain. Prakash et al. (2008) examined the post-buckling behaviour of the skew FG plate under thermal environment using the FSDT mid-plane kinematics and von-Karman nonlinear strain-displacement equations. Zhao et al. (2009) employed the element-free kp-Ritz method to examine the buckling responses of the FG plate under in-plane mechanical and thermal load using the FSDT mid-plane kinematics. Tung and Duc (2010) presented the buckling and the post-buckling behaviour of the geometrically imperfect FG plates under in-plane edge compression and thermal load using the CLPT and von-Karman type of nonlinear kinematics. The same authors (Duc and Tung, 2010b and 2011) extended the analysis for the shear deformable FG plates using the FSDT and the HSDT mid-plane kinematics with and without considering the temperature-dependent material properties. Lee et al. (2010) investigated the post-buckling behaviour of FG plates using the FSDT displacement field and von-Karman type nonlinear strain equations. The responses are obtained using an element-free kp-Ritz method under edge compression and temperature load. Sepahi et al. (2011) employed differential quadrature method to examine the thermal buckling and post-buckling responses of the FG annular plates using the FSDT kinematics and von-Karman nonlinear strain terms. Ghannadpour et al. (2012) analysed the buckling behaviour of the rectangular FG plates using a finite strip method under different thermal loadings (uniform, linear and nonlinear temperature rise) across the thickness. Valizadeh et al. (2013) examined the bending, vibration and buckling behaviour of FG plates under thermal using the non-uniform rational B-spline based Bubnov-Galerkin iso-geometric FEM and the FSDT mid-plane kinematics.

Huang and Han (2008, 2009a, 2009b, 2010a, 2010b, 2010c) used the Donnell shell theory to investigate the buckling/post-buckling behaviour of temperature dependent FG cylindrical shells with and without geometrical imperfections under

thermal/mechanical loading. Shen (2002b, 2003 and 2004) utilised the CLPT mid-plane displacement and von-Karman-Donnell-type nonlinear kinematics for the analysis of the FG thin shells with different loading conditions (pressure and axial loading) under thermal environment. Woo and Meguid (2003) proposed the analytical solution based on the mixed Fourier series to examine the post-buckling responses of FG flat and cylindrical shell panels under axial compression and thermal load using the CLPT mid-plane kinematics and von-Karman geometrical nonlinear strain terms. Shen and Noda (2005) examined the post-buckling responses of FG cylindrical shell of finite length subjected to combined axial and radial loads under thermal environment using the HSDT mid-plane and the von-Karman-Donnell-type nonlinear kinematic model. Wu et al. (2005) presented closed-form solution of the buckling responses of simply supported thin FG cylindrical shell under thermal loads based on the classical shell theory. Kadoli and Ganesan (2006) analysed thermal buckling and free vibration behaviour of clamped FG cylindrical panel with temperature-dependent material properties. Yang et al. (2006b) used the semi-analytical differential quadrature-Galerkin method to investigate the thermomechanical post-buckling behaviour of the FG cylindrical shell panel using the CLPT mid-plane kinematics and von-Karman–Donnell-type nonlinear strain. Bhangale et al. (2006) applied semi-analytical finite element method based on the FSDT mid-plane kinematics for the linear thermoelastic thermal buckling analysis of the FG truncated conical shells with different semi-vertex angles. Naj *et al.* (2008) studied the thermal and mechanical instability of FG truncated conical shells using the FSDT and Sanders nonlinear kinematics. Shen (2009a) presented the thermomechanical post-buckling behaviour the FG cylindrical shell panel resting on Pasternak elastic foundation using the HSDT mid-plane displacement and von-Karman–Donnell-type nonlinear strain terms. The same work has been extended under the internal pressure (Shen et al., 2010). The author (Shen, 2009b) also examined the post-buckling responses of the FG cylindrical shell by considering the torsional effect. Shahsiah et al. (2011) computed the equilibrium and stability equations for simply supported the FG deep spherical shells using the FSDT kinematics and Sanders kinematics relations. They have also analysed buckling of FG deep spherical shells for three different loading cases. Duc and Quan (2012) presented an analytical solution based on the Galerkin method for the buckling and post-buckling

responses of the thick FG doubly-curved shallow shell panels resting on elastic foundations under the thermal and thermomechanical loading conditions using CLPT mid-plane kinematics. Liew et al. (2012) utilised the element-free kp-Ritz method to investigate the post-buckling responses of the FG cylindrical shell panels under the thermal and in-plane edge compression using the FSDT in conjunction with the von-Karman geometrical nonlinearity. Lal et al. (2012) examined the post-buckling analysis of the FG plate under thermal and mechanical load with and without cut-outs. They formulated their model using the random material properties and utilised the HSDT and von-Karman nonlinear kinematics. Tung (2014) employed Galerkin method to study the nonlinear stability behaviour of FG circular flat and spherical shell panel resting on elastic foundations under uniform pressure and thermal field using the FSDT mid-plane kinematics.

It is noticeable from the past literature that most of the works are limited to the flat/single curved FG structures and utilised majorly the CLPT/FSDT mid-plane kinematic model and the von-Karman nonlinear strain-displacement relations. Based on the present review, a comprehensive knowledge gap is furnished in the later section for a better understanding of the present problem.

2.5 Observations

It is now clear from the above review that very few work have addressed the nonlinear flexural and vibration, and post-buckling responses of the FG single/doubly-curved shell panels under the elevated thermal field. Based on the available published literature and the subsequent discussions, the following points are drawn to mention the knowledge gap of the past contributions:

- The review confirms that most of the analyses are performed for the flat and singly-curved FG shell panels instead of doubly-curved shell panel.
- It is also observed from the previously reported literature that the geometrical nonlinearity is introduced using von-Karman type strain-displacement relation and

which is inadequate to capture the true structural responses under the large deformation regime.

- In the past studies indicate, the linear/nonlinear flexural and the free vibration and, the buckling/post-buckling analyses of the FG flat/curved shell panels are performed using the CLPT and/or FSDT type mid-plane kinematics. It is well known that, in the CLPT kinematic model, the transverse shear terms are ignored and limited to the thin panel structures. However, the FSDT kinematics can be used for the thin to moderately thick panels but requires shear correction factor.

- A more general mathematical model is needed to predict the realistic responses of FG curved shell panels which can be capable of dealing the individual and/or the combined loading cases with and without considering the temperature-dependent material properties.

- It is also noted that no study has been reported yet on the nonlinear analysis of the FG single/doubly curved shell panel under the uniform and non-uniform elevated thermal environment using the HSDT mid-plane kinematics and the geometrical nonlinearity in Green-Lagrange sense by considering the temperature-dependent material properties.

Finally, based on the above-identified points, a brief motive of the present work is outlined here for the sake of completeness. Based on the earlier discussion in the previous chapter, the present study aims to analyse the nonlinear flexural and free vibration, and the buckling and the post-buckling behaviour of the FG single/doubly curved shell panel under the combined loading effect. In this regard, a general nonlinear mathematical model of the FG curved shell panel is proposed to be developed using the HSDT mid-plane kinematics and Green-Lagrange nonlinear equations. In addition, to the above all the nonlinear higher-order terms and the temperature-dependent material properties are incorporated in the proposed mathematical model to achieve the general case. In order to obtain the desired responses under uniform and non-uniform loading case, a suitable nonlinear isoparametric FEM model utilised for the discretisation purpose. The desired nonlinear responses are computed numerically using the direct iterative method. In the

subsequent chapter, a general nonlinear mathematical formulation is proposed for the FG shell panels under thermomechanical loading.

CHAPTER 3

GENERAL MATHEMATICAL FORMULATION

3.1 Introduction

In general, structural components experience different loadings and environment conditions during their service life. The actual performance of the structural component continuously deteriorates over its lifespan which result in the failure of the structural component. Therefore, from the design and analysis aspects, the structural responses like frequency, deformation, critical load, etc. are very much essential for the structural sustainability under the severe environmental conditions. There are two ways to find the structural responses, viz. the laboratory experimentation and/or the numerical simulation. The present study focuses on the numerical analysis of the FGM structure which is microscopically inhomogeneous in nature. Due to their inhomogeneity in terms of grading between two distinguish materials (the metal and the ceramic), the prototype testing of such structural component are very much difficult to achieve under the uniform and non-uniform temperature fields. It is also true that the closed-form solutions are easy for the simple geometries, the material model and the support conditions, but it is difficult when the problem become complex by considering the combined situation. These complex problems can be solved easily by implementing the so-called numerical technique, i.e., FEM, with less mathematical complexity. The accuracy of structural response is maintained by inclusion of geometrical nonlinearity and the higher-order

terms in the kinematic model. The necessity and the knowledge gap regarding the present mathematical model and numerical analysis have already been discussed in the previous chapter.

In this chapter, a general mathematical formulation is proposed and developed for the FG curved shell panel in the framework of the HSDT kinematics using the nonlinear finite element steps. The proposed formulation is developed using some of the general and specific assumptions and stated in Section 3.2. Section 3.3 presents the evaluation step of the effective material properties of FG panel using Voigt's micromechanical model via power-law distribution. In the present analysis, the FGM constituents (metal and ceramic) are assumed to be temperature-dependent. Section 3.4 describes different types of the FG shell geometries in Cartesian co-ordinate system for the analysis purpose. In this study, a general doubly-curved shallow shell panel model has been developed and extended to achieve different shell configurations using necessary conditions. Section 3.5 presents the HSDT mid-plane kinematics used as displacement model for the FG curved shell panel. The geometrical nonlinearity is introduced through the strain-displacement relation using Green-Lagrange sense and presented in Section 3.6. In the present study, three different types of temperature distribution across the thickness direction of the shell panel are considered and presented in Section 3.7. The thermoelastic constitutive relations of the FG shell panel are presented in Section 3.8. The finite element formulation and the desired governing equation of the desired analysis are discussed in Section 3.9 and Section 3.10, respectively. The solution techniques are through the suitable finite element steps in Section 3.11. In the Section 3.12, various types of support conditions are mentioned for the analysis purpose. At last, this chapter is summarised in Section 3.13.

3.2 Basic Assumptions

The present general mathematical formulation is developed based on the following basic assumptions:

i. The basic geometric configuration of the problem considered here is a doubly curved shell panel on a rectangular plan form.

ii. Doubly-curved panel geometry is considered as a basic configuration so that depending on the values of curvature parameters, flat, spherical, cylindrical, hyperbolic and elliptical panel configuration can be considered.

iii. A 2D equivalent single layer theory is adopted for the modelling of 3D shell panel.

iv. The mid-plane of the shell panel is considered as the reference plane.

v. The transverse normal is assumed to be inextensible.

vi. The effect of transverse normal stress on the gross response of the shell panel is assumed to be negligible (plane stress condition).

vii. The FGM is assumed to be isotropic and inhomogeneous.

viii. The undamped system is assumed for the present analysis.

ix. The metal-rich and ceramic-rich phases are assumed to be at the bottom and the top surfaces of the FG shell panel, respectively.

x. The unidirectional gradation of FGM constituents is assumed, i.e., along the thickness direction only.

xi. The flexural behaviour of the FG shell panel is assumed to be within the elastic limit.

3.3 Effective Material Properties of FGM

FGMs are known to be inhomogeneous in nature, and the properties are varying gradually from the one surface to the other along with the thickness direction. The bottom of the panel is considered to be metal-rich and the top as ceramic-rich. The FGM constituents are temperature-dependent and can be expressed as (Reddy and Chin, 1998)

$$P_{c,m}(T) = P_0(P_{-1}T^{-1} + 1 + P_1T + P_2T^2 + P_3T^3) \qquad \ldots(3.1)$$

The effective material properties of FGM (P) can be evaluated by using Voigt's micromechanics model (Gibson et al., 1995) and expressed as

$$P(T,z) = P_c(T)V_c(z) + P_m(T)V_m(z) \qquad \ldots(3.2)$$

where, subscript '*c*' and '*m*' denotes the ceramic and the metal, respectively and *V(z)* is the volume fraction, follows the power-law distribution (Shen, 2009c) and expressed as

$$V_c(z)=\left(\frac{z}{h}+\frac{1}{2}\right)^n \quad \text{and} \quad V_m(z)=1-V_c(z)=1-\left(\frac{z}{h}+\frac{1}{2}\right)^n \qquad \ldots(3.3)$$

where, n ($0 \le n < \infty$) is the power-law index that characterizes the material variation profile to generate the infinite number of composition distributions in between the metal and the ceramic phase. In the above equation, z is any arbitrary point within the transverse direction whereas, h represents the total thickness of the assumed panel. The effect of the power-law index on the volume fractions of the ceramic and the metal along with the thickness direction is plotted in Figure 3.1. The effective FGM properties are obtained using the following equation as:

$$P(T,z)=\left\{P_c(T,z)-P_m(T,z)\right\}\left(\frac{z}{h}+\frac{1}{2}\right)^n+P_m(T,z) \qquad \ldots(3.4)$$

Eq. (3.4) can be expressed for different elastic and the thermal properties of the FGM such as Young's modulus (E), Poisson's ratio (υ), density (ρ), thermal expansion coefficient (α) and thermal conductivity (k). Here in this analysis, the mass density (ρ) and the thermal conductivity (k) are assumed to be temperature-independent and Poisson's ratio (v) is taken as constant throughout the thickness of the FG panel.

$$E(T,z)=\left\{E_c(T,z)-E_m(T,z)\right\}\left(\frac{z}{h}+\frac{1}{2}\right)^n+E_m(T,z) \qquad \ldots(3.5)$$

$$\alpha(T,z)=\left\{\alpha_c(T,z)-\alpha_m(T,z)\right\}\left(\frac{z}{h}+\frac{1}{2}\right)^n+\alpha_m(T,z) \qquad \ldots(3.6)$$

$$\rho(z)=\left\{\rho_c(z)-\rho_m(z)\right\}\left(\frac{z}{h}+\frac{1}{2}\right)^n+\rho_m(z) \qquad \ldots(3.7)$$

$$k(z)=\left\{k_c(z)-k_m(z)\right\}\left(\frac{z}{h}+\frac{1}{2}\right)^n+k_m(z) \qquad \ldots(3.8)$$

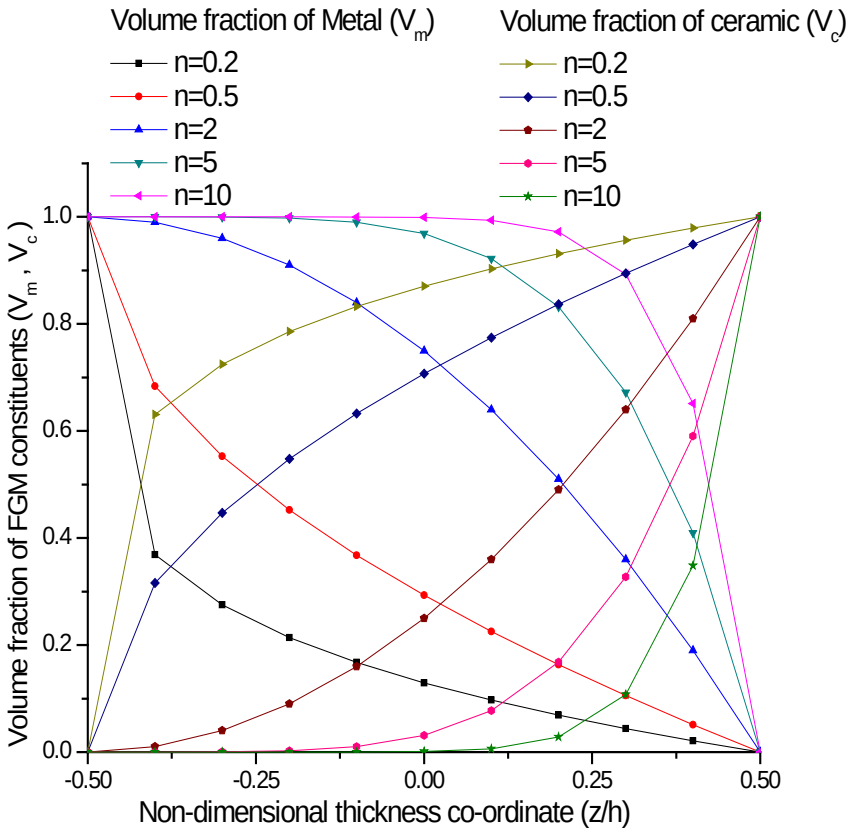

Figure 3.1 Variations of volume fractions of FGM constituents along with the non-dimensional thickness co-ordinate

3.4 Shell Description

A general doubly curved FG panel of uniform thickness '*h*' with a rectangular base of sides *a* and *b* is considered for the present analysis as shown in Figure 3.2. R_x and R_y are the principal radii of curvature of the shell panel along *x* and *y* directions, respectively. The principal radii of curvature of flat, cylindrical, spherical, hyperbolic paraboloid and ellipsoid panels can be represented as $R_x=R_y=\infty$; $R_x=R$, $R_y=\infty$; $R_x=R_y=R$; $R_x=R$, $R_y=-R$; and $R_x=R$, $R_y=2R$, respectively as shown in Figure 3.3.

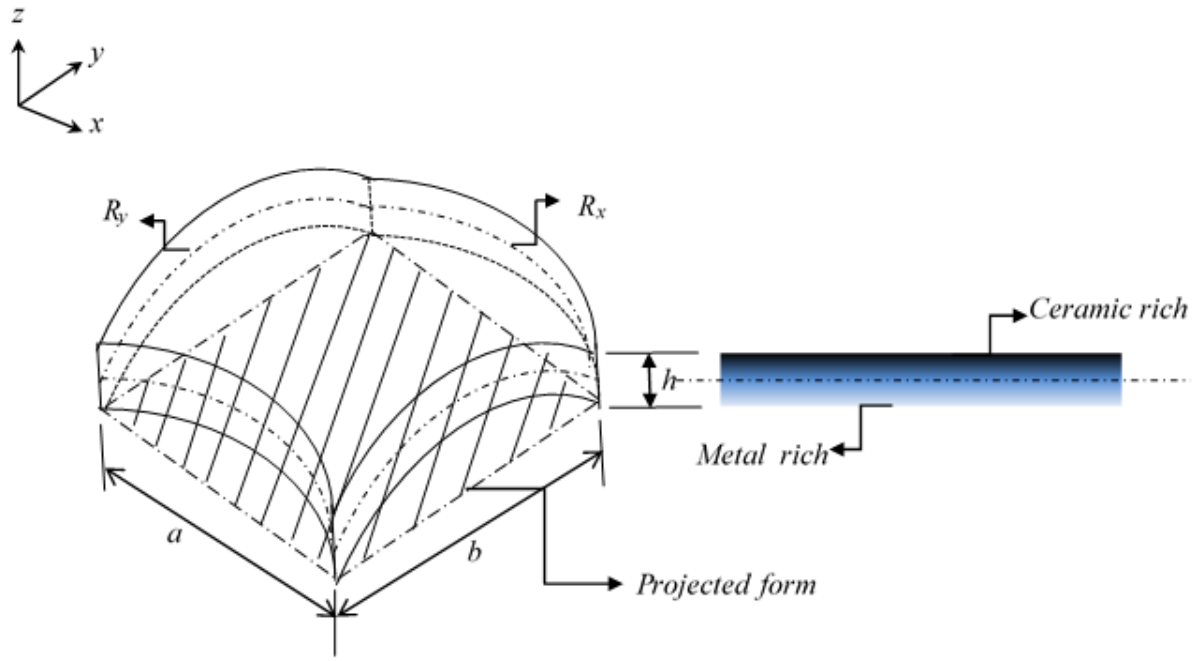

Figure 3.2 Geometry and dimension of the doubly-curved FG shell panel

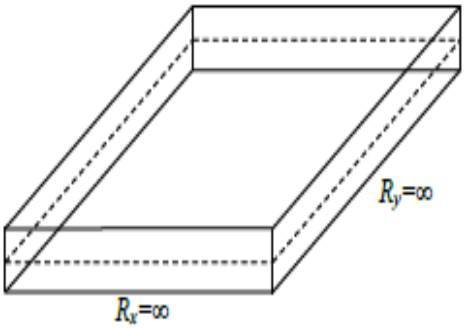

(a) Flat panel

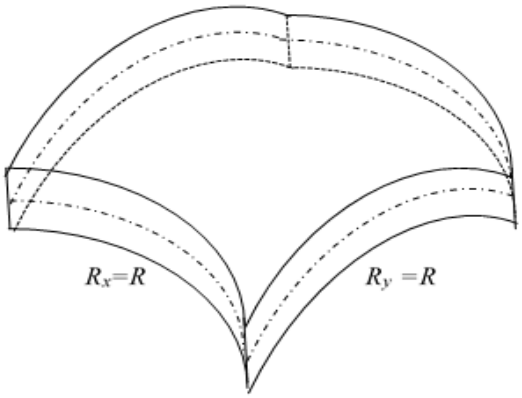

(b) Spherical panel

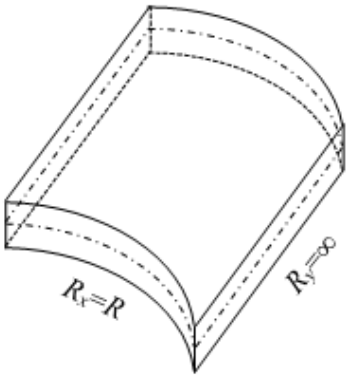

(c) Cylindrical panel

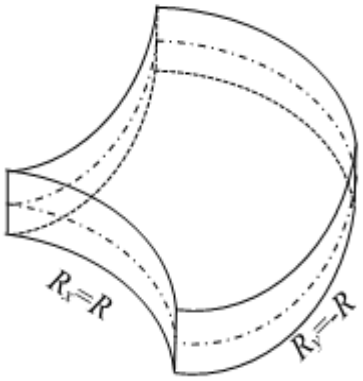

(d) Hyperbolic panel

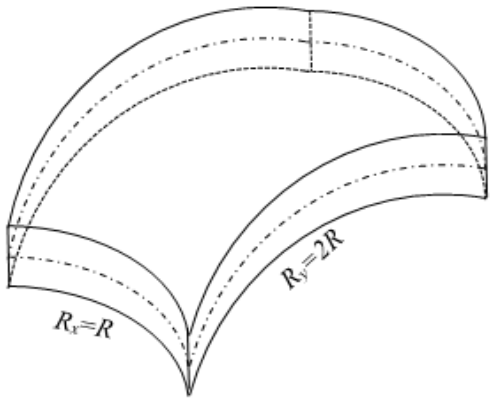

(e) Elliptical panel

Figure 3.3 Geometries of various shell configurations generated from a general doubly-curved shell panel

3.5 Displacement Field

In this study, the displacement field of the FG curved shell panel is derived based on the HSDT kinematics in the mid-plane of the shell panel (at z = 0). The global displacements (u, v, w) are defined in the following polynomial form of nine unknown parameters $\left(u_0, v_0, w_0, \theta_x, \theta_y, u_0^*, v_0^*, \theta_x^*, \theta_y^*\right)$ as in (Pandya and Kant, 1988)

$$\left.\begin{aligned} u\left(x,y,z,t\right) &= u_0\left(x,y,t\right) + z\theta_x\left(x,y,t\right) + z^2u_0^*(x,y,t) + z^3\theta_x^*\left(x,y,t\right) \\ v\left(x,y,z,t\right) &= v_0\left(x,y,t\right) + z\theta_y\left(x,y,t\right) + z^2v_0^*(x,y,t) + z^3\theta_y^*\left(x,y,t\right) \\ w\left(x,y,z,t\right) &= w_0\left(x,y,t\right) \end{aligned}\right\} \quad \ldots(3.9)$$

where, (u_0, v_0, w_0) denote the mid-plane displacements along (x, y, z) co-ordinates, respectively. θ_y and θ_x are the shear rotations about the x- and y-axis, respectively and $\left(u_0^*, v_0^*, \theta_x^*, \theta_y^*\right)$ are the higher-order terms defined in the mid-plane of the curved panel. These nine unknowns can be defined in the mid-plane, i.e., at z = 0 as $u_0 = u(x,y,t)$,

$v_0 = v(x,y,t)$, $w_0 = w(x,y,t)$, $\theta_x = \dfrac{\partial u}{\partial z}, \theta_y = \dfrac{\partial v}{\partial z}$, $u_0^* = \dfrac{1}{2}\left(\dfrac{\partial^2 u}{\partial z^2}\right)$,

$v_0^* = \dfrac{1}{2}\left(\dfrac{\partial^2 v}{\partial z^2}\right), \theta_x^* = \dfrac{1}{6}\left(\dfrac{\partial^3 u}{\partial z^3}\right)$ and $\theta_y^* = \dfrac{1}{6}\left(\dfrac{\partial^3 v}{\partial z^3}\right)$.

Now, the Eq. (3.9) can also be represented in the matrix form as follows:

$$\{\lambda\} = [f]\{\lambda_0\} \qquad \ldots(3.10)$$

where, $\{\lambda\} = \{u\ v\ w\}^T$ and $\{\lambda_0\} = \left[u_0\ \ v_0\ \ w_0\ \ \theta_x\ \ \theta_y\ \ u_0^*\ \ v_0^*\ \ \theta_x^*\ \ \theta_y^*\right]^T$ are the global and mid-plane displacement vectors, and $[f]$ is the function of thickness co-ordinate. The expanded form of $[f]$ is conceded as in the following lines.

$$[f] = \begin{bmatrix} 1 & 0 & 0 & z & 0 & z^2 & 0 & z^3 & 0 \\ 0 & 1 & 0 & 0 & z & 0 & z^2 & 0 & z^3 \\ 0 & 0 & 1 & 0 & 0 & 0 & 0 & 0 & 0 \end{bmatrix} \qquad \ldots(3.11)$$

3.6 Strain-Displacement Relations

The small strain and large deformation behaviour of the FG shell panel is expressed by considering Green-Lagrange type nonlinear strain-displacement field as (Reddy, 2004b)

$$\{\varepsilon\} = \begin{Bmatrix} \varepsilon_{xx} \\ \varepsilon_{yy} \\ \varepsilon_{xy} \\ \varepsilon_{xz} \\ \varepsilon_{yz} \end{Bmatrix} = \begin{Bmatrix} \left(\frac{\partial u}{\partial x} + \frac{w}{R_x}\right) \\ \left(\frac{\partial v}{\partial y} + \frac{w}{R_y}\right) \\ \left(\frac{\partial u}{\partial y} + \frac{\partial v}{\partial x} + \frac{2w}{R_{xy}}\right) \\ \left(\frac{\partial u}{\partial z} + \frac{\partial w}{\partial x} - \frac{u}{R_x}\right) \\ \left(\frac{\partial v}{\partial z} + \frac{\partial w}{\partial y} - \frac{v}{R_y}\right) \end{Bmatrix} + \begin{Bmatrix} \frac{1}{2}\left[\left(\frac{\partial u}{\partial x} + \frac{w}{R_x}\right)^2 + \left(\frac{\partial v}{\partial x} + \frac{w}{R_{xy}}\right)^2 + \left(\frac{\partial w}{\partial x} - \frac{u}{R_x}\right)^2\right] \\ \frac{1}{2}\left[\left(\frac{\partial u}{\partial y} + \frac{w}{R_{xy}}\right)^2 + \left(\frac{\partial v}{\partial y} + \frac{w}{R_y}\right)^2 + \left(\frac{\partial w}{\partial y} - \frac{v}{R_y}\right)^2\right] \\ \left[\left(\frac{\partial u}{\partial x} + \frac{w}{R_x}\right)\left(\frac{\partial u}{\partial y} + \frac{w}{R_{xy}}\right) + \left(\frac{\partial v}{\partial x} + \frac{w}{R_{xy}}\right)\left(\frac{\partial v}{\partial y} + \frac{w}{R_y}\right) + \left(\frac{\partial w}{\partial x} - \frac{u}{R_x}\right)\left(\frac{\partial w}{\partial y} - \frac{v}{R_y}\right)\right] \\ \left[\frac{\partial u}{\partial z}\left(\frac{\partial u}{\partial x} + \frac{w}{R_x}\right) + \frac{\partial v}{\partial z}\left(\frac{\partial v}{\partial x} + \frac{w}{R_{xy}}\right) + \frac{\partial w}{\partial z}\left(\frac{\partial w}{\partial x} - \frac{u}{R_x}\right)\right] \\ \left[\frac{\partial u}{\partial z}\left(\frac{\partial u}{\partial y} + \frac{w}{R_{xy}}\right) + \frac{\partial v}{\partial z}\left(\frac{\partial v}{\partial y} + \frac{w}{R_y}\right) + \frac{\partial w}{\partial z}\left(\frac{\partial w}{\partial y} - \frac{v}{R_y}\right)\right] \end{Bmatrix} \qquad \ldots(3.12)$$

$$\{\varepsilon\} = \{\varepsilon_l\} + \{\varepsilon_{nl}\} \qquad \ldots(3.13)$$

where, $\{\varepsilon_l\}$ and $\{\varepsilon_{nl}\}$ are the linear and the nonlinear strain tensors, respectively and the strain tensors are modified further in matrix form as follows:

$$\{\varepsilon_l\} = \begin{Bmatrix} \varepsilon_x^0 \\ \varepsilon_y^0 \\ \varepsilon_{xy}^0 \\ \varepsilon_{xz}^0 \\ \varepsilon_{yz}^0 \end{Bmatrix} + z\begin{Bmatrix} k_x^1 \\ k_y^1 \\ k_{xy}^1 \\ k_{xz}^1 \\ k_{yz}^1 \end{Bmatrix} + z^2\begin{Bmatrix} k_x^2 \\ k_y^2 \\ k_{xy}^2 \\ k_{xz}^2 \\ k_{yz}^2 \end{Bmatrix} + z^3\begin{Bmatrix} k_x^3 \\ k_y^3 \\ k_{xy}^3 \\ k_{xz}^3 \\ k_{yz}^3 \end{Bmatrix} = [T_l]\{\bar{\varepsilon}_{nl}\}$$

$$\{\varepsilon_{nl}\} = \begin{Bmatrix} \varepsilon_x^4 \\ \varepsilon_y^4 \\ \varepsilon_{xy}^4 \\ \varepsilon_{xz}^4 \\ \varepsilon_{yz}^4 \end{Bmatrix} + z\begin{Bmatrix} k_x^5 \\ k_y^5 \\ k_{xy}^5 \\ k_{xz}^5 \\ k_{yz}^5 \end{Bmatrix} + z^2\begin{Bmatrix} k_x^6 \\ k_y^6 \\ k_{xy}^6 \\ k_{xz}^6 \\ k_{yz}^6 \end{Bmatrix} + z^3\begin{Bmatrix} k_x^7 \\ k_y^7 \\ k_{xy}^7 \\ k_{xz}^7 \\ k_{yz}^7 \end{Bmatrix} + z^4\begin{Bmatrix} k_x^8 \\ k_y^8 \\ k_{xy}^8 \\ k_{xz}^8 \\ k_{yz}^8 \end{Bmatrix} + z^5\begin{Bmatrix} k_x^9 \\ k_y^9 \\ k_{xy}^9 \\ k_{xz}^9 \\ k_{yz}^9 \end{Bmatrix} + z^6\begin{Bmatrix} k_x^{10} \\ k_y^{10} \\ k_{xy}^{10} \\ k_{xz}^{10} \\ k_{yz}^{10} \end{Bmatrix} = [T_{nl}]\{\bar{\varepsilon}_{nl}\} \quad \ldots(3.14)$$

where, $\{\bar{\varepsilon}_l\} = \left[\varepsilon_x^0\ \varepsilon_y^0\ \varepsilon_{xy}^0\ \varepsilon_{xz}^0\ \varepsilon_{yz}^0\ k_x^1 k_y^1 k_{xy}^1 k_{xz}^1 k_{yz}^1 k_x^2 k_y^2 k_{xy}^2 k_{xz}^2 k_{yz}^2 k_x^3 k_y^3 k_{xy}^3 k_{xz}^3 k_{yz}^3\right]^T$ and

$\{\bar{\varepsilon}_{nl}\} = \begin{bmatrix} \varepsilon_x^4 \varepsilon_y^4 \varepsilon_{xy}^4 \varepsilon_{xz}^4 \varepsilon_{yz}^4\ k_x^5 k_y^5 k_{xy}^5 k_{xz}^5 k_{yz}^5 k_x^6 k_y^6 k_{xy}^6 k_{xz}^6 k_{yz}^6 k_x^7 k_y^7 k_{xy}^7 k_{xz}^7 k_{yz}^7 \\ k_x^8 k_y^8 k_{xy}^8 k_{xz}^8 k_{yz}^8 k_x^9 k_y^9 k_{xy}^9 k_{xz}^9 k_{yz}^9 k_x^{10} k_y^{10} k_{xy}^{10} k_{xz}^{10} k_{yz}^{10} \end{bmatrix}^T$ are the linear and the nonlinear mid-plane strain vectors. The individual linear and the nonlinear strain terms are provided in Appendix A. Here, the terms associated with superscripts 0 and 4 are the membrane, 1 and 5 are curvature, and the rest are higher order strain terms. $[T_l]$ and $[T_{nl}]$ are the linear and the nonlinear thickness co-ordinate matrices, respectively and the detailed individual terms are given in Appendix B.

3.7 Temperature Distributions

In order to achieve a general case, different temperature fields across the thickness direction of FG curved panels are considered here, namely, uniform, linear and nonlinear temperature fields.

3.7.1 Uniform Temperature Field

The temperature field is assumed to be uniform across the thickness direction. Let the ambient temperature is T_0 =300K and the temperature field is denoted as

$$T = T_0 + \Delta T \quad \ldots(3.15)$$

3.7.2 Linear Temperature Field

The temperature field is assumed to be linear across the thickness direction. Let T_m and T_c are the temperatures at the bottom and top surfaces, respectively. The temperature field with linear variation across the thickness direction is expressed as

$$T(z) = T_m + (T_c - T_m)\left(\frac{z}{h} + \frac{1}{2}\right) \qquad \ldots(3.16)$$

3.7.3 Nonlinear Temperature Field

The temperature field with nonlinear variation across the thickness direction is obtained by using one-dimensional heat conduction equation and expressed as

$$-\frac{d}{dz}\left(k(z)\frac{dT}{dz}\right) = 0 \qquad \ldots(3.17)$$

where, $T=T_m$ at the bottom surface ($z=-h/2$) and $T=T_c$ at the top surface ($z=+h/2$). The analytical solution to Eq. (3.17) and presented as:

$$T(z) = T_t - \frac{(T_c - T_m)}{\int_{-h/2}^{+h/2} \frac{1}{k(z)}dz} \int_{-h/2}^{z} \frac{1}{k(z)}dz \qquad \ldots(3.18)$$

In the above equation, the thermal conductivity is assumed to be temperature independent and it does not affect the results (Miyamoto et al., 1999). The equation is further solved using the polynomial series (Javaheri and Eslami, 2002b).

$$T\left(z\right) = T_m + \left(T_c - T_m\right) \times \zeta\left(z\right) \qquad \ldots(3.19)$$

where,

$$\zeta(z) = \frac{1}{\mu}\left[\left(\frac{z}{h}+\frac{1}{2}\right) - \frac{k_{cm}}{(n+1)k_m}\left(\frac{z}{h}+\frac{1}{2}\right)^{(n+1)} + \frac{k_{cm}^2}{(2n+1)k_m^2}\left(\frac{z}{h}+\frac{1}{2}\right)^{(2n+1)}\right.$$
$$\left. - \frac{k_{cm}^3}{(3n+1)k_m^3}\left(\frac{z}{h}+\frac{1}{2}\right)^{(3n+1)} + \frac{k_{cm}^4}{(4n+1)k_m^4}\left(\frac{z}{h}+\frac{1}{2}\right)^{(4n+1)} - \frac{k_{cm}^5}{(5n+1)k_m^5}\left(\frac{z}{h}+\frac{1}{2}\right)^{(5n+1)}\right]$$

and $\mu = 1 - \frac{k_{cm}}{(n+1)k_m} + \frac{k_{cm}^2}{(2n+1)k_m^2} - \frac{k_{cm}^3}{(3n+1)k_m^3} + \frac{k_{cm}^4}{(4n+1)k_m^4} - \frac{k_{cm}^5}{(5n+1)k_m^5}$

where, $k_{cm} = k_c - k_m$.

Now, Eq. (3.19) can be simplified for the isotropic material (fully metal/ceramic-rich) as:

$$T(z) = \frac{T_c - T_m}{2} + \frac{T_c - T_m}{h} z \qquad \ldots(3.20)$$

3.8 Constitutive Equations

The thermoelastic stress field for FG shell panel can be written as

$$\{\sigma\} = [C]\left(\{\varepsilon\} - \{\varepsilon_{th}\}\right) \qquad \ldots(3.21)$$

where, $\{\sigma\} = \begin{Bmatrix}\sigma_{xx} & \sigma_{yy} & \sigma_{xy} & \sigma_{xz} & \sigma_{yz}\end{Bmatrix}^T$ and $\{\varepsilon_{th}\} = \begin{Bmatrix}1 & 1 & 0 & 0 & 0\end{Bmatrix}^T \alpha(T,z)\Delta T$ are the stress and thermal strain tensor at any point within the shell panel, respectively.

Now, Eq. (3.21) can also be rewritten in the following form as

$$\begin{Bmatrix}\sigma_{xx}\\ \sigma_{yy}\\ \sigma_{xy}\\ \sigma_{xz}\\ \sigma_{yz}\end{Bmatrix} = \begin{bmatrix}C_{11} & C_{12} & 0 & 0 & 0\\ C_{21} & C_{22} & 0 & 0 & 0\\ 0 & 0 & C_{66} & 0 & 0\\ 0 & 0 & 0 & C_{44} & 0\\ 0 & 0 & 0 & 0 & C_{55}\end{bmatrix}\left(\begin{Bmatrix}\varepsilon_{xx}\\ \varepsilon_{yy}\\ \varepsilon_{xy}\\ \varepsilon_{xz}\\ \varepsilon_{yz}\end{Bmatrix} - \begin{Bmatrix}1\\ 1\\ 0\\ 0\\ 0\end{Bmatrix}\alpha(T,z)\Delta T\right) \qquad \ldots(3.22)$$

where,

$C_{11} = C_{22} = E(T,z)/(1-\upsilon^2)$, $C_{12} = C_{21} = E(T,z)\upsilon/(1-\upsilon^2)$, $C_{66} = C_{44} = C_{55} = E(T,z)/2(1+\upsilon)$.

The total strain energy due to the linear and the nonlinear strains of the FG shell panel can be written as

$$\left.\begin{aligned} U_\varepsilon &= \frac{1}{2}\int\left(\int_{-h/2}^{+h/2}\{\varepsilon\}^T[C]\{\varepsilon\}\,dz\right)dA \\ &= \frac{1}{2}\int_A\left(\{\bar{\varepsilon}_l\}^T[D_1]\{\bar{\varepsilon}_l\}+\{\bar{\varepsilon}_l\}^T[D_2]\{\bar{\varepsilon}_{nl}\}+\{\bar{\varepsilon}_{nl}\}^T[D_3]\{\bar{\varepsilon}_l\}+\{\bar{\varepsilon}_{nl}\}^T[D_4]\{\bar{\varepsilon}_{nl}\}\right)dA \end{aligned}\right\} \ldots(3.23)$$

where, $[D_1]=\int_{-h/2}^{+h/2}[T_{nl}]^T[C][T_l]\,dz$, $[D_2]=\int_{-h/2}^{+h/2}[T_l]^T[C][T_{nl}]\,dz$,

$[D_3]=\int_{-h/2}^{+h/2}[T_{nl}]^T[C][T_l]\,dz$ and $[D_4]=\int_{-h/2}^{+h/2}[T_{nl}]^T[C][T_{nl}]\,dz$.

The total external work done on the FG shell panel due to the transverse load (q) and the temperature rise (ΔT) can be expressed as:

$$W=\int_A\{\lambda_0\}^T\{q\}\,dA+\int_A\left(\{\varepsilon\}^T[C]\{\varepsilon_{th}\}\right)dA \qquad \ldots(3.24)$$

The kinetic energy of the FG shell panel is given by

$$T=\frac{1}{2}\int_V\rho\{\dot{\lambda}\}^T\{\dot{\lambda}\}\,dV \qquad \ldots(3.25)$$

where, ρ and $\{\dot{\lambda}\}$ are the mass density and the first-order differential of the global displacement vector with respect to time. The global displacement field vector can be represented in the form of the mid-plane displacement vector as well.

By substituting Eq. (3.10) in Eq. (3.25), the kinetic energy expression of the FG shell panel can be rewritten as

$$T=\frac{1}{2}\int_A\left(\int_{-h/2}^{+h/2}\{\dot{\lambda}_0\}^T[f]^T\rho[f]\{\dot{\lambda}_0\}\,dz\right)dA=\frac{1}{2}\int_A\{\dot{\lambda}_0\}^T[m]\{\dot{\lambda}_0\}\,dA \qquad \ldots(3.26)$$

where, $[m]=\int_{-h/2}^{+h/2}[f]^T\rho[f]\,dz$ is the inertia matrix.

The strain energy (U_m) due to the in-plane force resultants (N_x, N_y, N_{xy}) can be expressed as (Cook et al., 2009):

$$U_m = \int_v \begin{Bmatrix} \frac{1}{2}\left\{(u_{,x})^2 + (v_{,x})^2 + (w_{,x})^2\right\} N_x \\ + \frac{1}{2}\left\{(u_{,y})^2 + (v_{,y})^2 + (w_{,y})^2\right\} N_y \\ + \left\{u_{,x}\, u_{,y} + v_{,x}\, v_{,y} + w_{,x}\, w_{,y}\right\} N_{xy} \end{Bmatrix} dv \qquad \ldots(3.27)$$

$$U_m = \int_v \begin{Bmatrix} u_{,x} \\ u_{,y} \\ v_{,x} \\ v_{,y} \\ w_{,x} \\ w_{,y} \end{Bmatrix}^T \begin{bmatrix} N_x & N_{xy} & 0 & 0 & 0 & 0 \\ N_{xy} & N_y & 0 & 0 & 0 & 0 \\ 0 & 0 & N_x & N_{xy} & 0 & 0 \\ 0 & 0 & N_{xy} & N_y & 0 & 0 \\ 0 & 0 & 0 & 0 & N_x & N_{xy} \\ 0 & 0 & 0 & 0 & N_{xy} & N_y \end{bmatrix} \begin{Bmatrix} u_{,x} \\ u_{,y} \\ v_{,x} \\ v_{,y} \\ w_{,x} \\ w_{,y} \end{Bmatrix} dv \qquad \ldots(3.28)$$

where, $N_x = N_x^M + N_x^T$, $N_y = N_y^M + N_y^T$ and $N_{xy} = 0$. N_x^M and N_y^M are the in-plane edge compressive/tensile loading along x and y-directions, respectively. $N_x^T = N_y^T = (C_{11} + C_{12})\alpha\Delta T$ is the in-plane thermal force resultant.

$$U_m = \frac{1}{2}\iint \left[[\varepsilon_G]^T [S_G][\varepsilon_G] \right] dxdy \qquad \ldots(3.29)$$

where, $[\varepsilon_G]$ and $[S_G]$ are the in-plane strain vector and the in-plane force resultant matrix, respectively.

3.9 Nonlinear Finite Element Formulation

It is well known that the exact or closed-form solutions are the efficient way to predict the structural responses. However, to achieve the exact solutions of the complex geometry/material model/boundary conditions are almost impossible as discussed earlier. In this regard, numerical methods (especially, finite element method) have been effectively implemented by the many researchers for the complex structural problems

from last few decades. In the present study, a suitable finite element approach is employed to obtain the set of algebraic equations and solved subsequently using the direct iterative method. In order to discretise the proposed FG shell domain, a nine node quadrilateral isoparametric Lagrangian element is employed. This element is framed in Natural co-ordinate system as shown in Figure 3.4.

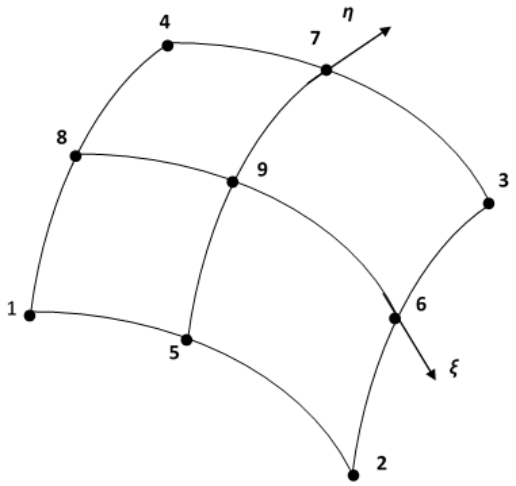

Figure 3.4 A nine node quadrilateral Lagrange isoparametric element

The shape functions (N_i) for the corner (i =1 to 4), mid-side (i =5 to 8) and centre (i =9) nodes are defined in the following manner (Cook et al., 2009):

$$\left.\begin{aligned} N_1 &= \frac{1}{4}(\xi^2-\xi)(\eta^2-\eta) & N_2 &= \frac{1}{4}(\xi^2+\xi)(\eta^2-\eta) \\ N_3 &= \frac{1}{4}(\xi+\xi^2)(\eta+\eta^2) & N_4 &= \frac{1}{4}(\xi^2-\xi)(\eta^2+\eta) \\ N_5 &= \frac{1}{2}(1-\xi^2)(\eta^2-\eta) & N_6 &= \frac{1}{2}(\xi+\xi^2)(1-\eta^2) \\ N_7 &= \frac{1}{2}(1-\xi^2)(\eta^2+\eta) & N_8 &= \frac{1}{2}(\xi^2-\xi)(1-\eta^2) \\ N_9 &= (1-\xi^2)(1-\eta^2) \end{aligned}\right\} \quad \ldots(3.30)$$

The elemental displacement vector is expressed using the corresponding shape function as

$$\{\lambda_0\} = \sum_{i=1}^{9} N_i \{\lambda_{0_i}\} \quad \ldots(3.31)$$

where, $\{\lambda_{0_i}\} = \left[u_{0_i} \;\; v_{0_i} \;\; w_{0_i} \;\; \theta_{x_i} \;\; \theta_{y_i} \;\; u^*_{0_i} \;\; v^*_{0_i} \;\; \theta^*_{x_i} \;\; \theta^*_{y_i} \right]^T$ is the nodal displacement vector at node *i*. N_i is the shape function for the i^{th} node.

The linear and nonlinear mid-plane strain vector in terms of nodal displacement vector can be written as

$$\{\bar{\varepsilon}_l\} = [B]\{\lambda_{0_i}\}, \quad \{\bar{\varepsilon}_{nl}\} = [A][G]\{\lambda_{0_i}\} \qquad \ldots(3.32)$$

where, [*B*] and [*G*] are the product form of the differential operator matrix and the shape functions for the linear and the nonlinear strain vectors, respectively. However, [*A*] is the function of displacements associated with the nonlinear strain terms. The details of [*B*], [*A*] and [*G*] matrices are provided in Appendix C.

Now, Eqs. (3.23), (3.24), (3.26) and (3.29) for strain energy, work done, kinetic energy and membrane strain energy respectively can be transformed into the elemental form using Eqs. (3.31) and (3.32).

3.9.1 Elemental Stiffness Matrix

The elemental equation for strain energy due to linear and nonlinear strains may be expressed as

$$U^e_\varepsilon = \frac{1}{2}\int_A \begin{pmatrix} \{\lambda_{0_i}\}^T [B]^T [D_1][B]\{\lambda_{0_i}\} + \{\lambda_{0_i}\}^T [B]^T [D_2][A][G]\{\lambda_{0_i}\} \\ + \{\lambda_{0_i}\}^T [G]^T [A]^T [D_3][B]\{\lambda_{0_i}\} + \{\lambda_{0_i}\}^T [G]^T [A]^T [D_4][A][G]\{\lambda_{0_i}\} \end{pmatrix} dA \qquad \ldots(3.33)$$

$$U^e_\varepsilon = \frac{1}{2}\begin{pmatrix} \{\lambda_{0_i}\}^T [K_l]^e \{\lambda_{0_i}\} + \{\lambda_{0_i}\}^T [K_{nl1}]^e \{\lambda_{0_i}\} \\ + \{\lambda_{0_i}\}^T [K_{nl2}]^e \{\lambda_{0_i}\} + \{\lambda_{0_i}\}^T [K_{nl3}]^e \{\lambda_{0_i}\} \end{pmatrix} \qquad \ldots(3.34)$$

where, $[K_l]^e = \int_{-1}^{1}\int_{-1}^{1} [B]^T [D_1][B]|J|\,d\xi\,d\eta$ is the linear/linear elemental stiffness matrix, $[K_{nl1}]^e = \int_{-1}^{1}\int_{-1}^{1} [B]^T [D_2][A][G]|J|\,d\xi\,d\eta$ is the linear/nonlinear elemental stiffness matrix,

$[K_{nl2}]^e = \int_{-1}^{1}\int_{-1}^{1}[G]^T[A]^T[D_3][B]|J|d\xi d\eta$ is the nonlinear/linear elemental stiffness matrix and $[K_{nl}]^e = \int_{-1}^{1}\int_{-1}^{1}[G]^T[A]^T[D_4][A][G]|J|d\xi d\eta$ is the nonlinear/nonlinear elemental stiffness matrix.

3.9.2 Elemental Force Matrix

The elemental equation of work done due to thermomechanical loads may be written in the following form as

$$W^e = \{\lambda_{0_i}\}^T\left(\{F_m\}^e + \{F_{th}\}^e\right) \quad \ldots(3.35)$$

where, $\{F_m\}^e = \int_{-1}^{1}\int_{-1}^{1}[N]^T\{q\}|J|d\xi d\eta$ and $\{F_{th}\}^e = \int_{-1}^{1}\int_{-1}^{1}\left(\int_{-h/2}^{+h/2}[B]^T[T]^T[C]\{\varepsilon_{th}\}dz\right)|J|d\xi d\eta$ are the mechanical and thermal load vectors, respectively.

3.9.3 Elemental Mass Matrix

The elemental equation of kinetic energy of FG shell panel may be expressed as

$$T^e = \frac{1}{2}\{\dot{\lambda}_{0_i}\}^T[M]^e\{\dot{\lambda}_{0_i}\} \quad \ldots(3.36)$$

where, $[M]^e = \int_{-1}^{1}\int_{-1}^{1}[N]^T[m][N]|J|d\xi d\eta$ is the elemental mass matrix at any node *i.*

3.9.4 Elemental Geometric Stiffness Matrix

The elemental equation of strain energy due to in-plane loading can be expressed as

$$U_m^e = \frac{1}{2}\int_A\{\lambda_{0_i}\}^T[B_G]^T[D_G][B_G]\{\lambda_{0_i}\}dA \quad \ldots(3.37)$$

$$U_m^e = \frac{1}{2}\left\{\lambda_{0_i}\right\}^T [K_G]^e \left\{\lambda_{0_i}\right\} \qquad \ldots(3.38)$$

where, $[D_G]$ represents the material property matrix and $[B_G]$ is the product form of differential operator matrix and shape functions for the in-plane strain vector. The details of $[B_G]$ matrix can be seen in Appendix C. Here, $[K_G]^e$ is the elemental geometric stiffness matrix which may be expressed as

$$[K_G]^e = \int_{-1}^{1}\int_{-1}^{1} [B_G]^T [D_G][B_G]|J|\, d\xi d\eta \qquad \ldots(3.39)$$

3.10 Governing Equations

The generalised governing equation can be obtained using variational principle and this can be expressed as

$$\delta \int_{t_1}^{t_2} (T^e - (U_\varepsilon^e + U_m^e + W^e))dt = 0 \qquad \ldots(3.40)$$

The equilibrium equation for any element within the shell panel can be obtained by substituting Eqs. (3.34), (3.35), (3.36) and (3.38) in Eq. (3.40) as

$$\left([K_l]^e + [K_{nl}]^e\right)\{\lambda_0\} + [K_G]^e\{\lambda_0\} + [M]^e\{\ddot{\lambda}_0\} = \{F_m\}^e + \{F_{th}\}^e \qquad \ldots(3.41)$$

where, $[K_{nl}]^e = [K_{nl1}]^e + [K_{nl2}]^e + [K_{nl3}]^e$.

The above elemental equation can be rewritten in the global form as

$$\left([K_l] + [K_{nl}]\right)\{\lambda\} + [K_G]\{\lambda\} + [M]\{\ddot{\lambda}\} = \{F_m\} + \{F_{th}\} \qquad \ldots(3.42)$$

where, $[K_l]$, $[K_{nl}]$, $[M]$ and $[K_G]$ are the corresponding global matrices of $[K_l]^e$, $[K_{nl}]^e$, $[M]^e$ and $[K_G]^e$, respectively. $\{F_m\}$ and $\{F_{th}\}$ are the global force vectors, and $\{\ddot{\lambda}\}$ is the global acceleration vector.

Now, the Eq. (3.42) is utilised for the analysis of different linear and nonlinear static, linear and nonlinear structural problem (free vibration, buckling and post-buckling) by dropping appropriate terms.

3.10.1 Nonlinear Static Analysis

The equilibrium equation for the nonlinear static analysis of FG shell panel subjected to thermomechanical load can be obtained by dropping the inertia matrix and the geometric stiffness matrix terms from Eq. (3.42). The final form of the equilibrium equation may be expressed as

$$\left([K_l]+[K_{nl}]\right)\{\lambda\}=\{F_m\}+\{F_{th}\} \qquad \ldots(3.43)$$

3.10.2 Nonlinear Free Vibration Analysis

The equilibrium equation of the nonlinear free vibration behaviour of FG shell panel under thermal environment can be obtained by dropping the load vector terms from Eq. (29) and presented as

$$\left([K_l]+[K_{nl}]+[K_G]\right)\{\lambda\}+[M]\{\ddot{\lambda}\}=0 \qquad \ldots(3.44)$$

The above equation is further solved by substituting $\{\lambda\}=ae^{i\omega t}\{\Delta\}$. The final form of equilibrium equation for the thermally vibrated FG panel can be expressed as

$$\left([K_l]+[K_{nl}]+[K_G]-\omega_n^2[M]\right)\{\Delta\}=0 \qquad \ldots(3.45)$$

where, ω_n is the eigenvalue (natural frequency) of the free vibrated FG panel and Δ is the corresponding eigenvector (mode shapes).

3.10.3 Buckling and Post-buckling Analysis

The equilibrium equation for the buckling analysis of FG shell panel due the in-plane mechanical and thermal loading can be achieved by dropping the nonlinear

stiffness and mass matrix terms and, load vector terms from Eq. (3.42) as

$$\left(([K_l]) + \gamma_{cr}\left[K_G\right]\right)\{\Delta\} = 0 \qquad \ldots(3.46)$$

where, γ_{cr} is the critical buckling load factor.

The equilibrium equation for the post-buckling analysis can be obtained by adding nonlinear stiffness matrix term in the above equation (Eq. 3.46) and conceded as

$$\left(([K_l] + [K_{nl}]) + \gamma_{cr}\left[K_G\right]\right)\{\Delta\} = 0 \qquad \ldots(3.47)$$

3.11 Solution Technique

The required responses are obtained by solving the appropriate governing equations using a direct iterative method (Reddy, 2004a). The steps of direct iterative methods are as follows:

i. As a first step, the linear governing equation has been solved by dropping the appropriate nonlinear terms.

ii. For the eigenvalue problems, the corresponding eigenvector is extracted by using standard eigenvector extraction algorithm. Subsequently, the eigenvector is normalized and scaled up using desired amplitude ratio (W_{max}/h, where W_{max} is the maximum central deflection and h is the thickness of the panel).

iii. Based on the amplitude ratio, the nonlinear stiffness matrices are evaluated and will be used as the first input to obtain the nonlinear responses. Whereas for the flexural analysis, the initial linear response will be used as the first input to compute the nonlinear response.

iv. Now, by continuing the step (ii) and (iii) till two successive iterations will achieve the convergence criteria ($\sim 10^{-3}$) for the required flexural and eigenvalue solutions.

3.12 Support Conditions

In this study, different sets of support conditions (clamped (C), simply-supported (S), hinged (H) and free (F)) are considered on the panel edges to restrict the rigid body motion and to reduce the number of unknowns from the final equilibrium equation. These support conditions are presented in Table 3.1.

Table 3.1 Sets of support conditions

CCCC	At $x = 0, a$ and $y = 0, b$ $u_0 = v_0 = w_0 = \theta_x = \theta_y = u_0^* = v_0^* = \theta_x^* = \theta_y^* = 0$
SSSS	At $x = 0, a$: $v_0 = w_0 = \theta_y = v_0^* = \theta_y^* = 0$ At $y = 0, b$: $u_0 = w_0 = \theta_x = u_0^* = \theta_x^* = 0$
SCSC	At $x = 0, a$: $v_0 = w_0 = \theta_y = v_0^* = \theta_y^* = 0$ At $y = 0, b$: $u_0 = v_0 = w_0 = \theta_x = \theta_y = u_0^* = v_0^* = \theta_x^* = \theta_y^* = 0$
HHHH	At $x = 0, a$: $u_0 = v_0 = w_0 = \theta_y = v_0^* = \theta_y^* = 0$ At $y = 0, b$: $u_0 = v_0 = w_0 = \theta_x = u_0^* = \theta_x^* = 0$
SFSF	At $x = 0, a$: $v_0 = w_0 = \theta_y = v_0^* = \theta_y^* = 0$
CFCF	At $x = 0, a$: $u_0 = v_0 = w_0 = \theta_x = \theta_y = u_0^* = v_0^* = \theta_x^* = \theta_y^* = 0$

3.13 Computer Implementation

The computer implementation of the present FEM formulation is executed through developing a suitable computer code in MATLAB R2012b environment. Different programs are built for various analyses, viz. nonlinear free vibration, nonlinear bending, buckling and post-buckling under thermomechanical loading conditions. The MATLAB codes for different analyses are performed using a desktop computer with the specification of Intel(R) Core(TM) i7-2600 CPU @ 3.4GHz, 6.00GB RAM, 64-bit Operating system. In addition, a 32 node high performance computing system with 64-Intel Sandy Bridge CPU @2GHz is also utilised for the purpose of result generation.

3.14 Summary

In this chapter, the general nonlinear mathematical model is developed for the analysis of FG shell panel under thermal environment. The effective material properties of the FGM are evaluated through Voigt's micromechanical model through the power-law distribution. The properties of FGM is assumed to be temperature-dependent and

graded along the thickness direction. The mathematical model has been developed using Green-Lagrange nonlinear kinematics in the framework of the HSDT to achieve the parabolic variation of the transverse shear stresses. In this study, three different types of temperature distribution across the thickness direction (uniform, linear and nonlinear) are considered. The domain is discretised using suitable finite element steps through a nine node quadrilateral isoparametric Lagrange element. The equilibrium equations for different structural problems such as nonlinear static, free vibration and, buckling and post-buckling responses are computed individually using the direct iterative method and discussed in the forthcoming chapters.

CHAPTER 4
FLEXURAL BEHAVIOUR OF FG SHELL PANEL UNDER THERMOMECHANICAL LOAD

4.1 Introduction

The FG shell panel structures and structural components are mainly designed to perform under severe environmental condition including the excessive compressive load due to the elevated thermal field. Therefore, the FGM structures need to model accurately for the prediction of the deformation behaviour under the hostile environment condition including the geometrical distortion. It is well known that the deflection varies linearly within a certain load limit and beyond that the behaviour becomes nonlinear. Hence, this chapter attempts to analyse and to discuss the linear and the nonlinear flexural behaviour of the FG (flat, spherical, cylindrical, hyperbolic and elliptical) shell panels under mechanical and/or thermal loading conditions including the temperature-dependent material properties. In order to do so, a general nonlinear mathematical model has already been developed by taking Green-Lagrange type nonlinear kinematics in the framework of the HSDT, and it is utilised to compute the desired responses. In Section 4.2, the governing equation of the FG shell panel under thermomechanical loading condition is obtained, and its solution steps are provided. Section 4.3 presents the convergence and validation behaviour of the developed mathematical model for the linear and the nonlinear flexural behaviour of the flat/curved FG shell panel under mechanical and thermal loading through various numerical examples. In continuation, the robustness and the efficacy of the presently developed nonlinear model have been revealed through the

comprehensive parametric study. The effects of various geometrical and material parameters and the support conditions on the linear and the nonlinear flexural responses with TD and TID properties of the FG shell panels are examined under different loading conditions. Finally, this chapter is summarised with the concluding remarks in Section 4.4.

4.2 Solution Methodology

The final form of equilibrium equation of the FG shell panel under thermomechanical loading condition is derived using the variational principle and presented in Eq. (3.43). The nonlinear static responses of the FG shell panel are solved using the direct iterative method and the detailed solution steps using the steps as mentioned in Section 3.11. In this analysis, the FG shell panels are exposed to uniformly distributed load along with three different temperature distributions (uniform, linear and nonlinear) across the thickness direction of the FG shell panel. In this regard, a customised homemade computer code has been developed in MATLAB environment to compute the desired flexural responses. In order to exhibit the flexural behaviour of the FG shell panel, the transverse deflection at the middle of the shell panel $\left(\frac{a}{2},\frac{b}{2},0\right)$ is computed and presented throughout in the analysis.

4.3 Results and Discussion

The linear and the nonlinear flexural responses are obtained using developed mathematical model through a homemade customised MATLAB code that can extend for any general case. The convergence study of the TD and the TID-FG shell panel under thermomechanical load is performed for various geometrical and material configurations. Consequently, a variety of examples is solved for the validation purposes and compared with those available published literature. After the exhaustive testing of the present model, an inclusive parametric study of the flat/curved FG shell panel under thermomechanical load is performed. Here, the linear and the nonlinear flexural responses of the TD and the TID-FG shell panels are analysed for various geometrical

and material parameters, support conditions and temperature fields. In continuation to that, the effects of different parameters on the flexural response are discussed in detail. The TD material properties of FGM constituents used in throughout the analysis are taken same as in Table 4.1. If not stated otherwise, the following non-dimensional parameters are used throughout the analysis for the linear central deflection (w_l), the nonlinear central deflection (w_{nl}), and the uniformly distributed load (UDL, q) as:

Non-dimensional linear central deflection, $\overline{w}_l = w_l / h$

Non-dimensional nonlinear central deflection, $\overline{w}_{nl} = w_{nl} / h$

Load parameter, $Q = (q / E_0) \times (a / h)^4$ where E_0 denotes the Young's modulus of metal at ambient temperature, i.e., at T=300K.

Table 4.1 Temperature-dependent material properties of FGM constituents (Haung and Shen, 2004)

Material	Properties	P_0	P_{-1}	P_1	P_2	P_3
	E (Pa)	2.0104×10^{11}	0	3.0790×10^{-04}	-6.5340×10^{-07}	0
	α (K^{-1})	1.2330×10^{-05}	0	8.0860×10^{-04}	0	0
SUS304	υ	0.28	0	0	0	0
	k (W/mK)	12.04	0	0	0	0
	ρ (kg/m^3)	8166	0	0	0	0
	E (Pa)	1.2256×10^{11}	0	4.5860×10^{-04}	0	0
	α (K^{-1})	7.5788×10^{-06}	0	6.6380×10^{-04}	-3.1470×10^{-06}	0
Ti-6Al-4V	υ	0.3	0	0	0	0
	k (W/mK)	7.82	0	0	0	0
	ρ (kg/m^3)	4427	0	0	0	0
	E (Pa)	3.4843×10^{11}	0	-3.0700×10^{-04}	2.1600×10^{-07}	-8.9460×10^{-11}
	α (K^{-1})	5.8723×10^{-06}	0	9.0950×10^{-04}	0	0
Si_3N_4	υ	0.28	0	0	0	0
	k (W/mK)	9.19	0	0	0	0
	ρ (kg/m^3)	2370	0	0	0	0
	E (Pa)	2.4427×10^{11}	0	-1.3710×10^{-03}	1.2140×10^{-06}	-3.6810×10^{-10}
	α (K^{-1})	1.2766×10^{-05}	0	-1.4910×10^{-03}	1.0060×10^{-05}	-6.7780×10^{-11}
ZrO_2	υ	0.3	0	0	0	0
	k (W/mK)	1.80	0	0	0	0
	ρ (kg/m^3)	3000	0	0	0	0

4.3.1 Convergence and Validation Study

The consistency and the stability of the proposed FE model are demonstrated by computing the responses for different mesh refinement. The linear and nonlinear flexural responses are computed for different FG flat and curved panels under thermomechanical loading conditions. The validity of the present numerical model has been checked by comparing the responses with those available published literature for different geometrical configurations (flat/spherical/cylindrical), and for the TD/TID FGM constituents.

4.3.1.1 Convergence behaviour of linear and nonlinear central deflection of FG panels

In this present example, the convergence behaviour of the linear and the nonlinear non-dimensional central deflections of the simply supported FG (Al/ZrO_2) shell panel (a/h=100, R/a=5, a/b=1) under UDL (Q=50) is examined for three different power-law indices (n=0.5, 2, 10). The metal and ceramic constituents of the FG shell panel are taken as aluminium (Al) and zirconia (ZrO_2) at the bottom and the top surfaces of the panel, respectively. The Young's modulus of Al and ZrO_2 are taken to be 70GPa and 151GPa, respectively. For both the material constituents (metals and ceramic), the Poisson's ratio is assumed to be same as, $\upsilon = 0.3$. The responses are obtained for five different geometries viz., flat, spherical, cylindrical, hyperbolic and elliptical and plotted in Figure 4.1. It is clear from the figure that both the linear and the nonlinear responses are converging well, and a (5×5) mesh is adequate to compute the desired responses further. In addition, it is noted that the metal-rich FG panels (i.e., n=10) are more flexible than that of the ceramic-rich FG panels (n=0.5).

4.3.1.2 Comparison study of linear central deflection of FG panel

The linear deflection responses of the simply supported FG (Al/ZrO_2) flat/curved FG shell panel (a/h=10, R/a=5, a/b=1) is analysed under the transverse loading for different power-law indices (n=0, 0.5, 1, 2, 5, 10 and ∞) and simultaneously compared with the previous published literature (Kiani et al., 2012) and the simulation results obtained using commercial finite element package (ANSYS). The non-dimensional

central deflections ($\bar{w}_l = (E_m \times w \times h)/(a^2 \times q)$, where q is the uniformly distributed load) are computed for three different panel geometries viz., flat, spherical (R/a=5) and cylindrical (R/a=5) shells and presented in Figure 4.2. The geometrical and material parameters are taken to be same as the reference. It is observed that the present results are following the same trend as in the other two cases. However, the present responses are showing comparatively higher than the references, i.e., the present model indicates the flexible behaviour as the results are obtained using the HSDT kinematic model instead of the FSDT as in the reference and the ANSYS.

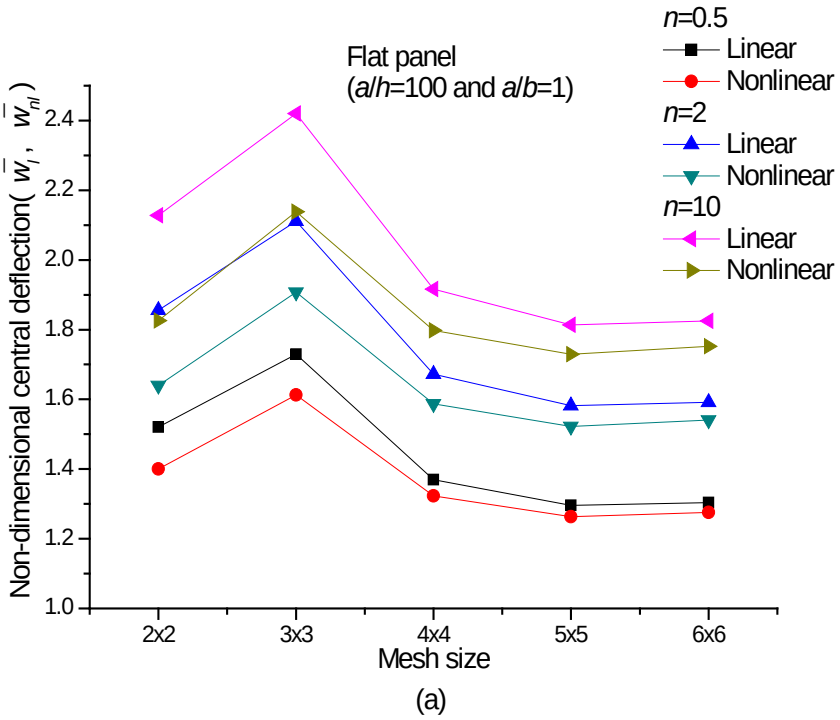

(a)

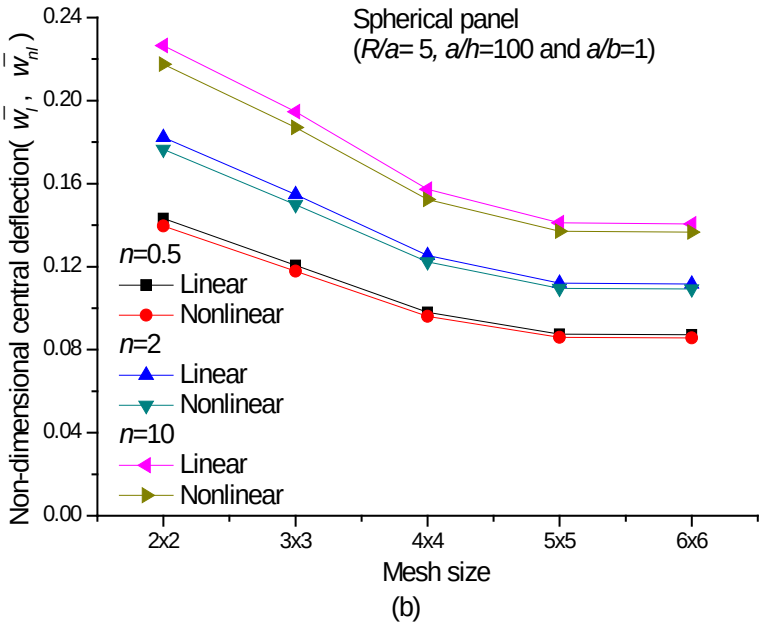
Spherical panel
(R/a= 5, a/h=100 and a/b=1)
Non-dimensional central deflection($\bar{w}_l$, $\bar{w}_{nl}$)
0.24
0.20
0.16
0.12
0.08
0.04
0.00
n=0.5
Linear
Nonlinear
n=2
Linear
Nonlinear
n=10
Linear
Nonlinear
2x2
3x3
4x4
5x5
6x6
Mesh size

(b)

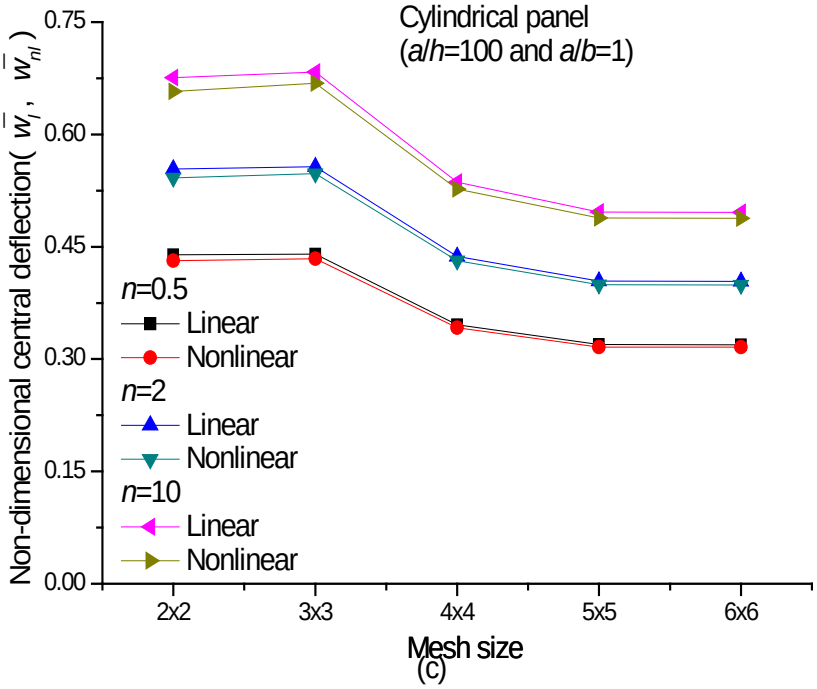
Cylindrical panel
(a/h=100 and a/b=1)
Non-dimensional central deflection($\bar{w}_l$, $\bar{w}_{nl}$)
0.75
0.60
0.45
0.30
0.15
0.00
n=0.5
Linear
Nonlinear
n=2
Linear
Nonlinear
n=10
Linear
Nonlinear
2x2
3x3
4x4
5x5
6x6
Mesh size

(c)

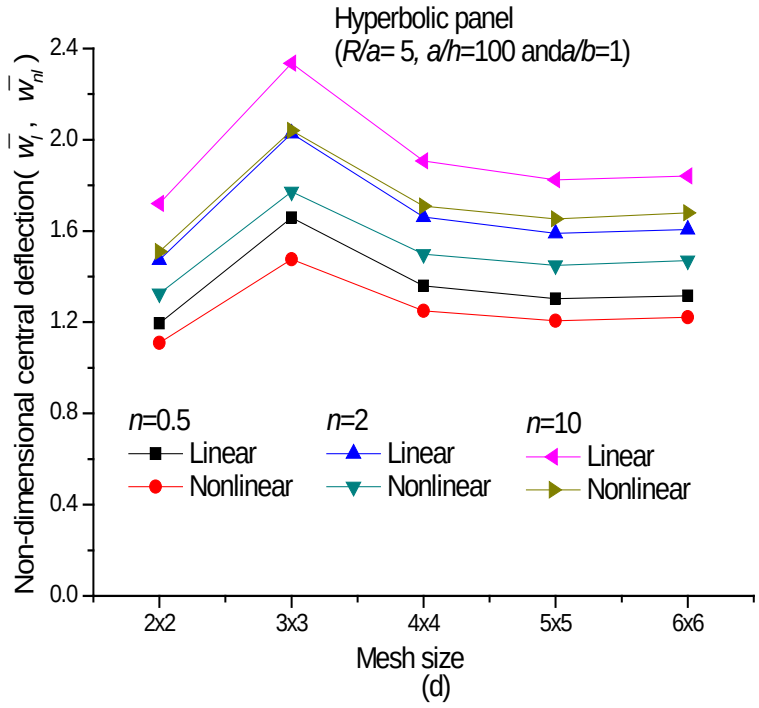

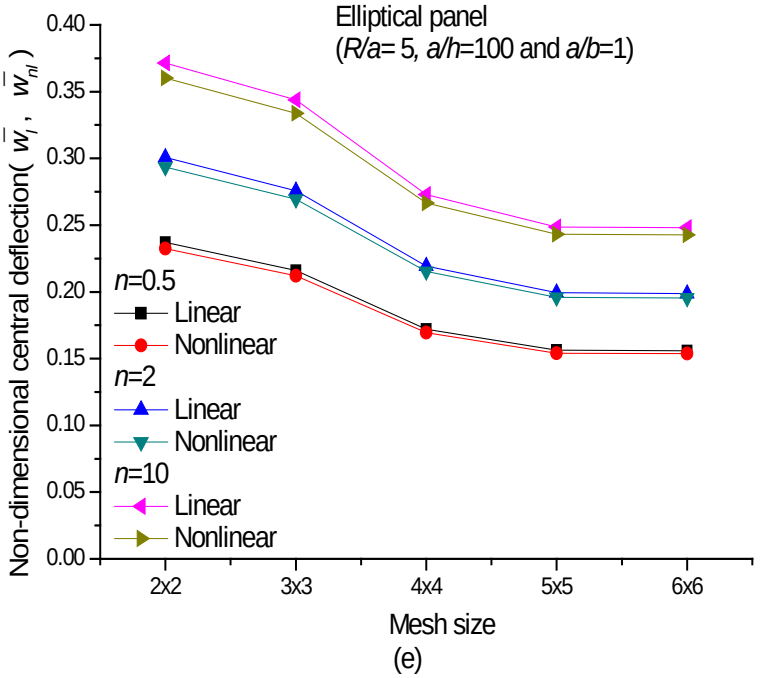

Figure 4.1 Convergence behaviour of linear and nonlinear non-dimensional central deflection of simply supported FG panel for different power-law indices (a) flat, (b) spherical, (c) cylindrical, (d) hyperbolic, and (e) elliptical panel.

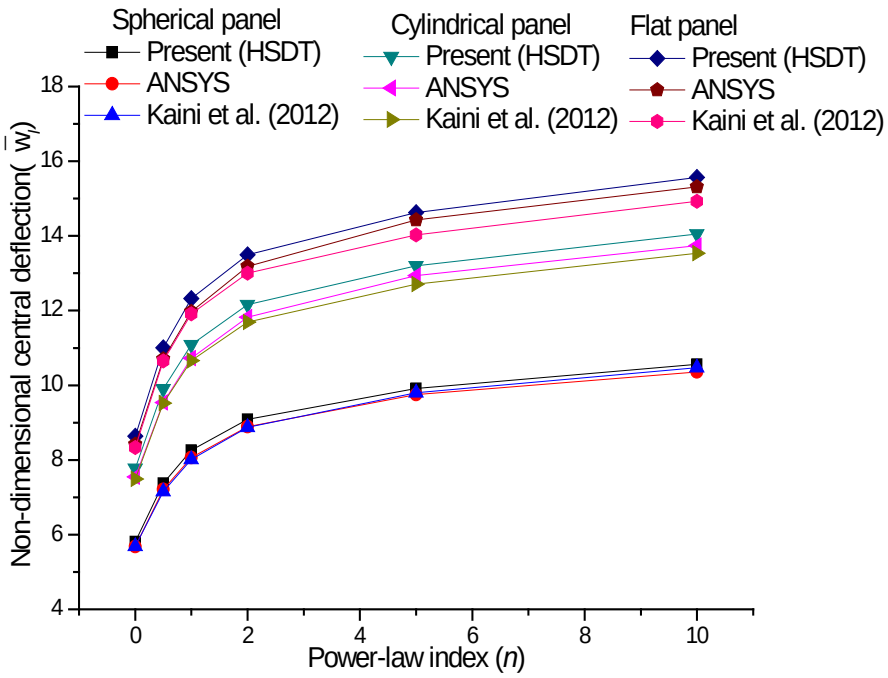

Figure 4.2 Comparison of non-dimensional central deflection of simply supported FG flat/curved panel for different power-law indices

4.3.1.3 Comparison study of nonlinear deflections of FG shell panel

In order to check the validity of the present nonlinear numerical model, the results are computed for various FG flat and curved panel example. The material properties are taken to be same as in the previous examples. Initially, the nonlinear responses of the simply supported FG (Al/ZrO_2) flat panel (a/h=20, n=0.5) are examined for different load parameters. The results are compared with the previously published results of Zhao and Liew (2009a) and the developed ANSYS model and presented in Figure 4.3. The non-dimensional central deflections are obtained using the present HSDT model and showing good agreement with that of the references with very small differences. It is also interesting to note that the responses are almost following the linear trend for every load case, and it may be due to the small load parameters.

In continuation of the above, one more example has been solved further for different power-law indices and compared with available reported literature (Reddy, 2000 and Yang and Shen, 2003) and presented in Figure 4.4. It is worthy to mention that, the reference models are developed using von-Karman nonlinearity in the framework of the FSDT (Reddy, 2000) and the HSDT mid-plane kinematics (Yang and Shen, 2003),

respectively. It is also interesting to note that the differences between the results are within 4% for both the cases, which indicate the efficacy and applicability of present nonlinear model for small strain and large but finite deformation problems.

Based on the earlier comparison study of the FG flat problem, it is understood that the present model is working satisfactorily for the flat panel problems. Further, the model has been extended to analyse for the curved panel problems. In order to do so, another example of square simply supported FG spherical shell panel (R/a =5, a/h=20, n=1) problem has been taken for higher load parameter (Q=100, 200, 300, 400 and 500) and the responses are presented in Figure 4.5**.** The results are compared with Woo and Meguid (2001) and ANSYS results, and considerable difference can be observed clearly. It is due to the fact that the reference and ANSYS results are computed using the CLPT and FSDT, respectively and structure becomes stiffer in comparison to the HSDT kinematics as in the present case. It is well known that the CLPT/FSDT overestimates the shear strain terms and this in turn increases the differences between the published and the present results.

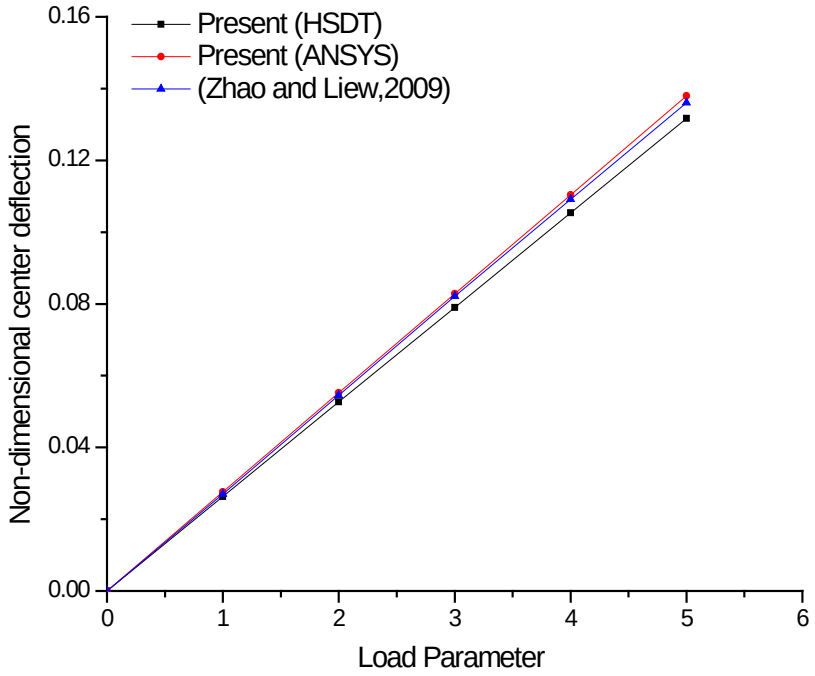

Figure 4.3 Variation of nonlinear non-dimensional central deflection with load parameters for simply supported FG flat panel

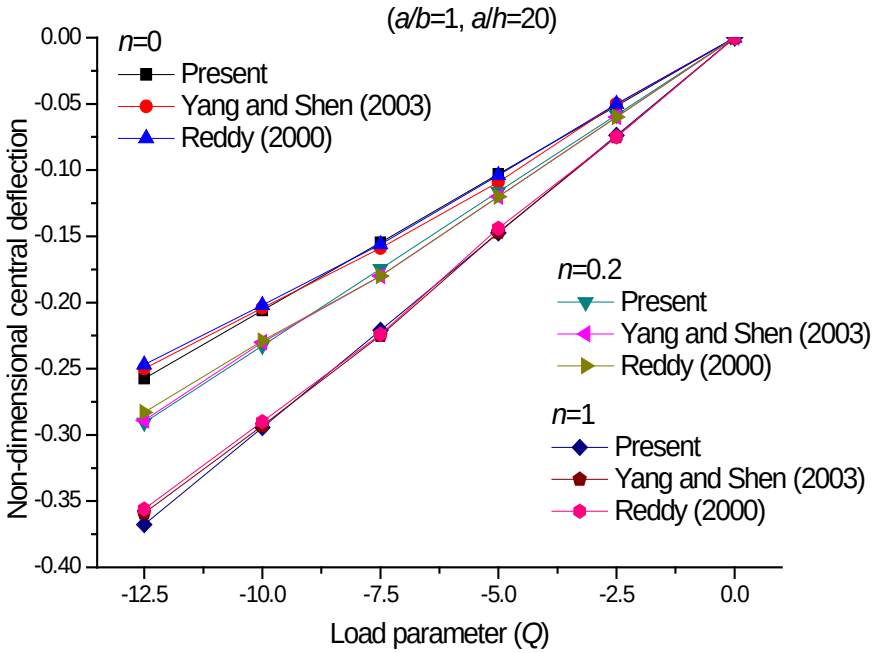

Figure 4.4 Nonlinear non-dimensional central deflection of simply supported FG flat panel for different power-law indices

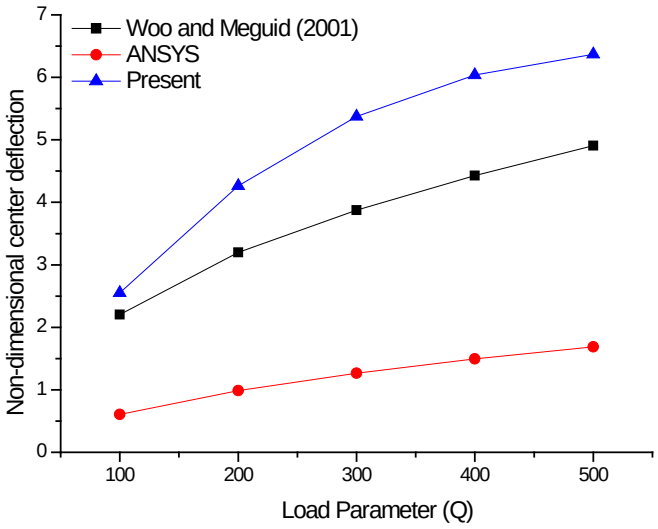

Figure 4.5 Variation of non-dimensional central deflection with load parameters for simply supported FG spherical panel

In the similar line, the nonlinear deflection behaviour of the simply supported square FG (Al/ZrO_2) cylindrical shell panel (a/h=20, R/a=5) are analysed for various transverse load parameters (Q= 10, 20, 30, 40, 50 and 60) and power-law indices (n=0.5, 1, 2), and compared with the results of Zhao and Liew (2009b) and presented in Figure

4.6. In this case also, the considerable amount of difference between the results is observed. Here, the reference results are computed using the FSDT mid-plane kinematics and von-Karman nonlinearity instead of the HSDT kinematics and Green-Lagrange nonlinear strain as in the present case. In addition to the above, the present model also included all the nonlinear higher order terms in the mathematical model to achieve more general. It is important to note from all the above examples that the present model is showing flexible behaviour in comparison to the reference, and the results are within the expected line.

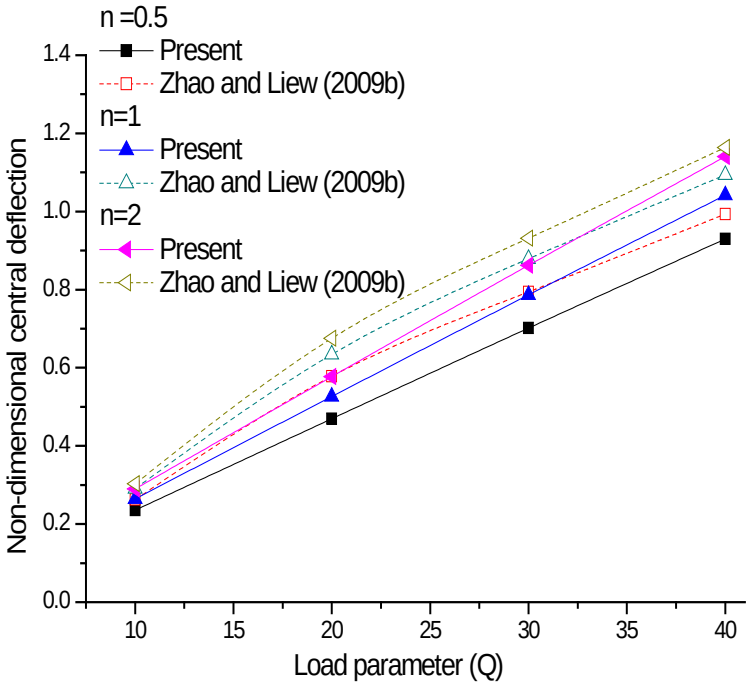

Figure 4.6 Nonlinear non-dimensional central deflection of simply supported FG cylindrical panel for different power-law indices

4.3.1.4 Convergence and comparison behaviour of linear and nonlinear deflections of FG Panel under Thermomechanical Load

In this example, the convergence behaviour of the clamped FG spherical shell panel (R/a=50, a/h=10) under thermomechanical load (ΔT=0, 300K and Q=100) are computed. The FG panel is comprised of Stainless steel (*SUS304*) as metal and silicon nitride (Si_3N_4) as a ceramic material, and the corresponding TD material properties are taken from Table 4.1. The linear and the nonlinear central deflection parameters are computed for different power-law indices at various mesh size and conceded in Figure 4.7. It is clearly understood from the figure that the responses converging well and a (5×5) mesh is sufficient to compute the desired responses further. In continuation of the convergence study, the nonlinear model has been extended further for the validation purpose for square FG ($SUS304/Si_3N_4$) flat panel (a/h=10) under combined thermomechanical (ΔT=300K and Q=10-100). The nonlinear responses are computed for three different support conditions (CFCF, CSCF and CCCC) and two different power-law indices (n=0.2, 2) and presented in Table 4.2. In particular, the support conditions are taken same as in the reference (Yang and Shen, 2003) where movable and immovable in-plane support conditions are considered in the x and y-directions, respectively. The present results are showing good agreement with Yang and Shen (2003) for each case of the support conditions. It is also interesting to note that, the differences are higher for the clamped support and the higher load parameters. The difference between the results may be due to the support condition including the Green-Lagrange nonlinearity in the framework of the HSDT kinematics instead of von-Karman geometrical nonlinearity as adopted in the reference.

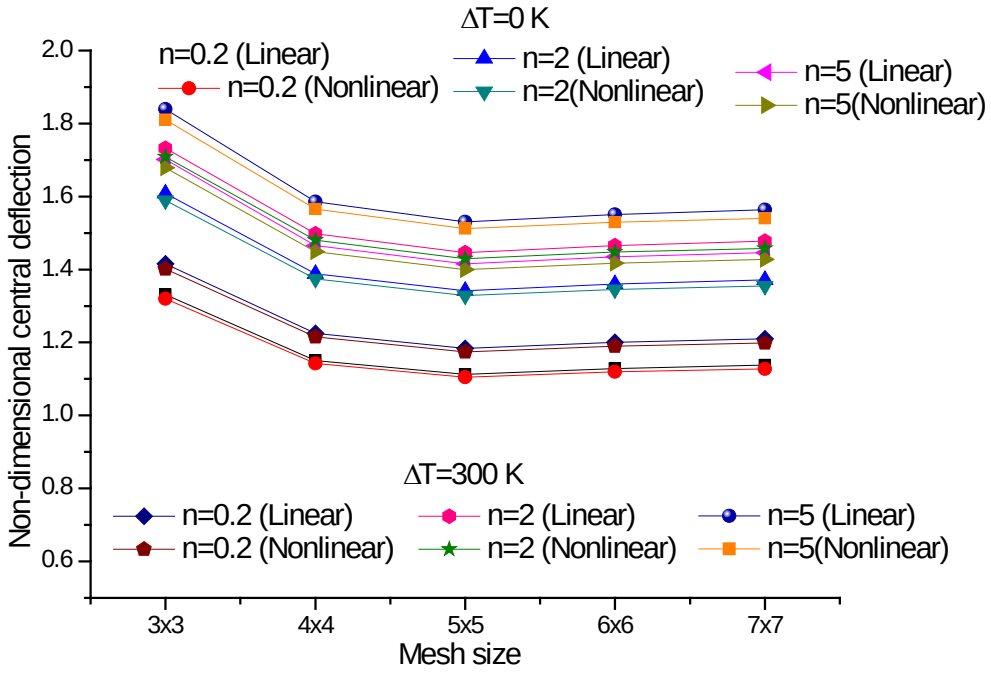

Figure 4.7 Convergence of a clamped FG spherical panel under thermomechanical loading

Table 4.2 Comparison study of nonlinear non-dimensional central deflection of FG flat panel under uniform temperature field

Q	CFCF				CCCC				CSCF			
	n=0.2		*n*=2		*n*=0.2		*n*=2		*n*=0.2		*n*=2	
	Present	Ref*	Present	Ref	Present	Ref	Present	Ref	Present	Ref	Present	Ref
10	0.236	0.175	0.287	0.202	0.117	0.126	0.143	0.139	0.206	0.202	0.252	0.229
20	0.473	0.484	0.576	0.525	0.235	0.247	0.287	0.277	0.411	0.418	0.502	0.458
30	0.710	0.740	0.866	0.834	0.353	0.350	0.431	0.402	0.615	0.633	0.750	0.701
40	0.947	1.009	1.155	1.143	0.471	0.457	0.574	0.519	0.818	0.835	0.996	0.957
50	1.184	1.265	1.445	1.413	0.589	0.556	0.718	0.626	1.020	1.024	1.239	1.186
60	1.422	1.507	1.736	1.749	0.706	0.645	0.860	0.733	1.219	1.226	1.480	1.388
70	1.660	1.776	2.027	2.085	0.823	0.726	1.002	0.818	1.417	1.401	1.717	1.576
80	1.899	2.072	2.319	2.395	0.940	0.798	1.144	0.885	1.613	1.562	1.951	1.778
90	2.130	2.354	2.612	2.717	1.056	0.856	1.285	0.952	1.807	1.697	2.181	1.926
100	2.377	2.623	2.906	3.000	1.172	0.909	1.425	1.014	1.998	1.844	2.408	2.074

** Yang and Shen (2003)*

4.3.2 Numerical Illustrations and Parametric Study

Based on the various illustrations in earlier sections, it clearly indicates the importance and inevitability of the present higher-order nonlinear mathematical model. In continuation of the above section, the robustness of the present nonlinear finite element model is demonstrated through a variety of numerical problems for different shell geometries such as spherical, cylindrical, hyperbolic and elliptical and flat panels, respectively. For each shell geometry, the linear and the nonlinear flexural responses are computed under mechanical and/or thermal loads for different geometrical (the thickness ratios, the curvature ratios and the aspect ratios) and material parameter (the power-law indices, n), the temperature field and the support conditions are examined and discussed in detailed in the following subsections.

Firstly, the linear and the nonlinear flexural responses of FG shell panel are examined without considering the thermal load, i.e., the FG shell panel is subjected to mechanical load only. For the computational purpose, the aluminium, (E_m=70 GPa, ρ_m=2707 kg/m^3, υ_m= 0.3) and zirconia (E_c=151GPa, ρ_c=3000 kg/m^3, υ_c = 0.3) are considered as a metal (at the bottom) and ceramic material (at the top) constituent of the FG material, respectively. Further, the linear and the nonlinear flexural responses of FG panels are examined under combined loading conditions, i.e., mechanical and thermal loading. For the thermal load case, three temperature distributions are considered across the thickness direction of the FG panel are assumed to be uniform, linear and nonlinear. In each case of the thermal load, the responses are obtained for both the TD and the TID properties of the FG panel structure. For the computational purpose under thermal load, *SUS304* is taken as the metal and Si_3N_4 as the ceramic material considered at the bottom and at the top surface of the FG shell panel, respectively and their properties are taken as in Table 4.1. If not stated otherwise, the linear ($\bar{w}_l$) and the nonlinear ($\bar{w}_{nl}$) non-dimensional central deflections are computed throughout the analysis for the square simply supported FG panels by setting the geometrical and the material parameters as R/a=5 and 50, a/h=10, and n=2 under UDL (Q=0, 50, 50, 100, 150 and 200). In addition to that, the top and the bottom surface temperatures are taken as T_c=600K and T_m=300K, respectively.

4.3.2.1 Spherical FG shell panel

In the following subsections, the influence of different parameters (material and geometry) on the linear and the nonlinear flexural responses of the FG spherical (R_x=R_y=R) shell panel under mechanical and/or thermal load including the TD and TID properties are discussed.

4.3.2.1.1 Effect of power-law index on the flexural behaviour of FG spherical panel under mechanical load

It is well known that the grading has a considerable effect on the effective FGM elastic properties and the grading via the power-law index also decides the volume fraction of each constituent in that material. The effect of volume fractions of each (metal and ceramic) constituent on the stiffness behaviour of the FG panel and the corresponding deflection response is analysed in this present example (Kar and Panda, 2015a). Figure 4.8 shows the non-dimensional central deflection of the simply supported square FG (Al/ZrO_2) shell panel (R/a=5 and a/h=10) for six load parameters (Q = 0, 50, 100, 150, 200 and 250) and three power-law indices (n= 0.5, 2 and 10). It can be easily observed that the linear and the nonlinear non-dimensional central deflections are increasing with the increase in the power-law indices. It is because of the fact that, when the 'n' value increases the FG panel becomes metal-rich and which has lower elastic stiffness as compared the ceramic counterpart.

4.3.2.1.2 Effect of thickness ratio on the linear and the nonlinear flexural behaviour of FG spherical panel under mechanical load

The elastic properties of any FG structural components are the functions of thickness co-ordinate and it has a great influence on the overall structural stiffness. Here, the effect of thickness ratios on the linear and the nonlinear flexural responses of the FG spherical panel are investigated. For the computational purpose, the square simply supported FG (Al/ZrO_2) spherical shell panel (R/a=5, n=2) is investigated for four thickness ratios (a/h = 5, 10, 20 and 50) and six load parameters (Q =0, 50, 100, 150, 200

and 250) and presented in Figure 4.9. It is clearly observed that the linear and the nonlinear non-dimensional central deflections decrease monotonously as the thickness ratio increases. It is because the thin FG structures are comparatively less stiff than the thick panel.

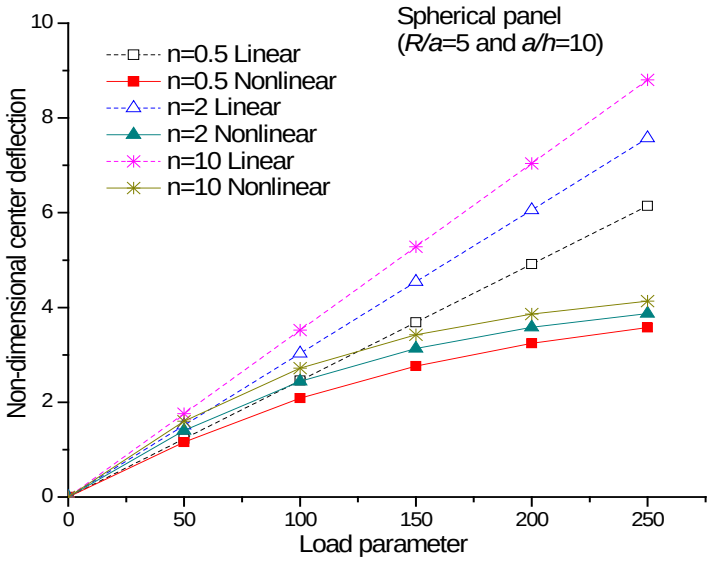

Figure 4.8 Variation of non-dimensional central deflection with power-law indices and load parameters for simply supported FG spherical panel

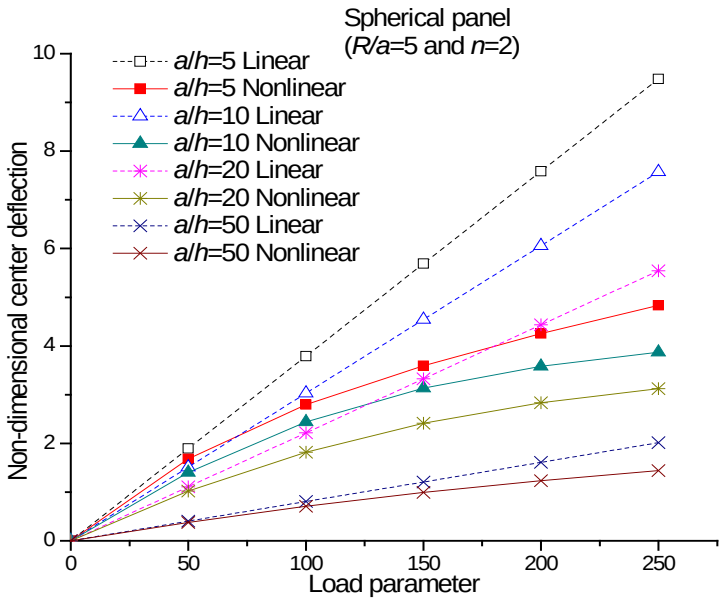

Figure 4.9 Variation of non-dimensional central deflection with thickness ratios and load parameters for simply supported FG spherical panel

4.3.2.1.3 Effect of curvature ratio on the linear and the nonlinear flexural behaviour of FG spherical panel under mechanical load

It is true that the curved panels have higher membrane energy as compared to the bending energy, and the degree of shallowness of any panel is being described in terms of its curvature. In order to address the effect of the curvature ratio on the bending behaviour of the FG shell panel, this example has been solved and presented in Figure 4.10. The linear and nonlinear non-dimensional central deflections of the simply supported square FG (Al/ZrO_2) spherical shell panel (a/h=10 and n=2) is analysed for four curvature ratios (R/a=5, 10, 20 and 50). It is observed that both the linear and the nonlinear central deflections are increasing with the increase in the curvature ratios, i.e., the flat structures exhibit larger deflection than the curved one, and the responses are well within the expected line.

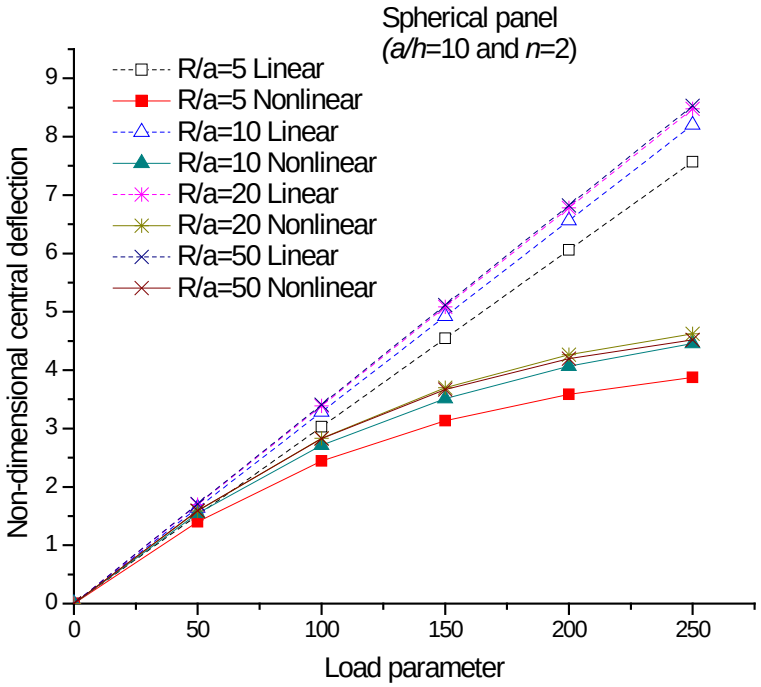

Figure 4.10 Variation of non-dimensional central deflection with curvature ratios and load parameters for simply supported FG spherical panel

4.3.2.1.4 *Effect of aspect ratio on the linear and the nonlinear flexural behaviour of FG spherical panel under mechanical load*

The aspect ratio is the deciding factor for any panel geometry which contributes to the stiffness calculation of the structure. The variation of non-dimensional central deflections of the simply supported square FG (Al/ZrO_2) spherical shell panel (n=2, a/h=100, R/a=50) is examined for four aspect ratios (a/b = 1, 1.5, 2 and 2.5) and shown in Figure 4.11. The loading conditions and material parameters are taken same as in the previous example. It can be observed that the linear and nonlinear central deflection parameters are reducing as the aspect ratios increase. It is also noted that the nonlinearity effect becomes insignificant for the higher aspect ratios.

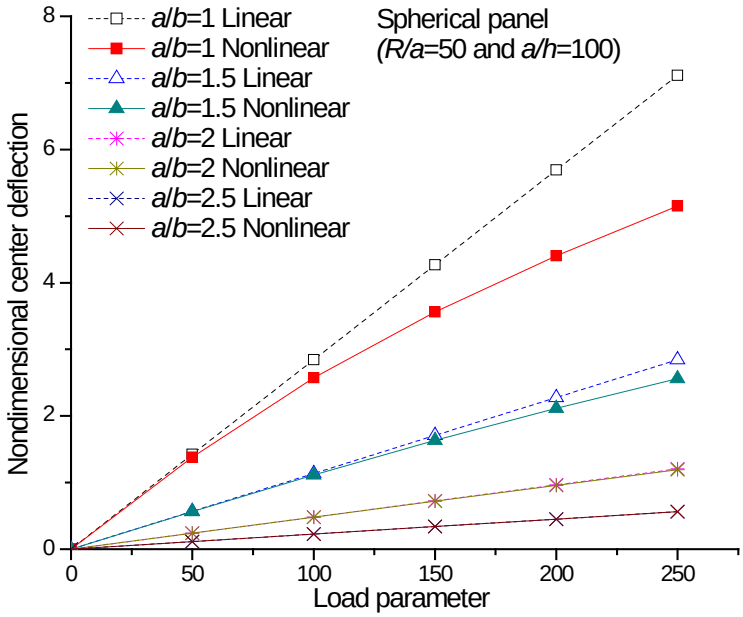

Figure 4.11 Variation of non-dimensional central deflection with aspect ratios and load parameters for simply supported FG spherical panel

4.3.2.1.5 *Effect of support condition on the linear and the nonlinear deflections of FG spherical panel under mechanical load*

In any analysis of the deformable structure, the structural model needs to be constrained properly to avoid rigid body motion. In order to achieve the same, the spatial

degree of freedom is being removed from the structure. It is also true that the support conditions play a significant role for the flexural strength of any structure and structural components. In this example, the effect of four support conditions (SSSS, CCCC, SCSC and HHHH) on the linear and the nonlinear non-dimensional central deflections of the square FG (Al/ZrO_2) spherical shell panel (n=2, a/h=100, R/a=50) under five different load parameters as discussed earlier are computed and plotted in Figure 4.12. It is observed that the deflection parameters are increasing as the number of constraints decreases, i.e., the non-dimensional central deflections are lower and higher for the clamped (CCCC) and the simply support (SSSS) supports, respectively. However, the nonlinearity is insignificant for the CCCC and the SCSC supports. Further, to demonstrate the realistic flexural responses of the FG spherical shell panels, the combined effect of thermal and mechanical loadings are considered and corresponding deflection responses for various parameters in the subsequent examples.

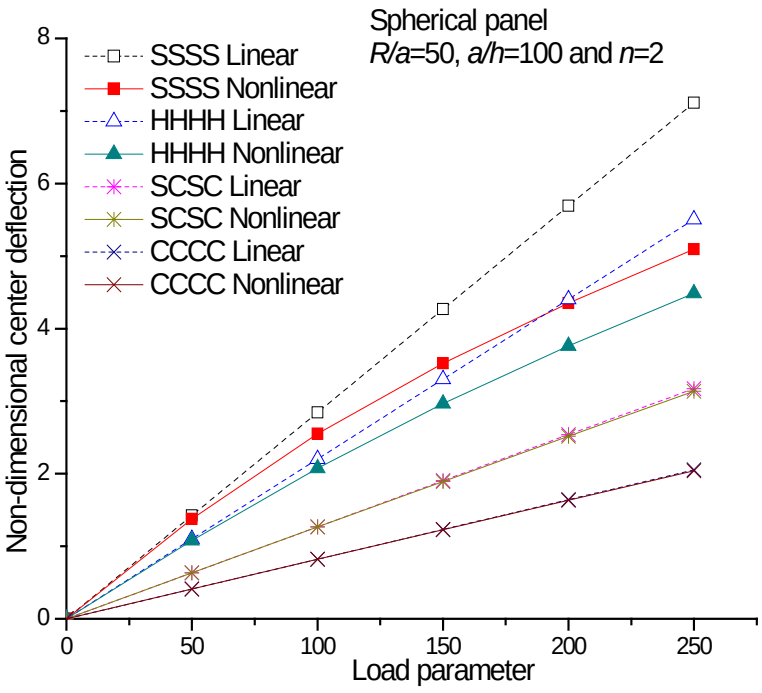

Figure 4.12 Variation of non-dimensional central deflection with load parameters for different support conditions of simply supported FG spherical panel

4.3.2.1.6 Effect of power-law indices on the linear and the nonlinear deflection parameter of FG spherical panel under thermomechanical load

In this example, the effect of power-law indices on the linear and the nonlinear deflection parameters of FG ($Si_3N_4/SUS304$) spherical shell (R/a=50, a/h=10, a/b=1) panel are examined under thermomechanical loading. The responses are obtained under three temperature field (uniform, linear and nonlinear) and five UDL (Q=0, 50, 100, 150 and 200) and presented in Table 4.3. It is observed that the linear and the nonlinear deflection parameters are increasing with the increase in power-law indices. It is also noted that the deflection parameters are higher in the case of the TD-FG spherical shell panel than the TID-FG panel irrespective of the temperature field. In the case of the TD-FG spherical shell panel, the maximum and the minimum deflections are observed for the uniform and the nonlinear temperature field. However, a reverse trend is observed in the TID-FG type shell panels. It is also interesting to note that the differences between the deflection parameters of TID-FG spherical shell panel subjected to the linear and the nonlinear temperature field are insignificant.

Table 4.3 The linear and the nonlinear deflection parameters of simply supported FG spherical panel under thermomechanical loading for different power-law indices

Temperature distribution	Q	TD				TID			
		n=0.2		n=5		n=0.2		n=5	
		$\bar{w}_l$	$\bar{w}_{nl}$	$\bar{w}_l$	$\bar{w}_{nl}$	$\bar{w}_l$	$\bar{w}_{nl}$	$\bar{w}_l$	$\bar{w}_{nl}$
Uniform	0	0.0014	0.0013	0.0006	0.0005	0.0010	0.0009	0.0004	0.0004
	50	1.7414	1.5726	2.2247	1.9239	1.6388	1.4987	2.0625	1.8161
	100	3.4814	2.8767	4.4488	3.4448	3.2765	2.7413	4.1246	3.2707
	150	5.2214	3.9377	6.6729	4.7031	4.9142	3.7833	6.1866	4.4418
	200	6.9614	4.8645	8.897	5.7646	6.552	4.6597	8.2487	5.4682
Linear	0	0.0132	0.0129	0.0181	0.0175	0.0109	0.0107	0.0151	0.0146
	50	1.6986	1.5753	2.1411	1.9221	1.6487	1.5235	2.0772	1.8764
	100	3.3841	2.8641	4.2641	3.4288	3.2864	2.7915	4.1392	3.3263
	150	5.0696	3.9167	6.3870	4.6439	4.9241	3.8374	6.2013	4.5264
	200	6.7550	4.8474	8.5100	5.6602	6.5619	4.7181	8.2634	5.5547
Nonlinear	0	0.0132	0.0129	0.0179	0.0173	0.0109	0.0107	0.0149	0.0144
	50	1.6982	1.5754	2.1397	1.9223	1.6487	1.5240	2.0770	1.8774
	100	3.3832	2.8642	4.2616	3.4289	3.2864	2.7922	4.1390	3.3278
	150	5.0682	3.9167	6.3834	4.6438	4.9242	3.8381	6.2011	4.5281
	200	6.7532	4.8473	8.5053	5.6601	6.5619	4.7188	8.2632	5.5564

4.3.2.1.7 Effect of thickness ratio on the linear and the nonlinear deflection parameter of FG spherical panel under thermomechanical load

Table 4.4 presents the linear and the nonlinear deflection parameters of FG (*Si_3N_4/SUS304*) spherical shell panel for two thickness ratios (*a*/*h*=10 and 20). The loading conditions are taken same as in the previous example. It is observed that the linear and the nonlinear deflection parameters are decreasing with the increase in thickness ratios. The other observations related to the TD/TID and the temperature fields on the deflection parameters are similar to the aforementioned example.

Table 4.4 The linear and the nonlinear deflection parameters of simply supported FG spherical panel under thermomechanical loading for different thickness ratios

Temperature distribution	*Q*	TD				TID			
		a/*h*=10		*a*/*h*=20		*a*/*h*=10		*a*/*h*=20	
		$\bar{w}_l$	$\bar{w}_{nl}$	$\bar{w}_l$	$\bar{w}_{nl}$	$\bar{w}_l$	$\bar{w}_{nl}$	$\bar{w}_l$	$\bar{w}_{nl}$
Uniform	0	-0.0027	-0.0025	0.0196	0.0125	-0.0034	-0.0031	0.0116	0.0074
	50	2.1106	1.8415	2.037	1.2917	1.9668	1.7243	1.8964	1.19
	100	4.2239	3.31	4.0543	2.4787	3.9371	3.1101	3.7813	2.3142
	150	6.3373	4.5225	6.0716	3.5924	5.9073	4.2143	5.6662	3.3374
	200	8.4506	5.5475	8.089	4.568	7.8775	5.1804	7.5511	4.2877
Linear	0	0.0153	0.0148	0.0753	0.06	0.0133	0.0128	0.0654	0.0508
	50	2.0355	1.8406	2.0038	1.5531	1.9835	1.7911	1.9503	1.4913
	100	4.0558	3.2948	3.9323	2.8908	3.9537	3.1726	3.8351	2.783
	150	6.0761	4.4706	5.8608	4.0568	5.924	4.3077	5.72	3.9315
	200	8.0964	5.4567	7.7893	5.1005	7.8942	5.2756	7.6049	4.9401
Nonlinear	0	0.0151	0.0146	0.0742	0.0596	0.0125	0.0121	0.0624	0.0509
	50	2.0343	1.8412	2.0017	1.5656	1.9775	1.7997	1.9382	1.5363
	100	4.0534	3.2953	3.9292	2.8934	3.9426	3.2046	3.814	2.8667
	150	6.0726	4.471	5.8567	4.0907	5.9076	4.3656	5.6899	4.0178
	200	8.0918	5.4569	7.7841	5.1197	7.8726	5.3597	7.5657	5.0711

4.3.2.1.8 Effect of curvature ratio on the linear and the nonlinear deflections of FG spherical panel under thermomechanical load

Now, the effect of curvature ratios on the linear and the nonlinear central deflections of the FG (*Si_3N_4/SUS304*) spherical shell panel is examined under thermomechanical loading and presented in Table 4.5. It is observed that the linear and

the nonlinear deflection parameters are increasing with the increase in curvature ratios. The influences of other parameters such as TD/TID and the temperature distribution on the deflection parameters of FG spherical panel are following the same line in the previous sections.

Table 4.5 The linear and the nonlinear deflection parameters of simply supported FG spherical panel under thermomechanical loading for different curvature ratios

Temperature distribution	Q	TD				TID			
		R/a=10		R/a=20		R/a=10		R/a=20	
		$\bar{w}_l$	$\bar{w}_{nl}$	$\bar{w}_l$	$\bar{w}_{nl}$	$\bar{w}_l$	$\bar{w}_{nl}$	$\bar{w}_l$	$\bar{w}_{nl}$
Uniform	0	0.0301	0.0221	0.0099	0.0083	0.0234	0.017	0.0068	0.0058
	50	2.0876	1.5237	2.1108	1.7124	1.9412	1.4138	1.9655	1.5898
	100	4.1451	2.8742	4.2118	3.1206	3.859	2.6587	3.9241	2.9244
	150	6.2025	4.0211	6.3128	4.2966	5.7769	3.7385	5.8828	4.0301
	200	8.26	5.0011	8.4138	5.339	7.6947	4.6785	7.8414	4.9825
Linear	0	0.0296	0.0255	0.0208	0.0192	0.0258	0.0219	0.0181	0.0165
	50	1.9965	1.6595	2.0293	1.7706	1.9436	1.5963	1.9768	1.7169
	100	3.9635	3.0281	4.0378	3.1897	3.8614	2.9260	3.9354	3.0923
	150	5.9304	4.1840	6.0463	4.3655	5.7793	4.0255	5.8941	4.1914
	200	7.8973	5.166	8.0547	5.3391	7.6971	4.9519	7.8527	5.1535
Nonlinear	0	0.0290	0.025	0.0205	0.019	0.0249	0.0219	0.0173	0.0161
	50	1.9948	1.664	2.0278	1.7731	1.9380	1.6348	1.9709	1.7386
	100	3.9606	3.0345	4.0352	3.1930	3.8511	2.9888	3.9244	3.1151
	150	5.9264	4.1900	6.0425	4.3685	5.7641	4.0963	5.8779	4.2670
	200	7.8922	5.1719	8.0499	5.3423	7.6772	5.0687	7.8315	5.2545

4.3.2.1.9 Effect of aspect ratio on the linear and the nonlinear deflections of FG spherical panel under thermomechanical load

The effect of the aspect ratios on the linear and the nonlinear deflection parameters of the FG (Si_3N_4/*SUS304*) spherical shell panel is investigated under thermomechanical loading conditions and presented in Table 4.6. It is observed that the linear and the nonlinear deflection parameters are decreasing with the increase in aspect ratios. The deflection parameters are following the similar fashion for TD/TID and temperature fields as in the earlier example.

Table 4.6 The linear and the nonlinear deflection parameters of simply supported FG spherical panel under thermomechanical load for different aspect ratios

Temperature distribution	Q	TD				TID			
		a/b=2		a/b=2.5		a/b=2		a/b=2.5	
		$\overline{w}_l$	$\overline{w}_{nl}$	$\overline{w}_l$	$\overline{w}_{nl}$	$\overline{w}_l$	$\overline{w}_{nl}$	$\overline{w}_l$	$\overline{w}_{nl}$
Uniform	0	0.0166	0.0134	0.009	0.0078	0.0139	0.0115	0.0075	0.0067
	50	0.3633	0.295	0.1799	0.1569	0.3362	0.281	0.1664	0.1483
	100	0.71	0.5794	0.3508	0.3068	0.6585	0.5528	0.3253	0.2904
	150	1.0566	0.8645	0.5218	0.4572	0.9808	0.8245	0.4842	0.4329
	200	1.4033	1.1482	0.6927	0.6078	1.3031	1.0945	0.6432	0.5755
Linear	0	0.0088	0.0079	0.0042	0.0039	0.0077	0.007	0.0037	0.0035
	50	0.3402	0.3073	0.1676	0.1572	0.3301	0.3015	0.1626	0.153
	100	0.6715	0.6067	0.331	0.3106	0.6524	0.5899	0.3215	0.3026
	150	1.0029	0.9034	0.4944	0.464	0.9747	0.8862	0.4805	0.4522
	200	1.3343	1.1959	0.6578	0.6171	1.297	1.1729	0.6394	0.6013

4.3.2.1.10 Effect of support condition on the linear and the nonlinear deflection parameter of FG spherical panel under thermomechanical load

The effect of support conditions on the linear and the nonlinear deflection parameters of the FG ($Si_3N_4/SUS304$) spherical shell panel is analysed under thermomechanical loading conditions and reported in Table 4.7. The responses are obtained under two different temperature distributions (uniform and linear). It is observed that the linear and the nonlinear deflection parameters are maximum in case of the SCSC type FG panel and minimum in case of clamped (CCCC) support, i.e., the increase in the number of support constraints reduces the deflection parameters. The TD-FG spherical panel exhibits maximum deflection parameter than the TID-FG spherical panel.

Similarly, the present study is being extended to the cylindrical type shell geometry in Section *4.3.2.2*, and the corresponding deflection responses are examined under mechanical and/or thermal.

4.3.2.2 Cylindrical FG shell panel

The influence of different parameters on the linear and the nonlinear flexural responses of the FG cylindrical (R_x=R and R_y=∞) shell panel under mechanical and/or thermal load are presented in the following subsections.

4.3.2.2.1 Effect of power-law indices on the linear and the nonlinear flexural behaviour of FG cylindrical panel under mechanical load

In this example, the effect of power-law indices on the linear and the nonlinear deflection behaviour of the FG cylindrical shell panel is examined and shown in Figure 4.13. For the computational purpose, the simply supported square FG (Al/ZrO_2) cylindrical shell (R/a=5 and a/h=10) panel for seven different load parameters (Q = 0, 50, 100, 150, 200, 250 and 300) and three power-law indices (n=0.5, 2 and 10) are considered (Kar and Panda, 2015b). It can be easily observed that the linear and the nonlinear non-dimensional central deflections are increasing with the increase in the power-law indices.

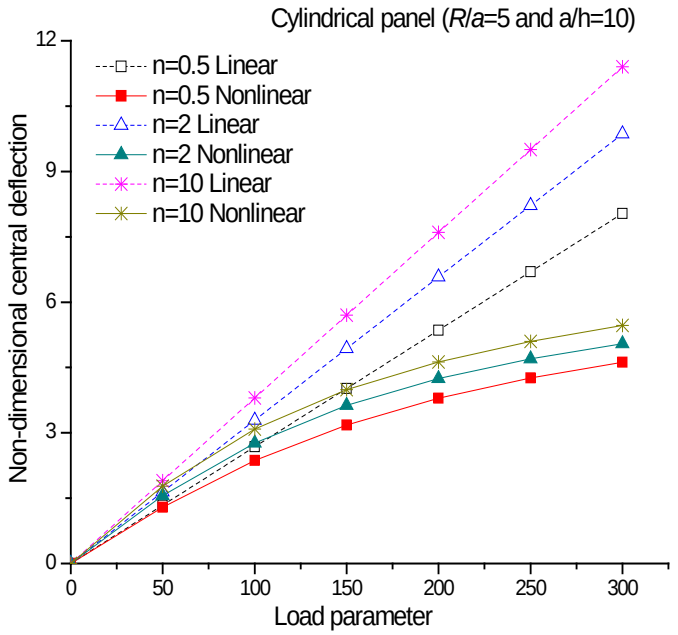

Figure 4.13 Variation of non-dimensional central deflection with power-law indices and load parameters

for simply supported FG cylindrical panel

4.3.2.2.2 Effect of thickness ratio on the linear and the nonlinear flexural behaviour of FG cylindrical panel under mechanical load

In this example, the effect of thickness ratios on the linear and the nonlinear central deflections on the FG cylindrical shell panels are examined. For the computational purpose, the simply supported square FG (Al/ZrO_2) cylindrical shell panel (R/a=5 and n=2) for four thickness ratios (a/h = 5, 10, 20 and 50) and six load parameters (Q =0, 50, 100, 150, 200 and 250) are taken and the responses are presented in Figure 4.14. It is clearly observed that the linear and the nonlinear non-dimensional central deflections decrease monotonously as the thickness ratio increases except few deviations in the nonlinear case. It is also important to mention that the deviation of the responses indicates the effect of full nonlinearity in the framework the HSDT kinematics for the small strain large (finite) deformation regime.

4.3.2.2.3 *Effect of curvature ratio on the linear and the nonlinear flexural behaviour of FG cylindrical panel under mechanical load*

The linear and the nonlinear non-dimensional central deflections of the simply supported square FG (Al/ZrO_2) cylindrical shell panel (a/h=10 and n=2) is analysed for three curvature ratios (R/a=10, 50 and 100) and presented in Figure 4.15. The loading conditions are considered to be same as in the previous problem. It is observed that the linear deflection parameters are not following any monotonous behaviour whereas the nonlinear responses are increasing with the increase in the curvature ratios.

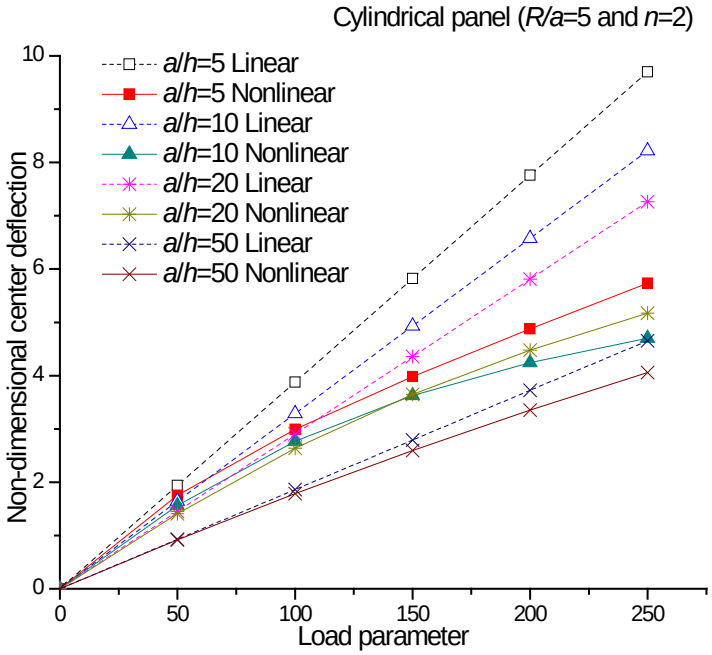

Figure 4.14 Variation of non-dimensional central deflection of simply supported FG cylindrical panel for different thickness ratios

4.3.2.2.4 *Effect of aspect ratio on the linear and the nonlinear flexural behaviour of FG cylindrical panel under mechanical load*

Now, the variation of the linear and the nonlinear non-dimensional central deflections of the simply supported square FG (Al/ZrO_2) cylindrical shell panel (n=2, a/h=100, R/a=50) for four aspect ratios (a/b = 1, 1.5, 2 and 2.5) is investigated and presented in Figure 4.16 in this example. It can be observed that the linear and nonlinear

central deflection parameters are reducing as the aspect ratios increase. It is also interesting to note that the geometrical nonlinearity is insignificant for the higher aspect ratios.

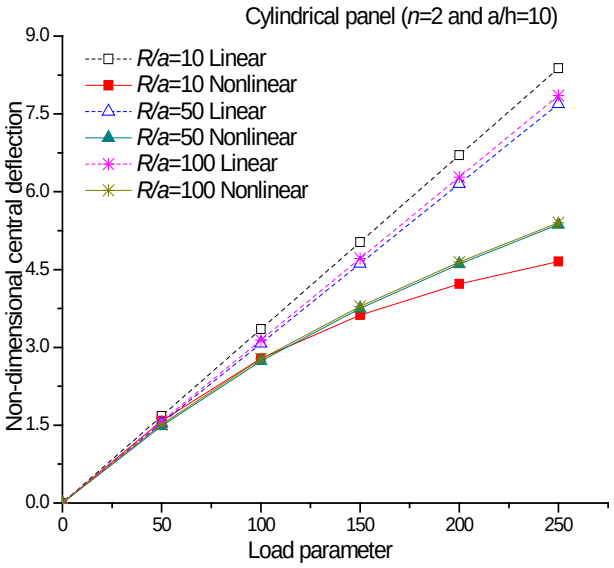

Figure 4.15 Variation of non-dimensional central deflection of simply supported square FG cylindrical shell panel for different curvature ratios

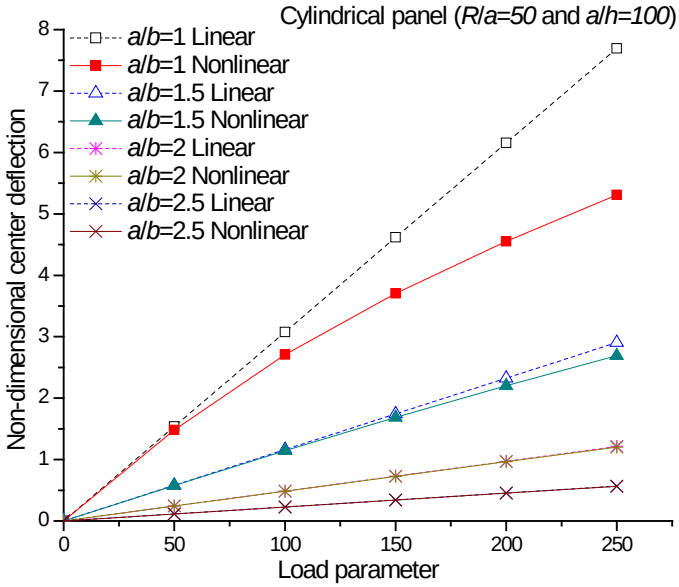

Figure 4.16 Variation of non-dimensional central deflection of simply supported FG cylindrical shell panel for aspect ratios

4.3.2.2.5 *Effect of support condition on the linear and the nonlinear central deflection of FG cylindrical panel under mechanical load*

The effect of support conditions (SSSS, CCCC, SCSC and HHHH) on the linear and the nonlinear non-dimensional central deflections of the square FG (Al/ZrO_2) cylindrical shell panel (n=2, a/h=100 and R/a=50) are computed and plotted in Figure 4.17. It is observed that the deflection parameters are increasing with the decrease in the number of constraints, i.e., the deflection parameters are maximum and minimum for SSSS and CCCC support conditions, respectively. It is also noted that the nonlinearity effect is minor in case of CCCC and SCSC support cases.

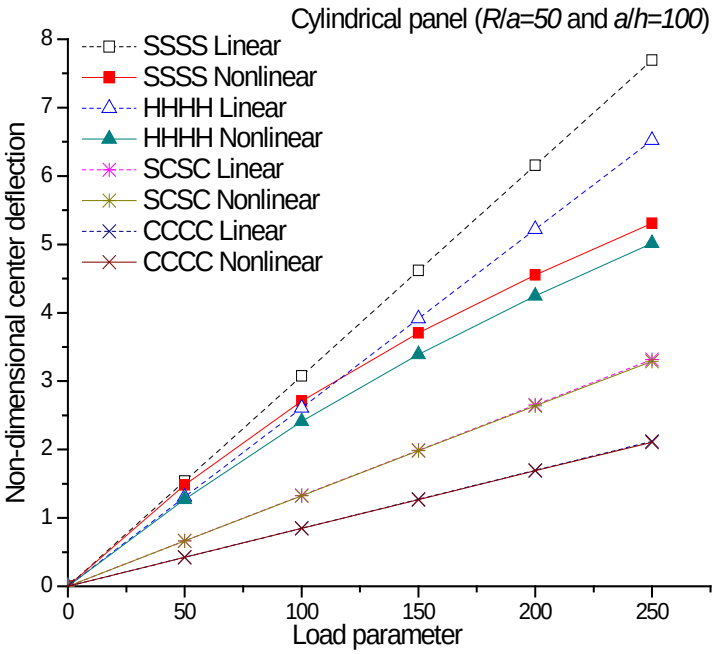

Figure 4.17 Variation of non-dimensional central deflection of square cylindrical FG panel for different support conditions

4.3.2.2.6 *Effect of power-law index on the linear and the nonlinear flexural behaviour of FG cylindrical panel under thermomechanical load*

Now, the thermomechanical flexural behaviour of the FG cylindrical shell panel is analysed for different geometrical, material parameters and support conditions. Initially, the effect of power-law indices on the linear and the nonlinear deflection parameters of

the FG (Si_3N_4/*SUS304*) cylindrical shell (R/a=50, a/h=10, a/b=1) panel is examined under thermomechanical loading and presented in Table 4.8. For the computational purpose, three temperature loads (uniform, linear and nonlinear) and five mechanical loads (Q=0, 50, 100, 150 and 200) are considered. It is observed that the linear and the nonlinear deflection parameters are increasing with the increase in power-law indices. It is because the stiffness of metal-rich FG panel has comparatively lower than the stiffness of ceramic-rich FG panel. It is also noted that the deflection parameters are higher in the case of the TD-FG shell panels than the TID-FG shell panels irrespective of the temperature field. In the case of the TD-FG shell panel, the maximum deflections are observed for uniform temperature field whereas the minimum for the nonlinear temperature field. However, a reverse trend is seen in the TID-FG shell panel where the FG cylindrical shell panel under uniform thermal field is exhibiting the minimum deflections. It is also interested to note that the differences between the deflection parameters of the TID-FG cylindrical shell panel subjected to the linear and the nonlinear temperature field are insignificant.

4.3.2.2.7 Effect of thickness ratio on the linear and the nonlinear flexural behaviour of FG cylindrical panel under thermomechanical load

In this example, the effect of thickness ratios on the linear and the nonlinear deflection parameters of the FG (Si_3N_4/*SUS304*) cylindrical shell panel is examined under thermomechanical loading and presented in Table 4.9. It is observed that the linear deflection parameters are decreasing with the increase in thickness ratios. However, the nonlinear deflection parameters are showing a reverse trend than in the linear case. The other observations related to the TD and the TID case and the temperature field are similar to the previous section.

4.3.2.2.8 Effect of curvature ratio on the linear and the nonlinear flexural behaviour of FG cylindrical panel under thermomechanical load

The effect of curvature ratios on the linear and the nonlinear deflection parameters of the FG (Si_3N_4/*SUS304*) shell panel is examined under the thermomechanical loading

and presented in Table 4.10. It is clear from the tabulated responses that the linear and the nonlinear deflection parameters are increasing with the increase in curvature ratios for all the different cases. The influences of other parameters such as the TD/TID, the temperature distribution on the deflection parameters of the FG cylindrical shell panel are following the same trend as in the previous sections.

4.3.2.2.9 Effect of aspect ratio on the linear and the nonlinear flexural behaviour of FG cylindrical panel under thermomechanical load

In this example, the effect of aspect ratios on the linear and the nonlinear central deflections of the FG (*Si_3N_4/SUS304*) cylindrical shell panel is examined under thermomechanical loading conditions and presented in Table 4.11. It is observed that the linear and the nonlinear deflection parameters are decreasing with the increase in the aspect ratios. However, the deflection parameters are following the similar fashion for the TD/TID and temperature fields as mentioned in the previous examples.

4.3.2.2.10 Effect of support condition on the linear and the nonlinear flexural behaviour of FG cylindrical panel under thermomechanical load

The effect of support conditions on the linear and the nonlinear deflection parameters of the FG (*Si_3N_4/SUS304*) cylindrical shell panel are examined under thermomechanical loading and presented in Table 4.12. It is noted that the linear and the nonlinear deflection parameters are maximum and minimum for the SCSC and the CCCC supports, i.e., the increase in the number of support constraints reduces the deflection parameters. It is also noted that the deflection parameters are higher in the case of the TD-FG cylindrical panels than the TID-FG shell panels irrespective of the temperature field.

4.3.2.3 Hyperbolic FG shell panel

The earlier sections discussed the deflection behaviour of the FG spherical/cylindrical shell panel under mechanical and/or thermal loadings. Here, in this subsection the linear and the nonlinear central deflections are examined for the FG hyperbolic (R_x=R and R_y=-R) shell panel. The responses are obtained for different geometrical, material, and loading conditions and discussed in detailed.

4.3.2.3.1 Effect of power-law indices on the linear and the nonlinear deflections of the FG hyperbolic shell panel under thermomechanical load

In this example, the effect of power-law indices on the linear and the nonlinear deflection parameters of the FG hyperbolic shell panel subjected to UDL is examined (Kar and Panda, 2015b). Figure 4.18 shows the non-dimensional central deflections of the simply supported square FG (Al/ZrO_2) hyperbolic shell panel (R/a=50 and a/h=100) for three power-law indices (n= 0.5, 2 and10) and six load parameters (Q =0, 50, 100, 150, 200 and 250). It can be easily observed that the linear and the nonlinear central deflection parameters are increasing with the increase in the power-law indices, i.e., the metal-rich FG hyperbolic shell panel is comparatively more flexible than the ceramic-rich panel.

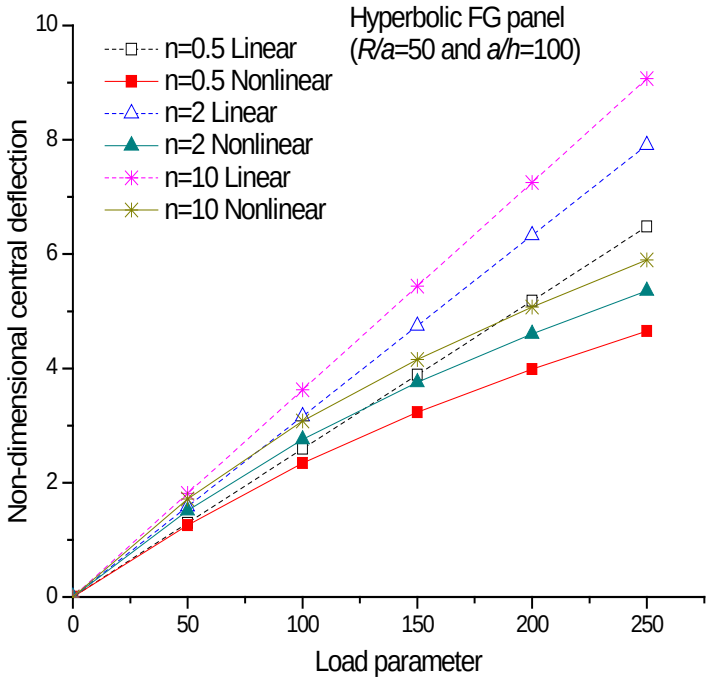

Figure 4.18 Variation of non-dimensional central deflection of simply supported hyperbolic FG panel for different power-law indices

4.3.2.3.2 Effect of thickness ratio on the linear and the nonlinear flexural behaviour of FG hyperbolic panel under mechanical load

In continuation of the above, the effect of thickness ratios on the linear and the nonlinear flexural behaviour of the FG hyperbolic shell panel under the mechanical loading is investigated. For the computational purpose, the square simply supported FG (Al/ZrO_2) hyperbolic shell panel (R/a=50 and n=2) is analysed for four thickness ratios (a/h = 5, 10, 20 and 50) and presented in Figure 4.19. The load parameters are taken same as in the previous example. It is clearly observed that the linear non-dimensional central deflections are decreasing as the thickness ratio increases whereas the nonlinear responses are not following any monotonous behaviour. It is also important to mention that the deviation of the responses indicates the effect of full nonlinearity in the framework the HSDT kinematics for small strain large deformation regime. In addition, such behaviour may be due to the unequal curvature of the hyperbolic panel.

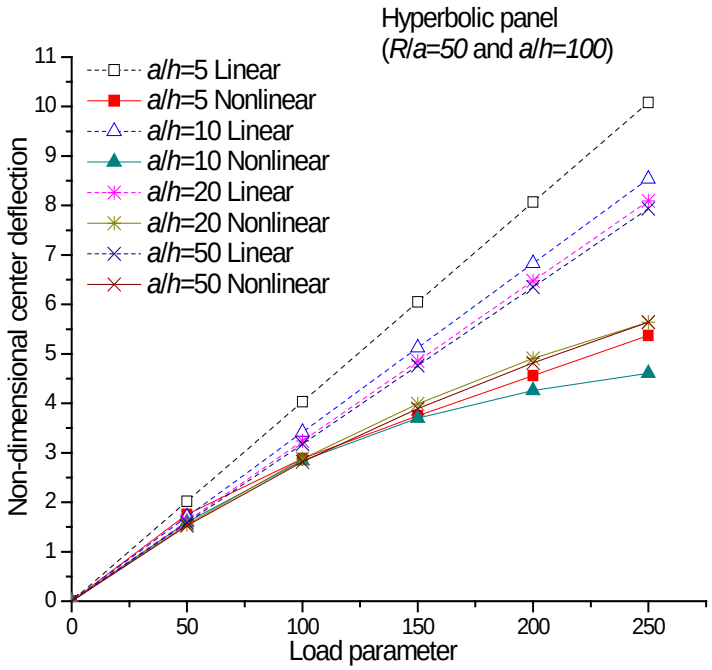

Table 4.19 Variation of non-dimensional central deflection with thickness ratios and load parameters for simply supported curved FG panels

4.3.2.3.3 Effect of curvature ratio on the linear and the nonlinear flexural behaviour of FG hyperbolic panel under mechanical load

Now in this example, the linear and the nonlinear non-dimensional central deflections of the simply supported square FG (Al/ZrO_2) shell panel (a/h=100 and n=2) is analysed for three curvature ratios (R/a=10, 50 and 100) and six load parameters (Q =0, 50, 100, 150, 200 and 250) and presented in Figure 4.20. It is observed that the effect of the curvature ratios on the linear and the nonlinear central deflection parameters of the FG hyperbolic shell panel are insignificant. It may be due the positive and the negative curvatures of hyperbolic shell panel.

4.3.2.3.4 Effect of aspect ratio on the linear and the nonlinear flexural behaviour of FG hyperbolic panel under mechanical load

The variation of non-dimensional central deflections of the square simply supported FG (Al/ZrO_2) hyperbolic shell panel (n=2, a/h=100, R/a=50) for four aspect ratios (a/b = 1, 1.5, 2 and 2.5) is investigated in this example and presented in Figure

4.21. It is observed that the linear and the nonlinear central deflection parameters are decreasing as the aspect ratios increase. It is also noted that the nonlinearity effect becomes insignificant for the higher aspect ratios as well.

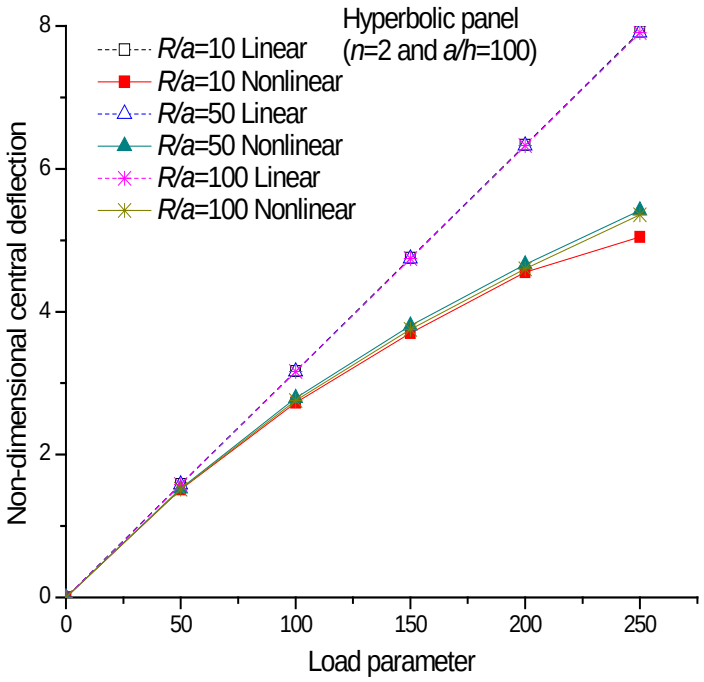

Figure 4.20 Variation of non-dimensional central deflection of square simply supported FG hyperbolic shell panel for different curvature ratios

4.3.2.3.5 Effect of support condition on the linear and the nonlinear flexural behaviour of FG hyperbolic panel under mechanical load

In this example, the effect of support conditions (SSSS, CCCC, SCSC and HHHH) on the linear and the nonlinear non-dimensional central deflections of the square FG (Al/ZrO_2) hyperbolic shell panel (n=2, a/h=100, R/a=50) is examined and plotted in Figure 4.22. It is observed that the deflection parameters are increasing with the decrease in the number of constraints, i.e., the non-dimensional central deflections are maximum

and minimum in SSSS and CCCC type support cases, respectively. However, the linear and the nonlinear responses are almost same in the case of CCCC and SCSC supports. Further, in the subsequent examples, the flexural behaviour of the FG hyperbolic shell panels are examined under the thermomechanical loading including the effect of temperature-dependent material properties.

4.3.2.3.6 Effect of power-law indices on the linear and the nonlinear flexural behaviour of FG hyperbolic panel under thermomechanical load

The influence of power-law indices (n=0.2, 5) on the linear and the nonlinear deflection parameters of the FG (Si_3N_4/*SUS304*) hyperbolic shell (R/a=50, a/h=10, a/b=1) panel is analysed under thermomechanical loading. The responses are computed for three temperature field (uniform, linear and nonlinear) and five mechanical loads (Q=0, 50, 100, 150 and 200), and presented in Table 4.13. It is observed that the linear and the nonlinear deflection parameters are increasing with the increase in power-law indices. It is also noted that the deflection parameters are higher in the case of the TD-FG hyperbolic shell panel than the TID-FG panel irrespective of the thermal fields. In the case of the TD-FG shell panel, the maximum deflection is observed for the uniform temperature field whereas minimum in case of the nonlinear temperature field. However, a reverse trend is also noticed for the TID-FG shell panel, i.e., the deflection parameter is minimum for uniform temperature field in conjunction with the mechanical load. It is also interesting to note that the differences between the deflection parameters of the TID-FG panel subjected to the linear and the nonlinear temperature fields are insignificant.

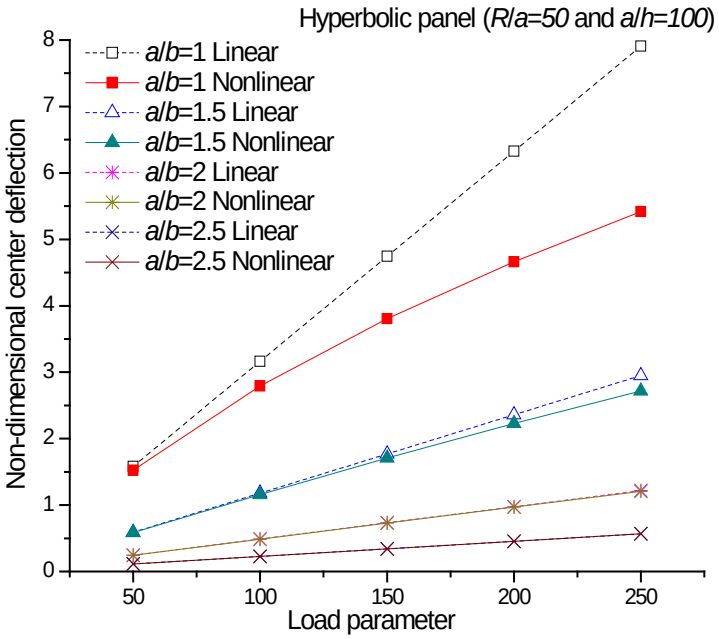

Figure 4.21 Variation of non-dimensional central deflection of simply supported FG hyperbolic shell panel for different aspect ratios

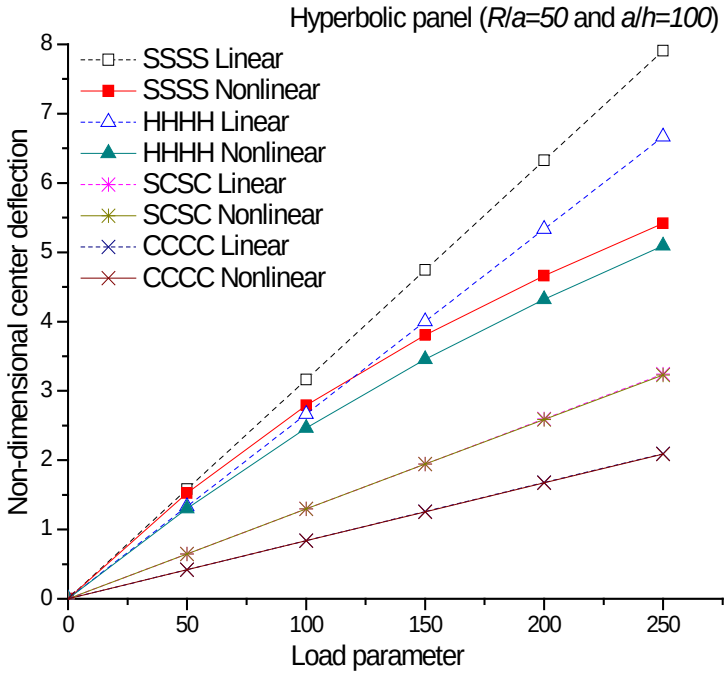

Figure 4.22 Variation of non-dimensional central deflection of square hyperbolic FG panel for different support conditions

4.3.2.3.7 Effect of thickness ratio on the linear and the nonlinear flexural behaviour of FG hyperbolic panel under thermomechanical load

In this example, the effect of thickness ratios on the linear and the nonlinear deflection parameters of the FG (Si_3N_4/*SUS304*) hyperbolic shell panel is examined under the thermomechanical load and presented in Table 4.14. The loading conditions are taken same as in the previous example. It is observed that the linear deflection parameters are decreasing with the increase in the thickness ratios. However, the nonlinear deflection parameters are increasing with the increase in the thickness ratios. The other observations related to the TD/TID and the temperature fields on the deflection parameters are similar as reported in the previous example.

4.3.2.3.8 *Effect of curvature ratio on the linear and the nonlinear flexural behaviour of FG hyperbolic panel under thermomechanical load*

Table 4.15 presents the linear and the nonlinear deflection parameters of the FG (Si_3N_4/*SUS304*) hyperbolic shell panel for different curvature ratios (R/a=10 and 20). The thermal and the mechanical loads are taken same as in the previous example. It is observed that the linear and the nonlinear deflection parameters are reducing with the increase in curvature ratios. The influences of other parameters such as the TD/TID, the temperature distribution on the deflection parameters of the FG hyperbolic shell panel are following the same trend as in the previous examples.

4.3.2.3.9 *Effect of aspect ratio on the linear and the nonlinear flexural behaviour of FG hyperbolic panel under thermomechanical load*

Here in this example, the effect of aspect ratios (a/b=2, 2.5) on the linear and the nonlinear deflection parameters of the FG (Si_3N_4/*SUS304*) hyperbolic shell panel is examined under thermomechanical loading conditions and presented in Table 4.16. It is observed that the linear and the nonlinear deflection parameters are decreasing with the increase in the aspect ratios. The deflection parameters are following the similar fashion for the TD/TID and the temperature fields as in the previous sections.

4.3.2.3.10 *Effect of support condition on the linear and the nonlinear flexural behaviour of FG hyperbolic panel under thermomechanical load*

Table 4.17 presents the linear and the nonlinear deflection parameters of the FG (Si_3N_4/*SUS304*) hyperbolic shell panel under thermomechanical loading conditions. The responses are obtained for two different support conditions (CCCC and SCSC). It is observed that the linear and the nonlinear central deflection parameters are maximum in the FG hyperbolic shell panel with SCSC support condition and minimum in CCCC support case, i.e., the increment in the number of support constraints reduces the deflection parameters.

4.3.2.4 Elliptical FG shell panel

The previous sections discussed the flexural responses of the FG (spherical/cylindrical/hyperbolic) shell panels under mechanical and/or thermal load. Now, to show the effect of different parameters on the flexural responses of the FG elliptical (R_x=R, R_y=$2R$) shell panel under thermomechanical loading, various numerical experimentations are conducted and discussed in the following subsections.

4.3.2.4.1 Effect of power-law index on the linear and the nonlinear flexural behaviour of FG elliptical panel under mechanical load

In this example, the influence of power-law indices on the deflection parameters of the FG elliptical shell panel are examined under UDL (Q = 0, 50, 100, 150, 200 and 250). Figure 4.23 shows the non-dimensional central deflections of the square simply supported FG (Al/ZrO_2) elliptical shell panel (R/a=50 and a/h=100) for three power-law indices (n= 0.5, 2 and 10) (Kar and Panda, 2015b). It is observed that the linear and the nonlinear non-dimensional central deflections are increasing with the increase in the power-law indices, i.e., the deflection parameter of the ceramic-rich FG elliptical shell panel is lower than the metal-rich FG panel, and the responses are within the expected line.

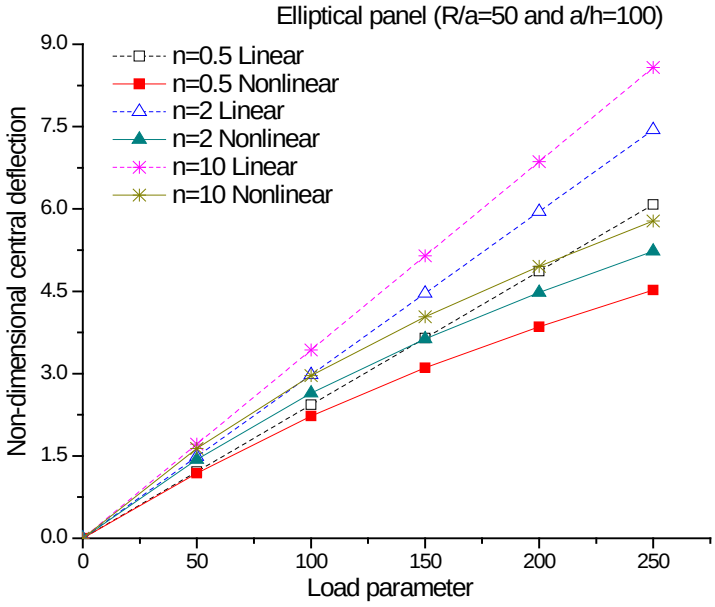

Figure 4.23 Variation of non-dimensional central deflection of simply supported elliptical FG shell panel for different power-law indices

4.3.2.4.2 Effect of thickness ratio on the linear and the nonlinear flexural behaviour of FG elliptical panel under mechanical load

In this example, the effect of thickness ratio on the linear and the nonlinear non-dimensional central deflection parameter of the FG elliptical shell panel is analysed and shown in Figure 4.24. For the computational purpose, the square simply supported FG (Al/ZrO_2) elliptical shell panel (R/a=50 and n=2) is considered for four different thickness ratios (a/h = 5, 10, 20 and 50). It is clearly observed that the linear non-dimensional central deflections are decreasing with the increase in the thickness ratios whereas the nonlinear responses are not following any monotonous behaviour, and it may be due the inclusion of all the nonlinear higher-order terms in the mathematical model.

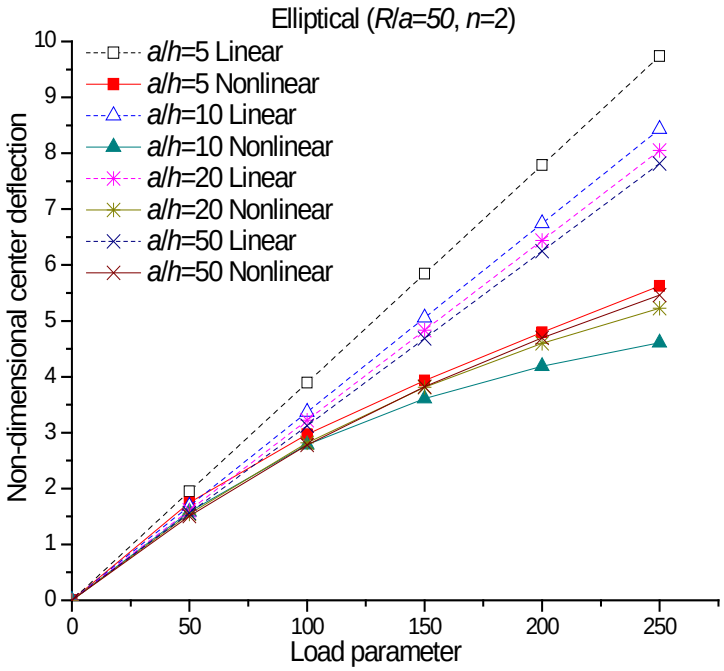

Figure 4.24 Variation of non-dimensional central deflection of simply supported elliptical FG shell panel for thickness ratios

4.3.2.4.3 Effect of curvature ratio on the linear and the nonlinear flexural behaviour of FG elliptical panel under mechanical load

The effect of the curvature ratios on the flexural behaviour of the FG elliptical shell panel is investigated in the present problem. Figure 4.25 presents the linear and

nonlinear non-dimensional central deflections of the square simply supported FG (Al/ZrO_2) elliptical shell panel (a/h=100 and n=2) for three different curvature ratios (R/a=10, 50 and 100). The load parameters are considered to be same as in the earlier example. It is observed that both the linear and the nonlinear central deflection parameters are increasing with the increase in curvature ratios.

4.3.2.4.4 Effect of aspect ratio on the linear and the nonlinear flexural behaviour of FG elliptical panel under mechanical load

In this example, the non-dimensional central deflections of the simply supported square FG (Al/ZrO_2) elliptical shell panel (n=2, a/h=100 and R/a=50) are investigated for four aspect ratios (a/b=1, 1.5, 2 and 2.5) and presented in Figure 4.26. It can be observed that the linear and nonlinear central deflection parameters are decreasing as the aspect ratios increase. It is also noted that the nonlinearity effect becomes insignificant for higher aspect ratios.

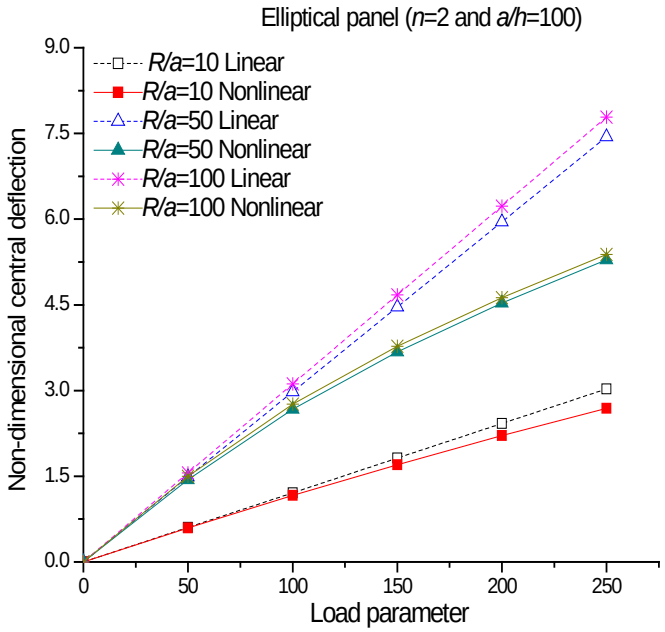

Figure 4.25 Variation of non-dimensional central deflection of square simply supported elliptical FG shell panel for different curvature ratios

4.3.2.4.5 Effect of support condition on the linear and the nonlinear flexural behaviour of FG elliptical panel under mechanical load

The effect of different support conditions (SSSS, CCCC, SCSC and HHHH) on the non-dimensional central deflections of the square FG (Al/ZrO_2) elliptical shell panel (n=2, a/h=100 and R/a=50) is examined in this example and presented in Figure 4.27. It is observed that the deflection parameters are increasing with the decrease in the number of constraints, i.e., the non-dimensional central deflections are lower for the CCCC support case and higher in the SSSS support case. However, the nonlinearity is insignificant for the CCCC and the SCSC support cases.

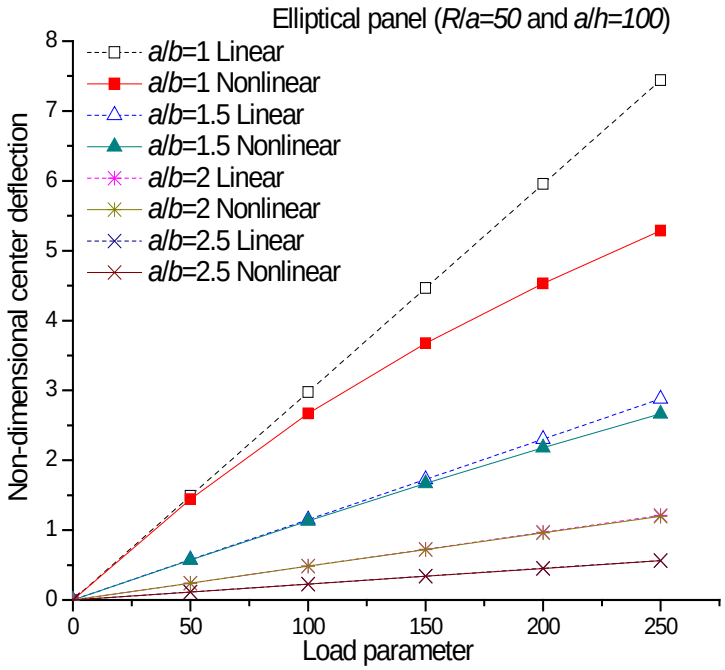

Figure 4.26 Variation of non-dimensional central deflection of simply supported elliptical FG shell panel for different aspect ratios

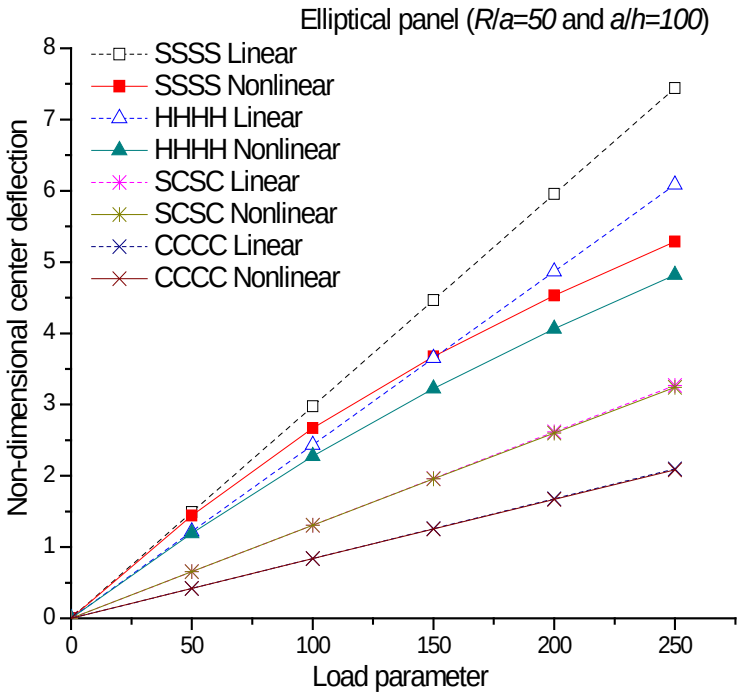

Figure 4.27 Variation of non-dimensional central deflection of square elliptical FG panel for different support conditions

4.3.2.4.6 Effect of power-law index on the linear and the nonlinear flexural behaviour of FG elliptical panel under thermomechanical load

In the previous examples of FG elliptical shell panel, the flexural responses are obtained for the mechanical load only. Here, the effect of power-law indices (n=0.2 and 5) on the linear and the nonlinear deflection parameters of the FG ($Si_3N_4/SUS304$) elliptical shell (R/a=50, a/h=10 and a/b=1) panel is examined under the combined mechanical and the thermal loading. The responses are obtained for three different temperature loads (uniform, linear and nonlinear) and UDL (Q=0, 50, 100, 150 and 200), and presented in Table 4.18. It is observed that the linear and the nonlinear deflection parameters are increasing with the increase in power-law indices. It is also noted that the deflection parameters are higher for the TD-FG elliptical shell panel than the TID case irrespective of the temperature field. In case of the TD-FG elliptical shell panel, the maximum and the minimum deflection parameters are observed for the uniform and the

nonlinear temperature fields, respectively. However, a reverse trend is noticed in the TID-FG elliptical shell panel, i.e., the minimum deflection is observed for the panel under uniform temperature field. It is also interesting to note that the differences between the deflection parameters of the TID-FG panel subjected to the linear and the nonlinear temperature field are also insignificant.

4.3.2.4.7 Effect of thickness ratio on the linear and the nonlinear flexural behaviour of FG elliptical panel under thermomechanical load

The effect of thickness ratios (a/h=10, 20) on the linear and the nonlinear deflection parameters of the FG ($Si_3N_4/SUS304$) elliptical shell panel is examined under thermomechanical load and presented in Table 4.19. It is observed that the linear deflection parameters are decreasing with the increase in the thickness ratios. However, the nonlinear deflection parameters are increasing with the increase in the thickness ratios. The other observations related to the TD/TID and the temperature field on the deflection parameters are similar to the previous example.

4.3.2.4.8 Effect of curvature ratio on the linear and the nonlinear flexural behaviour of FG elliptical panel under thermomechanical load

The effect of curvature ratios (R/a=10 and 20) on the linear and the nonlinear deflection parameters of FG ($Si_3N_4/SUS304$) elliptical shell panel are examined under thermomechanical loading conditions and presented in Table 4.20. It is observed that the linear and the nonlinear deflection parameters are increasing with the increase in curvature ratios. The influences of other parameters such as TD/TID and the temperature distribution on the deflection parameters of FG elliptical shell panel are following the same trend as in the previous examples.

4.3.2.4.9 Effect of aspect ratio on the linear and the nonlinear flexural behaviour of FG elliptical panel under thermomechanical load

Now, the effect of aspect ratios (a/b=2, 2.5) on the linear and the nonlinear deflection parameters of the FG ($Si_3N_4/SUS304$) elliptical shell panel is examined under

thermomechanical loading and presented in Table 4.21. It is observed from the table that the linear and the nonlinear deflection parameters are decreasing with the increase in aspect ratios. The deflection parameters are following the similar behaviour for the TD/TID and the temperature fields as in the previous section.

4.3.2.4.10 Effect of support condition on the linear and the nonlinear flexural behaviour of FG elliptical panel under thermomechanical load

Table 4.22 presents the linear and the nonlinear deflection parameters of the FG (Si_3N_4/*SUS304*) elliptical shell panel under thermomechanical loading for two different support conditions (CCCC and SCSC). It is observed that the linear and the nonlinear deflection parameters are maximum and the minimum for the SCSC and the CCCC type supports, respectively, i.e., the increase in the number of support constraints reduces the deflection parameters.

4.3.2.5 Effect of Shell Geometry on Flexural Behaviour

In this example, the effects of various FG (Si_3N_4/*SUS304*) shell geometries (flat, spherical, cylindrical, hyperbolic and elliptical) on the linear and the nonlinear deflection parameters are examined under thermomechanical load. The responses are obtained for two support conditions (*SSSS* and *SCSC*) under UDL and nonlinear temperature field. The responses are provided in Table 4.23. It is observed that the linear and the nonlinear deflection parameters are increasing in the ascending order of spherical, hyperbolic, elliptical, cylindrical and flat, i.e., the spherical FG shell panel is stiffer than other shell geometries.

4.4 Conclusions

In this chapter, the linear and nonlinear flexural behaviour of different geometries of FG shell panels (spherical, cylindrical, hyperbolic and elliptical) are analysed under the thermomechanical load. The flexural responses are obtained for both the TD and TID material properties under the uniform, linear and nonlinear temperature fields. The responses are computed using the general nonlinear mathematical model of the FG shell panel developed based on the HSDT kinematics and Green-Lagrange nonlinearity. In addition, all the nonlinear higher order terms are included in the mathematical model to compute the exact flexure of the shell panel under the combined action of loading. The effective properties of the FG shell panels are evaluated using Voigt micromechanical model in conjunction with the power-law distribution. The governing differential equation is derived using the variational principle and discretised with the help of suitable isoparametric FE steps. The desired responses are computed numerically using a direct iterative method. The convergence behaviour of the present model has been checked and validated by comparing the present responses to that of the available published literature and with the commercial finite element tool, i.e., ANSYS. In order to show the efficacy of the present model, the study has been extended for different geometrical and material parameters of FG shell panels under thermomechanical load. Wide varieties of numerical

examples have been solved, and the final closures on the various parametric studies are discussed in the following lines.

a) It is evident from the validation study that the presently developed nonlinear higher-order model with Green-Lagrange type geometrical nonlinearity is more realistic as compared to the FSDT/HSDT and von-Karman type nonlinearity under mechanical and/or thermal load.

b) The metal-rich FG shell panel exhibits maximum deflection than the ceramic-rich FG shell panel, irrespective of the geometrical parameters, the shell geometries and the loading conditions.

c) The flexural responses of FG shell panel are prominently affected by varying the aspect ratios in all the considered cases. It is observed that the linear and nonlinear central deflection parameters are reducing as the aspect ratios increase. However, the nonlinearity effect is insignificant for the shell geometries at higher aspect ratios.

d) The non-dimensional linear deflection parameters are reducing with the increase in the thickness ratios whereas the nonlinear deflections are not following the same trend for each type of FG shell panel.

e) The effect of the curvature ratios on the flexural behaviour is profound in the synclastic type FG shell panels (spherical, cylindrical and elliptical) whereas, in the anticlastic type shell panel, the effect of curvature ratios on the deflection parameters are insignificant. However, the linear and the nonlinear deflection parameters are increasing as the curvature ratios increase.

f) The type of support conditions affects the flexural behaviour of the FG shell panels significantly. The linear and the non-dimensional nonlinear deflection parameters are reducing with the increase in the number of support constraints, i.e., the central deflections are maximum and minimum for the SSSS and the CCCC type of support conditions, respectively.

g) The TD-FG shell panels are more flexible as compared to TID-FG shell panels irrespective of the panel geometry and the thermal field.

h) In the case of the TD-FG shell panel, the maximum and the minimum deflections are observed for the uniform and the nonlinear temperature field.

i) The TID-FG shell panels exhibit minimum deflections under combined thermomechanical loading at uniform temperature field. It is also interesting to note that the differences between the deflection parameters of the TID-FG panel under the linear and the nonlinear temperature field are insignificant.

j) It is also noted that the deflection parameter increase with the increase in load parameters, whereas the hard spring type of nonlinearity is observed for all the

other cases of the FG shell panel.

k) The deflection parameters are increasing in the ascending order of spherical, hyperbolic, elliptical, cylindrical and flat, i.e., the spherical FG shell panel is stiffer than other shell geometries.

l) It can be concluded from the present results that the developed nonlinear mathematical model in the framework of the HSDT kinematics and Green-Lagrange nonlinearity is capable of examining the linear and the nonlinear flexural behaviour of the FG shell panels under thermomechanical loading with the desired accuracy.

CHAPTER 5
FREE VIBRATION ANALYSIS OF FG SHELL PANEL UNDER THERMAL ENVIRONMENT

5.1 Introduction

In general, the vibration can be either desirable or undesirable with respect to its application. The structural designer always strives to eliminate or to reduce the undesirable vibration effect which is the major cause of fatigue failure in any structure and/or structural components. The natural frequency of any structure needs to be evaluated for the prevention of resonance and to achieve the desired safety before the finished product. In particular, the FGM structures are developed for space related structural application to overcome the shortcomings of the laminated structure under elevated thermal environment. Hence, the FGM structure needs critical attention for the issues related to undesirable vibration under such complex environment without hampering the structural integrity. It is also true that these structures are very often exposed to the large amplitude vibration under elevated thermal environment and therefore only the linear solutions are not sufficient for the accurate prediction of the desired responses.

In this chapter, the linear/nonlinear free vibration responses of the FG shell panel have been computed numerically using the developed general mathematical model including the temperature-dependent material properties. In Section 5.2, the governing equation of the free vibrated FG shell panel under thermal environment and its solution steps are mentioned. Section 5.3 presents the convergence and validation study of the proposed mathematical model for the flat/curved FG panel with/ without temperature

field by solving the variety of numerical illustrations. The robustness and the efficacy of the presently developed model have been revealed through the comprehensive parametric study. The effects of various geometrical and material parameters and the support conditions on the linear and the nonlinear frequency responses with TD/TID properties of the FG flat/curved panels are examined under three different kind of the temperature field. Finally, the concluding remarks are drawn in Section 5.4 based on the results obtained for different parameters in Section 5.3.

5.2 Solution Methodology

The equilibrium equation of the vibrated FG shell panel under the different thermal environment (uniform and non-uniform temperature field) is derived using the variational principle as presented in Eq. (3.45). The nonlinear free vibration responses of the FG shell panel are solved using the steps of the solution technique as mentioned in Section 3.11. In this analysis, the first mode of the fundamental frequency is obtained for all different cases discussed throughout, if not specified otherwise. The nonlinearity in the system of the equation is introduced through the amplitude ratio (W_{max}/h, where W_{max} is the maximum central deflection and h is the thickness of the panel). The desired frequency responses are computed using the customised homemade computer code developed in MATLAB environment. The temperature dependent properties of the FGM constituents are obtained and utilised for the computational purpose as in Table 4.1. The effects of nonlinearity on the structural frequencies are computed in the form of frequency ratio ($\bar{\omega}_{nl} / \bar{\omega}_{l}$, ratio of nonlinear frequency and linear frequency) throughout the analysis.

5.3 Results and Discussion

The desired frequency responses are computed using a homemade customised computer code developed in MATLAB environment based on the nonlinear mathematical formulation. The convergence behaviour of the present numerical model has been obtained for the TD or TID properties of the FG shell panel under thermal environment for different geometrical configurations and material sets. Subsequently, the validation of the present nonlinear model is also established by comparing the responses with that of the previously published results. In order to exhibit the robustness and the applicability

of the present model wide variety of numerical examples are solved for various geometrical and material parameters, support conditions and temperature fields. Finally, the influences of different parameters on the linear and the nonlinear vibration responses of the FG shell panel under different thermal fields are discussed in details. Table 4.1 shows the TD material properties of each constituent of the FGM used in the present analysis.

5.3.1 Convergence and Validation Study

In this section, the convergence and the validation behaviour of the proposed nonlinear FE model of the FG flat/curved panel have been shown by computing the linear/nonlinear frequencies. The convergence behaviour of the present numerical results of the FG shell panel is obtained for different mesh division with TD and TID properties. Subsequently, the nonlinear model has also been validated by comparing the responses with those available published literature. The convergence and the comparison studies of the linear/nonlinear free vibration responses of the FG shell panel are performed for different geometrical configurations (flat/spherical/cylindrical), material properties (TD and TID), and the FGM constituents as well and discussed in the following subsections.

5.3.1.1 Convergence behaviour of linear free vibration responses of FG spherical panel

In this example, the convergence behaviour of the present numerical model has been obtained for the simply-supported square FG spherical shell panel and presented in Figure 5.1. The figure shows the non-dimensional fundamental frequency parameters $\left(\overline{\omega} = \omega ab / h\sqrt{(12(1-\nu_m^2)\rho_m / E_m)}\right)$ of the shell panel for three power-law indices (n= 0.5, 2 and 10) with different mesh division by taking R/a=50 and a/h=100. The metal and the ceramic constituents of the FG shell panel are taken as Aluminium (*Al*) and Zirconia (ZrO_2) at the bottom and the top surfaces of the panel, respectively. The material properties utilised for the present computational purpose are: E_m=70 GPa, ρ_m=2707 kg/m^3 for *Al*, and E_c=151GPa, ρ_c=3000 kg/m^3 for ZrO_2. For both the material constituents (metals and ceramic), the Poisson's ratio is assumed to be same, υ = 0.3. It

can easily be observed that the responses are converging well with the mesh refinement and a (6×6) mesh is sufficient to compute the desired responses further.

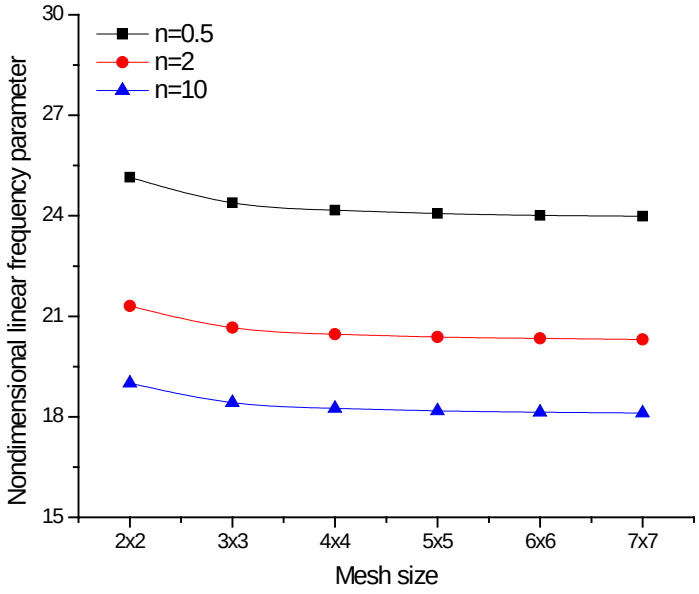

Figure 5.1 Non-dimensional linear frequency parameter of simply-supported square FG spherical panel

5.3.1.2 Convergence and comparison study of linear free vibration responses of FG spherical/cylindrical panel

In continuation of the above, another example has also been solved to show the convergence and the validation behaviour of the linear frequency parameter of the FG cylindrical panel with different FG material constituent and geometry. Figure 5.2 shows the convergence behaviour of the non-dimensional linear fundamental frequency parameters $\left(\overline{\omega} = \omega ab / h\sqrt{(12(1-\nu_m^2)\rho_m / E_m)}\right)$ of the simply-supported square FG cylindrical shell panel ($R/a=10$, $a/h=10$) for different power-law indices (n = 0, 0.5, 2, 10 and ∞). In this example, the FGM constituents are taken as alumina (Al_2O_3) and aluminium (Al) at the top and bottom surfaces, respectively. The material properties utilised for the present computational purpose are: E_m=70 GPa, ρ_m=2707 kg/m^3 and E_c=380 GPa, ρ_c=3800 kg/m^3 and υ = 0.3 for both the materials. It is observed that the responses are converging well and a (6×6) mesh is also adequate to compute the responses further as in the earlier example.

Now, the linear frequency parameters ($\bar{\omega}_l = \omega h\sqrt{\rho_c / E_c}$) are obtained for the simply-supported FG spherical shell panel using the present higher-order model and compared with Matsunaga (2008). The responses are computed for two curvature ratios and six power-law indices and presented in Table 5.1. In this example, the FGM constituents (*Al* and Al_2O_3) and the geometrical parameters (a/h=10) are taken same as in the reference. It is observed that the responses obtained using the present numerical model has good agreement with that to the 2D exact solutions and each parameter as well.

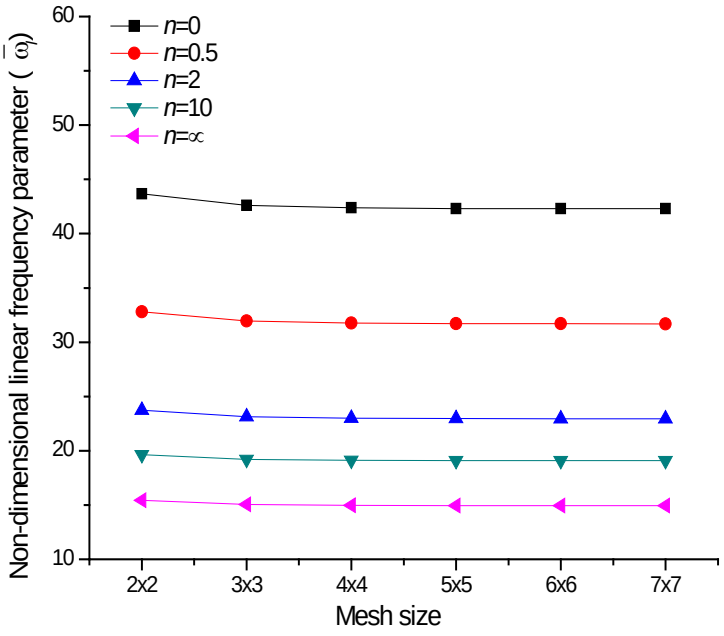

Figure 5.2 Non-dimensional linear frequency parameter of a simply-supported square FG cylindrical panel for different mesh size.

In continuation to the earlier examples, one more example has also been solved to show the validation behaviour of the present numerical model by comparing the responses with other available published literature (Pradyumna and Bandyopadhya, 2008). Table 5.2 shows the comparison study of the frequency responses of simply-supported FG (Al/Al_2O_3) spherical and cylindrical panels for three curvature ratios (R/a = 5, 10 and 50) and three power-law indices (n=0, 0.2 and 10). The present results are also showing good agreement with the finite element solutions in the framework of the HSDT in conjunction with Sander's assumption.

5.3.1.3 Convergence and comparison study of nonlinear free vibration responses of FG flat/cylindrical panel

Based on the convergence and the comparison behaviour of the linear responses, the present numerical model has been extended further to show the competency for the nonlinear analysis of the FG flat/curved panels. In the present example, the convergence and comparison behaviour of the nonlinear frequencies have been examined for the FG flat panel. It is well known that the flat panels are the simplest form of the curved panel of the infinite radius of curvature. Figure 5.3 presents the frequency ratios of the simply-supported square FG flat panel (a/h=10, n=2) for different amplitude ratios and mesh size. The present FG panel is comprised of stainless steel (*SUS304*) and silicon nitride (Si_3N_4) as the metal and the ceramic material constituents, respectively. The material properties of the FG constituents are evaluated using the relations as in Table 4.1 at ambient condition, i.e., T=300K. It is clearly observed that the present responses are converging well with the mesh refinement and a (6×6) mesh is also sufficient to compute the further nonlinear results as in the linear case. The present results are also compared with the available published results (Sundararajan et al., 2005) for different amplitude ratios. It is interesting to note that, the present frequency ratios are comparatively lower than the reference value for each amplitude ratios. It is because the present model is developed based on Green-Lagrange nonlinearity in the framework of the HSDT instead of the FSDT kinematics and von-Karman nonlinearity as in the reference. In addition to that, the present model has also included all the nonlinear higher order terms that make

the panel model more flexible as compared to the reference. It is also worthy to mention that the von-Karman nonlinearity is unable to count the large rotation and the translational terms in total. This in turn converts the model unrealistic in nature to predict the responses when exposed to the severe nonlinearity.

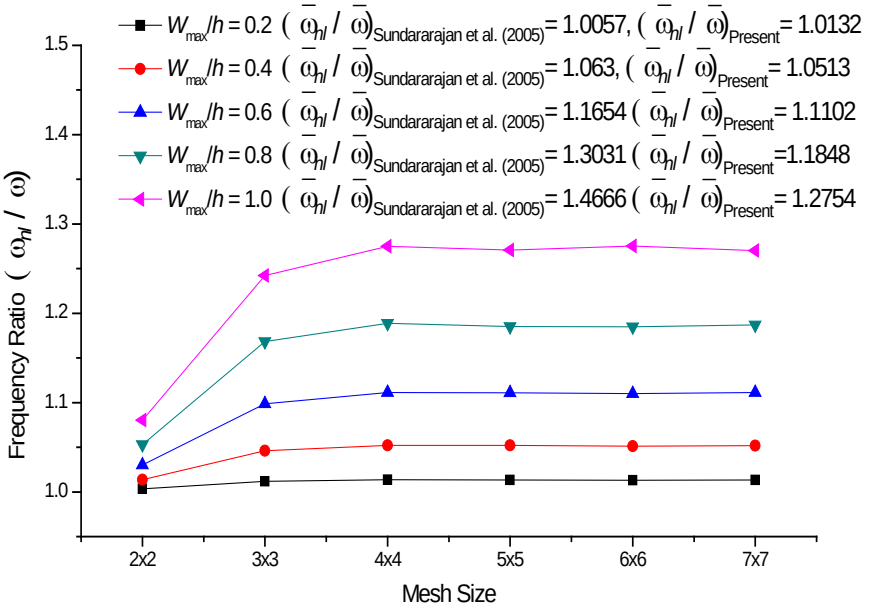

Figure 5.3 Convergence and comparison of frequency ratios of a simply-supported square FG flat panel for different amplitude ratios

In continuation of the earlier comparison study, the present model is further extended to compute for the curved panel cases. The nonlinear frequency responses of the simply-supported square FG (*Si_3N_4/SUS304*) cylindrical (*R*/*a*=2, 5, *a*/*h*=20, *n*=2.0) shell panels are obtained and presented in Table 5.3. The material properties, geometrical parameter and support conditions are taken same as Shen and Wang (2014). It is clear from the table that the present model is showing the hardened type of behaviour in all the cases for *R*/*a* = 2 however, the results follow revert behaviour for *R*/*a* = 5 and higher amplitude ratios. It is also interesting to note that the reference values are obtained based on the HSDT mid-plane kinematics and von-Karman nonlinearity instead of Green-Lagrange nonlinearity. The differences between the results are showing the necessity and requirement of the present model.

5.3.1.4 Convergence and comparison behaviour of linear and nonlinear free vibration behaviour of TD-FG flat panel under thermal environment

After the convergence and the comparison studies of the linear/nonlinear frequency parameters without thermal field and temperature independent properties of the FG flat/curved shell panel, the study is extended further for the temperature dependent properties and the elevated thermal environment. It is well known that the vibration analysis of the FG shell panel under the thermal environment with TD material properties is not only tough but also challenging. In addition, it is also necessary to incorporate the exact material behaviour for the accurate prediction of structural responses. In order to achieve the same, the present nonlinear model has been developed by introducing the TD properties of the FG panel under elevated thermal environment.

Now, the convergence behaviour of the FG shell panel model with TD properties is computed numerically using the developed nonlinear model and discussed in details. The metal and the ceramic constituents of the present FG shell panels are taken as Titanium alloy (*Ti-6Al-4V*) and zirconia (ZrO_2), respectively and the TD properties are evaluated as in Table 4.1. The responses of the simply-supported FG flat panel (a=0.2 m, a/h=8) are computed for five power-law indices (n = 0, 0.5, 1, 2, ∞) and two temperature fields (T_c=400K, T_m=300K and T_c=600K, T_m=300K) and presented in Figure 5.4. The non-dimensional fundamental frequency parameters ($\bar{\omega}_1 = \omega(a^2/h)\sqrt{(1-\nu_m^2)\rho_m / E_0}$, where E_0 denotes the Young's modulus of metal at ambient temperature) are obtained using the geometry and material properties are same as to the reference. It is observed that the present model is showing good convergence rate with mesh refinement for all different cases discussed here. It is also understood that a (6×6) mesh is sufficient to compute the linear frequency responses further. In order to show the validity of the present developed model under thermal environment, a simply-supported square FG (ZrO_2/ *Ti-6Al-4V*) flat (a =0.2 m, a/h = 8) panel is analysed for four different values of the power-law indices (n = 0, 0.5, 1 and 2) under nonlinear temperature field as shown in Figure 5.5. The material properties and geometrical parameters are taken same as in Huang and Shen (2004). The present results are showing good agreement with that to the analytical solutions except for the ceramic rich FG plate at higher temperature distribution (T_c=600K and T_m=300K). In continuation to the linear case, the convergence and comparison study of the nonlinear vibration behaviour of the FG panel under nonlinear temperature load has been computed and discussed in the following paragraphs.

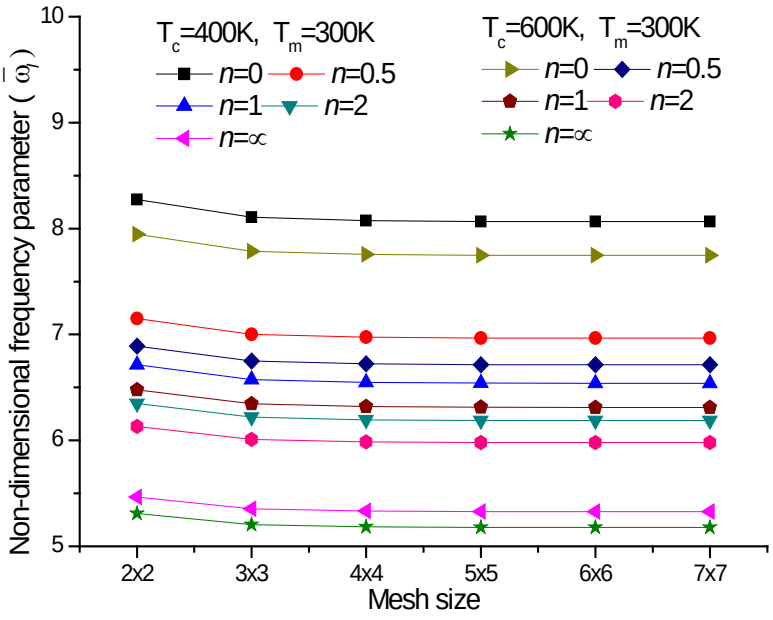

Figure 5.4 Convergence rate of frequency parameter of a square simply-supported FG flat panel

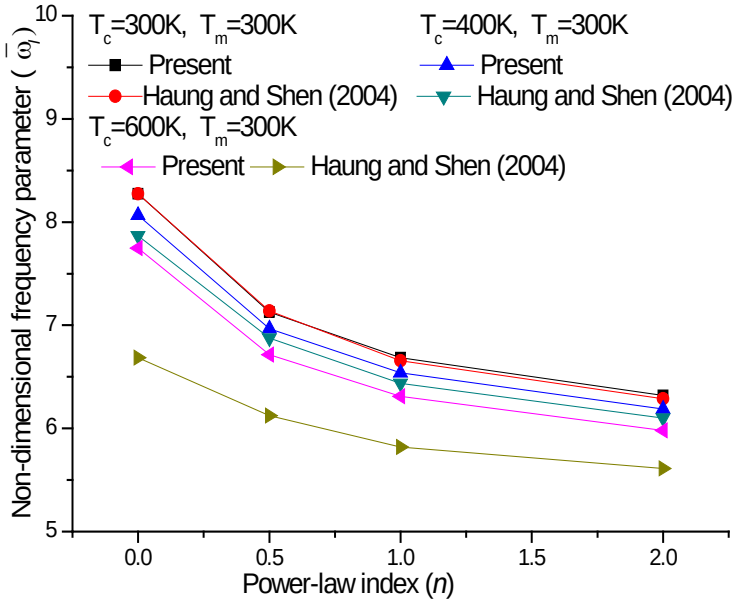

Figure 5.5 Comparison of frequency parameter of FG flat panel under nonlinear temperature field

Now, the previous example of linear vibration problem is further extended for the nonlinear analysis of the FG panel under thermal environment. The convergence

behaviour of the frequency ratios of the simply-supported square FG (*ZrO_2/Ti-6Al-4V*) flat panel is computed for different power-law indices and presented in Figure 5.6. Based on the convergence study, it is understood that a (6×6) mesh is adequate to compute both the linear and the nonlinear frequency responses comfortably. The validity of the present nonlinear model under elevated nonlinear thermal load is also established by comparing the responses with that of the available published literature. For the comparison purpose, the nonlinear frequency responses of the FG (*ZrO_2/Ti-6Al-4V*) flat panel under nonlinear temperature field with TD properties are computed based on the developed higher-order nonlinear model for different power-law indices (n = 0, 0.5, 1, 2, ∞) and the amplitude ratios (W_{max}/h= 0.2, 0.4, 0.6, 0.8 and 1.0) and presented in Table 5.4. It is clearly observed that the difference between the results increases as the amplitude ratio increases and the differences are within the expected line. The difference between the results also indicates the necessity of the proposed nonlinear model, i.e., the HSDT mid-plane kinematics with Green-Lagrange type nonlinearity instead of the HSDT with von-Karman nonlinearity as in the reference (Haung and Shen, 2004).

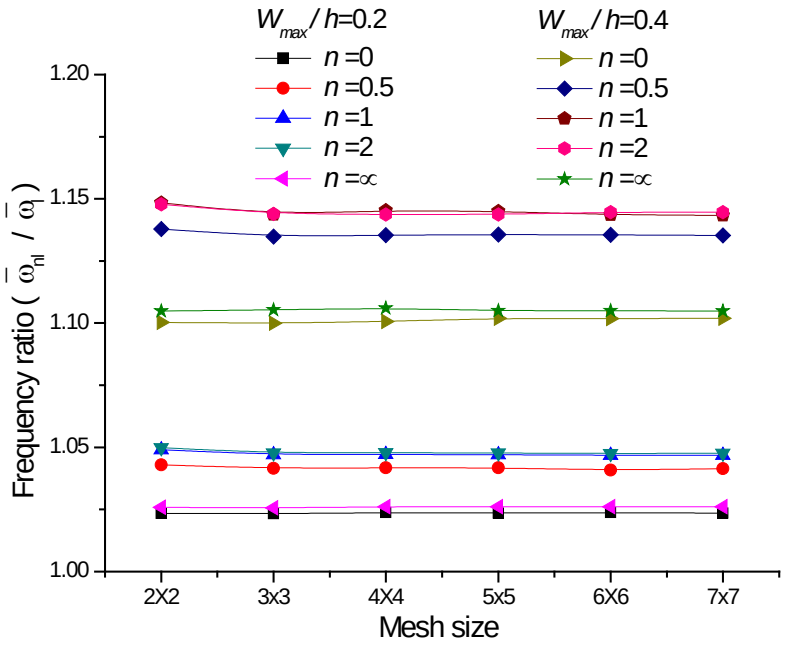

Figure 5.6 Convergence of frequency ratios of a simply supported square FG flat panel for different power-law indices

5.3.2 Numerical Illustrations and Parametric Study

The necessity and the importance of the presently developed nonlinear mathematical model have already been discussed based on various comparison and convergence study. It is also understood that the present model is capable of solving the linear and the nonlinear responses with sufficient accuracy for the FG structure under severe nonlinearity and the elevated thermal environment. In order to check the robustness of the present nonlinear finite element model, the study is extended further for different shell geometries (spherical, cylindrical, hyperbolic and elliptical), and the geometrical parameters with and without temperature field. The influences of different geometrical parameters (the thickness ratios, the curvature ratios, the aspect ratio, and the amplitude ratios), material parameter (the power-law indices), the temperature field (uniform, linear and nonlinear) and the support conditions on the linear and the nonlinear free vibration responses of the FG shell panels are examined by solving wide variety of numerical examples and discussed in details.

Further, the analysis is mainly categorised based on the type of shell geometries (spherical, cylindrical, hyperbolic and elliptical) and the effect of parameters in each panel geometries are discussed in the following subsections. The material considered for the FG shell panel without thermal field is taken as Al/ZrO_2 for throughout the analysis, if not stated otherwise. The corresponding material properties of individual constituents (metal and ceramic) of the FG shell panel at ambient temperature (300K) are taken as follows:

Aluminium (Al): E_m=70 GPa, ρ_m=2707 kg/m^3 and υ_m= 0.3 and

Zirconia (ZrO_2): E_c=151GPa, ρ_c=3000 kg/m^3 and υ_c = 0.3.

Similarly, the thermal load is also introduced in the present analysis by considering both the properties of FG shell panel say, TD and TID. The material constituents are considered for the analysis purpose as, $SUS304/Si_3N_4$. The TD material properties of the individual metal and ceramic constituents namely, $SUS304$ and Si_3N_4 are provided in Table 4.1. In addition to that the temperature variation through the thickness of the FG shell panel has been introduced by taking the top (ceramic-rich) and the bottom (metal-rich) surface temperatures as T_c=600K and T_m=300K, respectively. The linear and

the nonlinear frequency responses are non-dimensionalised using the following formula as:

$$\bar{\omega}_{l,nl} = \omega(a^2 / h)\sqrt{(1-\nu_m^2)\rho_m / E_0} \quad \ldots (5.1)$$

where, E_0 denotes the metal Young's modulus at ambient temperature, i.e., at T=300K.

5.3.2.1 Spherical FG shell panel

In the following subsections, the influence of different parameters (material and geometry) on the linear and the nonlinear vibration responses of the FG spherical (R_x=R_y=R) shell panel are computed for with and without thermal load including the TD and TID properties.

5.3.2.1.1 Effect of power-law index on the linear and the nonlinear vibration behaviour of FG spherical panel

The power-law index is one of the important factors for the FGM property evaluation and it also alters the stiffness behaviour of the structure subsequently. Figure 5.7 shows the frequency ratio of simply-supported square FG (Al/ZrO_2) shell panel (R/a=5, a/h=10) for five different amplitude ratios (W_{max}/h=0.2, 0.4, 0.6, 0.8 and 1.0) and

the power-law indices (n= 0.5, 2, 5). It is observed that the frequency ratios and the non-dimensional linear frequency parameters are decreasing with increase in power-law indices. It is because the n value decides the fraction of individual constituents, i.e., metal or ceramic rich FGM and the stiffness of the FG material also changes accordingly. It is true that the metal has comparatively low stiffness in comparison to the ceramic material and the present responses within the expected line (Kar and Panda, 2015c).

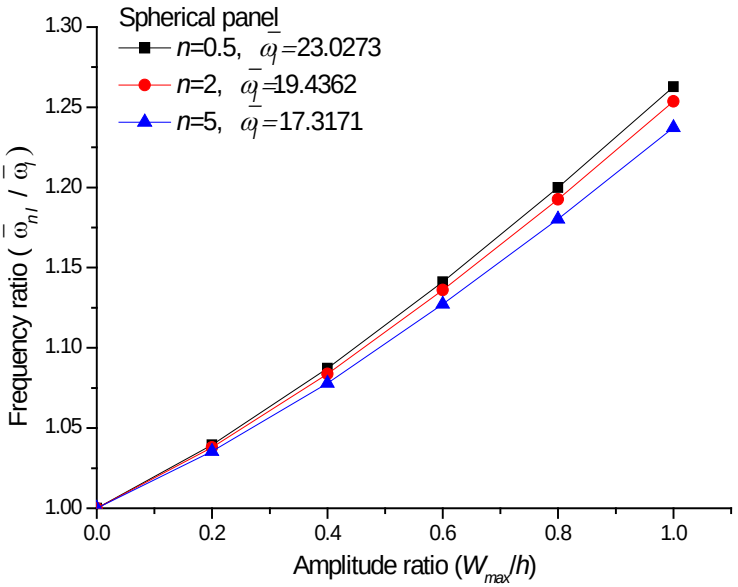

Figure 5.7 Influence of power-law index on frequency ratio of simply-supported square FG spherical (R/a=5, a/h=10) panel

5.3.2.1.2 Effect of thickness ratio on the linear and the nonlinear vibration behaviour of FG spherical panel

The stiffness of any structure or structural component majorly depends on their thickness value and this in turn affects the frequency responses largely. In this section, the linear and the nonlinear free vibration behaviour of the FG spherical panel are examined for different thickness ratios. Figure 5.8 represents the effect of four thickness ratios (a/h= 5, 10, 20 and 100) on the frequency responses of square simply-supported FG (Al/ZrO_2) spherical shell panel (R/a=5, n=2) for different amplitude ratios (W_{max}/h=0.2, 0.4, 0.6, 0.8 and 1.0). It is clearly observed that the linear frequency parameters and the frequency ratios are increasing as the thickness ratio increases. It is

also interesting to note that the frequency ratios are showing a reverse trend for the thin (a/h =100) FG spherical shell panel. This is because the thin structures may not follow the monotonous behaviour for small strain and large (finite) deformation problem.

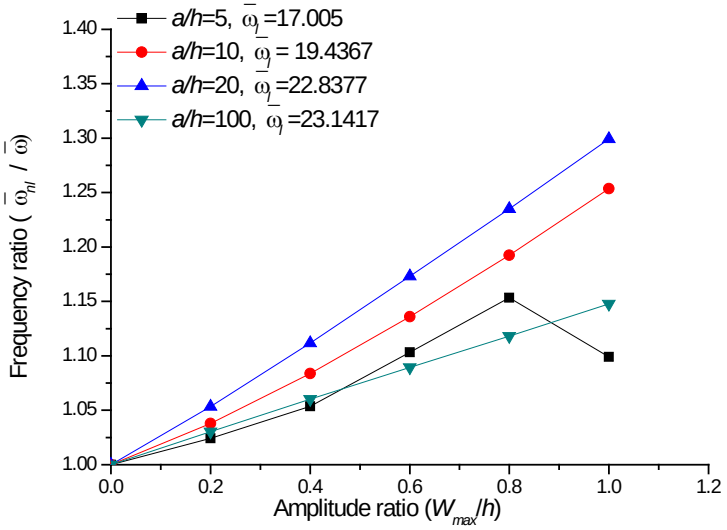

Figure 5.8 Influence of thickness ratio on frequency ratio of simply-supported square FG spherical panel

5.3.2.1.3 Effect of curvature ratio on the linear and the nonlinear vibration behaviour of FG spherical panel

The curved geometries are capable of bearing an extra amount of load due to their higher membrane strength in comparison to the flat geometries. In this example, the effect of different curvature ratios (R/a=5, 10, 20 and 50) and different amplitude ratios (W_{max}/h=0.2, 0.4, 0.6, 0.8 and 1.0) on the linear and the nonlinear frequency parameters are examined and presented in Figure 5.9. For the computational purpose, the simply-supported square FG (Al/ZrO_2) spherical shell panel is considered by setting other geometrical and material parameters as n=2, a/h=10. It is observed that the linear frequency parameters and the frequency ratios are decreasing with the increase in curvature ratios. It is because the curvature ratio increases the panel become flat and the

overall structural stiffness reduces considerably. It is also observed that the frequency ratios are increasing as the amplitude ratios increase.

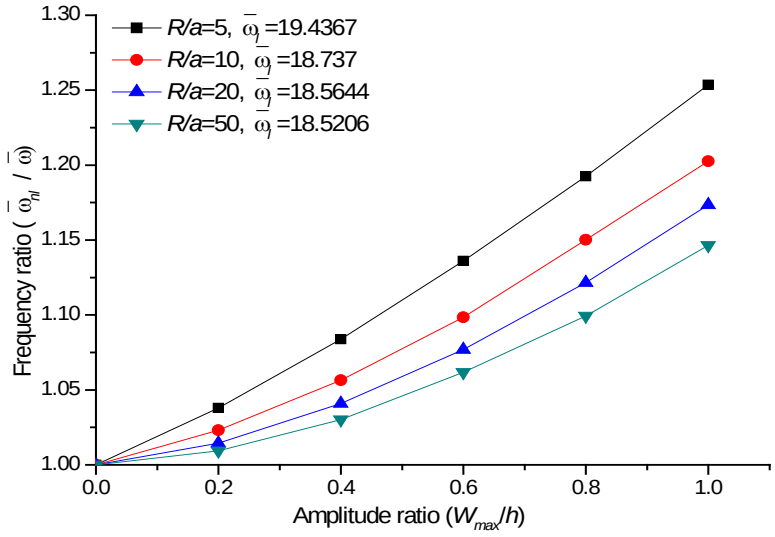

Figure 5.9 Influence of curvature ratio on frequency ratio of simply-supported square FG spherical panel

5.3.2.1.4 Effect of aspect ratio on the linear and the nonlinear vibration behaviour of FG spherical panel

The aspect ratio is one of the important factors for any panel geometry and it is prominent for thin structures in particular. It is because, as the structural components become thin the geometrical instability increases and finally it affects the vibration behaviour. Figure 5.10 shows the variation of frequency responses of simply-supported thin spherical FG (Al/ZrO_2) shell panel (n=2, a/h=100, R/a=50) for different aspect ratios (a/b=1, 1.5, 2, 2.5) and amplitude ratios (W_{max}/h= 0.2, 0.4, 0.6, 0.8 and 1.0). The linear responses of the FG spherical panel are increasing with the increase in aspect ratio whereas the frequency ratios are showing a reverse trend. It is true that the aspect ratio has a considerable effect on the stiffness matrix because the panel loses its square form as the aspect ratio increases.

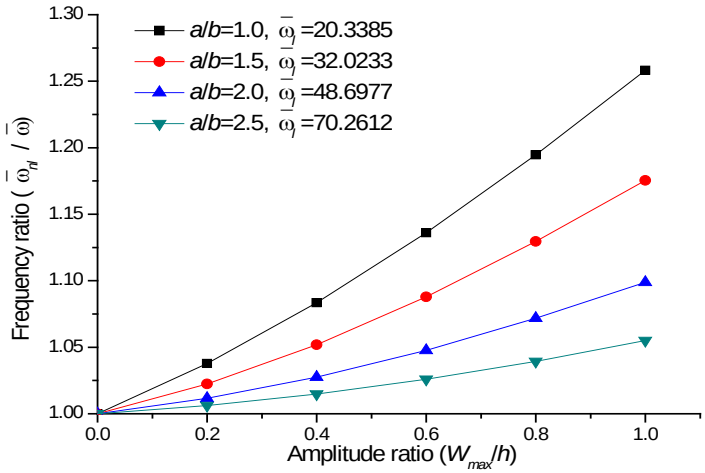

Figure 5.10 Influence of aspect ratio on frequency ratio of simply-supported FG spherical panel

5.3.2.1.5 Effect of support conditions on the linear and the nonlinear vibration behaviour of FG spherical panel

Figure 5.11 presents the frequency responses of the square FG (Al/ZrO_2) spherical shell panel (n=2, a/h=100, R/a=50) for four different support conditions (SSSS, CCCC, SCSC and HHHH) and the amplitude ratios (W_{max}/h=0.2, 0.4, 0.6, 0.8 and 1.0). It is observed that the linear responses are increasing with the increase in numbers of support constraints whereas the frequency ratios are not following any repetitive trend. The effect of nonlinearity is significant for the hinge support in comparison to all the other support cases. It is also observed that the frequency ratios are not following a monotonous behaviour with the amplitude ratios. It is because the nonlinear vibration is not only the functions of linear stiffness and mass matrix but also depending on the nonlinear stiffness matrices and their corresponding amplitude ratios as well. Hence, the non-monotonous behaviour can be observed in this example. It is interesting to note that the frequency ratios are increasing smoothly up to W_{max}/h=1.2 and then the slope changes considerably for two support conditions (HHHH and CCCC). This type of non-repetitive behaviour is observed due to the inclusion of all the nonlinear higher-order terms in the present mathematical model.

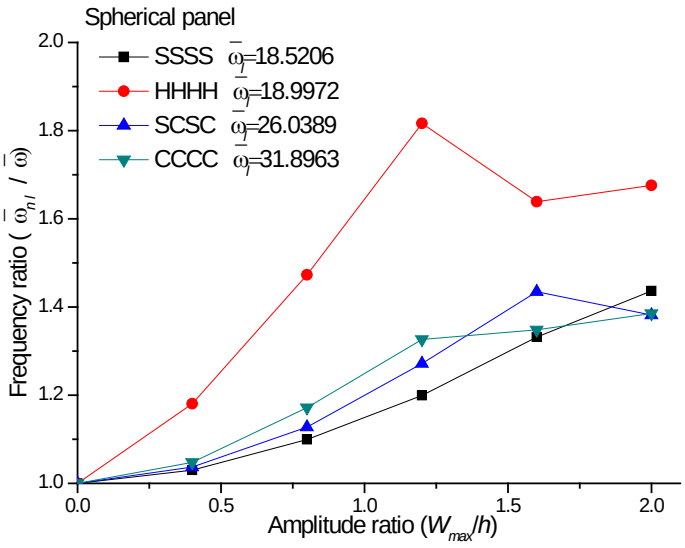

Figure 5.11 Influence of support condition on frequency ratio of square FG spherical panel

5.3.2.1.6 Effect of power-law index on the linear and the nonlinear vibration behaviour of FG spherical panel under thermal environment

Now, the frequency responses of simply-supported FG (Si_3N_4/*SUS304*) spherical (R/a=5, a/h=10 and a/b=1) panel are examined under different thermal loads for three different power-law indices (n=0.2, 2 and 5) and four amplitude ratios (W_{max}/h= 0.5, 1, 1.5 and 2). The responses are computed for three different temperature loads viz. uniform, linear and nonlinear temperature distribution through the thickness of the FG shell panel and presented in Table 5.5. The linear and the nonlinear frequency responses are decreasing with the increase in power-law indices for all three temperature distributions (uniform, linear and nonlinear). It is because of the fact that the linear and the nonlinear frequency parameters are the functions of stiffness matrix which is greatly dependent on the power-law indices. It is also true that the stiffness of the ceramic-rich ($n \to \infty$) FG panels have higher stiffness value in comparison to metal-rich ($n \to 0$). It is also noted that the frequency responses are higher in the case of TID-FG spherical panel than the TD-FG spherical panel, irrespective of the thermal fields. However, the linear frequency responses are increasing in the ascending order of nonlinear, linear and uniform temperature field, respectively. It is also observed that the frequency ratios are

maximum and minimum for the nonlinear and the uniform temperature fields, respectively.

5.3.2.1.7 Effect of thickness ratio on the linear and the nonlinear vibration behaviour of FG spherical panel under thermal environment

In this example, the linear and the nonlinear frequency responses of simply-supported FG ($Si_3N_4/SUS304$) spherical (R/a=5, n=2 and a/b=1) shell panel are examined for three different temperature loads, three different thickness ratios (a/h=20, 50 and 100) and four amplitude ratios (W_{max}/h= 0.5, 1, 1.5 and 2) and presented in Table 5.6. The linear and nonlinear frequency responses are increasing and decreasing as the thickness ratios increase for all three temperature distributions. It is due to the fact that the stiffness of any structure reduces when the structure becomes thin and the final structural frequencies are varying accordingly. It is also observed that the linear frequency parameters are higher for the FG spherical panel with TD properties whereas the frequency ratios are maximum for the TID-FG spherical panel. In addition to that the

linear frequency responses are increasing in an ascending order of the nonlinear, linear and the uniform temperature fields, respectively. However, the frequency ratios are showing a reverse trend with respect to the temperature fields.

5.3.2.1.8 Effect of curvature ratio on the linear and the nonlinear vibration behaviour of FG spherical panel under thermal environment

The linear and the nonlinear frequency responses of simply-supported FG (Si_3N_4/*SUS304*) spherical (a/h=10, n=2 and a/b=1) shell panel under different temperature load is examined for three different curvature ratios (R/a=10, 20 and 50) and four amplitude ratios (W_{max}/h= 0.5, 1, 1.5 and 2). The responses are computed under three different temperature loads namely, uniform, linear and nonlinear temperature distribution across the thickness direction, as presented in Table 5.7. In all the three cases of temperature variation the frequency (linear and nonlinear) responses are decreasing as the curvature ratios increase. It is because of the fact the membrane stiffness of the curved panel decreases as the curvature ratio increases, i.e., the overall stiffness of curved panels is comparatively higher than the flat panel. The frequency responses of the FG panels with TID properties are higher in comparison to the TD properties. It is also noted that the linear frequency responses are increasing in an ascending order of the temperature field, i.e., the nonlinear, linear and uniform, respectively, however, the frequency ratios are increasing in a reverse manner and it is expected.

5.3.2.1.9 Effect of aspect ratio on the linear and the nonlinear vibration behaviour of FG spherical panel under thermal environment

The linear and the nonlinear frequency responses of simply-supported FG (Si_3N_4/*SUS304*) spherical (a/h=10, n=2 and R/a=5) shell panel is analyzed under different temperature loads for the three aspect ratios (a/b=1.5, 2 and 2.5) and four amplitude ratios (W_{max}/h= 0.5, 1, 1.5 and 2). The responses are obtained under three different temperature loads as discussed earlier and presented in Table 5.8. In all the three cases of temperature variations, the linear frequency responses are increasing with the increase in aspect ratios whereas the frequency ratios are decreasing. It is also noted that the TID-FG panels exhibit higher linear frequencies ($\bar{\omega}_l$) as compared to the TD-FG panel.

The linear frequency responses are increasing in the ascending order of nonlinear, linear and uniform temperature field, respectively whereas the frequency ratios are not following any monotonous behaviour for the same.

5.3.2.1.10 Effect of support condition on the linear and the nonlinear vibration behaviour of FG spherical panel under thermal environment

The linear and the nonlinear frequency responses of FG ($Si_3N_4/SUS304$) spherical (a/h=10, n=2, a/b=1 and R/a=5) shell panel subjected to different temperature loads are examined for three different support conditions (CCCC, SCSC and SFSF) and four amplitude ratios (W_{max}/h= 0.5, 1, 1.5 and 2). The responses are obtained under three different temperature distributions across the thickness direction and presented in Table 5.9. In all the three cases of temperature variations, the linear frequency responses are increasing with the increase in number of support constraints, i.e., increasing in the ascending order of SFSF, SCSC and CCCC, respectively. The FG spherical panel with SFSF support condition is showing the softening type of nonlinearity whereas the hardening type of behaviour is observed in all the other cases. It is also noted that the linear frequency responses are higher in the case of TID-FG spherical panel whereas the frequency ratios are displaying non-repetitive behaviour for TD-FG shell panel. The linear frequency responses are increasing in the ascending order of nonlinear, linear and uniform temperature field, respectively whereas the frequency ratios are following the same trend as in the earlier example. The different mode shapes for two different support conditions (CCCC and SSSS) under linear temperature field are plotted in Figure 5.12.

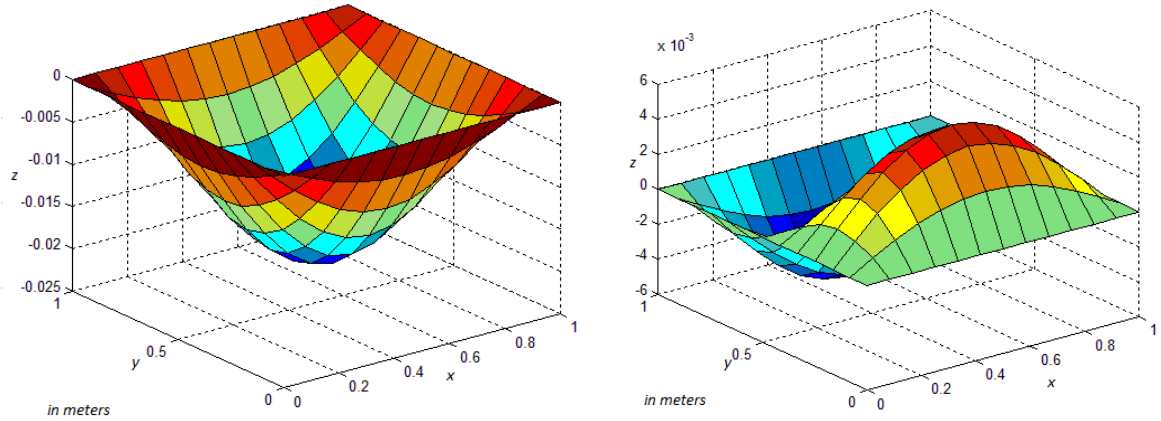

(a) 1st mode (SSSS) (b) 2nd mode (SSSS)

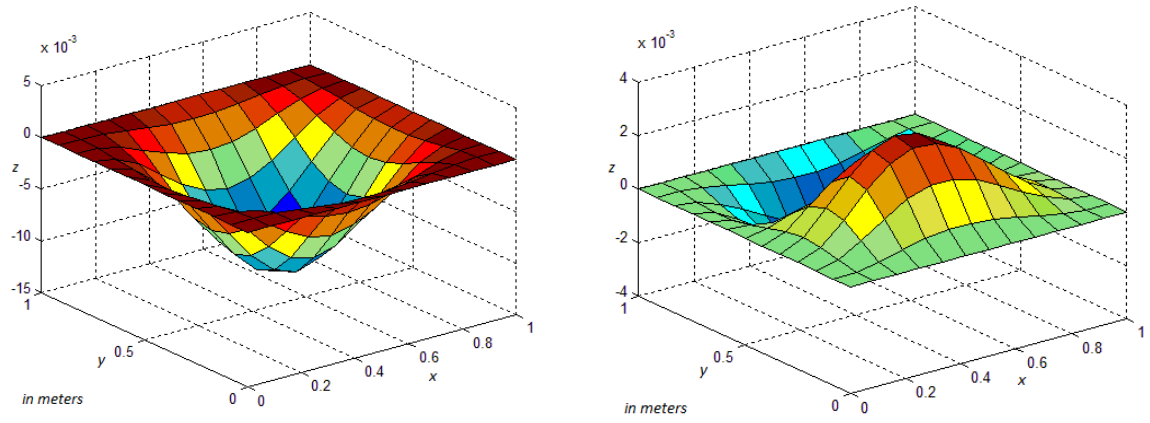

(c) 1st mode (CCCC) (d) 2nd mode (CCCC)

Figure 5.12. First and second vibration mode shapes of FG spherical panel under two different support condition (a) 1st Mode (SSSS) (b) 2nd Mode (SSSS) (c) 1st Mode (CCCC) (d) 2nd Mode (CCCC)

5.3.2.2 Cylindrical FG shell panel

The influence of different parameters on the linear and the nonlinear vibration behaviour of the FG cylindrical (R_x=R, R_y=∞) shell panel are computed with and without temperature dependent properties under various temperature field and discussed in detailed in the following subsections.

5.3.2.2.1 Effect of power-law index on the linear and the nonlinear vibration behaviour of FG cylindrical panel

Figure 5.13 show the frequency responses of simply-supported square FG (Al/ZrO_2) cylindrical shell (R/a=50, a/h=100) panel for five amplitude ratios (W_{max}/h= 0.4, 0.8, 1.2, 1.6 and 2) and three power-law indices (n=0.5, 2 and 10). It is noted that the linear and the nonlinear frequency responses are decreasing with increase in power-law indices. It is due to the fact that the FG shell panel becomes metal-rich when the 'n' value increases and the metal have comparatively low stiffness than the ceramic (Kar and Panda, 2015c).

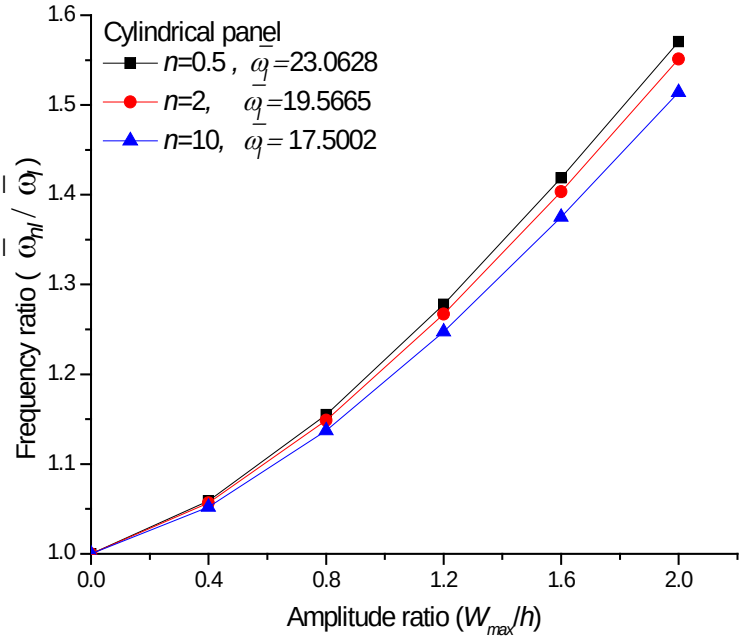

Figure 5.13 Frequency responses of FG cylindrical panel for different power-law indices

5.3.2.2.2 Effect of thickness ratio on the linear and the nonlinear vibration behaviour of FG cylindrical panel

Figure 5.14 represents the effect of four thickness ratios (a/h=10, 20, 50 and 100) on the frequency responses of square simply-supported FG (Al/ZrO_2) cylindrical shell panel (R/a=50 and n=2) for different amplitude ratios (W_{max}/h= 0.4, 0.8, 1.2, 1.6 and 2). The linear frequency and the frequency ratios are increasing with the increase in the thickness ratios and the responses are within the expected line.

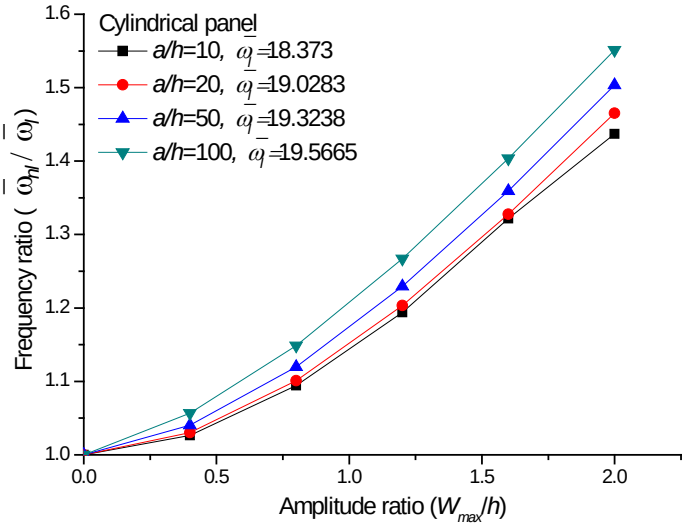

Figure 5.14 Frequency responses of FG cylindrical panel for various thickness ratios

5.3.2.2.3 Effect of curvature ratio on the linear and the nonlinear vibration behaviour of FG cylindrical panel

The effect of curvature ratios (R/a=5, 10, 20 and 50) on the frequency ratios of simply-supported square FG (Al/ZrO_2) cylindrical panel is (n=2 and a/h=100) computed for five amplitude ratios (W_{max}/h= 0.4, 0.8, 1.2, 1.6 and 2) and presented in Figure 5.15. It is observed that the non-dimensional linear frequency parameters are decreasing with the increase in curvature ratios because the overall stiffness of the panel structure reduces. However, the frequency ratios are also following the same trend as in the linear case, except for R/a=5 at W_{max}/h=1.6.

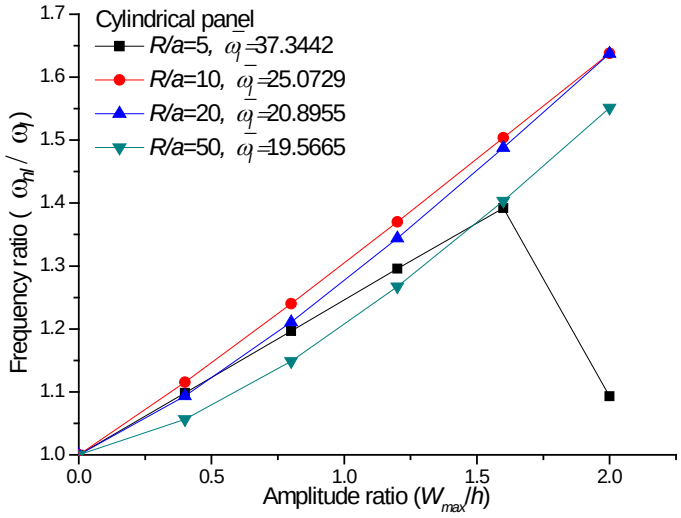

Figure 5.15 Frequency responses of FG cylindrical panel for different curvature ratios

5.3.2.2.4 Effect of aspect ratio on the linear and the nonlinear vibration behaviour of FG cylindrical panel

In this example the effect of aspect ratios (a/b=1, 1.5, 2, 2.5) on the nonlinear vibration behaviour of the simply-supported FG (Al/ZrO_2) cylindrical shell panel (n=2, a/h=100, R/a=50) is analysed for different amplitude ratios (W_{max}/h= 0.4, 0.8, 1.2, 1.6 and 2) and presented in Figure 5.16. The linear responses of the FG cylindrical shell panels are increasing with the increase in aspect ratio whereas the frequency ratios are showing a reverse trend.

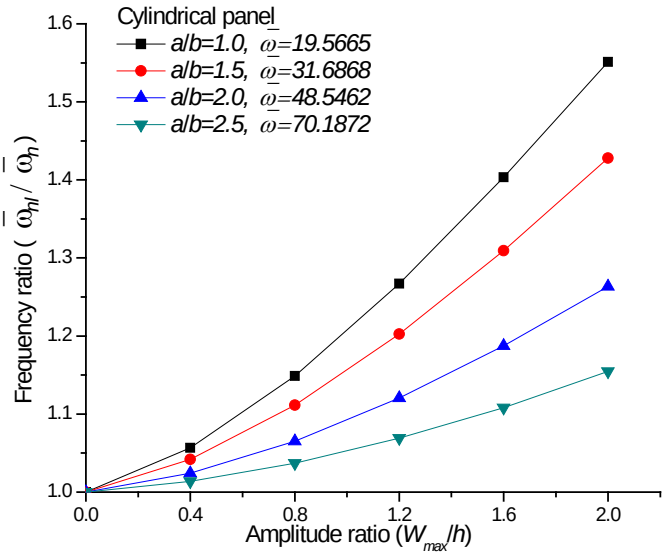

Figure 5.16 Frequency responses of FG cylindrical panel for different aspect ratios

5.3.2.2.5 Effect of support condition on the linear and the nonlinear vibration behaviour of FG cylindrical panel

The linear and the nonlinear frequency responses of square FG (Al/ZrO_2) cylindrical shell panel (n=2, a/h=100, R/a=50) are computed for five amplitude ratios (W_{max}/h= 0.4, 0.8, 1.2, 1.6 and 2) under four types of support conditions (SSSS, CCCC, SCSC and HHHH) and presented Figure 5.17. It can be clearly observed that the linear frequency responses are increasing with the increase in a number of support constraints. The effect of nonlinearity is predominant for the hinge support in comparison to other types of support conditions except for the higher amplitude ratio. It is interesting to note that the FG panels with hinge support, the frequency ratio is increasing smoothly up to W_{max}/h=1.6 and then drops suddenly. This type of non-repetitive behaviour is observed may be due to the inclusion of full nonlinearity in geometry.

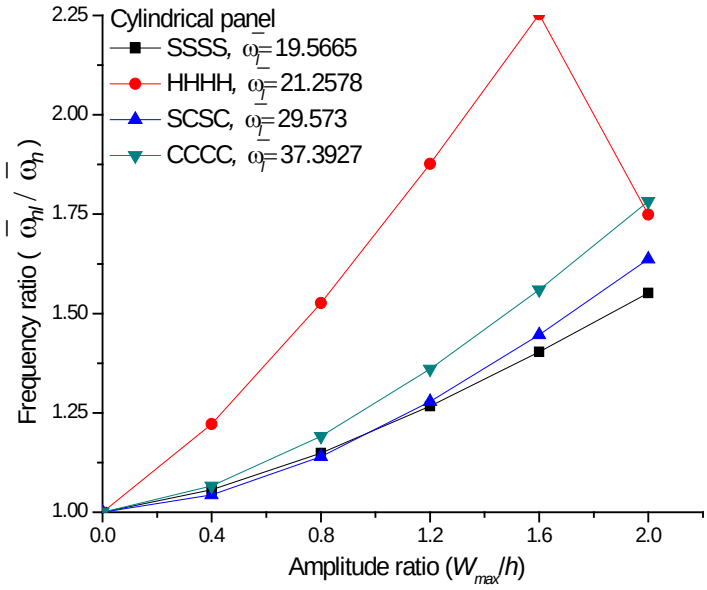

Figure 5.17 Frequency responses of FG cylindrical panel for different support conditions

5.3.2.2.6 Effect of power-law index on the linear and the nonlinear vibration behaviour of FG cylindrical panel under thermal environment

Now, the FG cylindrical panel is examined for the three temperature load distribution as discussed earlier with and without dependent material properties. In this example the frequency responses of simply-supported FG (Si_3N_4/*SUS304*) cylindrical (a/b=1, R/a=5 and a/h=10) shell panel is analysed for three power-law indices (n=0.2, 2 and 5) and four amplitude ratios (W_{max}/h= 0.5, 1, 1.5 and 2) under thermal load and presented in Table 5.10. The temperature distribution has been considered across the thickness direction, by taking the bottom and top surface temperatures as T_c=600K and T_m=300K, respectively. It observed from the results that the linear and the nonlinear frequency responses are decreasing with the increase in power-law indices for all three cases of temperature load. This is due to the fact that the stiffness of metal-rich FG panel has comparatively lower than the stiffness of ceramic-rich FG panel. It is also noted that the frequency responses are higher in the case of TID-FG cylindrical panel than the TD-FG cylindrical panel, irrespective thermal field. However, the linear frequency responses are increasing in an ascending order of nonlinear, linear and uniform temperature field,

respectively whereas the frequency ratios are observed maximum and minimum for the nonlinear and the uniform temperature field.

5.3.2.2.7 Effect of thickness ratio on the linear and the nonlinear vibration behaviour of FG cylindrical panel under thermal environment

In this example, the linear and the nonlinear frequency responses of simply-supported FG ($Si_3N_4/SUS304$) cylindrical (n=2, R/a=5 and a/b=1) shell panel under different temperature loads are examined for three different thickness ratios (a/h=20, 50 and 100) and four different amplitude ratios (W_{max}/h= 0.5, 1, 1.5 and 2). The responses are obtained under three different temperature loads namely uniform, linear and nonlinear temperature distribution across the thickness direction and presented Table 5.11. The linear frequency and the frequency ratios are increasing and decreasing with the increase in thickness ratios, respectively for all three cases of temperature variations. It is because the stiffness of any structure reduces along with its thickness value. The TD-FG panel is exhibiting maximum linear frequency parameter whereas frequency ratios are higher in

TID-FG panel. However, the linear frequency responses are increasing in an ascending order of the nonlinear, linear and the uniform temperature field, respectively and the frequency ratios are following a reverse trend.

5.3.2.2.8 Effect of curvature ratio on the linear and the nonlinear vibration behaviour of FG cylindrical panel under thermal environment

The linear and the nonlinear frequency responses of simply-supported FG ($Si_3N_4/SUS304$) cylindrical (a/b=1, n=2 and a/h=10) shell panel is analysed for three curvature ratios (R/a=10, 20 and 50) and four amplitude ratios (W_{max}/h= 0.5, 1, 1.5 and 2). The responses are computed for three temperature loads namely uniform, linear and nonlinear temperature distribution across the thickness direction and presented in Table 5.12. The linear and the nonlinear frequency responses are decreasing with the increase in curvature ratios under all three cases of temperature variations. It is because as the curvature ratio increases the membrane stiffness of the curved panel decreases, i.e., the overall stiffness of curved panels are comparatively higher than that of the flat panel case. It is also observed that the frequency responses of the TID-FG panel are higher as

compared to the TD-FG panel. It is interesting to note that the linear frequency responses are increasing in the ascending order of the nonlinear, linear and uniform temperature field, respectively whereas the frequency ratios are found to be minimum for the uniform temperature field.

5.3.2.2.9 Effect of aspect ratio on the linear and the nonlinear vibration behaviour of FG cylindrical panel under thermal environment

Further the linear and the nonlinear frequency responses of simply-supported FG ($Si_3N_4/SUS304$) cylindrical (R/a=5, n=2 and a/h=10) shell panels are analysed for three aspect ratios (a/b=1.5, 2 and 2.5) and four amplitude ratios (W_{max}/h= 0.5, 1, 1.5 and 2) under three temperature field as discussed earlier. The responses are computed using the material properties as in Table 4.1 and presented in Table 5.13. In all the three cases of temperature variations, the linear frequency responses are increasing with the increase in aspect ratios whereas the frequency ratios are decreasing with the increase in aspect ratios. It is also seen that the linear frequency responses are higher for the TID-FG panel

case in comparison to the TD-FG panel and increasing in an ascending order of nonlinear, linear and uniform temperature field. The frequency ratios of the FG cylindrical shell panel are not following any monotonous behaviour for the aspect ratios with respect to the TD properties and the thermal field.

5.3.2.2.10 Effect of support condition on the linear and the nonlinear vibration behaviour of FG cylindrical panel under thermal environment

Finally, the linear and the nonlinear frequency responses of the FG (Si_3N_4/*SUS304*) cylindrical (R/a=5, a/b=1, n=2 and a/h=10) shell panel is investigated for three different support conditions (CCCC, SCSC and SFSF) and the amplitude ratios (W_{max}/h= 0.5, 1, 1.5 and 2) under three temperature field. The responses are obtained using the TD and TID properties of the FG panel and presented in Table 5.14. In all the three cases of temperature variations, the linear frequency responses are increasing with the increase in number of support constraints, i.e., increasing in the ascending order of SFSF, SCSC and CCCC, respectively. The FG cylindrical panel with SFSF support condition is showing the softening type of nonlinearity whereas hardening type behaviour

is observed in all the other cases. It is also noted that the linear frequency responses are higher in the case of TID-FG cylindrical panel whereas the frequency ratios are displaying non-repetitive behaviour for the TD-FG cylindrical panel. The linear frequency responses are increasing in the ascending order of nonlinear, linear and uniform temperature field, respectively whereas the frequency ratios are not showing any monotonous trend for severe nonlinearity.

5.3.2.3 Hyperbolic FG shell panel

Now in this subsection, the effect of varying temperature field and the temperature dependent material properties on the linear and nonlinear vibration responses of the FG hyperbolic (R_x=R, R_y=-R) shell panel are analysed for different geometrical parameters and discussed in detailed.

5.3.2.3.1 *Effect of power-law index on the linear and the nonlinear vibration behaviour of FG hyperbolic panel*

Now, the effect of power-law indices (n= 0.5, 1, 2 and 10) on the frequency responses of simply-supported square FG (Al/ZrO_2) hyperbolic panel is analysed for different amplitude ratios (W_{max}/h= 0.4, 0.8, 1.2, 1.6 and 2) and presented in Figure 5.18 (Kar and Panda, 2014). The material properties for Al/ZrO_2 is utilised for the present analysis by setting the geometrical parameters as a/h = 100 and R/a = 50. It is noted that the frequency ratios and the non-dimensional linear frequency parameters are decreasing with increase in power-law indices and the responses are within the expected line. It is because the FG shell panel becomes metal-rich as the 'n' value increases and it is well known that the metal-rich FG panel structure has lower stiffness in comparison to the ceramic-rich.

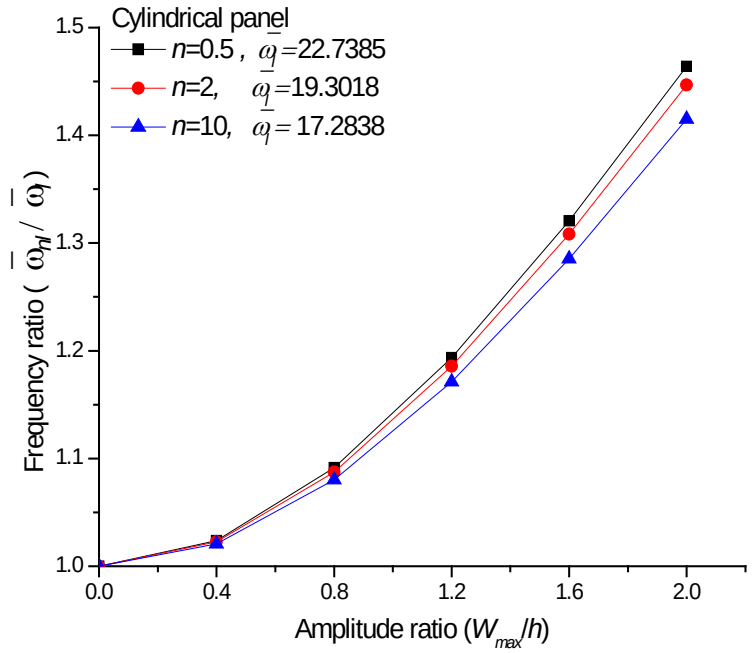

Figure 5.18 Frequency responses of FG hyperbolic panel for different power-law indices

5.3.2.3.2 Effect of thickness ratio on the linear and the nonlinear vibration behaviour of FG hyperbolic panel

In continuation of the above, the effect of four thickness ratios (a/h=10, 20, 50 and 100) on the frequency responses of the square simply-supported FG (Al/ZrO_2) hyperbolic shell panel (R/a=50 and n=2) is analysed for five amplitude ratios (W_{max}/h= 0.4, 0.8, 1.2, 1.6 and 2) and presented in Figure 5.19. From the figure, it is clearly observed that the non-dimensional linear frequency ($\bar{\omega}_l$) and the frequency ratio increases as the thickness ratio increase. It is also interesting to note that the effect of thickness ratio on the frequency ratios is insignificant and this may be due to the anticlastic curvature of the hyperbolic shell panel.

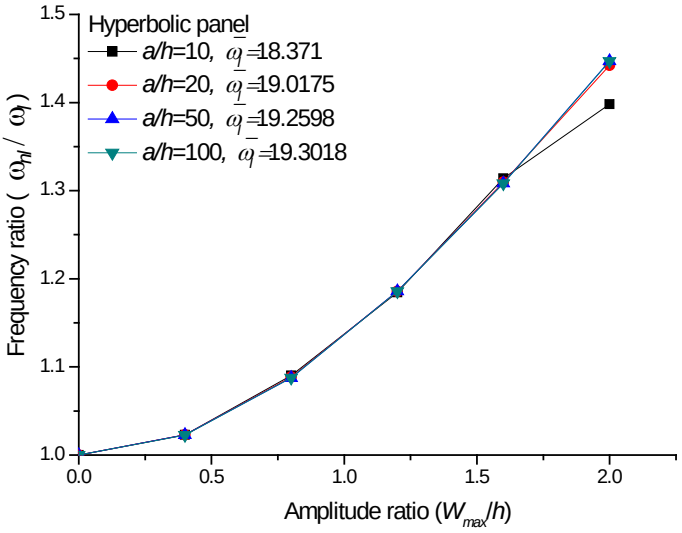

Figure 5.19 Frequency responses of FG hyperbolic panel for various thickness ratios

5.3.2.3.3 Effect of curvature ratio on the linear and the nonlinear vibration behaviour of FG hyperbolic panel

The effect of curvature ratios (R/a=5, 10, 20 and 50) on the frequency responses of simply-supported square FG (Al/ZrO_2) hyperbolic shell panel (n=2 and a/h=100) for different amplitude ratios (W_{max}/h= 0.4, 0.8, 1.2, 1.6 and 2) and presented in Figure 5.20. It is observed that the non-dimensional linear frequency parameters are increasing with increase in curvature ratios however the frequency ratios are not affected much as in the

earlier case. This may be due to the reason that the hyperboloid shell panels have unequal curvatures, i.e., the positive and the negative in different axis.

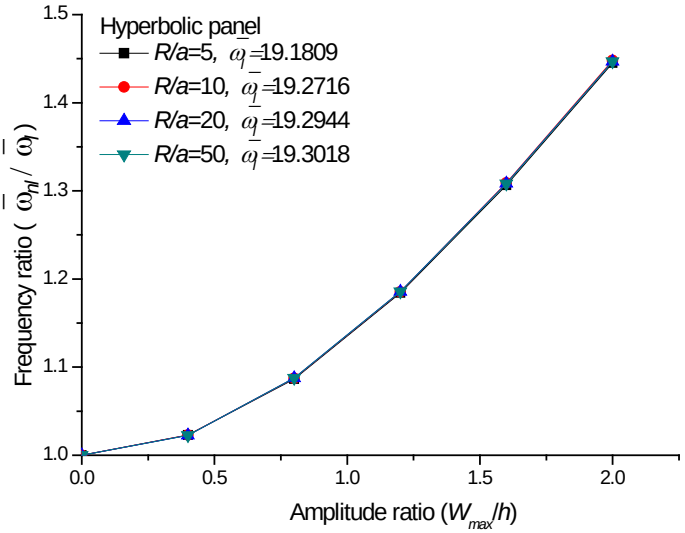

Figure 5.20 Frequency responses of FG hyperbolic panel for various curvature ratios

5.3.2.3.4 Effect of aspect ratio on the linear and the nonlinear vibration behaviour of FG hyperbolic panel

It is well known that the structural responses greatly depends on the aspect ratio and the effect of various aspect ratios (a/b=1, 1.5, 2 and 2.5) are analysed in this example. The responses are computed for simply-supported thin FG (Al/ZrO_2) hyperbolic shell panel (n=2, a/h=100 and R/a=50) by setting the different amplitude ratios (W_{max}/h= 0.4, 0.8, 1.2, 1.6 and 2) and presented in Figure 5.21. The linear responses of the FG shell panel are increasing as the aspect ratio increases whereas the frequency ratios are showing an opposite trend.

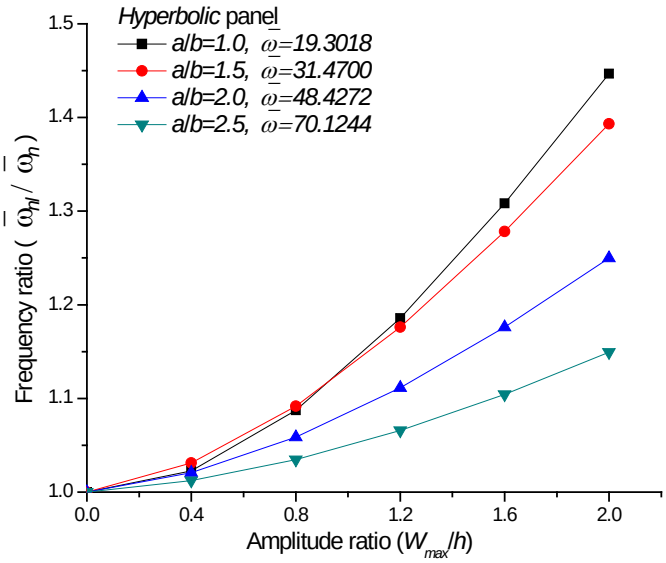

Figure 5.21 Frequency responses of FG shell hyperbolic panel for different aspect ratios

5.3.2.3.5 Effect of support conditions on the linear and the nonlinear vibration behaviour of FG hyperbolic panel

The structural stiffness largely depends on their type of support conditions and it also affects the final structural responses as well. Now in this example effect of four different support conditions (SSSS, CCCC, SCSC and HHHH) and five different amplitude ratios (W_{max}/h= 0.4, 0.8, 1.2, 1.6 and 2) on the frequency responses are analysed. The responses are computed for the square FG (Al/ZrO_2) hyperbolic shell panel (n=2, a/h=100 and R/a=50) is analysed and presented Figure 5.22. It is observed that the linear responses are increasing with the increase in a number of constraints whereas a non-repetitive type of behaviour is seen in the nonlinear case.

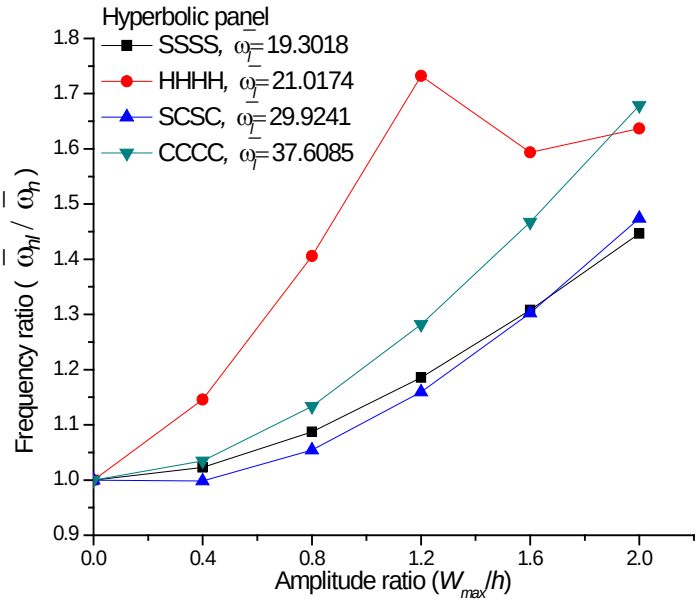

Figure 5.22 Frequency responses of FG hyperbolic panel for different support conditions

5.3.2.3.6 Effect of power-law index on the linear and the nonlinear vibration behaviour of FG hyperbolic panel under thermal environment

Now the effect temperature load on the frequency responses of simply-supported FG (*Si_3N_4/SUS304*) hyperbolic (*R/a*=5, *a/b*=1 and *a/h*=10) shell panel is examined for three different power-law indices (*n*=0.2, 2 and 5) and four amplitude ratios (W_{max}/h= 0.5, 1, 1.5 and 2). The responses are obtained under three different temperature loads namely uniform, linear and nonlinear temperature distribution across the thickness direction and presented in Table 5.15. In all the three cases of temperature variations, the linear and the nonlinear frequency responses are decreasing with the increase in power-law indices. It is also noted that the frequency responses are higher for the TID-FG panel than the TD-FG panels, irrespective thermal field. However, the linear frequency responses are increasing in the ascending order of nonlinear, linear and uniform temperature field, respectively whereas the frequency ratios are observed to be maximum and minimum for the nonlinear and uniform temperature field.

5.3.2.3.7 Effect of thickness ratio on the linear and the nonlinear vibration behaviour of FG hyperbolic panel under thermal environment

In this example, the linear and the nonlinear frequency responses of simply-supported FG ($Si_3N_4/SUS304$) hyperbolic (R/a=5, a/b=1 and n=2) panel under three temperature loads are examined for different thickness ratios (a/h=20, 50 and 100) and four amplitude ratios (W_{max}/h= 0.5, 1, 1.5 and 2). The responses are obtained using the defined material properties and presented in Table 5.16. The linear frequency responses are increasing with the increase in thickness ratios whereas the frequency ratios are decreasing for all three cases of temperature load. It is because the stiffness of any structure reduces as the thickness ratio increases. The TD-FG panel is exhibiting maximum linear frequency parameter whereas frequency ratios are higher in TID-FG panel. However, the linear frequency responses are increasing in the ascending order of nonlinear, linear and uniform temperature field, respectively whereas the frequency ratios are increasing in a reverse manner as in the linear case.

5.3.2.3.8 Effect of curvature ratio on the linear and the nonlinear vibration behaviour of FG hyperbolic panel under thermal environment

The linear and the nonlinear frequency responses of simply-supported FG ($Si_3N_4/SUS304$) hyperbolic (n=2, a/b=1 and a/h=10) panel subjected to different temperature loads are examined for three different curvature ratios (R/a=10, 20 and 50) and four different amplitude ratios (W_{max}/h= 0.5, 1, 1.5 and 2). The responses are obtained under three different temperature loads namely uniform, linear and nonlinear temperature distribution across the thickness direction, as presented in Table 5.17. In all the three cases of temperature variations, the linear frequency responses are increasing with the increase in curvature ratios, whereas the effect of curvature ratio on the frequency ratios is almost insignificant. It may be due to the anticlastic nature of the hyperbolic panel. The frequency responses of the TID-FG panel are higher as compared to TD-FG panel. It is also noted that the linear frequency responses are increasing in the

ascending order of nonlinear, linear and uniform temperature field, respectively whereas the frequency ratios are increasing in a reverse order as in the linear case.

5.3.2.3.9 Effect of aspect ratio on the linear and the nonlinear vibration behaviour of FG hyperbolic panel under thermal environment

The effect of aspect ratios (a/b=1.5, 2 and 2.5) on the linear and the nonlinear frequency responses of simply-supported FG ($Si_3N_4/SUS304$) hyperbolic (R/a=5, n=2 and a/h=10) shell panel is analysed for different temperature loads and four different amplitude ratios (W_{max}/h= 0.5, 1, 1.5 and 2) in this example. The responses are obtained under three different temperature loads (uniform, linear and nonlinear) and presented in Table 5.18. In all the three cases of temperature variations, the linear frequency responses are increasing with the increase in aspect ratios whereas the frequency ratios are decreasing with the increase in aspect ratios. It is also noted that the linear frequency responses are higher for the TID-FG panel as compared to the TD-FG panel. The linear frequencies are increasing in the ascending order of nonlinear, linear and uniform temperature field. The frequency ratios of the FG hyperbolic panels are not showing any

monotonous trend with respect to the aspect ratios including the temperature dependent material properties and thermal field.

5.3.2.3.10 Effect of support condition on the linear and the nonlinear vibration behaviour of FG hyperbolic panel under thermal environment

Finally, the effect of different support conditions (CCCC, SCSC and SFSF) on the linear and the nonlinear frequency responses of the FG (Si_3N_4/*SUS304*) hyperbolic (R/a=5, n=2, a/b=1 and a/h=10) under different temperature loads are examined for four amplitude ratios (W_{max}/h= 0.5, 1, 1.5 and 2). The responses are computed using the temperature dependent material properties and presented in Table 5.19. The linear frequency responses are increasing with the increase in numbers of support constraints, i.e., increasing in an ascending order of SFSF, SCSC and CCCC, respectively for all the temperature variations. It is observed that the nonlinearity is insignificant for the SFSF supported FG hyperbolic panel whereas the hardening type behaviour for all the other supports. It is also noted that the linear frequency responses are higher in case of the TID-FG panel whereas the frequency ratios are displaying non-repetitive behaviour for the

TD-FG panel. The linear frequency responses are increasing in the ascending order of the nonlinear, the linear and the uniform temperature field, respectively whereas the frequency ratios are not following any monotonous trend.

5.3.2.4 Elliptical FG shell panel

In this subsection, the effect of different parameters on the linear and the nonlinear vibration responses of the FG elliptical ($R_x=R$, $R_y=2R$) shell panel with and without temperature dependent material properties under three thermal field are analysed and discussed in details.

5.3.2.4.1 Effect of power-law index on the linear and the nonlinear vibration behaviour of FG elliptical panel

Figure 5.23 shows the frequency responses of simply-supported square FG (Al/ZrO_2) elliptical shell ($R/a=50$, $a/h=100$) panel for different power-law indices (n= 0.5, 2, 10) and five different amplitude ratios (W_{max}/h= 0.4, 0.8, 1.2, 1.6 and 2). It is noted

that the frequency ratios and the non-dimensional linear frequency parameters are decreasing with increase in power-law indices. It is because the FG shell panel becomes metal-rich when the '*n*' value increases and the metal have comparatively lower stiffness in comparison to the ceramic material.

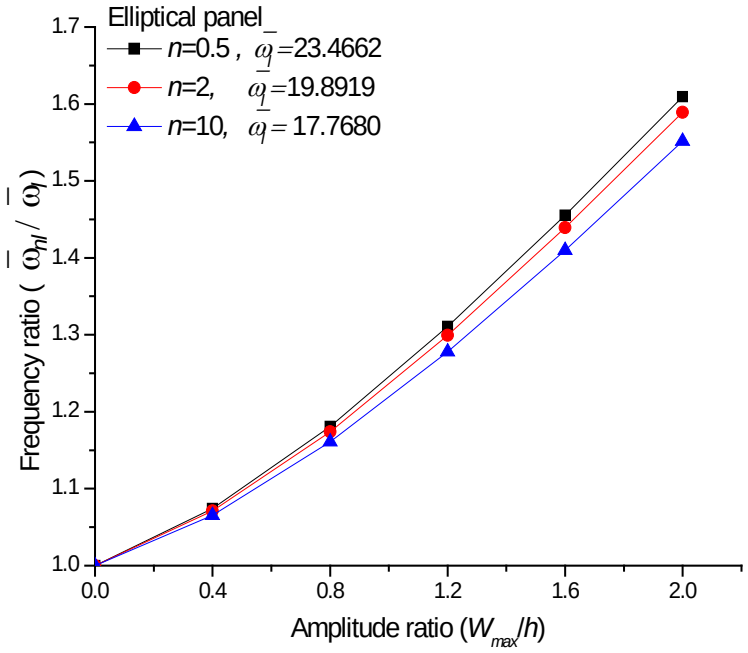

Figure 5.23 Frequency responses of FG elliptical panel for different power-law index

5.3.2.4.2 Effect of thickness ratio on the linear and the nonlinear vibration behaviour of FG elliptical panel

The frequency responses of square simply-supported FG (Al/ZrO_2) elliptical shell panel (R/a=50, n=2) is analysed for four thickness ratios (a/h=10, 20, 50 and 100) by setting different amplitude ratios (W_{max}/h= 0.4, 0.8, 1.2, 1.6 and 2). The responses are computed using the material properties same as discussed earlier in the example *5.3.2.4.1* and presented in Figure 5.24. It is observed that both the linear and the nonlinear frequency responses are increasing with the increase in the thickness ratios.

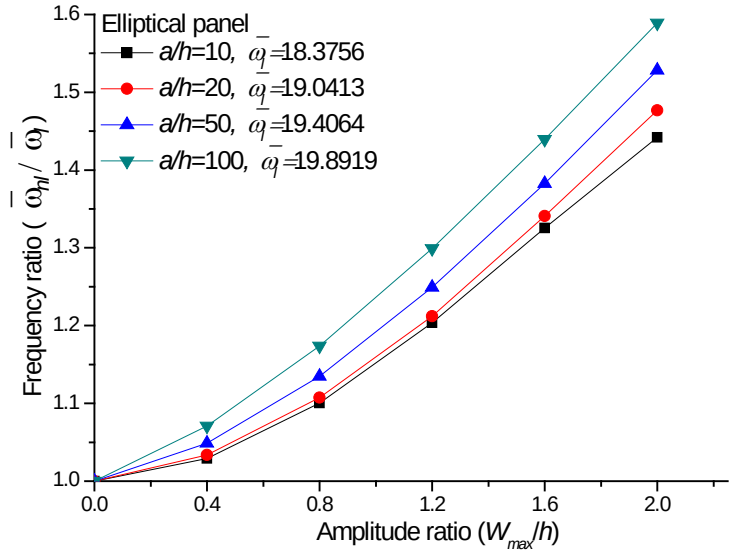

Figure 5.24 Frequency responses of FG shell panel for various thickness ratios

5.3.2.4.3 Effect of curvature ratio on the linear and the nonlinear vibration behaviour of FG elliptical panel

Figure 5.25 shows the effect of curvature ratios (R/a=5, 10, 20 and 50) on the frequency responses of simply-supported square FG (Al/ZrO_2) elliptical shell panel (n=2, a/h=100) for five different amplitude ratios (W_{max}/h= 0.4, 0.8, 1.2, 1.6 and 2). It is observed that the non-dimensional linear frequency parameters are decreasing with the increase in curvature ratios whereas the frequency ratios are not following any regular fashion. It is also noted that the frequency responses are increasing with the amplitude ratio for all FG elliptical panels except R/a=5. This can be clearly observed that frequency ratio drops drastically after W_{max}/h=1.2 and it may be due to the dome effect of unequal curvature of the elliptical panel ($R_x = R$ and $R_y = 2R$).

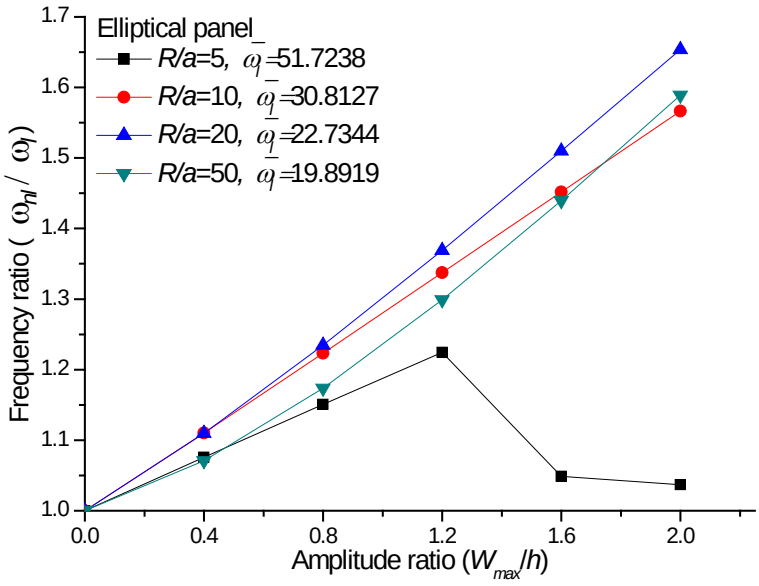

Figure 5.25 Frequency responses of FG elliptical panel for different curvature ratios

5.3.2.4.4 Effect of aspect ratio on the linear and the nonlinear vibration behaviour of FG elliptical panel

Figure 5.26 shows the variation of the frequency responses of simply-supported FG (Al/ZrO_2) elliptical shell panel (n=2, a/h=100, R/a=50) for four aspect ratios (a/b=1, 1.5, 2 and 2.5) and five amplitude ratios (W_{max}/h= 0.4, 0.8, 1.2, 1.6 and 2). It is observed that the linear frequency responses of the FG elliptical panel are increasing with the increase in aspect ratios whereas the frequency ratios are showing a reverse trend and the responses are within the expected line.

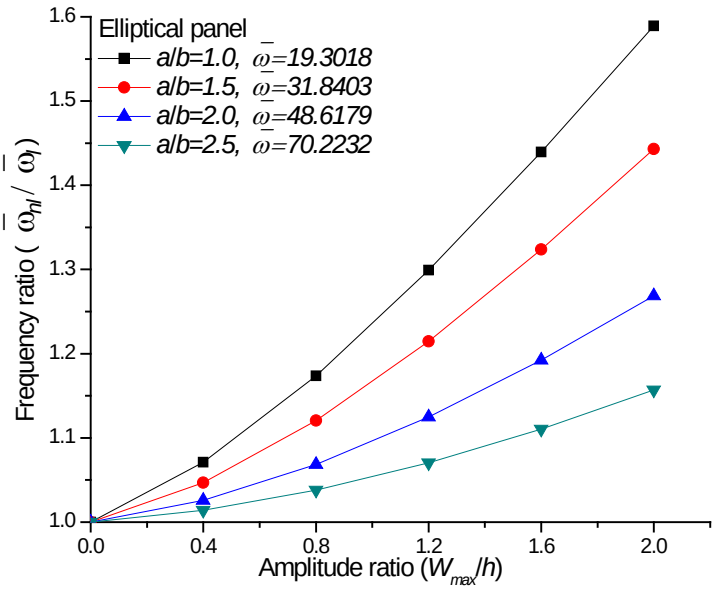

Figure 5.26 Frequency ratios of FG elliptical panel with different aspect ratios

5.3.2.4.5 Effect of support condition on the linear and the nonlinear vibration behaviour of FG elliptical panel

The effect of four different support conditions (SSSS, SCSC, HHHH and CCCC) on the linear and nonlinear frequency behaviour of the square FG (Al/ZrO_2) elliptical panel (n=2, a/h=100, R/a=50) are analysed in this example and presented in Figure 5.27. The present frequency ratios are computed for five different amplitude ratios (W_{max}/h= 0.4, 0.8, 1.2, 1.6 and 2) by setting the same material properties as discussed earlier. It is observed that the linear responses are increasing with the increase in numbers of support constraints whereas the effect of nonlinearity is predominant for hinge (HHHH) supported FG elliptical panel. It is also observed that the frequency ratios fall suddenly for two support conditions (HHHH and CCCC) at W_{max}/h=1.2 and 1.6, respectively. This type of non-repetitive behaviour of frequencies are observed may be due to the inclusion of all the nonlinear higher-order terms in the mathematical model and it approaches towards any real-life situation as well.

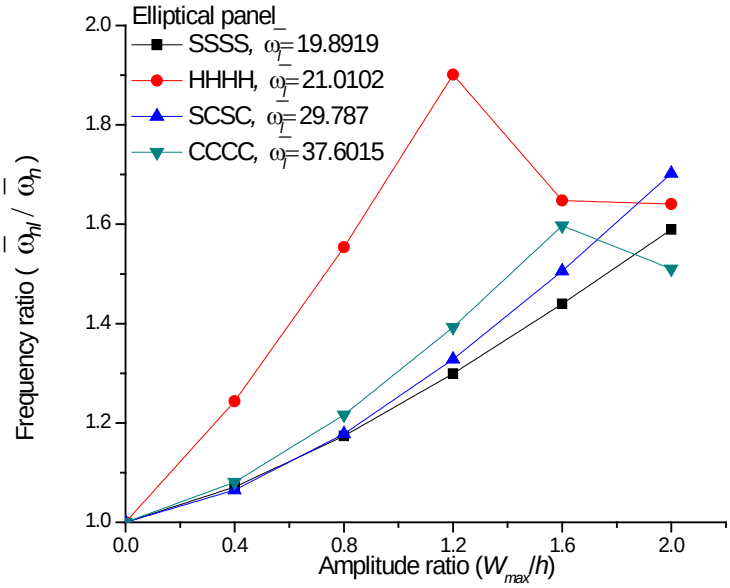

Figure 5.27 Frequency responses of FG elliptical panel for different support conditions

5.3.2.4.6 Effect of power-law index on the linear and the nonlinear vibration behaviour of FG elliptical panel under thermal environment

The frequency responses of simply-supported FG (Si_3N_4/*SUS304*) elliptical (*R*/*a*=5, *a*/*b*=1 and *a*/*h*=10) shell panel under three different temperature loads are examined (uniform, linear and nonlinear) in this example. The responses are computed for three power-law indices (*n*=0.2, 2 and 5) and four different amplitude ratios (W_{max}/*h*= 0.5, 1, 1.5 and 2) and presented in Table 5.20. The linear and the nonlinear frequency responses are decreasing with the increase in power-law indices for each of the temperature field. It is also noted that the frequency responses are higher and lower for the TID and TD-FG elliptical shell panel irrespective of the thermal field. However, the linear frequency responses are increasing in the ascending order of the nonlinear, the linear and the uniform temperature field, respectively. It is also observed that the frequency ratios are maximum and minimum for the nonlinear and the uniform temperature field, respectively.

5.3.2.4.7 Effect of thickness ratio on the linear and the nonlinear vibration behaviour of FG elliptical panel under thermal environment

In this example, the linear and the nonlinear frequency responses of simply-supported FG ($Si_3N_4/SUS304$) elliptical (R/a=5, a/b=1 and n=2) panel subjected to different temperature loads are examined for three different thickness ratios (a/h=20, 50 and 100) and four different amplitude ratios (W_{max}/h= 0.5, 1, 1.5 and 2). The responses are obtained under three different temperature loads namely uniform, linear and nonlinear temperature distribution across the thickness direction, as presented in Table 5.21. In all the three cases of temperature variations, the linear frequency responses are increasing with the increase in thickness ratios whereas the frequency ratios are decreasing with the increase in thickness ratios. It is because the stiffness of any structure reduces along with its thickness value. The TD-FG panel is exhibiting maximum linear frequency parameter whereas frequency ratios are higher in TID-FG panel. However, the linear frequency responses are increasing in the ascending order of nonlinear, linear and uniform

temperature field, respectively whereas the frequency ratios are increasing in a reverse fashion as in the linear case.

5.3.2.4.8 Effect of curvature ratio on the linear and the nonlinear vibration behaviour of FG elliptical panel under thermal environment

The linear and the nonlinear frequency responses of simply-supported FG ($Si_3N_4/SUS304$) elliptical (n=2, a/b=1 and a/h=10) shell panel under different temperature loads are examined in this example for three different curvature ratios (R/a=10, 20 and 50) and four amplitude ratios (W_{max}/h= 0.5, 1, 1.5 and 2). The responses are obtained under three temperature distributions (uniform, linear and nonlinear) and presented in Table 5.22. The linear and the nonlinear frequency responses are decreasing with the increase in curvature ratios for each case of the temperature distribution. It is because as the curvature ratio increases the structure become flat and the stiffness of the flat structural component is lower than that of the curved panel. The frequency responses of the TID-FG panels are higher as compared to the TD-FG panel. It is also noted that the linear frequency responses are increasing in the ascending order of nonlinear, linear and uniform temperature field, respectively whereas the frequency ratios are increasing in a reverse manner with reference to the linear case.

5.3.2.4.9 Effect of aspect ratio on the linear and the nonlinear vibration behaviour of FG elliptical panel under thermal environment

In this example, the linear and the nonlinear frequency responses of simply-supported FG ($Si_3N_4/SUS304$) elliptical (R/a=5, n=2 and a/h=10) shell panel under different temperature loads (uniform, linear and nonlinear) are examined. The responses are computed for three aspect ratios (a/b=1.5, 2 and 2.5) and four different amplitude ratios (W_{max}/h= 0.5, 1, 1.5 and 2) and presented in Table 5.23. In all the three cases of temperature variations, the linear frequency responses are increasing with the increase in aspect ratios whereas the frequency ratios are decreasing with the increase in aspect ratios. It is noted that the linear frequency responses are higher for the TID-FG panel in comparison to the TD-FG panel and also increasing in the ascending order of nonlinear, linear and uniform temperature field. The frequency ratios of the FG elliptical shell

panels with temperature dependent material properties are not showing any monotonous behaviour under different temperature field and the aspect ratios.

5.3.2.4.10 Effect of support condition on the linear and the nonlinear vibration behaviour of FG elliptical panel under thermal environment

The linear and the nonlinear frequency responses of FG (Si_3N_4/*SUS304*) elliptical (R/a=5, a/b=1, n=2 and a/h=10) shell panel is analysed for three different support conditions (CCCC, SCSC and SFSF) under three temperature loads. The responses are obtained for four amplitude ratios (W_{max}/h= 0.5, 1, 1.5 and 2) and presented in Table 5.24. In all the three cases of temperature variations, the linear frequency responses are increasing with the increase in number of support constraints, i.e., increasing in the ascending order of SFSF, SCSC and CCCC, respectively. The FG elliptical shell panel is showing soft spring type of behaviour under SFSF support condition whereas hardening type behaviour is observed for all other support condition. It is also noted that the linear frequency responses are higher for the TID-FG elliptical panel whereas the frequency ratios are following non-repetitive behaviour with temperature dependent FG panel properties. The linear frequency responses are increasing in the ascending order of nonlinear, linear and uniform temperature field, respectively whereas the frequency ratios are not showing any monotonous trend.

5.3.2.5 *Effect of Shell Geometry on Frequency Responses*

In this example, the effect of different shell geometries (spherical, cylindrical, elliptical, hyperbolic and flat) on the frequency ratios of FG (Si_3N_4/*SUS304*) panels under different temperature loads (uniform, linear and nonlinear) are examined under CFCF support condition and presented in Table 5.25. It is observed that the linear frequency parameters are increasing in the ascending order of flat, cylindrical, elliptical, hyperbolic and spherical, respectively. However, the frequency ratios are increasing in the order of hyperbolic, cylindrical, flat, elliptical and spherical.

5.4 Conclusions

In this present chapter, the linear and the nonlinear free vibration responses of the FG shell panels of various geometries (spherical, cylindrical, hyperbolic and elliptical) are analysed with and without thermal loading. The responses are obtained for both the TD and TID material properties of the individual FG constituents under the uniform, linear and nonlinear temperature fields. The FG shell panel model is developed

mathematically in the framework of the HSDT kinematics and Green-Lagrange geometrical nonlinearity. The present mathematical model included all the nonlinear higher-order terms to achieve the generality. In addition to the above, the effective FGM properties are evaluated using Voigt's micromechanical model through the power-law distribution of volume fractions. The governing equations of vibrated FG shell panels are derived using variational principle and discretised using the suitable finite element steps. The domain is discretised using a nine node isoparametric Lagrangian element with nine degrees of freedom per node. The desired linear and/or nonlinear responses are computed further numerically for all types of shell geometries using the direct iterative method based on the customised computer code developed in MATLAB environment. The convergence and validation behaviour of the present numerical model for the linear and the nonlinear responses are verified for each case. The influences of various geometry and material parameters on the linear non-dimensional frequency and the frequency ratios of the FG shell panels have been examined thoroughly. Based on the comprehensive parametric study, the following concluding remarks are drawn.

(a) It is observed that the temperature-dependent material properties and the type of temperature distributions across the thickness direction of FG shell panel affect the vibration behaviour of the FG panels considerably.

(b) The non-dimensional linear frequency parameters of FG shell panels are increasing for each panel geometry as the thickness ratios, the aspect ratios and the number of support constraints increase.

(c) The non-dimensional linear frequency parameters of FG shell panels are decreasing as the power-law indices and the curvature ratios increase for each case, whereas the hyperbolic shell panels exhibit the reverse trend for the curvature ratios.

(d) The FG shell panel with TID material properties is showing the maximum linear frequency irrespective of the panel geometries. It is also noted that the FG shell panels are exhibiting the maximum and minimum linear frequencies for the uniform and nonlinear temperature field.

(e) The linear frequency parameters increase in an ascending order of flat, cylindrical, elliptical, hyperbolic and spherical FG shell panels.

(f) The frequency ratios of the FG shell panels are increasing with the decrease in power-law indices for all the cases analysed in the present chapter, i.e., the nonlinearity is significant in the case of the ceramic-rich FG panel irrespective geometry, material and temperature load.

(g) The frequency ratios of the FG shell panels under the ambient condition are increasing with the increase in thickness ratio except for the hyperbolic panel. However, it follows a reverse trend for the elevated thermal field.

(h) The frequency ratios are decreasing with the increase in the curvature ratios for each case of the panel geometries. However, the variation is insignificant for hyperbolic FG shell panel.

(i) The frequency ratios of the FG shell panel are not following the monotonous behaviour for the support conditions.

(j) The frequency ratios of the FG shell panels are increasing with the decrease in aspect ratio, i.e., the nonlinearity is higher in the case of square FG shell panel.

(k) The FG shell panels with TID material properties are showing the higher frequency ratios. However, the frequency ratios are following an increasing trend in an ascending order of the uniform, linear and the nonlinear temperature field.

(l) It is also noted that the nonlinear free vibration responses increase with the increase in amplitude ratios, however, few deviations are observed after $W_{max} / h \geq 1.5$.

(m) The frequency ratios are increasing in an ascending order of hyperbolic, cylindrical, flat, elliptical and spherical FG shell panel.

(n) The present higher-order mathematical model with Green-Lagrange nonlinearity is showing good adaptability for the analysis of linear and/or nonlinear vibration problems of FG shell panels with and without thermal effects.

CHAPTER 6
BUCKLING AND POST-BUCKLING OF FG SHELL PANEL UNDER THERMOMECHANICAL LOAD

6.1 Introduction

In this chapter, the buckling and the post-buckling responses of the FG shell panel under the in-plane mechanical and/or the transverse thermal loading condition are computed numerically using the presently developed general nonlinear mathematical model including the temperature-dependent material properties. The shell panels have known for their significantly higher membrane stiffness than that of the bending stiffness, and, therefore, a shell panel is capable of absorbing a larger amount of membrane strain energy without excessive deformation. If the shell is subjected to such a loading condition in which most of the strain energy in the form of membrane compression, and if there is a way that this stored-up membrane energy can be converted into bending energy, the shell may fail dramatically in a process called 'buckling'. It is also known that the buckling doesn't mean the ultimate failure of the structural components and they are still capable of carrying extra amount of load beyond the buckling point without failure, i.e., known as the post-buckling strength.

In Section 6.2, the governing equation of the FG shell panel under the thermal and mechanical environment and its solution steps are already mentioned. Section 6.3 presents the convergence and the validation studies of the proposed mathematical model for the flat/curved FG panel by solving the wide variety of numerical illustrations. In continuation to this, the robustness and the efficacy of the presently developed model have been revealed through the comprehensive parametric study. The effects of various

geometrical and material parameters and the support conditions on the buckling and the post-buckling responses with TD/TID properties of the FG curved panels are examined under individual and/or combined loading conditions. Finally, the concluding remarks are drawn in Section 6.4 based on the results obtained for different parameters in Section 6.3.

6.2 Solution Methodology

The equilibrium equations for the buckling and the post-buckling of the FG shell panel due to in-plane mechanical and thermal loading are derived using the variational principle and presented in Eq. (3.46) and (3.47), respectively. The buckling and the post-buckling responses of the FG shell panel are solved using the steps of the solution technique as mentioned in Section 3.11. For the computational purpose, the critical buckling load parameter of the FG shell panel is computed in the first mode of the eigenvalue solution, if not specified otherwise. The post-buckling responses are obtained for the said system of the equation by introducing the amplitude ratio (W_{max}/h, where W_{max} is the maximum central deflection and h is the thickness of the panel). The desired responses are computed using the customised homemade computer code developed in MATLAB environment. The temperature dependent properties of the FGM constituents are obtained and utilised for the computational purpose as in Table 4.1.

6.3 Results and Discussion

The desired critical buckling load responses are computed using a homemade customised computer code developed in MATLAB environment based on the developed mathematical formulation. The convergence behaviour of the present numerical model has been obtained for the FG shell panel under in-plane mechanical/thermal loading environment for different geometrical and material configurations. Subsequently, the validation of the present model is also established by comparing the responses with that of the previously published results. In order to exhibit the robustness and the applicability of the present model wide variety of numerical examples are solved for various geometrical and material parameters, support conditions and temperature fields. Finally, the influences of different parameters on the buckling and the post-buckling responses of

the FG shell panel are discussed in details. Table 4.1 shows the TD material properties of each constituent of the FGM used in the present analysis.

6.3.1 Convergence and Validation Study

In this section, the convergence and the validation behaviour of the proposed FE model of the FG flat/curved panel have been shown by computing the critical buckling load parameters. The convergence behaviour of the present numerical results of the FG shell panel is obtained for different mesh division with the TD and the TID properties. Subsequently, the present FG panel model has also been validated by comparing the responses with those available published literature. The convergence and the comparison studies of the buckling/post-buckling responses of the FG shell panel are performed for the different geometrical configurations (flat/spherical/cylindrical), material properties (TD and TID), and the FGM constituents and discussed in the following subsections in detailed.

6.3.1.1 Convergence and comparison study of buckling responses of FG panel under uniform temperature rise

As discussed earlier, the efficacy and the competency of the developed numerical model have been checked initially using the material properties (E_m = 70 GPa, υ_m = 0.3 and α_m = 23.0×10^{-6} K^{-1}, for *Al* and E_c = 380 GPa, υ_c = 0.3 and α_m =7.4×10^{-6} K^{-1} for Al_2O_3, respectively) and the support conditions same as to Zhao et al. (2009). The convergence behaviour of the buckling load parameters of the square simply supported FG (Al/Al_2O_3) flat panel (a/h=50) are computed under the influence of the unit temperature rise for different mesh size and presented in Figure 6.1. It can be observed that the present results are converging well and a (6×6) mesh is sufficient to compute the further responses.

Now, the present model is extended for the validation purpose to show the efficacy of the proposed FG shell panel model. Figure 6.2 shows the critical buckling temperature load of the clamped FG (Al/Al_2O_3) flat panels for two different thickness ratios (a/h=50 and 100). The responses are compared with Zhao et al. (2009) and the simulation model

developed in ANSYS using APDL code. It is clearly observed that the differences between the reference, ANSYS and present results are very insignificant. It is also interesting to note that the present results are showing the bit higher value as compared to the reference and the ANSYS. This is because of the fact that the present geometrical distortion has been modelled using Green-Lagrange type geometrical nonlinearity in the framework of the HSDT instead of the FSDT kinematics as in the reference and the ANSYS.

Similarly, the thermal buckling responses are obtained for the simply supported square FG (Al/Al_2O_3) flat panel for two different thickness ratios (a/h=50 and 100) and presented in Figure 6.3. It is observed that from the figure that the present HSDT results are matching well with that of the FSDT results of Zhao et al. (2009).

6.3.1.2 Convergence behaviour of post-buckling responses of FG panels under thermal environment

In this example, the post-buckling responses of the FG curved (spherical and cylindrical) panel are computed under three different thermal fields (uniform, linear and nonlinear). Figure 6.4 shows the critical buckling load parameters of the simply supported FG shell panel (a/h=10, a/b=1, R/a=5) for different mesh size and the amplitude ratios (W_{max}/h=0, 0.5, 1 and 1.5). For the computational purpose, the stainless steel (SUS304) and the silicon nitride (Si_3N_4) are considered at the bottom and at the top surface of the shell panel as the metal and the ceramic constituent, respectively and the corresponding TD material properties are mentioned in Table 4.1. It can be observed that the responses are converging well for each of the case considered here and a (6×6) mesh is sufficient to compute the further post-buckling responses.

6.3.1.3 Comparison study of post-buckling responses of FG panel under thermal environment

In order to validate the present nonlinear model, the thermal post-buckling responses of FG flat panel is computed and compared with Duc and Tung (2011). Figure 6.5 presents the post-buckling responses of the simply supported FG (Al/Al_2O_3) flat (a/h=20 and a/b=1) panel under the uniform temperature rise for three different power-

law indices (n = 0, 1 and 5) and the amplitude ratios. The material and geometrical parameters are taken same as to Duc and Tung (2011). It is observed that the present results are exhibiting higher critical buckling temperature as compared to Duc and Tung (2011). It is because the present model accounts the full nonlinearity in Green-Lagrange sense whereas, in the reference, the nonlinearity is introduced through von-Karman strain terms and which unable to consider exact geometrical distortion under the thermal load.

6.3.1.4 Comparison study of post-buckling responses of FG panel under uniaxial compression load

In continuation of the previous example, now the post-buckling responses of FG flat panel are obtained under uniaxial compression and compared with the available published results. Figure 6.6 shows the non-dimensional critical buckling load parameter $\left(\overline{\gamma}_{cr} = \gamma_{cr} b^2 / E_c h^3\right)$ of the clamped FG (Al/Al_2O_3) flat panel (a/h=40, a/b=1) for different power-law indices (n=0, 1, 2, 5, 10 and ∞) at different amplitude ratios. The material and the geometrical parameters are taken same as in Wu et al. (2007). The present results are compared with the results of Wu et al. (2007) and Lal et al. (2012) which are based on the FSDT/HSDT mid-plane kinematics and von-Karman nonlinearity. It is observed that the present results are showing good agreement with that of the references.

6.3.2 Numerical Illustrations and Parametric Study

The previous section has demonstrated the efficacy and the necessity of the presently developed nonlinear mathematical model for the buckling/post-buckling analysis of the FG panel under in-plane mechanical and/or the thermal loading through by solving various examples. It is also evident the developed computer code is capable enough to solve the buckling and the post-buckling problems of the FG shell panel under thermal and the mechanical loading conditions. In this section, the stability behaviour of various curved shell geometries (spherical, cylindrical, hyperbolic and elliptical) are examined by varying different parameters such as the power-law indices, the thickness ratios, the curvature ratios, the aspect ratio, the amplitude ratios, the support conditions and the loading conditions. For the computational purpose, *SUS304* and Si_3N_4 are

considered as the metal and the ceramic materials, respectively throughout in the section. The mechanical and the thermal properties of each constituent are given in Table 4.1. The forthcoming subsections are broadly classified based on the shell panel geometries where

the buckling/post-buckling responses are computed under three different type of loadings, such as temperature fields, uniform edge compression loads and combined uniform temperature and edge compression loading cases. The details of buckling and the post-buckling responses under these three loading conditions are discussed in the following lines.

- In the thermal buckling and the post-buckling analysis, the critical buckling temperature load parameter (γ_{cr}) of the FG shell panel are examined under three different type of thermal loadings (uniform, linear and nonlinear) for different amplitude ratios (W_{max}/h=0, 0.5, 1 and 1.5). For the computational purpose, the TD/TID-FG (*SUS304/Si$_3$N$_4$*) shell panel with a/h=10, n=2, R/a=5, SSSS and a/b=1 is considered, if not stated otherwise. The temperatures at the top and the bottom are assumed to be T_c=600K and T_m=300K, respectively.
- Similarly, the mechanical buckling and the post-buckling analysis, the non-dimensional critical buckling load parameter $\left(\overline{\gamma}_{cr} = \gamma_{cr} b^2 / E_c h^3\right)$ of the FG shell panel are examined under uniaxial (along x direction) and biaxial (along x and y directions) compression loadings for different amplitude ratios (W_{max}/h=0, 0.5, 1 and 1.5). For the computational purpose, the TID-FG (*SUS304/Si$_3$N$_4$*) shell panel with a/h=10, n=2, R/a=5, SSSS and a/b=1 is considered, if not stated otherwise.
- In the thermomechanical buckling/post-buckling analysis, the critical buckling temperature load parameter (γ_{cr}) of the TD-FG (*SUS304/Si$_3$N$_4$*) shell panel are examined under uniaxial compression load and uniform temperature field for different amplitude ratios (W_{max}/h=0, 0.5, 1, 1.5 and 2). The temperatures at the top and the bottom are assumed to be same as the earlier case.

6.3.2.1 Spherical FG shell panel

In the following subsections, the influence of different parameters (material and geometry) on the buckling and the post-buckling strength of the FG spherical (R_x=R_y=R) shell panel under mechanical and/or thermal load including the TD and TID properties are discussed.

6.3.2.1.1 Effect of power-law index on thermal post-buckling strength of FG spherical panel

The power-law index is one of the deciding factors in FGM property evaluation which alters the stiffness of the FGM structure. Table 6.1 presents the buckling and the post-buckling responses (γ_{cr}) of simply supported square FG (*SUS304/Si$_3$N$_4$*) spherical shell panel (*R*/*a*=5, *a*/*h*=10 and *a*/*b*=1) for different power-law indices (*n*= 0.2 and 5) and amplitude ratios. It is observed that the buckling and the post-buckling responses are reducing with the increase in power-law indices, i.e., the ceramic-rich FG spherical panel has the higher buckling and the post-buckling strength under the thermal environment than the metal-rich FG spherical panel. The FG spherical panel under the nonlinear temperature field exhibits maximum buckling and the post-buckling strength as compared to other temperature distributions. However, the FG spherical panel with the TID properties is showing the higher buckling and the post-buckling strength than the TD-FG spherical panel.

6.3.2.1.2 Effect of thickness ratio on thermal post-buckling strength of FG spherical panel

In general, the stiffness of any structure greatly depends on its thickness value. Table 6.2 presents the buckling and the post-buckling responses (γ_{cr}) of the simply supported square FG (*SUS304/Si$_3$N$_4$*) spherical shell panel (*R*/*a*=5, *n*=2 and *a*/*b*=1) for different thickness ratios (*a*/*h*=20 and 100) and the amplitude ratios. It is observed that the buckling and the post-buckling responses are reducing with the increase in thickness ratios, i.e., the thick FG spherical panel exhibits higher buckling and post-buckling strength under the thermal environment than the thin FG spherical panel. However, the other observations of the buckling and post-buckling responses of the FG spherical panel under the temperature fields and the temperature dependent (TD/TID) material properties are following the same trend as in the previous example.

6.3.2.1.3 Effect of curvature ratio on thermal post-buckling strength of FG spherical panel

The influence of curvature ratios on the buckling and the post-buckling responses (γ_{cr}) of the FG spherical shell panel is examined under three temperature field and presented in Table 6.3. For the computational purpose, the simply supported square FG (*SUS304/Si$_3$N$_4$*) spherical shell panel (*a*/*h*=10, *n*=2 and *a*/*b*=1) is considered and the responses are obtained for two curvature ratios (*R*/*a*=10 and 50) and different amplitude ratios. It is observed that the buckling and the post-buckling responses are reducing with the increase in curvature ratios, i.e., the curved FG panel exhibits higher buckling and post-buckling strength than the flat panel. However, the other observations of the buckling and the post-buckling responses of the FG spherical panel related to the temperature fields and the temperature dependent (TD/TID) material properties are exhibiting the same fashion as in the previous examples.

6.3.2.1.4 *Effect of aspect ratio on thermal post-buckling strength of FG spherical panel*

In this example, the effect of aspect ratios on the buckling and the post-buckling responses (γ_{cr}) of the FG spherical shell panel is examined under the thermal environment. Table 6.4 presents the buckling and the post-buckling responses of the simply supported FG ($SUS304/Si_3N_4$) spherical shell panel (a/h=10, n=2 and R/a=5) for different aspect ratios (a/b=1 and 2) and the amplitude ratios. It is observed that the buckling and the post-buckling responses are increasing with the increase in aspect ratios, i.e., the slender FG spherical panel exhibits higher buckling and the post-buckling strength than the square FG panel. However, the other observations of the buckling and the post-buckling responses of the FG spherical panel related to the temperature fields and the temperature dependent material properties are exhibiting same trend as in the case of previous examples.

6.3.2.1.5 *Effect of support condition on thermal post-buckling strength of FG spherical panel*

The influence of support conditions on the buckling and the post-buckling responses (γ_{cr}) of the FG spherical shell panel is examined under thermal fields as in Table 6.5. For the computational purpose, the square FG ($SUS304/Si_3N_4$) spherical shell panel (a/h=10, n=2, R/a=5 and a/b=1) is considered and the responses are obtained for different support cases (*SSSS* and *CCCC*) and the amplitude ratios. It is observed that the buckling and the post-buckling responses are increasing with the increase in number of

support constraints, i.e., the fully clamped (*CCCC*) FG spherical shell panel has maximum buckling and post-buckling strength. The FG spherical panel under the linear temperature field exhibits maximum buckling and the post-buckling strength as compared to the uniform temperature field. However, the FG spherical panel with the TID properties is showing the higher buckling and the post-buckling strength than the TD-FG spherical panel. Figure 6.7 shows the buckling mode shapes (first and second) of the FG spherical shell panel (a/h=10, R/a=5, n=2) for CFCF support conditions under linear temperature field.

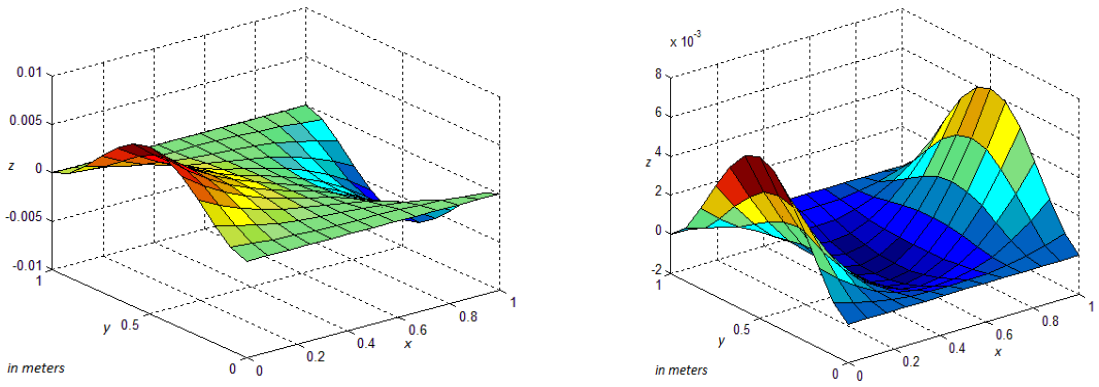

(a) 1st mode (b) 2nd mode

Figure 6.7. First and second buckling mode shapes of FG spherical panel under CFCF support condition (a) 1st Mode (b) 2nd Mode

6.3.2.1.6 Effect of power-law indices on mechanical post-buckling strength of FG spherical panel

The previous examples have already demonstrated the buckling and the post-buckling behaviour of the FG spherical panel under thermal loadings. Now, the buckling and the post-buckling responses of the FG spherical panel are presented under the uniaxial and biaxial compression loads without considering the temperature effect. In this example, the buckling and the post-buckling responses $\left(\overline{\gamma}_{cr} = \gamma_{cr} b^2 / E_c h^3\right)$ of the simply

supported square FG (*SUS304/Si$_3$N$_4$*) spherical shell panel (*R*/*a*=5, *a*/*h*=10 and *a*/*b*=1) are examined for different power-law indices (*n*= 0.2 and 5) and amplitude ratios and presented in Table 6.6. It is observed that the buckling and the post-buckling responses are decreasing with the increase in power-law indices, i.e., the ceramic-rich FG spherical panel is showing the maximum buckling and the post-buckling strength under the in-plane mechanical loading condition than the metal-rich FG spherical panel. It is also noted that the FG spherical panel under uniaxial compression loading exhibits higher buckling and post-buckling strength.

6.3.2.1.7 Effect of thickness ratio on mechanical post-buckling strength of FG spherical panel

In this example, the critical buckling load parameters $\left(\overline{\gamma}_{cr} = \gamma_{cr} b^2 / E_c h^3\right)$ of the simply supported square FG (*SUS304/Si$_3$N$_4$*) spherical shell panel (*R*/*a*=5, *n*=2 and *a*/*b*=1) is examined for different thickness ratios (*a*/*h*=20 and 100) and the amplitude ratios and presented in Table 6.7. It is observed that the buckling and the post-buckling responses are increasing with the increase in the thickness ratios, i.e., the thick FG spherical panel is showing the maximum buckling and the post-buckling strength under the in-plane mechanical loading condition than the thin FG spherical panel. It is also noted that the FG spherical panel under the uniaxial edge compression loading along the *x* direction exhibits higher buckling and the post-buckling strength than in the case of biaxial edge compression and the results are within the expected line.

6.3.2.1.8 Effect of curvature ratio on mechanical post-buckling strength of FG spherical panel

The influence of curvature ratios on the buckling and the post-buckling responses $\left(\overline{\gamma}_{cr} = \gamma_{cr} b^2 / E_c h^3\right)$ of the simply supported square FG (*SUS304/Si$_3$N$_4$*) spherical shell panel (*a*/*h*=10, *n*=2 and *a*/*b*=1) is examined under in-plane mechanical loading condition. The responses are obtained for different curvature ratios (*R*/a=10 and 50) and the amplitude ratios and presented in Table 6.8. It is observed that the buckling and the post-buckling responses are reducing with the increase in curvature ratios, i.e., the curved FG

spherical panel is having maximum buckling and the post-buckling strength than the flat FG panel. It is also noted that the FG spherical panel under uniaxial edge compression loading along the x direction has higher buckling and post-buckling strength than in the case of biaxial edge compression.

6.3.2.1.9 Effect of support condition on mechanical post-buckling strength of FG spherical panel

The influence of different support conditions on the buckling and the post-buckling responses $\left(\overline{\gamma}_{cr} = \gamma_{cr} b^2 / E_c h^3\right)$ of the square FG (*SUS304/Si$_3$N$_4$*) spherical shell panel (a/h=10, n=2, R/a=5 and a/b=1) is examined under the uniaxial and the biaxial edge compression. The responses are computed for two support conditions (*SSSS* and *CCCC*) and the amplitude ratios and presented in Table 6.9. It is observed that the buckling and the post-buckling responses are increasing with the increase in number of support constraints, i.e., the fully clamped (*CCCC*) FG spherical panel is exhibiting the maximum buckling and the post-buckling strength. It is also noted that the FG spherical panel under the uniaxial edge compression loading has higher buckling and the post-buckling strength than in the case of the biaxial edge compression.

6.3.2.1.10 Thermomechanical post-buckling strength of FG spherical panel

In this example, the buckling and the post-buckling behaviour of the FG spherical shell panel are examined under uniaxial compression and uniform temperature field. Table 6.10 presents the critical buckling load parameter (γ_{cr}) of the square FG (*SUS304/Si$_3$N$_4$*) spherical shell panel (a/h=10, R/a=5 and a/b=1) under two support conditions (*SSSS* and *CCCC*), three power-law indices (n=0.2, 2 and 5) and five amplitude ratios ($W_{\max}/h$ = 0, 0.5, 1, 1.5 and 2). It is observed that the buckling and the post-buckling responses are increasing with the increase in the number of support constraints and reducing with the increase in power-law indices, i.e., the fully clamped (*CCCC*) and ceramic-rich FG spherical panel exhibits maximum buckling and the post-buckling strength.

6.3.2.2 Cylindrical FG shell panel

The previous section discussed the stability behaviour of the spherical shell panel under various conditions. Now, the buckling and the post-buckling strength of the FG

cylindrical (R_x=R and R_y=∞) shell panel under the in-plane mechanical and/or the thermal load are examined for different geometrical and the material parameters.

6.3.2.2.1 Effect of power-law index on thermal post-buckling strength of FG cylindrical panel

In this example, the influence of power-law indices on the buckling and the post-buckling responses (γ_{cr}) of the FG cylindrical shell panel are examined. Table 6.11 presents the buckling and the post-buckling responses of simply supported square FG (*SUS304/Si$_3$N$_4$*) cylindrical shell panel (R/a=5, a/h=10 and a/b=1) for different power-law indices (n= 0.2 and 5) and the amplitude ratios. It is observed that the ceramic-rich FG cylindrical panel exhibits higher buckling and the post-buckling strength under the thermal environment than the metal-rich FG panel. It is also noted that the FG cylindrical panel under the nonlinear temperature field exhibits maximum buckling and the post-buckling strength as compared to other temperature cases. However, the FG cylindrical panel with TID material properties is showing higher buckling and the post-buckling strength than the TD-FG cylindrical panel.

6.3.2.2.2 Effect of thickness ratio on thermal post-buckling strength of FG cylindrical panel

The influence of thickness ratios on the buckling and the post-buckling behaviour of the FG (*SUS304/Si$_3$N$_4$*) cylindrical shell panel (R/a=5, n=2 and a/b=1) are examined under thermal environment and presented in Table 6.12. The buckling and the post-buckling responses (γ_{cr}) are obtained for different thickness ratios (a/h=20 and 100) and four amplitude ratios. It is observed that the buckling and the post-buckling responses are reducing with the increase in thickness ratios, i.e., the thick FG cylindrical panel exhibits higher buckling and the post-buckling strength under the thermal environment than the thin FG panel. However, the buckling and post-buckling strength of the FG cylindrical panel under different temperature field with TD and the TID properties are following the same line as expected.

6.3.2.2.3 Effect of curvature ratio on thermal post-buckling strength of FG cylindrical panel

In this example, the effect of the curvature ratios (R/a=10 and 50) on the buckling and the post-buckling responses (γ_{cr}) of FG ($SUS304/Si_3N_4$) cylindrical shell panel (a/h=10, n=2 and a/b=1) are examined at different thermal fields and the amplitude ratios and presented in Table 6.13. It is observed that the curved FG panel exhibits higher buckling and the post-buckling strength than the FG flat panel. It is also observed that the buckling and the post-buckling responses of the FG cylindrical panel with temperature dependent and the independent properties of the FG panel under various temperature fields follow the same fashion as in the earlier.

6.3.2.2.4 Effect of aspect ratio on thermal post-buckling strength of FG cylindrical panel

Now, the effect of aspect ratios on the buckling and the post-buckling responses of the FG cylindrical shell panel is examined under the thermal environment**.** Table 6.14 presents the critical buckling temperature load parameter (γ_{cr}) of the simply supported FG (*SUS304/*Si_3N_4) cylindrical shell panel (*a*/*h*=10, *n*=2 and *R*/a=5) for different aspect ratios (*a*/*b*=1 and 2) and the amplitude ratios. It is observed that the buckling and the post-buckling responses are increasing with the increase in aspect ratios, i.e., the slender FG cylindrical panel exhibits the higher buckling and the post-buckling strength than the square FG panel. However, the buckling and the post-buckling strength of the FG cylindrical panel under different temperature field and the temperature dependent material properties are demonstrating repetitive behaviour as expected.

6.3.2.2.5 Effect of support condition on thermal post-buckling strength of FG cylindrical panel

The influence of two support conditions on the buckling and the post-buckling responses (γ_{cr}) of the FG cylindrical shell panel (*a*/*h*=10, *n*=2, *R*/*a*=5 and *a*/*b*=1) is examined under two temperature fields and shown in Table 6.15. The responses are obtained for the different support cases (*SSSS* and *CCCC*) and the amplitude ratios. It is observed that the fully clamped (*CCCC*) FG cylindrical shell panels demonstrates nearly double the buckling and the post-buckling strength in comparison the simply support condition. It is also noted that the FG cylindrical panel under the linear temperature field exhibits maximum buckling and the post-buckling strength. However, the FG cylindrical panel with TID material properties is showing higher buckling and the post-buckling strength than the TD-FG cylindrical panel.

Effect of power-law indices on mechanical post-buckling strength of FG cylindrical panel

The previous examples have demonstrated the buckling and the post-buckling behaviour of the FG cylindrical panel under thermal loadings. Now, the buckling and the post-buckling responses of the FG cylindrical shell panel is examined under the uniaxial and biaxial compression loads without considering the temperature effect. In this example, the buckling and the post-buckling responses $\left(\overline{\gamma}_{cr} = \gamma_{cr} b^2 / E_c h^3\right)$ of the simply supported square FG (*SUS304/*Si_3N_4) cylindrical shell panel (*R*/*a*=5, *a*/*h*=10 and *a*/*b*=1) are examined for two different power-law indices (*n*= 0.2 and 5) and amplitude ratios and presented in Table 6.16. It is observed that the buckling and the post-buckling responses are reducing with the increase in power-law indices, i.e., the ceramic-rich FG cylindrical panel is having maximum buckling and post-buckling strength under the in-plane mechanical loading condition than the metal-rich FG cylindrical panel. It is also noted that the FG cylindrical shell panel under uniaxial compression loading exhibits higher buckling and post-buckling strength than that of the biaxial compression and the responses are within the expected line.

Effect of thickness ratio on mechanical post-buckling strength of FG cylindrical panel

Further, the critical buckling load parameter $\left(\overline{\gamma}_{cr} = \gamma_{cr} b^2 / E_c h^3\right)$ of the simply supported square FG (*SUS304/Si$_3$N$_4$*) cylindrical shell panel (*R*/*a*=5, *n*=2 and *a*/*b*=1) is analysed in this example for different thickness ratios (*a*/*h*=20 and 100) and the amplitude ratios and presented in Table 6.17. It is observed that the buckling and the post-buckling responses are increasing with the increase in thickness ratios, i.e., the thick FG cylindrical panel is showing higher buckling and the post-buckling strength under the in-plane mechanical load than that of the thin FG cylindrical panel. It is also noted that the FG cylindrical panel under uniaxial edge compression load has higher buckling and the post-buckling strength than that of the biaxial edge compression.

6.3.2.2.6 Effect of curvature ratio on mechanical post-buckling strength of FG cylindrical panel

The influence of curvature ratios on the buckling and the post-buckling responses $\left(\overline{\gamma}_{cr} = \gamma_{cr} b^2 / E_c h^3\right)$ of the simply supported square FG (*SUS304/Si$_3$N$_4$*) cylindrical shell panel (*a*/*h*=10, *n*=2 and *a*/*b*=1) is examined under the in-plane mechanical load. The responses are obtained for different curvature ratios (*R*/a=10 and 50) and amplitude ratios and presented in Table 6.18. It is observed that the buckling and the post-buckling responses are reducing with the increase in curvature ratios, i.e., the curved FG shell panel has higher buckling and the post-buckling strength than that of the flat FG panel. It is also noted that the FG cylindrical shell panel under the uniaxial edge compression loading displays higher buckling and post-buckling strength than the biaxial edge compression.

6.3.2.2.7 Effect of support condition on mechanical post-buckling strength of FG cylindrical panel

The influence of support conditions on the buckling and the post-buckling responses $\left(\overline{\gamma}_{cr} = \gamma_{cr} b^2 / E_c h^3\right)$ of square FG (*SUS304/Si$_3$N$_4$*) spherical shell panel (*a*/*h*=10, *n*=2, *R*/*a*=5 and *a*/*b*=1) are examined under in-plane mechanical loading. The responses

are obtained for different support conditions (*SSSS* and *CCCC*) and amplitude ratios and presented in Table 6.19. It is observed that the buckling and the post-buckling response are increasing with the increase in number of support constraints, i.e., the fully clamped (*CCCC*) FG cylindrical panel is exhibiting the maximum buckling and post-buckling. It is also noted that the FG cylindrical shell panel under the uniaxial edge compression load show higher buckling and post-buckling strength than the biaxial compression.

In previous problems of the FG cylindrical shell panels are investigated for the buckling and the post-buckling responses are computed under the temperature and the in-plane (uniaxial and biaxial) mechanical load individually. Now, in this example, the combined effect of thermomechanical load on the FG cylindrical shell panel is examined. Table 6.20 presents the buckling and the post-buckling responses (γ_{cr}) of the square FG (*SUS304/Si$_3$N$_4$*) cylindrical shell panel (a/h=10, R/a=5 and a/b=1) for two support conditions (*SSSS* and *CCCC*), three power-law indices (n=0.2, 2 and 5) and four amplitude ratios (W_{max}/h = 0, 0.5, 1 and 1.5). It is observed that the buckling and the post-buckling responses are increasing with the increase in number of support constraints, i.e., the fully clamped (*CCCC*) FG cylindrical panel have higher buckling and the post-buckling strength as in the earlier examples. It is also interesting to note that the ceramic-rich FG cylindrical panel, i.e., for the lower power indices the FG shell panels are exhibiting higher buckling and the post-buckling strength than the metal-rich FG shell panel.

6.3.2.3 Hyperbolic FG shell panel

In this section, the buckling and the post-buckling responses of the FG hyperbolic (R_x=R and R_y=-R) shell panel under the in-plane mechanical, the thermal and the thermomechanical loads are examined for various geometrical and material parameters.

6.3.2.3.1 Effect of power-law index on thermal post-buckling strength of FG hyperbolic panel

The influence of power-law indices on the buckling and the post-buckling responses (γ_{cr}) of the simply supported square FG (*SUS304/Si$_3$N$_4$*) hyperbolic shell

(R/a=5, a/h=10 and a/b=1) panel are examined under thermal environment and presented in Table 6.21. The responses are obtained for different power-law indices (n=0.2 and 5) and the amplitude ratios. It is observed that the buckling and the post-buckling responses are reducing with the increase in power-law indices, i.e., the ceramic-rich FG hyperbolic shell panel has higher buckling and the post-buckling strength than the metal-rich FG hyperbolic panel. The FG hyperbolic shell panel under the nonlinear temperature distribution exhibits maximum buckling and the post-buckling strength as compared to the linear and the uniform temperature distribution. However, the FG hyperbolic panel with TID material properties are showing higher buckling and post-buckling strength than the TD case and it is expected.

6.3.2.3.2 Effect of thickness ratio on thermal post-buckling strength of FG hyperbolic panel

Table 6.22 presents the buckling and the post-buckling responses (γ_{cr}) of the simply supported square FG ($SUS304/Si_3N_4$) hyperbolic shell panel (R/a=5, n=2 and a/b=1) for different thickness ratios (a/h=20 and 100) and four amplitude ratios. It is observed that the buckling and the post-buckling strength are reducing with the increase in thickness ratios, i.e., the thick FG hyperbolic panel exhibits higher buckling and post-buckling strength under the thermal environment than the thin FG panel. The FG hyperbolic shell panel under the nonlinear temperature distribution exhibits maximum buckling and the post-buckling strength as compared to the other temperature cases. However, the FG hyperbolic shell panel with TID material properties are showing higher buckling and the post-buckling strength than the TD case, except in the case of the thin (a/h=100) FG hyperbolic panel under uniform temperature field.

6.3.2.3.3 Effect of curvature ratio on thermal post-buckling strength of FG hyperbolic panel

The influence of curvature ratios on the buckling and the post-buckling responses (γ_{cr}) of the FG hyperbolic shell panel is examined under three temperature load distributions as in Table 6.23. For the computational purpose, the simply supported

square FG (*SUS304/Si_3N_4*) hyperbolic shell panel (*a*/*h*=10, *n*=2 and *a*/*b*=1) is considered and the responses are obtained for different curvature ratios (*R*/*a*=10 and 50) and the amplitude ratios. It is observed that the buckling responses are reducing with the increase in curvature ratios whereas the post-buckling responses are following non-monotonous behaviour, may be due the anticlastic curvature of the hyperbolic shell panel. It is also noted that the FG hyperbolic shell panels of TID material properties under the nonlinear temperature field exhibit maximum buckling and the post-buckling strength as compared to other temperature distributions.

6.3.2.3.4 Effect of aspect ratio on thermal post-buckling strength of FG hyperbolic panel

In this example, the effect of aspect ratios on the buckling and the post-buckling responses (γ_{cr}) of the FG hyperbolic shell panel is examined under thermal environment. Table 6.24 presents the buckling and the post-buckling responses of the simply supported FG (*SUS304/Si_3N_4*) spherical shell panel (*a*/*h*=10, *n*=2 and *R*/a=5) for different aspect ratios (*a*/*b*=1 and 2) and amplitude ratios. It is observed that the buckling and the post-buckling responses are increasing with the increase in aspect ratios, i.e., the slender FG hyperbolic shell panel exhibits higher buckling and the post-buckling strength than the square FG panel. However, the other observations of the buckling and post-buckling responses of FG hyperbolic panel related to the temperature fields and the temperature dependent material properties are following the similar trend as in the previous example.

6.3.2.3.5 Effect of support condition on thermal post-buckling strength of FG hyperbolic panel

The influence of support conditions on the buckling and the post-buckling responses (γ_{cr}) of FG hyperbolic shell panel is examined under two temperature distributions (uniform and linear) and presented in Table 6.25. For the computational purpose, the square FG (*SUS304/Si_3N_4*) hyperbolic shell panel (*a*/*h*=10, *n*=2, *R*/*a*=5 and *a*/*b*=1) is considered and the responses are obtained for two support conditions (*SSSS* and *CCCC*) and the amplitude ratios. It is observed that the clamped (*CCCC*) FG hyperbolic

panel displays maximum buckling and the post-buckling strength. The FG hyperbolic shell panel under the nonlinear temperature distribution exhibits maximum buckling and the post-buckling strength as compared to other temperature distributions. It is also interesting to note that the FG hyperbolic shell panel with TID material properties are showing higher buckling and the post-buckling strength than that of the TD-FG panel, except few cases of the clamped FG hyperbolic panel under the uniform temperature field.

6.3.2.3.6 Effect of power-law indices on mechanical post-buckling strength of FG hyperbolic panel

The buckling and the post-buckling behaviour of the FG hyperbolic panel under thermal loading have already been discussed in earlier examples. Now, the buckling and the post-buckling responses of the FG hyperbolic shell panels under the uniaxial and the biaxial compression loads without considering the temperature effect are investigated further. In this example, the buckling and the post-buckling responses $\left(\overline{\gamma}_{cr} = \gamma_{cr} b^2 / E_c h^3\right)$ of the simply supported square FG (*SUS304/Si$_3$N$_4$*) hyperbolic shell panel (*R*/*a*=5, *a*/*h*=10 and *a*/*b*=1) are examined for different power-law indices (*n*= 0.2 and 5) and amplitude ratios and presented in Table 6.26. It is observed that the buckling and the post-buckling responses are reducing with the increase in power-law indices, i.e., the ceramic-rich FG hyperbolic panels have the maximum buckling and the post-buckling strength under the in-plane mechanical loading condition than the metal-rich FG hyperbolic panel. It is also noted that the FG hyperbolic shell panel under the uniaxial compression loading exhibits higher buckling and the post-buckling strength.

Effect of thickness ratio on mechanical post-buckling strength of FG hyperbolic panel

In this example, the buckling and the post-buckling $\left(\overline{\gamma}_{cr} = \gamma_{cr} b^2 / E_c h^3\right)$ behaviour of the simply supported square FG (*SUS304/Si$_3$N$_4$*) hyperbolic shell panel (*R*/*a*=5, *n*=2 and *a*/*b*=1) are examined for different thickness ratios (*a*/*h*=20 and 100) and the amplitude ratios and presented in Table 6.27. It is observed that the buckling and the post-buckling responses are increasing with the increase in thickness ratios, i.e., the thick

FG hyperbolic shell panel has maximum buckling and the post-buckling strength under the in-plane mechanical load than that of the thin FG panel. It is also noted that the FG hyperbolic shell panel under the uniaxial edge compression loading along the *x* direction exhibits higher buckling and the post-buckling strength than in the case of the biaxial edge compression.

6.3.2.3.7 Effect of curvature ratio on mechanical post-buckling strength of FG hyperbolic panel

The influence of curvature ratios on the buckling and the post-buckling responses $\left(\overline{\gamma}_{cr} = \gamma_{cr} b^2 / E_c h^3\right)$ of the simply supported square FG (*SUS304/Si$_3$N$_4$*) hyperbolic shell panel (*a*/*h*=10, *n*=2 and *a*/*b*=1) is examined under the in-plane mechanical loading conditions. The responses are computed for different curvature ratios (*R*/a=10 and 50) and the amplitude ratios and presented in Table 6.28. It is observed that the buckling and the post-buckling responses are reducing with the increase in curvature ratios, i.e., the curved FG shell panel has maximum buckling and the post-buckling strength than that of the flat FG panel. It is also noted that the FG hyperbolic shell panel under the uniaxial edge compression load has the higher buckling and the post-buckling strength than in the case of the biaxial edge compression.

6.3.2.3.8 Effect of support condition on mechanical post-buckling strength of FG hyperbolic panel

The influence of support conditions on the buckling and the post-buckling responses $\left(\overline{\gamma}_{cr} = \gamma_{cr} b^2 / E_c h^3\right)$ of square FG (*SUS304/Si$_3$N$_4$*) hyperbolic shell panel (*a*/*h*=10, *n*=2, *R*/*a*=5 and *a*/*b*=1) is examined under the in-plane mechanical load. The responses are obtained for two support conditions (*SSSS* and *CCCC*) and the amplitude ratios and presented in Table 6.29. It is observed that the buckling and the post-buckling responses are increasing with the increase in number of support constraints, i.e., the clamped FG hyperbolic shell panel is exhibiting the maximum buckling and the post-buckling strength. It is also noted that the FG hyperbolic shell panel under the uniaxial edge compression loading show higher buckling and the post-buckling strength than that of the biaxial edge compression.

6.3.2.3.9 Thermomechanical post-buckling strength of FG hyperbolic panel

In this example, the buckling and the post-buckling behaviour of the FG hyperbolic shell panel are examined under uniaxial compression and uniform temperature field. Table 6.30 presents the critical buckling load parameter (γ_{cr}) of the square FG (*SUS304/Si$_3$N$_4$*) hyperbolic shell panel (*a*/*h*=10, *R*/*a*=5 and *a*/*b*=1) under different support conditions (*SSSS* and *CCCC*), the power-law indices (*n*=0.2, 2 and 5) and the amplitude ratios. It is also observed that the buckling and the post-buckling responses are increasing with the increase in number of support constraints, i.e., the clamped (*CCCC*) FG hyperbolic shell panel is exhibiting the maximum buckling and the post-buckling strength than the simply supported case. However, the ceramic-rich FG hyperbolic panels

exhibit the maximum buckling and the post-buckling strength than the metal-rich FG panel and the results are within the expected line.

6.3.2.4 Elliptical FG shell panel

The thermomechanical stability behaviour of the spherical, cylindrical and hyperbolic panels have already been discussed considering the individual and/or combined effect of mechanical and thermal load for different geometrical and material parameters in previous sections. Now, the model has been extended further to analyse thermomechanical buckling and the post-buckling strength of the FG elliptical (R_x=R and R_y=$2R$) shell panel and discussed in the following lines.

6.3.2.4.1 Effect of power-law index on thermal post-buckling strength of FG elliptical panel

In this example, the effect of power-law indices on the buckling and the post-buckling responses (γ_{cr}) of the FG elliptical shell panel are examined under different thermal field as discussed earlier. Table 6.31 presents the buckling and the post-buckling responses of the simply supported square FG (*SUS304/*Si_3N_4) elliptical shell panel (R/a=5, a/h=10 and a/b=1) for different power-law indices (n= 0.2 and 5) and the amplitude ratios. It is observed that the ceramic-rich FG elliptical panel displays higher buckling and post-buckling strength under the thermal environment than the metal-rich FG shell panel. It is also noted that the FG elliptical shell panel under the nonlinear temperature field exhibits maximum buckling and the post-buckling strength as compared

to other two temperature field. However, the FG elliptical shell panel with TID material properties are showing higher buckling and the post-buckling strength than the TD-FG elliptical panel, except in the case of the uniform thermal field.

6.3.2.4.2 Effect of thickness ratio on thermal post-buckling strength of FG elliptical panel

The influence of thickness ratios on the buckling and the post-buckling behaviour of FG (*SUS304/Si_3N_4*) elliptical shell panel (*R*/*a*=5, *n*=2 and *a*/*b*=1) is examined under thermal environment and presented in Table 6.32. The buckling and the post-buckling responses (γ_{cr}) are obtained for different thickness ratios (*a*/*h*=20 and 100) and the amplitude ratios. It is observed that the buckling and the post-buckling responses are reducing with the increase in thickness ratios, i.e., the thick FG elliptical shell panel exhibits higher buckling and post-buckling strength under the thermal environment than the thin FG shell panel. However, the buckling and the post-buckling responses of the FG elliptical shell panel under different temperature fields and the temperature dependent material properties are following the same behaviour as in the previous example.

6.3.2.4.3 Effect of curvature ratio on thermal post-buckling strength of FG elliptical panel

In this example, the effect of the curvature ratios (*R*/*a*=10 and 50) on the buckling and the post-buckling responses (γ_{cr}) of the FG (*SUS304/Si_3N_4*) elliptical shell panel (*a*/*h*=10, *n*=2 and *a*/*b*=1) is examined under different thermal fields and the amplitude ratios and reported in Table 6.33. It is observed that the curved FG shell panels exhibit the higher buckling and the post-buckling strength than the flat panels. However, the buckling and the post-buckling responses of the FG elliptical shell panel shows higher for the TID-FG panel irrespective of the thermal field.

6.3.2.4.4 Effect of aspect ratio on thermal post-buckling strength of FG elliptical panel

In this example, the effect of aspect ratios on the buckling and the post-buckling responses of the FG elliptical shell panel are examined under three thermal environments. Table 6.34 presents the critical buckling temperature load parameter (γ_{cr}) of the simply supported FG (*SUS304/*Si_3N_4) elliptical shell panel (*a*/*h*=10, *n*=2 and *R*/a=5) for different

aspect ratios (a/b=1 and 2) and the amplitude ratios. It is also observed that the buckling and the post-buckling responses are increasing with the increase in aspect ratios, i.e., the slender FG elliptical shell panels exhibit higher buckling and the post-buckling strength than the square FG panel. However, the buckling and post-buckling responses of the FG elliptical panel with temperature dependent material properties are showing smaller values in comparison to the TID properties irrespective of the thermal field.

6.3.2.4.5 Effect of support condition on thermal post-buckling strength of FG elliptical panel

The influence of support conditions on the buckling and the post-buckling responses (γ_{cr}) of the FG elliptical shell panel (a/h=10, n=2, R/a=5 and a/b=1) is examined under thermal fields and shown in Table 6.35. The responses are obtained for different support conditions (*SSSS* and *CCCC*) and the amplitude ratios. It is observed that the clamped (*CCCC*) FG elliptical shell panels are showing the maximum buckling and the post-buckling strength as compared to the simply supported case. It is also noted that the FG elliptical shell panel under the linear temperature field exhibits maximum buckling and the post-buckling strength as compared to the uniform temperature field. It is also noted that the FG elliptical shell panel subjected to uniform temperature field displays higher buckling and post-buckling strength in case of TD material properties whereas, a reverse trend in found in the case of FG elliptical shell panel subjected to linear temperature field.

6.3.2.4.6 Effect of power-law indices on mechanical post-buckling strength of FG elliptical panel

The previous examples have been discussed on the buckling and the post-buckling behaviour of the FG elliptical shell panel under various thermal loading. Now,

the buckling and the post-buckling responses of the FG elliptical shell panel under the uniaxial and the biaxial compression load are analysed without considering the temperature effect. In this example, the buckling and the post-buckling responses $\left(\overline{\gamma}_{cr} = \gamma_{cr} b^2 / E_c h^3\right)$ of the simply supported square FG (*SUS304/Si$_3$N$_4$*) elliptical shell panel (*R*/*a*=5, *a*/*h*=10 and *a*/*b*=1) are examined for different power-law indices (*n*= 0.2 and 5) and the amplitude ratios and presented in Table 6.36. It is observed that the buckling and the post-buckling responses are reducing with the increase in power-law indices, i.e., the ceramic-rich FG elliptical panels are showing the maximum buckling and the post-buckling strength under the in-plane mechanical loading condition than the metal-rich FG elliptical panel. It is also noticed that the FG elliptical shell panel under the uniaxial compression loading exhibits higher buckling and post-buckling strength than the biaxial compression loading.

6.3.2.4.7 Effect of thickness ratio on mechanical post-buckling strength of FG elliptical panel

In this example, the critical buckling load parameter $\left(\overline{\gamma}_{cr} = \gamma_{cr} b^2 / E_c h^3\right)$ of the simply supported square FG (*SUS304/Si$_3$N$_4$*) elliptical shell panel (*R*/*a*=5, *n*=2 and *a*/*b*=1) is analysed for different thickness ratios (*a*/*h*=20 and 100) and amplitude ratios and presented in Table 6.37. It is observed that the buckling and the post-buckling responses are increasing as the thickness ratios increase, i.e., the thick FG elliptical panel is showing the maximum buckling and the post-buckling strength under the in-plane mechanical loading condition than the thin FG elliptical panel. It is also noted that the FG elliptical shell panel under uniaxial edge compression show higher buckling and the post-buckling strength than in the case of biaxial edge compression.

6.3.2.4.8 Effect of curvature ratio on mechanical post-buckling strength of FG elliptical panel

The influence of curvature ratios on the buckling and the post-buckling responses $\left(\overline{\gamma}_{cr} = \gamma_{cr} b^2 / E_c h^3\right)$ of the simply supported square FG (*SUS304/Si$_3$N$_4$*) elliptical shell panel (*a*/*h*=10, *n*=2 and *a*/*b*=1) is examined under in-plane mechanical load. The

responses are obtained for different curvature ratios (R/a=10 and 50) and the amplitude ratios and presented in Table 6.38. It is observed that the buckling and the post-buckling responses are reducing with the increase in curvature ratios, i.e., the curved FG panel have higher buckling and the post-buckling strength than the flat FG panel. It is also noted that the FG elliptical panel subjected to uniaxial edge compression loading displays higher buckling and the post-buckling strength than the biaxial edge compression.

6.3.2.4.9 Effect of support condition on mechanical post-buckling strength of FG elliptical panel

The influence of support conditions on the buckling and the post-buckling responses $\left(\overline{\gamma}_{cr} = \gamma_{cr} b^2 / E_c h^3\right)$ of the square FG (*SUS304/Si$_3$N$_4$*) elliptical shell panel (a/h=10, n=2, R/a=5 and a/b=1) is examined under the in-plane (uniaxial and biaxial) mechanical load and discussed in detailed. The responses are obtained for different support conditions (*SSSS* and *CCCC*) and the amplitude ratios and presented in Table 6.39. It is observed that the buckling and the post-buckling responses are increasing with the increase in number of support constraints, i.e., the clamped (*CCCC*) FG elliptical panel is exhibiting the maximum buckling and the post-buckling strength than the simply support case. It is also noted that the FG elliptical panel under uniaxial edge compression loading show higher buckling and the post-buckling strength than the biaxial compression.

6.3.2.4.10 Thermomechanical post-buckling strength of FG elliptical panel

Now, in this example, the combined effect of mechanical and the thermal load on the FG (*SUS304/Si$_3$N$_4$*) elliptical shell panel on the buckling and the post-buckling behaviour is investigated. Table 6.40 presents the buckling and the post-buckling responses (γ_{cr}) of the square FG elliptical shell panel (a/h=10, R/a=5 and a/b=1) for two support conditions (*SSSS* and *CCCC*), three power-law indices (n=0.2, 2 and 5) and four amplitude ratios. It is observed that the buckling and the post-buckling responses are increasing with the increase in number of support constraints, i.e., the clamped (*CCCC*) FG elliptical shell panel have higher buckling and the post-buckling strength than the

simply support case. However, the ceramic-rich FG elliptical panel exhibits maximum buckling and the post-buckling strength than the metal-rich FG panel as well.

6.3.2.5 Effect of Shell Geometry on Post-buckling Strength under Thermal Environment

Table 6.41 presents the buckling and the post-buckling responses (γ_{cr}) of different FG shell panels (a/h=10, n=2, and a/b=1) under nonlinear temperature field. The responses are obtained for five different shell geometries (spherical, cylindrical, hyperbolic, elliptical and flat) under two support conditions (*SSSS* and *CCCC*). It is observed that the buckling and the post-buckling strength are higher in the case of fully clamped (*CCCC*) FG shell panels. However, the TID-FG shell panels exhibit higher buckling and post-buckling strength, irrespective of shell geometries and support conditions. It is also noted that the buckling and the post-buckling responses are increasing in an ascending order of flat, cylindrical, hyperbolic, elliptical and spherical FG shell panels.

6.4 Conclusions

In this chapter, the buckling and the post-buckling responses of the FG shell panels are investigated under the in-plane (uniaxial and biaxial) mechanical, the thermal and thermomechanical load. The desired buckling and the post-buckling responses are computed using the customised computer code based on the developed mathematical model. The present model utilised both the TD and the TID material properties to achieve the realistic responses. The convergence and the validation behaviour of the present numerical model for the buckling and the post-buckling responses of the FG shell panel are examined. The influences of various geometrical and material parameters on the buckling and the post-buckling behaviour of the FG shell panels are analysed under the influence of the individual and/or combined thermomechanical load. Based on the numerical results, the following concluding remarks are drawn.

(a) The parametric study reveals that the thickness ratio, the curvature ratios, the power-law indices, the aspect ratios, the support conditions, the temperature dependent material properties and the loading conditions affect the buckling/post-buckling strength of FG shell panel noticeably.

(b) The FG shell panels under the nonlinear temperature field show higher buckling and the post-buckling strength as compared to other thermal fields.

(c) It is also observed that the TD-FG shell panels exhibit the higher buckling and post-buckling strength than the TD-FG panel under all different temperature distributions whereas few exceptions are also observed in the hyperbolic and the elliptical shell panels, especially for the uniform temperature field.

(d) The buckling and the post-buckling strength are higher for the FG shell panel under the uniaxial edge compression.

(e) It is also observed that the ceramic-rich FG shell panel exhibits the maximum buckling and the post-buckling strength under the mechanical and/or thermal loading conditions as compared to the metal-rich FG shell panels.

(f) The thick FG shell panel exhibits higher buckling and the post-buckling strength under the mechanical and/or the thermal loading.

(g) The FG shell panel with higher curvature exhibits higher buckling and the post-buckling strength under the mechanical or the thermal loading.

(h) The slender FG shell panel exhibits higher buckling and the post-buckling strength under the thermal loading conditions.

(i) The clamped FG shell panels display higher buckling and the post-buckling strength under the mechanical and/or thermal loading cases.

(j) It is also noticed that the post-buckling strength increases as the amplitude ratio increases for each type of the FG shell panels.

(k) The buckling and the post-buckling responses are increasing in the ascending order of flat, cylindrical, hyperbolic, elliptical and spherical FG shell panels.

(l) It can be concluded from the computed results that the present developed mathematical model based on the HSDT kinematics and Green-Lagrange nonlinearity is capable of solving the buckling and the post-buckling behaviour of FG shell panels under mechanical, the thermal and thermomechanical load.

CHAPTER 7

CLOSURES

7.1 Concluding Remarks

In this present work, a general nonlinear mathematical model of the FG shell panel is proposed and developed to investigate the linear and nonlinear structural responses (free vibration, buckling and bending) under thermomechanical loading. The present model is developed based on the HSDT mid-plane kinematics and Green-Lagrange geometrical nonlinearity. In addition, all the nonlinear higher-order terms are included in the present formulation for the sake of generality and to capture the exact flexure of the structure under the combined loading condition. The constitutive relations of the FG shell panels are obtained for both the temperature-dependent and independent material properties. The final forms of equilibrium equations for each type of analysis are derived using the variational principle and solved subsequently through a suitable nonlinear finite element approach in conjunction with the direct iterative method. The convergence and the validation study of the present numerical model have been performed through various illustrations and compared with the available published literature. The comparison study of the present analysis indicates the necessity and the importance of the presently proposed nonlinear model under the individual and/or combined loading condition. The influence of the various geometrical (the thickness ratio, the curvature ratio, the aspect ratio), material (the power-law index) parameters and the support conditions on the flexural, vibration and buckling and post-buckling

responses of the FG shell panels under the combined loading conditions are examined under different temperature loading and discussed in detail. Based on the outcomes of previous chapters (Chapters 4-6), the following concluding remarks are drawn:

- It is evident that the HSDT mid-plane kinematics in conjunction with Green-Lagrange type geometrical nonlinearity is more realistic for the small strain and large (finite) deformation problems.

- The convergence studies of different linear and nonlinear problems confirm the consistency and the stability of the present nonlinear FE model and it has been found that a (5×5) mesh is sufficient for the linear and the nonlinear flexural problems whereas the linear and nonlinear vibration and the buckling and the post-buckling problems converge well at (6×6) mesh.

- The comparison studies reveal the effectiveness and the necessity of the presently developed nonlinear mathematical model for different problems such as the bending, vibration and the buckling and post-buckling analysis of the FG flat/curved shell panels under thermal and/or mechanical loading.

- The numerous numerical illustrations under elevated environmental conditions exhibit the robustness and the stability of the present nonlinear FE model. It is also noted that the bending/vibration/buckling behaviour of the FG curved shell panels greatly depends on the geometrical and material parameters, and the loading and the support conditions. In continuation of the above, it is also observed that the various FG shell panel geometries (flat, spherical, cylindrical, hyperbolic and elliptical) have the substantial influence on the linear/nonlinear structural responses.

- The ceramic-rich ($n \rightarrow 0$) FG shell panel exhibits the maximum linear and nonlinear vibration response and the buckling and the post-buckling strength whereas the metal-rich ($n \rightarrow \infty$) FG shell panel displays maximum flexural strength irrespective of geometrical parameters, shell geometries and loading and the support conditions.

- The linear deflection parameters reduce with the increase in thickness ratios whereas the nonlinear deflection parameters follow a non-repetitive behaviour for each case of panel geometry. The thin (a/h=100) FG shell panel exhibits maximum linear frequency parameters under both the ambient and elevated thermal environment. However, the frequency ratios of the FG shell panels under the ambient condition increase with the increase in thickness ratios, except in the case of hyperbolic shell panel. However, the nonlinear vibration responses of the FG shell panel under elevated thermal field are showing a reverse trend. In addition, the FG shell panel with a/h=20 exhibits higher buckling and post-buckling strength under both the mechanical and thermal loading conditions.

- The effect of curvature ratios on the flexural behaviour is profound in the synclastic type FG shell panels (spherical, cylindrical and elliptical) whereas in the anticlastic type shell panel, the effects of curvature ratios on the deflection parameters are insignificant. However, the linear and the nonlinear deflection parameters are increasing with the increase in the curvature ratios ($R/a \rightarrow \infty$). The non-dimensional linear frequency parameters are decreasing as the power-law indices and the curvature ratios increase for each case, whereas the FG hyperbolic shell panel exhibits the reverse trend for the curvature ratios.

- It is also interesting to note that the frequency ratios are reducing with the increase in the curvature ratios for each case of the panel geometries. However, the effect of curvature ratio on the frequency ratios of the hyperbolic FG panels is insignificant. The FG shell panel with large curvature (R/a=50) exhibits higher buckling and post-buckling strength under the mechanical and the thermal loading conditions.

- The flexural responses of FG shell panel are prominently affected by varying the aspect ratios in all the cases analysed in this present study. It is observed that the linear and the nonlinear central deflection parameters are reducing as the aspect ratios increase. However, the nonlinearity effect is insignificant for

the higher aspect ratios. The non-dimensional linear frequency parameters are increasing for each of the FG panel geometries as the aspect ratios increases. The frequency ratios of the FG shell panels are increasing with the decrease in aspect ratio, i.e., the nonlinearity is higher in the case of square (*a/b*=1) FG shell panel. The slender FG shell panel structure exhibits higher buckling and the post-buckling strength under the thermal loading conditions.

- The type of support conditions affects greatly on the flexural behaviour of FG shell panels. The linear and the nonlinear non-dimensional deflection parameters are reducing with the increase in the number of support constraints, i.e., the central deflections are maximum and minimum in SSSS and CCCC type support conditions, respectively. The non-dimensional linear frequency parameters are increasing for each of the FG panel geometries as the number of support constraints increases. The frequency ratios of the FG shell panel are not showing any monotonous behaviour for the support conditions. It is also understood that the fully clamped FG shell panels have maximum buckling and post-buckling strength under the mechanical and/or thermal loading conditions and the results are within the expected line.

- The TD-FG shell panels are showing the flexible behaviour as compared to TID-FG shell panels irrespective of geometry and thermal field. In the case of TD-FG shell panel, the maximum and minimum deflections are observed for the uniform temperature and the nonlinear temperature field. The TID-FG shell panels under uniform thermomechanical load exhibit minimum deflection. It is also interesting to note that the differences between the deflection parameters of TID-FG panel under the linear and the nonlinear temperature field are insignificant.

- The FG shell panel with TID material properties is showing the maximum linear frequency parameters. It is also noted that the linear frequency parameters of the FG shell panel are showing the maximum and minimum under the uniform and the linear temperature field. The FG shell panel with TID

material properties is displaying the maximum frequency ratio. However, the frequency ratios are following an increasing trend with the ascending order of uniform, linear and nonlinear temperature field. The FG shell panels under the nonlinear temperature field display maximum buckling and the post-buckling strength as compared to other thermal fields. The FG shell panels with TID material properties exhibit the higher buckling and post-buckling strength than the TD case for each of the temperature distributions whereas few exceptions are also observed for the hyperbolic and the elliptical shell panels, especially under the uniform temperature case.

- The spherical FG shell panel demonstrates higher stiffness than the other FG shell geometries, irrespective of geometrical and material parameters, and loading/support conditions.

7.2 Significant Contributions of the Thesis

The contributions of the present research work are as follows:

- A general nonlinear mathematical model of the FG doubly-curved shell panel is developed using the HSDT mid-plane displacement field and the geometrical nonlinearity in Green-Lagrange sense. In addition, all the nonlinear higher-order nonlinear terms are incorporated in the present mathematical formulation to compute the exact flexure of the FG shell panel under severe geometrical nonlinearity and elevated thermal field.
- The effective material properties of the FGM panel are evaluated using the Voigt's micromechanical model via the power-law distribution of the volume fractions of the FGM constituents. Both the TD and TID material properties of FGM are incorporated in the constitutive relation. In this study, three different temperature fields (uniform, linear and nonlinear) are considered across the thickness direction of the FG shell panel.
- The linear and nonlinear flexural, linear and nonlinear vibration and the buckling and the post-buckling strength of different FG single/doubly curved panels (spherical,

cylindrical, hyperbolic and elliptical) are examined under combined thermomechanical loading.

- A comprehensive parametric study is performed to exhibit the influences of different geometrical (the thickness ratio, the curvature ratio, the aspect ratio) and material (the power-law index) parameters, support conditions and loading types on the linear and nonlinear flexural, vibration and the buckling behaviour of the FG shell panels.

7.3 Future Scope of the Research

- In this study, all the analyses are performed for the unidirectional grading of the FGM structure and it can be extended for the multi-directional grading further.
- The present study deals with the static responses of FG shell panel under thermomechanical loading conditions and that can be extended for the transient loading cases, as well.
- The present study is performed based on the deterministic assumptions of the material and environmental randomness. The probabilistic analysis can be done in order to consider the randomness in the system properties.
- The damped free vibration and forced vibration study can be performed for the FG shell panels.
- The present study of FG structures can also be extended by considered the initial geometric imperfections and the elastic foundations.
- The experimentations can be performed for the flexural/vibration/buckling behaviour of the FGM structures under unlike environment conditions.
- The optimization study can also be performed for the volume fractions of the FGM constituents.

REFERENCES

Alijani, F., Amabili, M. (2014). Non-linear vibrations of shells: A literature review from 2003 to 2013. *International Journal of Non-Linear Mechanics* 58:233–257.

Alijani, F., Amabili, M., Karagiozis, K., Bakhtiari-Nejad, F. (2011a) Nonlinear vibrations of functionally graded doubly curved shallow shells. *Journal of Sound and Vibration* 330: 1432–1454.

Alijani, F., Amabili, M., Karagiozis, K., Bakhtiari-Nejad, F. (2011b). Thermal effects on nonlinear vibrations of functionally graded doubly curved. *Composite Structures* 93: 2541–2553.

Alinia, M. M., Ghannadpour, S. A. M. (2009). Nonlinear analysis of pressure loaded FGM plates. *Composite Structures* 88:354–359.

Asemi, K., Salami, S. J., Salehi, M., Sadighi, M. (2014). Dynamic and static analysis of FGM skew plates with 3D elasticity based graded finite element modeling. *Latin American Journal of Solids and Structures* 11: 504–533.

Atmane, H. A., Tounsi A., Mechab, I., Bedia, E. A. A. (2010). Free vibration analysis of functionally graded plates resting on Winkler–Pasternak elastic foundations using a new shear deformation theory. *International Journal of Mechanics and Materials in Design* 6:113–121.

Baferani, A. H., Saidi, A. R., Jomehzadeh, E. (2012). Exact analytical solution for free vibration of functionally graded thin annular sector plates resting on elastic foundation. *Journal of Vibration and Control* 18(2): 246–267.

Bayat, M., Sahari, B. B., Saleem, M., Hamouda, A. M. S., Reddy, J. N. (2009). Thermo elastic analysis of functionally graded rotating disks with temperature-dependent material properties: uniform and variable thickness. *International Journal of Mechanics and Materials in Design* 5:263–279.

Bhangale, R. K., Ganesan, N., Padmanabhan C. (2006). Linear thermoelastic buckling and free vibration behavior of functionally graded truncated conical shells. *Journal of Sound and Vibration* 292:341–371.

Bich, D. H., Duc, N. D., Quan, T. Q. (2014). Nonlinear vibration of imperfect eccentrically stiffened functionally graded double curved shallow shells resting on elastic foundation using the first order shear deformation theory. *International Journal of Mechanical Sciences* 80:16–28.

Birman, V., Byrd, L. W. (2007). Modeling and analysis of functionally graded materials and structures. *Applied Mechanics Reviews* 60:195–216.

Cook, R. D., Malkus, D. S., Plesha, M. E., Witt, R. J. (2009). Concepts and applications of finite element analysis. Singapore: Fourth edition, John Wiley & Sons Pvt. Ltd.

Darabi, M., Darvizeh, M., Darvizeh, A. (2008). “Non-linear analysis of dynamic stability for functionally graded cylindrical shells under periodic axial loading. *Composite Structures* 83:201–211.

Desai, P., Kant, T. (2012). A mixed semi analytical solution for functionally graded (FG) finite length cylinders of orthotropic materials subjected to thermal load. *International Journal of Mechanics and Materials in Design* 8:89–100.

Duc N. D., Tung H. V. (2011). Mechanical and thermal postbuckling of higher order shear deformable functionally graded plates on elastic foundations. *Composite Structures* 93:2874–2881.

Duc, N. D., Anh, V. T. T., Cong, P. H. (2014). Nonlinear axisymmetric response of FGM shallow spherical shells on elastic foundations under uniform external pressure and temperature. *European Journal of Mechanics - A/Solids* 45:80-89.

Duc, N. D., Quan, T. Q. (2012). Nonlinear stability analysis of double-curved shallow FGM panels on elastic foundations in thermal environments. *Mechanics of Composite Materials* 48 (4):435-448.

Duc, N. D., Tung, H. V. (2010a). Nonlinear analysis of stability for functionally graded cylindrical panels under axial compression. *Computational Materials Science* 49:S313–S316.

Duc, N. D., Tung, H. V. (2010b). Mechanical and thermal postbuckling of shear-deformable FGM plates with temperature-dependent properties. *Mechanics of Composite Materials* 46(5):461-476.

Ebrahimi, F., Sepiani, H. (2010). Transverse shear and rotary inertia effects on the stability analysis of functionally graded shells under combined static and periodic axial loadings. *Journal of Mechanical Science and Technology* 24(12)2359-2366.

Farid, M., Zahedinejad, P., Malekzadeh, P. (2010). Three-dimensional temperature dependent free vibration analysis of functionally graded material curved panels resting on two-parameter elastic foundation using a hybrid semi-analytic, differential quadrature method. *Materials and Design* 31:2–13.

GhannadPour, S. A. M., Alinia, M. M. (2006). Large deflection behavior of functionally graded plates under pressure loads. *Composite Structures* 75:67–71.

Ghannadpour, S. A. M., Ovesy, H. R., Nassirnia, M. (2012). Buckling analysis of functionally graded plates under thermal loadings using the finite strip method. *Computers and Structures* 108(109):93–99.

Gibson, L. J., Ashby, M. F., Karam, G. N., Wegst, U., Shercliff, H. R. (1995). Mechanical properties of natural materials. II. Microstructures for mechanical efficiency. *Proceedings of The Royal Society of London. Series A* 450:141–162.

Haddadpour, H., Mahmoudkhani, S., Navazi, H. M. (2007). Free vibration analysis of functionally graded cylindrical shells including thermal effects. *Thin-Walled Structures* 45: 591–599.

Hosseini-Hashemi, S., Taher, H. R. D., Akhavan, H., Omidi, M. (2010). Free vibration of functionally graded rectangular plates using first-order shear deformation plate theory. *Applied Mathematical Modelling* 34: 1276–1291.

Huang, H., Han, Q. (2008). Buckling of imperfect functionally graded cylindrical shells under axial compression. *European Journal of Mechanics A/Solids* 27:1026–1036.

Huang, H., Han, Q. (2009a). Nonlinear buckling and postbuckling of heated functionally graded cylindrical shells under combined axial compression and radial pressure. *International Journal of Non-Linear Mechanics* 44:209-218.

Huang, H., Han, Q. (2009b). Nonlinear elastic buckling and postbuckling of axially compressed functionally graded cylindrical shells. *International Journal of Mechanical Sciences* 51:500–507.

Huang, H., Han, Q. (2010a). Nonlinear buckling of torsion-loaded functionally graded cylindrical shells in thermal environment. *European Journal of Mechanics A/Solids* 29:42–48.

Huang, H., Han, Q. (2010b). Nonlinear dynamic buckling of functionally graded cylindrical shells subjected to time-dependent axial load. *Composite Structures* 92:593–598.

Huang, H., Han, Q. (2010c). Research on nonlinear postbuckling of functionally graded cylindrical shells under radial loads. *Composite Structures* 92:1352–1357.

Huang, X. L., Shen, H. S. (2004). Nonlinear vibration and dynamic response of functionally graded plates in thermal environments. *International Journal of Solids and Structures* 41:2403–2427.

Huang, Z. Y., Lu, C. F., Chen, W. Q. (2008). Benchmark solutions for functionally graded thick plates resting on Winkler–Pasternak elastic foundations. *Composite Structures* 85:95–104.

Javaheri R, Eslami MR (2002a) Thermal buckling of functionally graded plates. *AIAA Journal* 40:162–169.

Javaheri, R., Eslami, M. R. (2002b). Thermal buckling of functionally graded plates based on higher order theory, *Journal of Thermal Stresses*, 25:603-625.

Jha, D. K., Kant, T., Singh, R. K. (2013). A critical review of recent research on functionally graded plates. *Composite Structures* 96:833–849.

Kadoli, R., Ganesan, N., (2006). Buckling and free vibration analysis of functionally graded cylindrical shells subjected to a temperature-specified boundary condition. *Journal of Sound and Vibration* 289:450–480.

Kar V R, Panda S K (2014). Nonlinear free vibration of functionally graded doubly curved shear deformable panels using finite element method, *Journal of Vibration and Control*, DOI: 10.1177/1077546314545102.

Kar V R, Panda S K (2015a). Large deformation bending analysis of functionally graded spherical shell using FEM, *Structural Engineering and Mechanics* 53(4):661-679.

Kar V R, Panda S K (2015b). Thermoelastic analysis of functionally graded doubly curved shell panels using nonlinear finite element method,*Composite Structures*, 129: 202-212.

Kar V R, Panda S K (2015c). Nonlinear flexural vibration of shear deformable functionally graded spherical shell panel, *Steel and Composite Structures*, 18(3):693-709.

Kashtalyan, M. (2004). Three-dimensional elasticity solution for bending of functionally graded rectangular plates. *European Journal of Mechanics - A/Solids* 23:853–864.

Khabbaz, R. S., Manshadi, B. D., Abedian, A. (2009). Nonlinear analysis of FGM plates under pressure loads using the higher-order shear deformation theories. *Composite Structures* 89:333–344.

Kiani, Y., Akbarzadeh, A. H., Chen, Z. T., Eslami, M. R. (2012). Static and dynamic analysis of an FGM doubly curved panel resting on the Pasternak-type elastic foundation. *Composite Structures* 94:2474–2484.

Koizomi, M. (1997). FGM activities in Japan. *Composites Part B: Engineering* 28:1-4.

Lal, A., Singh, H. N., Shegokar, N. L. (2012). FEM model for stochastic mechanical and thermal postbuckling response of functionally graded material plates applied to panels with circular and square holes having material randomness, *International Journal of Mechanical Sciences* 62: 18–33.

Lee, Y. Y., Zhao, X., Reddy, J. N., (2010). Post-buckling analysis of functionally graded plates subject to compressive and thermal loads. *Computer Methods in Applied Mechanics and Engineering* 199:1645–1653.

Li, Q., Iu, V. P., Kou, K. P. (2009). Three-dimensional vibration analysis of functionally graded material plates in thermal environment. *Journal of Sound and Vibration* 324:733–750.

Liew, K. M., Zhao, X., Ferreira, A. J. M. (2011). A review of meshless methods for laminated and functionally graded plates and shells. *Composite Structures* 93(8):2031–2041.

Liew, K.M., Zhao, X., Lee, Y.Y. (2012) Postbuckling responses of functionally graded cylindrical shells under axial compression and thermal loads. *Composites: Part B* 43 :1621–1630.

Miyamoto Y, Kaysser WA, Rabin BH, Kawasaki A, Ford RG (1999) *Functionally Graded Materials: Design, Processing and Applications.* Boston: Kluwer Academic.

Mojdehi A. R., Darvizeh, A., Basti, A., Rajabi, H. (2011). Three dimensional static and dynamic analysis of thick functionally graded plates by the meshless local Petrov–Galerkin (MLPG) method. *Engineering Analysis with Boundary Elements* 35:1168–1180.

Na, K. S., Kim, J. H. (2006a). Nonlinear bending response of functionally graded plates under thermal loads. *Journal of Thermal Stresses* 29:245–261.

Na, K. S., Kim, J. H. (2006b). Three-dimensional thermomechanical buckling analysis for functionally graded composite plates. *Composite Structures* 73:413–422.

Na, K. S., Kim, J. H. (2006c). Thermal postbuckling investigations of functionally graded plates using 3-D finite element method. *Finite Elements in Analysis and Design* 42:749 – 756.

Na, K. S., Kim, J. H., (2004). Three-dimensional thermal buckling analysis of functionally graded materials. *Composites: Part B* 35:429–437.

Naj, R., Sabzikar, B. M., Eslami, M. R. (2008). Thermal and mechanical instability of functionally graded truncated conical shells. *Thin-Walled Structures* 46:65–78.

Navazi, H. M., Haddadpour, H. (2008). Nonlinear cylindrical bending analysis of shear deformable functionally graded plates under different loadings using analytical methods. *International Journal of Mechanical Sciences* 50(12):1650–1657.

Oktem, A. S., Mantari, J. L., Soares, C. G., (2012). Static response of functionally graded plates and doubly-curved shells based on a higher order shear deformation theory. *European Journal of Mechanics - A/Solids* 36:163-172.

Ovesy, H. R., Ghannadpour, S. A. M. (2007). Large deflection finite strip analysis of functionally graded plates under pressure loads. *International Journal of Structural Stability and Dynamics* 7:193-211.

Pandya, B. N., Kant, T., (1988). Finite element analysis of laminated composite plates using a higher-order displacement model. Composites Science and Technology 32:137-155.

Panigrahi, B., Pohit, G. (2015). Nonlinear modelling and dynamic analysis of cracked Timoshenko functionally graded beams based on neutral surface approach. *Proceedings of the Institution of Mechanical Engineers, Part C: Journal of Mechanical Engineering Science,* doi: 10.1177/0954406215576560.

Park, J. S., Kim, J. H. (2006). Thermal postbuckling and vibration analyses of functionally graded plates. *Journal of Sound and Vibration* 289:77–93.

Patel, B. P., Gupta, S. S., Loknath, M. S., Kadu, C. P. (2005). Free vibration analysis of functionally graded elliptical cylindrical shells using higher-order theory. *Composite Structures* 69: 259–270.

Phung-Van, P., Nguyen-Thoi, T., Luong-Van, H., Lieu-Xuan, Q. (2014). Geometrically nonlinear analysis of functionally graded plates using a cell-based smoothed three-node plate element (CS-MIN3) based on the C^0-HSDT. *Computer Methods in Applied Mechanics and Engineering* 270:15-36.

Pradyumna, S., Bandyopadhyay, J. N. (2008). Free vibration analysis of functionally graded curved panels using a higher-order finite element formulation. *Journal of Sound and Vibration* 318: 176–192.

Pradyumna, S., Bandyopadhyay, J. N. (2010). Free vibration and buckling of functionally graded shell panels in thermal environments. *International Journal of Structural Stability and Dynamics* 10(5):1031-1053.

Pradyumna, S., Nanda, N. (2013). Geometrically nonlinear transient response of functionally graded shell panels with initial geometric imperfection. *Mechanics of Advanced Materials and Structures* 20: 217–226.

Pradyumna, S., Nanda, N., Bandyopadhyay, J. N. (2010). Geometrically nonlinear transient analysis of functionally graded shell panels using a higher-order finite element formulation. *Journal of Mechanical Engineering Research* 2: 39–51.

Prakash, T., Singha, M.K., Ganapathi, M. (2008). Thermal postbuckling analysis of FGM skew plates. *Engineering Structures* 30:22–32.

Praveen, G. N., Reddy, J. N. (1998). Nonlinear transient thermoelastic analysis of functionally graded ceramic-metal plates. *International Journal of Solids and Structures* 35(33):4457-4476.

Qatu, M. S. (2004). Vibration of Laminated Shells and Plates. Oxford, UK: Elsevier Academic Press.

Qatu, M. S., Sullivan R. W., Wang, W. (2010). Recent research advances on the dynamic analysis of composite shells: 2000–2009. *Composite Structures* 93:14–31

Rahimia, G. H., Ansari, R., Hemmatnezhada, M. (2011). Vibration of functionally graded cylindrical shells with ring support. *Scientia Iranica* 18 (6): 1313–1320.

Reddy, J. N. (2004a). An Introduction Nonlinear Finite Element Analysis. Cambridge, UK: Oxford University Press.

Reddy, J. N. (2004b). Mechanics of laminated composite: Plates and shells-Theory and analysis. Boca Raton, FL: Second Edition, CRC press.

Reddy, J. N., Cheng Z. Q. (2001). Three-dimensional thermo-mechanical deformations of functionally graded rectangular plates. *European Journal of Mechanics - A/Solids* 20:841–855.

Reddy, J. N., Chin, C. D. (1998). Thermoelastical analysis of functionally graded cylinders and plates. *Journal of Thermal Stresses* 21:593–626.

Santos, H., Soares, C. M. M., Soares, C. A. M., Reddy, J. N. (2009). A semi-analytical finite element model for the analysis of cylindrical shells made of functionally graded materials. *Composite Structures* 91: 427–432.

Sepahi, O., Forouzan, M.R., Malekzadeh. P. (2011). Thermal buckling and postbuckling analysis of functionally graded annular plates with temperature-dependent material properties. *Materials and Design* 32:4030–4041.

Shahsiah, R., Eslami, M. R., Sabzikar Boroujerdy M. (2011). Thermal instability of functionally graded deep spherical shell. *Arch Appl Mech* 81:1455–1471.

Shen, H. S. (2002a). Nonlinear bending response of functionally graded plates subjected to transverse loads and in thermal environments. *International Journal of Mechanical Sciences* 44(3): 561–584.

Shen, H. S. (2002b). Postbuckling analysis of axially-loaded functionally graded cylindrical shells in thermal environments. *Composites Science and Technology* 62:77–987.

Shen, H. S. (2003). Postbuckling analysis of pressure-loaded functionally graded cylindrical shells in thermal environments. *Engineering Structures* 25:487–497.

Shen, H. S. (2004). Thermal postbuckling behavior of functionally graded cylindrical shells with temperature-dependent properties. *International Journal of Solids and Structures* 41:1961–1974.

Shen, H. S. (2007a). Nonlinear thermal bending response of FGM plates due to heat conduction. *Composites Part B: Engineering* 38:201–215.

Shen, H. S. (2007b). Thermal postbuckling behavior of shear deformable FGM plates with temperature-dependent properties. *International Journal of Mechanical Sciences* 49:466–478.

Shen, H. S. (2007c). Thermal Postbuckling of Shear Deformable FGM Cylindrical Shells with Temperature-Dependent Properties. *Mechanics of Advanced Materials and Structures*, 14:439–452.

Shen, H. S. (2009a). Functionally graded material: Nonlinear analysis of plates & shells. Boca Raton, FL: CRC press.

Shen, H. S. (2009b). Postbuckling of shear deformable FGM cylindrical shells surrounded by an elastic medium, *International Journal of Mechanical Sciences* 51:372–383.

Shen, H. S. (2009c). Torsional buckling and postbuckling of FGM cylindrical shells in thermal environments. *International Journal of Non-Linear Mechanics* 44:644 – 657.

Shen, H. S., Noda, N. (2005). Postbuckling of FGM cylindrical shells under combined axial and radial mechanical loads in thermal environments. *International Journal of Solids and Structures* 42:4641–4662.

Shen, H. S., Wang, H. (2014). Nonlinear vibration of shear deformable FGM cylindrical panels resting on elastic foundations in thermal environments. *Composites*: *Part B* 60:167–177.

Shen, H. S., Wang, Z. X. (2010). Nonlinear bending of FGM plates subjected to combined loading and resting on elastic foundations. *Composite Structures* 92:2517–2524.

Shen, H. S., Yang, J., Kitipornchai, S., (2010). Postbuckling of internal pressure loaded FGM cylindrical shells surrounded by an elastic medium. *European Journal of Mechanics A/Solids* 29:448–460.

Shen, H.S., Wang, H. (2014). Nonlinear vibration of shear deformable FGM cylindrical panels resting on elastic foundations in thermal environments. *Composites Part B: Engineering* 60:167–177.

Sofiyev, A. H., (2003). Dynamic buckling of functionally graded cylindrical thin shells under non-periodic impulsive loading. *Acta Mechanica* 165:151–163.

Sofiyev, A. H., (2004). The stability of functionally graded truncated conical shells subjected to aperiodic impulsive loading. *International Journal of Solids and Structures* 41:3411–3424.

Sofiyev, A. H., (2007). The buckling of functionally graded truncated conical shells under dynamic axial loading. *Journal of Sound and Vibration* 305:808–826.

Sofiyev, A. H., Schnack, E. (2004). The stability of functionally graded cylindrical shells under linearly increasing dynamic torsional loading. *Engineering Structures* 26:1321–1331.

Sundararajan, N., Prakash, T., Ganapathi, M., (2005). Nonlinear free flexural vibrations of functionally graded rectangular and skew plates under thermal environments. *Finite Elements in Analysis and Design* 42: 152–168.

Swaminathan, K., Naveenkumar, D.T., Zenkour, A.M., Carrera, E. (2015). Stress, vibration and buckling analyses of FGM plates—A state-of-the-art review. *Composite Structures* 120:10–31.

Taj, G., Chakrabarti, A. (2013). Dynamic response of functionally graded skew shell panel. *Latin American Journal of Solids and Structures* 10:1243–1266.

Talha, M., Singh, B. N. (2010). Static response and free vibration analysis of FGM plates using higher order shear deformation theory. *Applied Mathematical Modelling* 34(12):3991–4011.

Talha, M., Singh, B. N. (2011). Large amplitude free flexural vibration analysis of shear deformable FGM plates using nonlinear finite element method. *Finite Elements in Analysis and Design* 47: 394–401.

Thai, H. T., Choi, D. H. (2013). A simple first-order shear deformation theory for the bending and free vibration analysis of functionally graded plates. *Composite Structures* 101:332-340.

Thai, H. T., Choi, D. H., (2012). An efficient and simple refined theory for buckling analysis of functionally graded plates. *Applied Mathematical Modelling* 36:1008–1022.

Thai, H. T., Kim, S. E. (2013). A simple higher-order shear deformation theory for bending and free vibration analysis of functionally graded plates. *Composite Structures* 96:165-173.

Thai, H. T., Kim, S. E. (2015). A review of theories for the modeling and analysis of functionally graded plates and shells. *Composite Structures* 128:70–86.

Tornabene, F. (2009). Free vibration analysis of functionally graded conical, cylindrical shell and annular plate structures with a four-parameter power-law distribution. *Computer Methods in Applied Mechanics and Engineering* 198(37–40):2911–2935.

Tornabene, F., Fantuzzi, N., Bacciocchi, M. (2014). Free vibrations of free-form doubly-curved shells made of functionally graded materials using higher-order equivalent single layer theories, *Composite Part B Engineering*, 67:490-509.

Tornabene, F., Reddy, J. N. (2013). FGM and Laminated Doubly-Curved and Degenerate Shells Resting on Nonlinear Elastic Foundations: A GDQ Solution for Static Analysis with a Posteriori Stress and Strain Recovery. *Journal of Indian Institute of Science* 93:635-688.

Tornabene, F., Viola E., Inman, D. J. (2009). 2-D differential quadrature solution for vibration analysis of functionally graded conical, cylindrical shell and annular plate structures. *Journal of Sound and Vibration* 328(3):259–290.

Tornabene, F., Viola, E. (2009). Free vibrations of four-parameter functionally graded parabolic panels and shells of revolution. *European Journal of Mechanics - A/Solids* 28(5):991–1013.

Tung, H. V. (2014). Nonlinear thermomechanical stability of shear deformable FGM shallow spherical shells resting on elastic foundations with temperature dependent properties. *Composite Structures* 114:107–116.

Tung, H. V., Duc, N. D. (2010). Nonlinear analysis of stability for functionally graded plates under mechanical and thermal loads. *Composite Structures* 92:1184–1191.

Udupa G., Rao S. S., Gangadharan K.V. (2014). Functionally graded composite materials: An overview. *Procedia Materials Science* 5: 1291–1299

Uymaz, B., Aydogdu, M. (2007). Three-dimensional vibration analysis of functionally graded plates under various boundary conditions. *Journal of Reinforced Plastics and Composites* 26(18): 1847–1863.

Valizadeh, N., Sundararajan, N., Gonzalez-Estrada, O. A., Rabczuk, T., Bui, T. Q., Bordas S. P. A. (2013). NURBS-based finite element analysis of functionally graded plates: Static bending, vibration, buckling and flutter. *Composite Structures* 99:309–326.

Viola, E., Tornabene, F. (2009). Free vibrations of three parameter functionally graded parabolic panels of revolution. *Mechanics Research Communications* 36(5):587–594.

Woo, J., Meguid, S. A. (2001). Nonlinear analysis of functionally graded plates and shallow shells. *International Journal of Solids and Structures* 38:7409-7421.

Woo, J., Meguid, S. A. (2003). Thermomechanical postbuckling analysis of functionally graded plates and shallow cylindrical shells. *Acta Mechanica* 165, 99–115

Woo, J., Meguid, S. A., Stranart J. C., Liew K. M. (2005) Thermomechanical postbuckling analysis of moderately thick functionally graded plates and shallow shells. *International Journal of Mechanical Sciences* 47:1147–1171.

Wu, L., Jiang, Z., Liu, J. (2005). Thermoelastic stability of functionally graded cylindrical shells. *Composite Structures* 70:60–68.

Wu, T. L., Shukla, K.K., Huang, J. H. (2007). Post-buckling analysis of functionally graded rectangular plates. *Composite Structures* 81:1–10.

Xiang, S., Kang, G. (2013). A nth-order shear deformation theory for the bending analysis on the functionally graded plates. *European Journal of Mechanics - A/Solids* 37:336-343.

Xu, Y., Zhou, D. (2009). Three-dimensional elasticity solution of functionally graded rectangular plates with variable thickness. *Composite Structures* 91:56–65.

Yang, J., Liew, K.M., Kitipornchai, S. (2006a). Imperfection sensitivity of the post-buckling behaviour of higher-order shear deformable functionally graded plates. *International Journal of Solids and Structures* 43:5247–5266.

Yang, J., Liew, K.M., Wu, Y.F., Kitipornchai, S. (2006b). Thermo-mechanical post-buckling of FGM cylindrical panels with temperature-dependent properties. *International Journal of Solids and Structures* 43:307–324.

Yang, J., Shen, H. S. (2003a). Non-linear analysis of functionally graded plates under transverse and in-plane loads. *International Journal of Non-Linear Mechanics* 38:467–482.

Yang, J., Shen, H. S. (2003b). Nonlinear bending analysis of shear deformable functionally graded plates subjected to thermomechanical loads under various boundary conditions. *Composites Part B: Engineering* 34:103–115.

Yang, J., Shen, H. S. (2003c). Free vibration and parametric resonance of shear deformable functionally graded cylindrical panels. *Journal of Sound and Vibration* 261:871–893.

Zhang, D. G. (2014). Nonlinear bending analysis of FGM rectangular plates with various supported boundaries resting on two-parameter elastic foundations. *Archive of Applied Mechanics* 48:1-20.

Zhao, X., Lee, Y. Y., Liew, K. M. (2009). Mechanical and thermal buckling analysis of functionally graded plates. *Composite Structures* 90:161–171.

Zhao, X., Liew, K. M. (2009a). Geometrically nonlinear analysis of functionally graded plates using the element-free kp-Ritz method. *Computer Methods in Applied Mechanics and Engineering* 198:2796–2811.

Zhao, X., Liew, K. M. (2009b). Geometrically nonlinear analysis of functionally graded shells. *International Journal of Mechanical Sciences* 51(2):131–144.

Zhu, P., Zhang, L. W., Liew, K. M. (2014). Geometrically nonlinear thermomechanical analysis of moderately thick functionally graded plates using a local Petrov–Galerkin approach with moving Kriging interpolation. *Composite Structures* 107: 298–314.

Appendix A

Linear $\{\bar{\varepsilon}_l\}$ and Nonlinear $\{\bar{\varepsilon}_{nl}\}$ Mid-plane Strain Terms Appeared in General Mathematical Formulation

Linear mid-plane strain terms as shown in Eq. (3.14)

$\varepsilon_x^0 = u_{,x}$, $\varepsilon_y^0 = v_{,y}$, $\varepsilon_{xy}^0 = u_{,y} + v_{,x}$, $\varepsilon_{xz}^0 = w_{,x} + \theta_x$, $\varepsilon_{yz}^0 = w_{,y} + \theta_y$, $k_x^1 = \theta_{x,x}$, $k_y^1 = \theta_{y,y}$,

$k_{xy}^1 = \theta_{x,y} + \theta_{y,x}$, $k_{xz}^1 = 2u_0^* - \theta_x / R_x$, $k_{yz}^1 = 2v_0^* - \theta_y / R_y$, $k_x^2 = u_{0,x}^*$, $k_y^2 = v_{0,y}^*$, $k_{xy}^2 = u_{0,y}^* + v_{0,x}^*$,

$k_{xz}^2 = 3\theta_x^* - u_0^* / R_x$, $k_{yz}^2 = 3\theta_y^* - v_0^* / R_y$, $k_x^3 = \theta_{x,x}^*$, $k_y^3 = \theta_{y,y}^*$, $k_{xy}^3 = \theta_{x,y}^* + \theta_{y,x}^*$, $k_{xz}^3 = -\theta_x^* / R_x$,

$k_{yz}^3 = -\theta_y^* / R_y$.

Nonlinear mid-plane strain terms as shown in Eq. (3.14)

$\varepsilon_x^4 = \frac{1}{2} u_{,x}^2 + \frac{1}{2} v_{,x}^2 + \frac{1}{2} w_{,x}^2$

$\varepsilon_y^4 = \frac{1}{2} u_{,y}^2 + \frac{1}{2} v_{,y}^2 + \frac{1}{2} w_{,y}^2$

$\varepsilon_{xy}^4 = u_{,x}u_{,y} + v_{,x}v_{,y} + w_{,x}w_{,y}$

$\varepsilon_{xz}^4 = u_{,x}\theta_x + v_{,x}\theta_y$

$\varepsilon_{yz}^4 = u_{,y}\theta_x + v_{,y}\theta_y$

$k_x^5 = u_{,x}\theta_{x,x} + v_{,x}\theta_{y,x} - w_{,x}\theta_x / R_x$

$k_y^5 = u_{,x}\theta_{x,y} + v_{,y}\theta_{y,y} - w_{,y}\theta_y / R_y$

$k_{xy}^5 = u_{,x}\theta_{x,y} + u_{,y}\theta_{x,x} + v_{,x}\theta_{y,y} + v_{,y}\theta_{y,x} - w_{,x}\theta_y / R_y - w_{,y}\theta_x / R_x$

$k_{xz}^5 = 2u_{,x}u_0^* + 2v_{,x}v_0^* + \theta_{x,x}\theta_x + \theta_{y,x}\theta_y$

$k_{yz}^5 = 2u_{,y}u_0^* + 2v_{,y}v_0^* + \theta_{x,x}\theta_x + \theta_{y,y}\theta_y$

$k_x^6 = u_{,x}u_{0,x}^* + v_{,x}v_{0,x}^* - w_{,x}u_0^*/R_x + \frac{1}{2}\theta_{x,x}^2 + \frac{1}{2}\theta_{y,x}^2 + \frac{1}{2}\theta_x^2 / R_x^2$

$k_y^6 = u_{,y}u_{0,y}^* + v_{,y}v_{0,y}^* - w_{,y}v_0^*/R_y + \frac{1}{2}\theta_{x,y}^2 + \frac{1}{2}\theta_{y,y}^2 + \frac{1}{2}\theta_y^2 / R_y^2$

$$k_{xy}^{6} = u_{,x}u_{0,y}^{*} + u_{,y}u_{0,x}^{*} + v_{,x}v_{0,y}^{*} + v_{,y}v_{0,x}^{*} - w_{,x}v_{0}^{*}/R_y - w_{,y}u_{0}^{*}/R_x + \theta_{x,x}\theta_{x,y} + \theta_{y,x}\theta_{y,y} + \theta_x\theta_y / R_xR_y$$

$$k_{xz}^{6} = 3u_{,x}\theta_x^{*} + 3v_{,x}\theta_y^{*} + 2\theta_{x,x}u_{0}^{*} + 2\theta_{y,x}v_{0}^{*} + u_{0,x}^{*}\theta_x + v_{0,x}^{*}\theta_y$$

$$k_{yz}^{6} = 3u_{,y}\theta_x^{*} + 3v_{,y}\theta_y^{*} + 2\theta_{x,y}u_{0}^{*} + 2\theta_{y,y}v_{0}^{*} + u_{0,y}^{*}\theta_x + v_{0,y}^{*}\theta_y$$

$$k_{x}^{7} = u_{,x}\theta_{x,x}^{*} + v_{,x}\theta_{y,x}^{*} - w_{,x}\theta_{x}^{*} / R_x + \theta_{x,x}u_{0,x}^{*} + \theta_{y,x}v_{0,x}^{*} + \theta_x u_{0}^{*}/R_x^2$$

$$k_{y}^{7} = u_{,y}\theta_{x,y}^{*} + v_{,y}\theta_{y,y}^{*} - w_{,y}\theta_{y}^{*} / R_y + \theta_{x,y}u_{0,y}^{*} + \theta_{y,y}v_{0,y}^{*} + \theta_y v_{0}^{*}/R_y^2$$

$$k_{xy}^{7} = u_{,x}\theta_{x,y}^{*} + u_{,y}\theta_{x,x}^{*} + v_{,x}\theta_{y,y}^{*} + v_{,y}\theta_{y,x}^{*} - w_{,x}\theta_{y}^{*} / R_y - w_{,y}\theta_{x}^{*} / R_x + \theta_{x,x}u_{0,y}^{*} + \theta_{x,y}u_{0,x}^{*} + \theta_{y,x}v_{0,y}^{*} + \theta_{y,y}v_{0,x}^{*} + \theta_x v_{0}^{*}/R_xR_y + \theta_y u$$

$$k_{xz}^{7} = 3\theta_{x,x}\theta_x^{*} + 3\theta_{y,x}\theta_y^{*} + 2u_{0,x}^{*}u_{0}^{*} + 2v_{0,x}^{*}v_{0}^{*} + \theta_{x,x}^{*}\theta_x + \theta_{y,x}^{*}\theta_y$$

$$k_{yz}^{7} = 3\theta_{x,y}\theta_x^{*} + 3\theta_{y,y}\theta_y^{*} + 2u_{0,y}^{*}u_{0}^{*} + 2v_{0,y}^{*}v_{0}^{*} + \theta_{x,y}^{*}\theta_x + \theta_{y,y}^{*}\theta_y$$

$$k_{x}^{8} = \theta_{x,x}\theta_{x,x}^{*} + \theta_{y,x}\theta_{y,x}^{*} + \tfrac{1}{2}\left(u_{0,x}^{*}\right)^2 + \tfrac{1}{2}\left(v_{0,x}^{*}\right)^2 + \theta_x\theta_x^{*}/R_x^2 + \tfrac{1}{2}(u_{0}^{*}/R_x)^2$$

$$k_{y}^{8} = \theta_{x,y}\theta_{x,y}^{*} + \theta_{y,y}\theta_{y,y}^{*} + \tfrac{1}{2}\left(u_{0,y}^{*}\right)^2 + \tfrac{1}{2}\left(v_{0,y}^{*}\right)^2 + \theta_y\theta_y^{*}/R_y^2 + \tfrac{1}{2}(v_{0}^{*}/R_y)^2$$

$$k_{xy}^{8} = \theta_{x,x}\theta_{x,y}^{*} + \theta_{x,y}\theta_{x,x}^{*} + \theta_{y,x}\theta_{y,y}^{*} + \theta_{y,y}\theta_{y,x}^{*} + u_{0,x}^{*}u_{0,y}^{*} + v_{0,x}^{*}v_{0,y}^{*} + \theta_x\theta_y^{*} / R_xR_y + \theta_y\theta_x^{*}/R_xR_y + u_{0}^{*}v_{0}^{*}/R_xR_y$$

$$k_{xz}^{8} = 3u_{0,x}^{*}\theta_x^{*} + 3v_{0,x}^{*}\theta_y^{*} + 2\theta_{x,x}^{*}u_0^{*} + 2\theta_{y,x}^{*}v_0^{*}$$

$$k_{yz}^{8} = 3u_{0,y}^{*}\theta_x^{*} + 3v_{0,y}^{*}\theta_y^{*} + 2\theta_{x,y}^{*}u_0^{*} + 2\theta_{y,y}^{*}v_0^{*}$$

$$k_{x}^{9} = u_{0,x}^{*}\theta_{x,x}^{*} + v_{0,x}^{*}\theta_{y,x}^{*} + u_0^{*}\theta_x^{*}/R_x^2$$

$$k_{y}^{9} = u_{0,y}^{*}\theta_{x,y}^{*} + v_{0,y}^{*}\theta_{y,y}^{*} + v_0^{*}\theta_y^{*}/R_y^2$$

$$k_{xy}^{9} = u_{0,x}^{*}\theta_{x,y}^{*} + u_{0,y}^{*}\theta_{x,x}^{*} + v_{0,x}^{*}\theta_{y,y}^{*} + v_{0,y}^{*}\theta_{y,x}^{*} + u_0^{*}\theta_y^{*}/R_xR_y + v_0^{*}\theta_x^{*}/R_xR_y$$

$$k_{xz}^{9} = 3\theta_{x,x}^{*}\theta_x^{*} + 3\theta_{y,x}^{*}\theta_y^{*}$$

$$k_{yz}^{9} = 3\theta_{x,y}^{*}\theta_x^{*} + 3\theta_{y,y}^{*}\theta_y^{*}$$

$$k_{x}^{10} = \tfrac{1}{2}(\theta_{x,x}^{*})^2 + \tfrac{1}{2}(\theta_{y,x}^{*})^2 + \tfrac{1}{2}(\theta_x^{*}/R_x)^2$$

$$k_{y}^{10} = \tfrac{1}{2}(\theta_{x,y}^{*})^2 + \tfrac{1}{2}(\theta_{y,y}^{*})^2 + \tfrac{1}{2}(\theta_y^{*}/R_y)^2$$

$$k_{xy}^{10} = \theta_{x,x}^{*}\theta_{x,y}^{*} + \theta_{y,x}^{*}\theta_{y,y}^{*} + \theta_x^{*}\theta_y^{*}/R_xR_y\,.$$

where, the expressions of $u_{,x}$, $u_{,y}$, $v_{,x}$, $v_{,y}$, $w_{,x}$ and $w_{,y}$ are

$$u_{,x} = \partial u_0 / \partial x + w_0 / R_x\,,\; u_{,y} = \partial u_0 / \partial y + w_0 / R_{xy}\,,\; v_{,x} = \partial v_0 / \partial x + w_0 / R_{xy}\,,\; v_{,y} = \partial v_0 / \partial y + w_0 / R_y\,,$$

$$w_{,x} = \partial w_0 / \partial x - u_0 / R_x\,,\quad w_{,y} = \partial w_0 / \partial y - v_0 / R_y\,.$$

Appendix B

Linear [T_l] and Nonlinear [T_{nl}] Thickness Co-ordinate Matrices

Linear thickness co-ordinate matrix [T_l] as appeared in Eq. (3.14)

$$\left[T_l\right]_{5\times 20}=\begin{bmatrix}1&0&0&0&0&z&0&0&0&0&z^2&0&0&0&0&z^3&0&0&0&0\\0&1&0&0&0&0&z&0&0&0&0&z^2&0&0&0&0&z^3&0&0&0\\0&0&1&0&0&0&0&z&0&0&0&0&z^2&0&0&0&0&z^3&0&0\\0&0&0&1&0&0&0&0&z&0&0&0&0&z^2&0&0&0&0&z^3&0\\0&0&0&0&1&0&0&0&0&z&0&0&0&0&z^2&0&0&0&0&z^3\end{bmatrix}$$

Nonlinear thickness co-ordinate matrix [T_{nl}] as appeared in Eq. (3.14)

$$\left[T_{nl}\right]_{5\times 35}=\begin{bmatrix}1&0&0&0&0&z&0&0&0&0&z^2&0&0&0&0&z^3&0&0&0&0\\0&1&0&0&0&0&z&0&0&0&0&z^2&0&0&0&0&z^3&0&0&0\\0&0&1&0&0&0&0&z&0&0&0&0&z^2&0&0&0&0&z^3&0&0\\0&0&0&1&0&0&0&0&z&0&0&0&0&z^2&0&0&0&0&z^3&0\\0&0&0&0&1&0&0&0&0&z&0&0&0&0&z^2&0&0&0&0&z^3\end{bmatrix}$$

$$\begin{bmatrix}z^4&0&0&0&0&z^5&0&0&0&0&z^6&0&0&0&0\\0&z^4&0&0&0&0&z^5&0&0&0&0&z^6&0&0&0\\0&0&z^4&0&0&0&0&z^5&0&0&0&0&z^6&0&0\\0&0&0&z^4&0&0&0&0&z^5&0&0&0&0&z^6&0\\0&0&0&0&z^4&0&0&0&0&z^5&0&0&0&0&z^6\end{bmatrix}$$

Appendix C

Linear, Nonlinear and Geometrical Strain-Displacement Functions

Individual terms of matrix [B] as appeared in Eq. (3.32)

$[B]_{1,1}= \partial/\partial x$, $[B]_{1,3} =1/R_x$, $[B]_{2,2}= \partial/\partial y$, $[B]_{2,3}=1/R_y$, $[B]_{3,1}= \partial/\partial y$, $[B]_{3,2}= \partial/\partial x$, $[B]_{3,3}= 2/R_{xy}$, $[B]_{4,1} = -1/R_x$, $[B]_{4,3} = \partial/\partial x$, $[B]_{4,4} =1$, $[B]_{5,2} = -1/R_y$, $[B]_{5,3} = \partial/\partial x$, $[B]_{5,5} =1$, $[B]_{6,4} = \partial/\partial x$, $[B]_{7,5} = \partial/\partial y$, $[B]_{8,4} = \partial/\partial y$, $[B]_{8,5} = \partial/\partial x$, $[B]_{9,4} = -1/R_x$, $[B]_{9,6} = 2$, $[B]_{10,5} = -1/R_y$, $[B]_{10,7} = 2$, $[B]_{11,6} = \partial/\partial x$, $[B]_{12,7} = \partial/\partial y$, $[B]_{13,6} = \partial/\partial y$, $[B]_{13,7} = \partial/\partial x$, $[B]_{14,6} = -1/R_x$, $[B]_{14,8} = 2$, $[B]_{15,7} = -1/R_y$, $[B]_{15,9} = 2$, $[B]_{16,8} = \partial/\partial x$, $[B]_{17,9} = \partial/\partial y$, $[B]_{18,8} = \partial/\partial y$, $[B]_{18,9} = \partial/\partial x$, $[B]_{19,8} = -1/R_x$, $[B]_{20,9} = -1/R_y$.

Individual terms of matrix [*A*] as appeared in Eq. (3.32)

$[A]_{1,1} = \tfrac{1}{2} u_{,x}$, $[A]_{1,3} = \tfrac{1}{2} v_{,x}$, $[A]_{1,5} = \tfrac{1}{2} w_{,x}$, $[A]_{2,2} = \tfrac{1}{2} u_{,y}$, $[A]_{2,4} = \tfrac{1}{2} v_{,y}$, $[A]_{2,6} = \tfrac{1}{2} w_{,y}$, $[A]_{3,1} = u_{,y}$, $[A]_{3,3} = v_{,y}$, $[A]_{3,5} = w_{,y}$, $[A]_{4,1} = \theta_x$, $[A]_{4,3} = \theta_y$, $[A]_{5,2} = \theta_x$, $[A]_{5,4} = \theta_y$, $[A]_{6,1} = \theta_{x,x}$, $[A]_{6,3} = \theta_{y,x}$, $[A]_{6,5} = -\theta_x/R_x$, $[A]_{7,2} = \theta_{x,y}$, $[A]_{7,4} = \theta_{y,y}$, $[A]_{7,6} = -\theta_y/R_y$, $[A]_{8,1} = \theta_{x,y}$, $[A]_{8,2} = \theta_{x,x}$, $[A]_{8,3} = \theta_{y,y}$, $[A]_{8,4} = \theta_{y,x}$, $[A]_{8,5} = -\theta_y/R_y$, $[A]_{8,6} = -\theta_x/R_x$, $[A]_{9,1} = 2u_0^*$, $[A]_{9,3} = 2v_0^*$, $[A]_{9,7} = \theta_x$, $[A]_{9,9} = \theta_y$, $[A]_{10,2} = 2u_0^*$, $[A]_{10,4} = 2v_0^*$, $[A]_{10,8} = \theta_x$, $[A]_{10,10} = \theta_y$, $[A]_{11,1} = u_{0,x}^*$, $[A]_{11,3} = v_{0,x}^*$, $[A]_{11,5} = -u_0^*/R_x$, $[A]_{11,7} = \tfrac{1}{2}\theta_{x,x}$, $[A]_{11,9} = \tfrac{1}{2}\theta_{y,x}$, $[A]_{12,2} = u_{0,y}^*$, $[A]_{12,4} = v_{0,y}^*$, $[A]_{12,6} = -v_0^*/R_y$, $[A]_{12,8} = \tfrac{1}{2}\theta_{x,y}$, $[A]_{12,10} = \tfrac{1}{2}\theta_{y,y}$, $[A]_{13,1} = u_{0,y}^*$, $[A]_{13,2} = u_{0,x}^*$, $[A]_{13,3} = v_{0,y}^*$, $[A]_{13,4} = v_{0,x}^*$, $[A]_{13,5} = -v_0^*/R_y$, $[A]_{13,6} = -u_0^*/R_x$, $[A]_{13,7} = \theta_{x,y}$, $[A]_{13,9} = \theta_{y,y}$,

$[A]_{14,1} = 3\theta_x^*$, $[A]_{14,3} = 3\theta_y^*$, $[A]_{14,7} = 2u_0^*$, $[A]_{14,9} = 2v_0^*$, $[A]_{14,11} = \theta_x$, $[A]_{14,13} = \theta_y$, $[A]_{15,2} = 3\theta_x^*$, $[A]_{15,4} = 3\theta_y^*$, $[A]_{15,8} = 2u_0^*$, $[A]_{15,10} = 2v_0^*$, $[A]_{15,12} = \theta_x$, $[A]_{15,14} = \theta_y$, $[A]_{16,1} = \theta_{x,x}^*$, $[A]_{16,3} = \theta_{y,x}^*$, $[A]_{16,5} = -\theta_x^* / R_x$, $[A]_{16,7} = u_{0,x}^*$, $[A]_{16,9} = v_{0,x}^*$, $[A]_{16,19} = u_0^* / R_x^2$, $[A]_{17,2} = \theta_{x,y}^*$, $[A]_{17,4} = \theta_{y,y}^*$, $[A]_{17,6} = -\theta_y^* / R_y$, $[A]_{17,8} = u_{0,y}^*$, $[A]_{17,10} = v_{0,y}^*$, $[A]_{17,20} = v_0^* / R_y^2$, $[A]_{18,1} = \theta_{x,y}^*$, $[A]_{18,2} = \theta_{x,x}^*$, $[A]_{18,3} = \theta_{y,y}^*$, $[A]_{18,4} = \theta_{y,x}^*$, $[A]_{18,5} = -\theta_y^* / R_y$, $[A]_{18,6} = -\theta_x^* / R_x$, $[A]_{18,7} = u_{0,y}^*$, $[A]_{18,8} = u_{0,x}^*$, $[A]_{18,9} = v_{0,y}^*$, $[A]_{18,10} = v_{0,x}^*$, $[A]_{18,19} = v_0^* / R_x R_y$, $[A]_{18,20} = u_0^* / R_x R_y$, $[A]_{19,7} = 3\theta_x^*$, $[A]_{19,9} = 3\theta_y^*$, $[A]_{19,11} = 2u_0^*$, $[A]_{19,13} = 2v_0^*$, $[A]_{19,15} = \theta_x$, $[A]_{19,17} = \theta_y$, $[A]_{20,8} = 3\theta_x^*$, $[A]_{20,10} = 3\theta_y^*$, $[A]_{20,12} = 2u_0^*$, $[A]_{20,14} = 2v_0^*$, $[A]_{20,16} = \theta_x$, $[A]_{20,18} = \theta_y$, $[A]_{21,7} = \theta_{x,x}^*$, $[A]_{21,9} = \theta_{y,x}^*$, $[A]_{21,11} = ½\, u_{0,x}^*$, $[A]_{21,13} = ½\, v_{0,x}^*$, $[A]_{21,19} = \theta_x^* / R_x^2$, $[A]_{21,21} = ½ u_0^* / R_x^2$, $[A]_{22,8} = \theta_{x,y}^*$, $[A]_{22,10} = \theta_{y,y}^*$, $[A]_{22,12} = ½\, u_{0,y}^*$, $[A]_{22,14} = ½\, v_{0,y}^*$, $[A]_{22,20} = \theta_y^* / R_y^2$, $[A]_{22,22} = ½ v_0^* / R_y^2$, $[A]_{23,7} = \theta_{x,y}^*$, $[A]_{23,8} = \theta_{x,x}^*$, $[A]_{23,9} = \theta_{y,y}^*$, $[A]_{23,10} = \theta_{y,x}^*$, $[A]_{23,11} = u_{0,y}^*$, $[A]_{23,13} = v_{0,y}^*$, $[A]_{23,19} = \theta_y^* / R_x R_y$, $[A]_{23,20} = \theta_x^* / R_x R_y$, $[A]_{23,21} = v_0^* / R_x R_y$, $[A]_{24,11} = 3\theta_x^*$, $[A]_{24,13} = 3\theta_y^*$, $[A]_{24,15} = 2u_0^*$, $[A]_{24,17} = 2v_0^*$, $[A]_{25,12} = 3\theta_x^*$, $[A]_{25,14} = 3\theta_y^*$, $[A]_{25,16} = 2u_0^*$, $[A]_{25,18} = 2v_0^*$, $[A]_{26,11} = \theta_{x,x}^*$, $[A]_{26,13} = \theta_{y,x}^*$, $[A]_{26,21} = \theta_x^* / R_x^2$, $[A]_{27,12} = \theta_{x,y}^*$, $[A]_{27,14} = \theta_{y,y}^*$, $[A]_{27,22} = \theta_y^* / R_y^2$, $[A]_{28,11} = \theta_{x,y}^*$, $[A]_{28,12} = \theta_{x,x}^*$, $[A]_{28,13} = \theta_{y,y}^*$, $[A]_{28,14} = \theta_{y,x}^*$, $[A]_{28,21} = \theta_y^* / R_x R_y$, $[A]_{28,22} = \theta_x^* / R_x R_y$, $[A]_{29,15} = 3\theta_x^*$, $[A]_{29,17} = 3\theta_y^*$, $[A]_{30,16} = 3\theta_x^*$, $[A]_{30,18} = 3\theta_y^*$, $[A]_{31,15} = ½\, \theta_{x,x}^*$, $[A]_{31,17} = ½\, \theta_{y,x}^*$, $[A]_{31,23} = ½\, \theta_x^* / R_x^2$, $[A]_{32,16} = ½\, \theta_{x,y}^*$, $[A]_{32,18} = ½\, \theta_{y,y}^*$, $[A]_{32,24} = ½\, \theta_y^* / R_y^2$, $[A]_{33,15} = \theta_{x,y}^*$, $[A]_{33,17} = \theta_{y,y}^*$, $[A]_{33,23} = \theta_y^* / R_x R_y$.

Individual terms of matrix [*G*] as appeared in Eq. (3.32)

$[G]_{1,1} = \partial / \partial x$, $[G]_{1,3} = 1/R_x$, $[G]_{2,1} = \partial / \partial y$, $[G]_{2,3} = 1/R_{xy}$, $[G]_{3,2} = \partial / \partial x$, $[G]_{3,3} = 2/R_{xy}$, $[G]_{4,1} = 1/R_{xy}$, $[G]_{4,2} = \partial / \partial y$, $[G]_{4,3} = 1/R_{xy}$, $[G]_{5,1} = -1/R_x$, $[G]_{5,3} = \partial / \partial x$, $[G]_{6,2} = -1/R_y$, $[G]_{6,3} = \partial / \partial y$, $[G]_{7,4} = \partial / \partial x$, $[G]_{8,4} = \partial / \partial y$, $[G]_{9,5} = \partial / \partial x$, $[G]_{10,5} = \partial / \partial y$, $[G]_{11,6} = \partial / \partial x$, $[G]_{12,6} = \partial / \partial y$, $[G]_{13,7} = \partial / \partial x$, $[G]_{14,7} = \partial / \partial y$, $[G]_{15,8} = \partial / \partial x$, $[G]_{16,8} = \partial / \partial y$, $[G]_{17,9}$

$= \partial / \partial x$, $[G]_{18,9} = \partial / \partial y$, $[G]_{19,4} = 1$, $[G]_{20,5} = 1$, $[G]_{21,6} = 1$, $[G]_{22,7} = 1$, $[G]_{23,8} = 1$, $[G]_{24,9} = 1$.

Individual terms of matrix $[B_G]$ as appeared in Eq. (3.37)

$[B_G]_{1,1} = \partial / \partial x$, $[B_G]_{1,3} = 1/R_x$, $[B_G]_{2,1} = \partial / \partial y$, $[B_G]_{3,2} = \partial / \partial x$, $[B_G]_{4,2} = \partial / \partial y$, $[B_G]_{4,3} = 1/R_y$, $[B_G]_{5,1} = -1/R_x$, $[B_G]_{5,3} = \partial / \partial x$, $[B_G]_{6,2} = -1/R_y$, $[B_G]_{6,3} = \partial / \partial y$, $[B_G]_{7,4} = \partial / \partial x$, $[B_G]_{8,4} = \partial / \partial y$, $[B_G]_{9,5} = \partial / \partial x$, $[B_G]_{10,5} = \partial / \partial y$, $[B_G]_{11,4} = -1/R_x$, $[B_G]_{12,5} = -1/R_y$, $[B_G]_{13,6} = \partial / \partial x$, $[B_G]_{14,6} = \partial / \partial y$, $[B_G]_{15,7} = \partial / \partial x$, $[B_G]_{16,7} = \partial / \partial y$, $[B_G]_{17,6} = -1/R_x$, $[B_G]_{18,7} = -1/R_y$, $[B_G]_{19,8} = \partial / \partial x$, $[B_G]_{20,8} = \partial / \partial y$, $[B_G]_{21,9} = \partial / \partial x$, $[B_G]_{22,9} = \partial / \partial y$, $[B_G]_{23,8} = -1/R_x$, $[B_G]_{24,9} = -1/R_y$.

Appendix D

Matlab Code for Nonlinear Static Analysis

```
clear
for curv=[1]
    R=[50];
for n=[0.2 5]
TD=2;
Tm=300;
for Tc=[600]
for bctype=[0]
a=1;
 for r=[10]
h=a/r;
  ar=[1]
b=a/ar;
   kc=10.1203;
km=12.1429;
mu=0.28;
 nel=25;
ndof_q=9;
ax=(nel)^.5 ;
ay=(nel)^.5;
L=(2*(nel)^.5)+1;
nnode=L^2;
edof_q=nnel*ndof_q;
sdof_q=nnode*ndof_q;
%
nglx=3; ngly=3;
for Q=[0 50 100 150 200]
    p=Q*E0*(h/a)^4;
f=[0 0 p 0 0 0 0 0 0];
Ntot=(ax*2+1)*(ay*2+1)*9;
CN=((ax*2+1)*(ay*2+1)+1)/2;
a4=(a)/(2*(nel)^.5);
b4=(b)/(2*(nel)^.5);
for k=1:L
  for i=((k-1)*L+1):(k*L)
      gcoord(i,2)=b4*(k-1);
  end
end
for k=1:L
  for i=k:L:(L*(L-1)+k)
      gcoord(i,1)=a4*(k-1);
  end
end
a0=nel^0.5;
for i=1:nel
for k=1:a0
  if i>(k-1)*a0 & i<=k*a0
      L=2*(nel)^.5+1;
      a1=i-(k-1)*a0;
```

```
      a2=2*a1-1+2*(k-1)*L;
  nodes(i,1)=a2;
  nodes(i,2)=a2+2;
  nodes(i,3)=a2+(2*L+2);
  nodes(i,4)=a2+2*L;
  nodes(i,5)=a2+1;
  nodes(i,6)=a2+(L+2);
  nodes(i,7)=a2+(2*L+1);
  nodes(i,8)=a2+L;
  nodes(i,9)=a2+(L+1);
  end
end
end
[bcdof]=bc_all(nel,ndof_q,bctype);
 ff_temp=ff_th(h,n,r,Tc,TD);
D_sys=D_matrix(mu,h,n,r,Tc,TD);
D_sys1=D_matrix1(mu,h,n,r,Tc,TD);
D_sys2=D_matrix2(mu,h,n,r,Tc,TD);
D_sys3=D_matrix3(mu,h,n,r,Tc,TD);
disp_u_e=zeros(nel,9);
disp_v_e=zeros(nel,9);
disp_w_e=zeros(nel,9);
disp_phix_e=zeros(nel,9);
disp_phiy_e=zeros(nel,9);
disp_six_e=zeros(nel,9);
disp_siy_e=zeros(nel,9);
disp_thetax_e=zeros(nel,9);
disp_thetay_e=zeros(nel,9);
for sh=1:100
KN_1=zeros(sdof_q,sdof_q);
KN_2=zeros(sdof_q,sdof_q);
KN_3=zeros(sdof_q,sdof_q);
K_q_q=zeros(sdof_q,sdof_q);
K_q_q_g=zeros(sdof_q,sdof_q);
index_q=zeros(nnel*ndof_q,1);
FF_q=zeros(sdof_q,1);
ff_q=zeros(sdof_q,1);
FF_T=zeros(sdof_q,1);
ff_T=zeros(sdof_q,1);
[point2,weight2]=feglqd2(nglx,ngly);
for iel=1:nel
    for i=1:nnel
    nd(i)=nodes(iel,i);
    xcoord(i)=gcoord(nd(i),1);
    ycoord(i)=gcoord(nd(i),2);
    end
k_q_q=zeros(edof_q,edof_q);
k_q_q_g=zeros(edof_q,edof_q);
kn_1=zeros(edof_q,edof_q);
kn_2=zeros(edof_q,edof_q);
kn_3=zeros(edof_q,edof_q);
M=zeros(edof_q,edof_q);
ff_q=zeros(edof_q,1);
ff_T=zeros(edof_q,1);

for intx=1:nglx
    x=point2(intx,1);
```

```
    wtx=weight2(intx,1);
  for inty=1:ngly
    y=point2(inty,2);
    wty=weight2(inty,2);
%
[shape,dhdr,dhds]=feisoq4(nnel,x,y);
jacob2=fejacob2(nnel,dhdr,dhds,xcoord,ycoord);
detjacob=det(jacob2);
invjacob=inv(jacob2);
[dhdx,dhdy]=federiv2(nnel,dhdr,dhds,invjacob);
B1_q=bmat_q(shape,dhdx,dhdy,R1,R2,h,1);
B2_q=bmat_q(shape,dhdx,dhdy,R1,R2,h,2);
B3_q=bmat_q(shape,dhdx,dhdy,R1,R2,h,3);
B4_q=bmat_q(shape,dhdx,dhdy,R1,R2,h,4);
B5_q=bmat_q(shape,dhdx,dhdy,R1,R2,h,5);
B6_q=bmat_q(shape,dhdx,dhdy,R1,R2,h,6);
B7_q=bmat_q(shape,dhdx,dhdy,R1,R2,h,7);
B8_q=bmat_q(shape,dhdx,dhdy,R1,R2,h,8);
B9_q=bmat_q(shape,dhdx,dhdy,R1,R2,h,9);
B_q=[B1_q B2_q B3_q B4_q B5_q B6_q B7_q B8_q B9_q];
B1_g=bmat_g(shape,dhdx,dhdy,R1,R2,h,1);
B2_g=bmat_g(shape,dhdx,dhdy,R1,R2,h,2);
B3_g=bmat_g(shape,dhdx,dhdy,R1,R2,h,3);
B4_g=bmat_g(shape,dhdx,dhdy,R1,R2,h,4);
B5_g=bmat_g(shape,dhdx,dhdy,R1,R2,h,5);
B6_g=bmat_g(shape,dhdx,dhdy,R1,R2,h,6);
B7_g=bmat_g(shape,dhdx,dhdy,R1,R2,h,7);
B8_g=bmat_g(shape,dhdx,dhdy,R1,R2,h,8);
B9_g=bmat_g(shape,dhdx,dhdy,R1,R2,h,9);
B_g=[B1_g B2_g B3_g B4_g B5_g B6_g B7_g B8_g B9_g];
[A_1,G]=a_g(disp_u_e,disp_v_e,disp_w_e,disp_phix_e,disp_phiy_e,disp_six
_e,disp_siy_e,disp_thetax_e,disp_thetay_e,shape,dhdx,dhdy,iel,R1,R2);
N(1,1)=shape(1);N(1,10)=shape(2);N(1,19)=shape(3);N(1,28)=shape(4);N(1,
37)=shape(5);N(1,46)=shape(6);
N(1,55)=shape(7);N(1,64)=shape(8);N(1,73)=shape(9);
N(2,2)=shape(1);N(2,11)=shape(2);N(2,20)=shape(3);N(2,29)=shape(4);N(2,
38)=shape(5);N(2,47)=shape(6);
N(2,56)=shape(7);N(2,65)=shape(8);N(2,74)=shape(9);
N(3,3)=shape(1);N(3,12)=shape(2);N(3,21)=shape(3);N(3,30)=shape(4);N(3,
39)=shape(5);N(3,48)=shape(6);
N(3,57)=shape(7);N(3,66)=shape(8);N(3,75)=shape(9);
N(4,4)=shape(1);N(4,13)=shape(2);N(4,22)=shape(3);N(4,31)=shape(4);N(4,
40)=shape(5);N(4,49)=shape(6);
N(4,58)=shape(7);N(4,67)=shape(8);N(4,76)=shape(9);
N(5,5)=shape(1);N(5,14)=shape(2);N(5,23)=shape(3);N(5,32)=shape(4);N(5,
41)=shape(5);N(5,50)=shape(6);
N(5,59)=shape(7);N(5,68)=shape(8);N(5,77)=shape(9);
N(6,6)=shape(1);N(6,15)=shape(2);N(6,24)=shape(3);N(6,33)=shape(4);N(6,
42)=shape(5);N(6,51)=shape(6);
N(6,60)=shape(7);N(6,69)=shape(8);N(6,78)=shape(9);
N(7,7)=shape(1);N(7,16)=shape(2);N(7,25)=shape(3);N(7,34)=shape(4);N(7,
43)=shape(5);N(7,52)=shape(6);
N(7,61)=shape(7);N(7,70)=shape(8);N(7,79)=shape(9);
N(8,8)=shape(1);N(8,17)=shape(2);N(8,26)=shape(3);N(8,35)=shape(4);N(8,
44)=shape(5);N(8,53)=shape(6);
N(8,62)=shape(7);N(8,71)=shape(8);N(8,80)=shape(9);
```

```
N(9,9)=shape(1);N(9,18)=shape(2);N(9,27)=shape(3);N(9,36)=shape(4);N(9,
45)=shape(5);N(9,54)=shape(6);
N(9,63)=shape(7);N(9,72)=shape(8);N(9,81)=shape(9);
k_q_q=k_q_q+B_q'*D_sys*B_q*wtx*wty*detjacob;
kn_1=kn_1+B_q'*D_sys1*A_1*G*wtx*wty*detjacob;
kn_2=kn_2+G'*A_1'*D_sys2*B_q*wtx*wty*detjacob;
kn_3=kn_3+G'*A_1'*D_sys3*A_1*G*wtx*wty*detjacob;
ff_q=ff_q+N'*f'*wtx*wty*detjacob;
ff_T=ff_T+B_q'*ff_temp*wtx*wty*detjacob;
end
end
index_q=feeldof(nd,nnel,ndof_q);
K_q_q=feasmbl1(K_q_q,k_q_q,index_q);
KN_1=feasmbl1(KN_1,kn_1,index_q);
KN_2=feasmbl1(KN_2,kn_2,index_q);
KN_3=feasmbl1(KN_3,kn_3,index_q);
FF_q=feasmbl3(FF_q,ff_q,index_q);
FF_T=feasmbl4(FF_T,ff_T,index_q);
end
K_q_q=K_q_q+1/2*KN_1+KN_2+1/2*KN_3;
Ks=K_q_q;
FF_q_q=FF_q+FF_T;
 [Ks,FF_q_q]=feaplycs1(Ks,FF_q_q,bcdof);
q=pinv(Ks)*FF_q_q;
w=q(:,1);
 wmax=w;
wcen=q((CN-1)*9+3,1);
w_nondimensional=wcen/h;
W_NONDIMEN(1)=w_nondimensional
 j=1;
     for i=3:9:sdof_q
    disp_w(j)=W_NONDIMEN;
    j=j+1;
  end
en=max(disp_w);
if en==0
    disp_w=-disp_w;
    en=max(disp_w);
end
for i=1:nel
    for j=1:9
        no=nodes(i,j);
        disp_w_e(i,j)=(disp_w(no));

    end
end
  j=1;
for i=1:9:sdof_q
    disp_u(j)=W_NONDIMEN(1);
    j=j+1;
end
en1=max(disp_u);
if en1==0
    disp_u=-disp_u;
    en1=max(disp_u);
for i=1:nel
    for j=1:9
```

```
        no=nodes(i,j);
        disp_u_e(i,j)=(disp_u(no));
end
        end
end
j=1;
for i=2:9:sdof_q
    disp_v(j)=W_NONDIMEN(1);
    j=j+1;
end
en2=max(disp_v);
if en2==0
    disp_v=-disp_v;
    en2=max(disp_v);
end
for i=1:nel
    for j=1:9
        no=nodes(i,j);
        disp_v_e(i,j)=(disp_v(no));
           end
end
j=1;
for i=4:9:sdof_q
    disp_six(j)=W_NONDIMEN(1);
    j=j+1;
end
en4=max(disp_six);
if en4==0
    disp_six=-disp_six;
    en4=max(disp_six);
end
for i=1:nel
    for j=1:9
        no=nodes(i,j);
        disp_six_e(i,j)=(disp_six(no));

    end
end
j=1;
for i=5:9:sdof_q
    j=j+1;
end
en5=max(disp_siy);
if en5==0
    disp_siy=-disp_siy;
    en5=max(disp_siy);
end
for i=1:nel
    for j=1:9
        no=nodes(i,j);
        disp_siy_e(i,j)=(disp_siy(no));

end
j=1;
for i=8:9:sdof_q
        j=j+1;
```

```
end
if en12==0
    disp_thetax=-disp_thetax;
    en12=max(disp_thetax);
end
for i=1:nel
    for j=1:9
        no=nodes(i,j);
        disp_thetax_e(i,j)=(disp_thetax(no));
    end
end
j=1;
for i=9:9:sdof_q
    disp_thetay(j)=W_NONDIMEN(1);
    j=j+1;
end
en13=max(disp_thetay);
if en13==0
    disp_thetay=-disp_thetay;
    en13=max(disp_thetay);
end
for i=1:nel
    for j=1:9
        disp_thetay_e(i,j)=(disp_thetay(no));
    end
end
w_nondimen(sh)=W_NONDIMEN(1);
if (sh~=1& (((w_nondimen(sh)-w_nondimen(sh-
1))^2/(w_nondimen(sh))^2)^0.5)<=(1e-3))
     Nonlinear_defelection= w_nondimen
    break
end
end
end
end
```

About the Author

Vishesh was born on 30th October 1984 in Raipur, one of the oldest cities in central India (now, the capital city of Chhattisgarh State). He completed his bachelor degree in Mechanical Engineering from Pt. Ravishankar Shukla University, Raipur in 2007 with honours. In 2010, he completed Master of Technology in Design Engineering from College of Engineering, Pune with first division. His master's project was sponsored by Design and Development Department, TATA TC Springs Ltd., Pune for the duration of one year. After his master's degree, he joined as Assistant Professor in Department of Mechanical Engineering at Pragati College of Engineering & Management, Raipur. Before enrolling in the doctoral programme in the Department of Mechanical Engineering, NIT Rourkela in 2012, he was in O. P. Jindal Institute of Technology (now, O. P. Jindal University), Raigarh as Assistant Professor. The author's current research interest lies in the field of Advanced Composites, Smart Structures, Solid Mechanics and Finite Element Method. He has some journal and conference publications in his credit. Lists of papers that have been published /communicated are given below:

Published/Accepted in International Journals

1. Kar V R, Panda S K (2014). Nonlinear free vibration of functionally graded doubly curved shear deformable panels using finite element method, *Journal of Vibration and Control*, DOI: 10.1177/1077546314545102.
2. Kar V R, Panda S K (2015). Large deformation bending analysis of functionally graded spherical shell using FEM, *Structural Engineering and Mechanics* 53(4):661-679.
3. Kar V R, Panda S K (2015). Nonlinear flexural vibration of shear deformable functionally graded spherical shell panel, *Steel and Composite Structures*, 18(3):693-709.

4. Kar V R, Panda S K (2015). Thermoelastic analysis of functionally graded doubly curved shell panels using nonlinear finite element method, *Composite Structures*, 129: 202-212.
5. Kar V R, Panda S K (2015). Free vibration responses of temperature dependent functionally graded doubly curved panels under thermal environment, *Latin American Journal of Solids & Structures*, 12(11):2006-2024.
6. Kar V R, Mahapatra T R, Panda S K (2015) Nonlinear flexural analysis of laminated composite flat panel under hygro-thermo-mechanical loading, *Steel and Composite Structures*, 19(4):1011-1033.
7. Mahapatra T R, Kar V R, Panda S K (2015) Nonlinear free vibration analysis of laminated composite doubly curved shell panel in hygrothermal environment, *Journal of Sandwich Structures and Materials*, 17(5):511-545.
8. Kar V R, Panda S K, Nonlinear thermomechanical deformation behaviour of P-FGM spherical shallow shell panel, *Chinese Journal of Aeronautics,* DOI:10.1016/j.cja.2015.12.007.
9. Mahapatra T R, Kar V R, Panda S K (2015) Large amplitude free vibration analysis of laminated composite spherical panel under hygrothermal environment, *International Journal of Structural Stability and Dynamics*, DOI: 10.1142/S0219455414501053.
10. Mahapatra T R, Panda S K, Kar V R (2015) Geometrically nonlinear flexural analysis of hygro-thermo-elastic laminated composite doubly curved shell panel. *International Journal of Mechanics & Materials in Design*, DOI: 10.1007/s10999-015-9299-9.
11. Mahapatra T R, Panda S K, Kar V R, (2015) Nonlinear hygro-thermo-elastic vibration analysis of doubly curved composite shell panel using finite element micromechanical model, *Mechanics of Advanced Materials and Structures*, DOI: 10.1080/15376494.2015.1085606.
12. Mahapatra T R, Kar V R, Panda S K (2015) Large amplitude bending behaviour of laminated composite curved panels, *Engineering Computations*, DOI: 10.1108/EC-05-2014-0119.

13. Mehar K, Panda S K, Dehengia A, Kar V R, Vibration analysis of functionally graded carbon nanotube reinforced composite plate in thermal environment. *Journal of Sandwich Structures and Materials*, DOI:10.1177/1099636215613324.
14. Mahapatra T R, Kar V R, Panda S K, Nonlinear flexural analysis of laminated composite spherical shells under hygro-thermo-mechanical loading-a micromechanical approach. *International Journal of Computational Method* (Accepted).
15. Kar V R, Panda S K, Nonlinear thermo-mechanical behaviour of FGM cylindrical/hyperbolic/elliptical shell panel with TD and TID properties", *Journal of Pressure Vessel Technology - ASME* (Revised).
16. Kar V R, Panda S K, Geometrical nonlinear free vibration analysis of FGM spherical panel under nonlinear thermal loading with TD and TID properties. *Journal of Thermal Stresses* (Revised).
17. Kar V R, Panda S K, Geometrical nonlinear free vibration behaviour of functionally graded doubly curved panel under non-uniform thermal field. *Computational and Nonlinear Dynamics - ASME*, (Under review).
18. Kar V R, Panda S K, Thermal buckling of shear deformable functionally graded doubly curved shell panel with TD and TID properties. *Latin America Journal of Solids and Structures* (Under review).
19. Kar V R, Panda S K, Nonlinear free vibration behaviour of temperature-dependent functionally graded spherical shallow shell panel under uniform/linear temperature distribution. *Mechanics of Advanced Materials & Structures* (Communicated).
20. Kar V R, Panda S K, Nonlinear free vibration behaviour of shear deformable functionally graded doubly curved panel uniform and linear thermal field. *International Journal of Pressure Vessel & Piping* (Communicated).

Published/Accepted in International/National Conferences:

1. Kar V R, Panda S K (2015), Effect of volume fraction on the nonlinear flexural behaviour of shear deformable functionally graded plate, 5th National Conference

on Processing and Characterization of Materials (NCPCM 2015), NIT Rourkela, India. Dec 12-13.

2. Kar V R, Panda S K (2014), Thermal buckling of temperature dependent functionally graded cylindrical panel, 5th International & 26th All India Manufacturing Technology, Design and Research Conference (AIMTDR 2014) IIT Guwahati, India, Dec 12-14.
3. Kar V R, Panda S K (2014), Effect of temperature on stability behaviour of functionally graded spherical panel, 4th National Conference on Processing and Characterization of Materials (NCPCM 2014), NIT Rourkela, India. Dec 5-6. (*Scopus Indexed*: IOP Conference Series: Materials Science and Engineering 75 (2015) 012014 doi:10.1088/1757-899X/75/1/012014).
4. Kar V R, Panda S K (2014), Bending responses of functionally graded cylindrical panel, International Conference on Emerging Materials and Processes (ICEMP 2014), CSIR-IMMT, Bhubaneswar, India. Feb 26-28.
5. Kar V R, Panda S K (2014), Nonlinear bending responses of functionally graded cylindrical panels, International Conference on Functional Materials (ICFM 2014) IIT Kharagpur, India. Feb 5 -7.
6. Kar V R, Panda S K (2013), Bending behaviour of functionally graded spherical shell panels, 2nd KIIT International Symposium on Advances in Automotive Technology (2nd KIIT SAAT-2013), KIIT, Bhubaneswar, India. Dec 20-21.
7. Kar V R, Panda S K (2013), Thermal Stability Analysis of Functionally Graded Panels, International Conference on Structural Engineering and Mechanics (ICSEM 2013) NIT-Rourkela, India. Dec 20-22.
8. Kar V R, R K Singh, Panda S K (2013). Effect of gradation on bending behaviour of functionally graded spherical panels, 3th National Conference on Processing and Characterization of Materials (NCPCM 2013), NIT Rourkela, India. Dec 6-7.
9. Kar V R, Panda S K (2013), Free Vibration Responses of Functionally Graded Spherical Shell Panels using Finite Element Method, ASME 2013 Gas Turbine India Conference (ASME GTINDIA2013), CSIR-NAL, Bangalore, India. Dec 5-6. (*Scopus Indexed*: doi: 10.1115/GTINDIA20133693).

10. Kar V R, Panda S K (2013). Free vibration responses of functionally graded cylindrical shell panels using finite element method, All India Seminar on Recent Advances in Mechanical Engineering, Institute of Engineers (India), Bhubaneswar, India. March 16-17.
11. Kar V R, Panda S K (2013). Scope and study of functionally graded plate structures in automotives, 1st KIIT International Symposium on Advances in Automotive Technology (1st KIIT SAAT-2013), KIIT, Bhubaneswar, India. Jan 11-12.
12. Katariya P V, Panda S K, Kar V R (2015). Free vibration analysis of skew laminated composite curved shell panels. International Conference on Computer Aided Engineering (CAE 2015), GITAM University, Hyderabad, India, Dec 2015.